UNIVERSIDAD DE EXTREMADURA

TESIS DOCTORAL

ESTUDIO TEÓRICO-EXPERIMENTAL DE LA REACTIVIDAD 1,3-DIPOLAR DE TIOISOMÜNCHNONAS BICÍCLICAS

JUAN GARCÍA DE LA CONCEPCIÓN

PROGRAMA DE DOCTORADO EN QUÍMICA SOSTENIBLE

Conformidad de los directores:

Martín Ávalos González José Luis Jiménez Requejo

2018

This PhD Thesis has given rise to five publications:

1. *"Computational insights into cycloadditions of thioisomünchnones with acetylenes: how does sulfur escape from cycloadducts?"* Juan García de la Concepción, Martín Ávalos, Reyes Babiano, Pedro Cintas, José L. Jiménez, Mark E. Light and Juan C. Palacios. *Tetrahedron* **2016**, *72*, 4665-4670. DOI: 10.1016/j.tet.2016.06.041

2. *"Assessing stereoelectronic effects in dipolar cycloadditions yielding fused thiazolopyridone rings"* Juan García de la Concepción, Martín Ávalos, Reyes Babiano, Pedro Cintas, José L. Jiménez, Mark E. Light and Juan C. Palacios. *Tetrahedron* **2017**, *73*, 1551-1560. DOI: 10.1016/j.tet.2017.01.064

3. *"Computational screening of new orthogonal metal-free dipolar cycloadditions of mesomeric betaines"* Juan García de la Concepción, Martín Ávalos, Pedro Cintas and José L. Jiménez. *Chem. Eur. J.* **2018**, *24*, 7507–7512. DOI: 10.1002/chem.201800869

4. *"Mechanistic studies of 1,3-dipolar cycloadditions of bicyclic thioisomünchnones with alkenes. A computational rationale focused on donor–acceptor interactions"* Juan García de la Concepción, Martín Ávalos, Pedro Cintas, José L. Jiménez and Mark E. Light. *Org. Biomol. Chem.* **2018**, *16*, 3438–3452. DOI: 10.1039/C8OB00683K

5. 5. *"On the dual reactivity of a Janus-type mesoionic dipole: experiments and theoretical validation"* Juan García de la Concepción, Martín Ávalos, Pedro Cintas, José L. Jiménez and Mark E. Light. *Org. Biomol. Chem.* **2018**, *16*, 4778-4783. DOI: 10.1039/C8OB01195H.

In addition, the doctoral candidate has collaborated in another research line, by performing mechanistic studies aided by DFT calculations, which has resulted in the following paper:

6. *"Formation of cyanamide–glyoxal oligomers in aqueous environments relevant to primeval and astrochemical scenarios: A spectroscopic and theoretical Study"* Nieves Lavado, Juan García de la Concepción, Reyes Babiano and Pedro Cintas. *Chem. Eur. J*. **2018**, *24*, 4069–4085. DOI: 10.1002/chem.201705747

Finally, the doctoral student has co-authored a book chapter on mesoionic heterocycles, within the scope of the present PhD Thesis:

7. *"Cycloadditions with mesoionic dipoles: strategy and control"* Juan García de la Concepción, Rafael Fernando Martínez, Pedro Cintas and José L. Jiménez. In *Targets in Heterocyclic Systems: Chemistry and Properties, Vol. 21*; O. Attanasi, P. Merino and D. Spinelli, Eds.; Italian Society of Chemistry, Rome (Italy), 2018, Ch 11*,* pp 228-253. ISBN: 978-88-86208-87-1

Resumen

En esta Tesis Doctoral se ha llevado a cabo un estudio teórico y experimental de las reacciones de cicloadición 1,3-dipolar de heterociclos mesoiónicos bicíclicos con dipolarófilos que presentan insaturaciones carbono-carbono.

Los heterociclos mesoiónicos (entre ellos tioisomünchnonas, estudiadas en particular aquí) son heterociclos de cinco miembros que no puede ser adecuadamente representados por una estructura covalente o dipolar sin separación de cargas, que poseen un sextete de electrones π asociado a los cinco átomos del anillo y que se describen mejor como un híbrido en resonancia de todas las posibles formas cargadas. Las reacciones de cicloadición de heterociclos mesoiónicos con dobles y triples enlaces carbono-carbono dan lugar a aductos ricos en heteroátomos, que son difíciles de obtener a través de otras rutas sintéticas.

Se ha estudiado la reactividad de heterociclos mesoiónicos de estructura rígida derivados de tiazolidin-2-tionas frente a olefinas y acetilenos simétricos y asimétricos, que dan lugar a tiazolopiridonas y cicloaductos que contienen oxígeno, nitrógeno y azufre. Las reacciones de cicloadición con dipolarófilos asimétricamente sustituidos fueron regioespecificas. Esta regioselectividad se ha justificado a través de un estudio teórico que, además, ha permitido elucidar el mecanismo por el cual los cicloaductos iniciales evolucionan hacia los productos. El análisis de los efectos estereoelectrónicos que controlan estas cicloadiciones ha permitido justificar la selectividad que se aprecia tras evaluar las barreras de energía que conducen a los cicloaductos y la estereoseleccion facial que ejerce un dipolo mesoiónico quiral.

Debido a la importancia de emplear reactivos baratos, fácilmente accesibles e inventar nuevas rutas sintéticas, se ha sintetizado una tioisomünchnona derivada de un aminoácido natural. Dicha tioisomünchnona presentó una reactividad dual que conduce a productos estructuralmente muy diferentes. La detección experimental y verificación teorica de este comportamiento dual ha permitido abrir una línea de investigación dirigida a la síntesis de reactivos dipolares que presenten esta doble reactividad.

En los últimos años el desarrollo de nuevas reacciones que sean muy selectivas y rápidas ha adquirido una gran importancia debido a su posible aplicación en química bio-ortogonal. En este campo las cicloadiciones dipolares de sidnonas con acetilenos tensionados han sido muy utilizadas. Las sidnonas son heterociclos mesoiónicos que

reaccionan con acetilenos para dar pirazoles. Aunque estas cicloadiciones son selectivas, son generalmente lentas, limitando en ocasiones su utilidad. Debido a este inconveniente, se ha realizado un cribado computacional de varios heterociclos mesoiónicos con ciclooctinos y se han estudiado los procesos electrónicos que controlan estas cicloadiciones. Este análisis ha permitido diseñar teóricamente nuevos dipolos que presentarían reactividades con ciclooctinos muy superiores a las descritas hasta el momento.

Summary

This PhD Thesis involves both theoretical and experimental studies on the 1,3-dipolar cycloadditions of bicyclic mesoionic heterocycles with dipolarophiles bearing unsaturated carbon-carbon bonds.

The mesoionic heterocycles (among them thioisomünchnones, a family explored here in particular) are a five-membered rings that cannot be represented by a covalent or dipolar structure without charge separation, possess a π-electron sextet associated to the five atoms of the ring, and being actually a hybrid structure of all the charged canonical forms. The cycloaddition reactions of mesoionic dipoles with unsaturated carbon-carbon bonds give rise to rich-heteroatom heterocycles that can hardly be obtained by other synthetic routes.

Firstly, the reactivity of rigid mesioionic heterocycles derived from thiazolidin-2-thiones against symmetrical and unsymmetrical olefins, as well as acetylenes has been studied. These reactions led to thiazolopyridones and other cycloadducts containing oxygen, nitrogen and sulfur atoms. The reactions with unsymmetrically-substituted dipolarophiles were regioselective and that selectivity could be justified through a theoretical analysis, thus allowing us to elucidate the reaction mechanisms by which the initial 1:1 cycloadducts evolve into the products. Moreover, the stereoelectronic effects that control these cycloadditions helped us to rationalize the observed selectivity by assessing the corresponding energy barriers and the facial stereocontrol exerted by a chiral mesoionic dipole.

Due to the importance of using cheap, easily available reagents, and inventing new synthetic routes, a thioisomünchnone derived from a natural amino acid has been synthesized. That mesoionic ring, showed a dual reactivity leading to structurally different products. The experimental detection and theoretical verification of this behavior opens the door to a research line focused on the synthesis of dipolar reagents susceptible of dual reactivity.

In recent years the development of new, selective and fast cycloadditions has gained increased importance due to their potential application in bio-orthogonal chemistry. In this field, dipolar cycloadditions of sydnones with strained acetylenes have been widely used. Sydnones constitute a type of mesoionic heterocycle capable of reacting with acetylenes to give pyrazoles. Although such cycloadditions are quite selective, they are generally slow,

often limiting their usefulness. To overcome this drawback, a computational screening of several mesoionic heterocycles and cyclooctynes has been carried out, evaluating in addition the electronic features that control these cycloadditions. This analysis has allowed us to design theoretically new dipoles that exhibit reactivities vastly superior to those described so far.

Acknowledgements

We acknowledge the financial support from the *Ministerio de Economía y Competitividad* (Project No. CTQ2013-44787P) and the *Junta de Extremadura and Fondo Europeo de Desarrollo Regional* (Ayuda a Grupos de Investigación Consolidados, Grants GR15022 and IB16167). We also thank *Cénits* and *Fundación Computaex* for permitting the use of Supercomputer LUSITANIA.

From my personal corner, I would like to thank my supervisors, Profs. Martín Ávalos González and José Luis Jiménez Requejo for giving me the opportunity to work with them over the past years, and especially for their constant and unconditional support, and for allowing me to develop my own ideas. All in all, these predoctoral studies have boosted my academic and personal skills.

Thanks also to Drs. Pedro Cintas and Reyes Babiano, who have followed my trajectory as well, and gave me the opportunity of collaborating in additional research proyects.

Special thanks to Isabel, Victoria, Juan Carlos, Verónica, Pilar and Esther for their help whenever I needed it and to my MSc mates for sharing great leisure times.

Big thanks to my friends, who always offered their support and understanding.

To Nieves for being there, for her patience, stimulus, and unconditional support, which made everything easier.

Finally, many thanks to my sister and parents, without their support nothing would have been possible. This Thesis, and much more, is especially dedicated to them.

Index

1. Introduction

This Doctoral Thesis focuses on theoretical and experimental studies of the 1,3-dipolar cycloadditions of mesoionic heterocycles, specifically 1,3-thiazolium-4-olates, against double and triple carbon-carbon bonds. The dipolar reactivity of mesoionic heterocycles has long been explored by the QUOREX research group at the Department of Organic and Inorganic Chemistry of the University of Extremadura, Spain. In this context, the work presented through this thesis deals mainly with stereoelectronic effects in [3+2]-cycloadditions reactions of ring-fused mesoionic heterocycles, derived from thiazolidine-2-thiones, with double and triple bonds, as well as preliminary results aimed at exploring the dipolar duality of one bicyclic mesoionic derived from a proteinogenic amino acid. Moreover, we show the contribution of mesoionic dipoles to the so-called bio-orthogonal chemistry, thus extending the application of such dipoles into future biological labeling methodology. For the purpose of these introductory remarks, some recent book chapters and monographs, in mesoionic chemistry[1] and computational methods,[2-4] should be mentioned.

1.1. The 1,3-dipolar cycloaddition

Since pioneering studies in the early 1960s, the 1,3-dipolar cycloaddition has become a versatile tool for the construction of five-membered rings.[5] Nowadays, it is still a powerful strategy en route to diverse heterocyclic systems and especially in the elaboration of natural products and their analogs.

A 1,3-dipole is a kind of zwitterionic octet structure that can undergo 1,3-dipolar cycloadditions with unsaturated systems (dipolarophiles), leading to rings whose atoms are devoid of formal charges (Scheme 1.1).

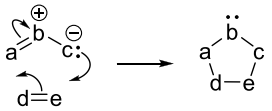

Scheme 1.1. 1,3-dipolar cycloaddition.

The 1,3-dipoles can be classified in either allylic or propargyl/allenyl type. Allyl type dipoles show four electrons in two π molecular orbitals. Contrary to the allyl anion, whose central atom does not show any formal charge, the corresponding 1,3-dipoles possess a *b* center whose positive charge offsets the negative charge delocalized between the terminal atoms *a* and *c* in two octet structures (Figure 1.1). In this way, the whole system can be considered as a heteroallylic anion without net charge. As depicted in the resonance structures in Figure 1.1, the *b* atom can localize two π allylic electrons of the dipole while creating electron sextets in *a* or *c*. On the other hand, although the allyl anion atoms *a* and *c* are always nucheophiles, such atoms in the 1,3-dipoles can be both nucleophiles and electrophiles. This ambivalence is a key feature for ascertaining the reaction mechanism as well as the regiochemistry of the 1,3-dipolar cycloaddition, as the termini of a dipole may exhibit different nucleophilic and electrophilic activities.

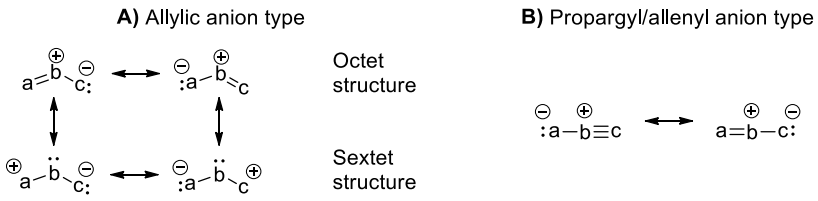

Figure 1.1. Types of 1,3-dipoles.

The 1,3-dipolar cycloaddition with unsaturated carbon-carbon systems involves four π electrons of the dipole (D) and two π electrons of the dipolarophile (d). This is a process classified as $[\pi 4_s + \pi 2_s]$ according to the Woodward-Hoffman rules. It implies that π molecular orbitals of the dipole and the dipolarophile interact each other when they are positioned in parallel planes (Figure 1.2). This arrangement precedes the formation and

rupture of the new bonds and involves a re-hybridization of the molecular orbitals. The transition states of 1,3-dipolar cycloadditions are controlled by the frontier molecular orbitals (FMO) of reactants, namely, the HOMO and LUMO orbitals. Sustmann classified the dipolar cycloadditions in *Type I, II* and *III* based on the energy gaps between the FMOs.[6,7] Figure 1.3 shows the energy gaps between the FMOs of a dipole and dipolarophile, where red and green colors denote the least and the most favorable interactions respectively. In Type I dipolar cycloaddition, the most favorable interaction is the $HOMO_D$-$LUMO_d$, also called *direct electron demanding* cycloaddition. On the contrary, the $HOMO_d$-$LUMO_D$ interaction is characteristic of *Type III* cycloadditions or *inverse electron demanding*. Sustmann's *Type II* cycloadditions consider that both $HOMO_D$-$LUMO_d$ interactions and *vice versa* are possible due to the energetic similarity of the frontier molecular orbitals.

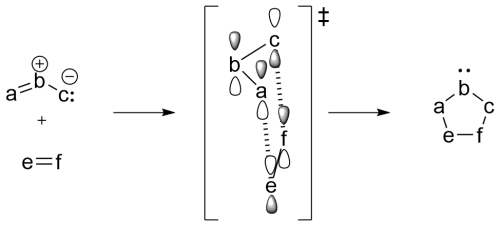

Figure 1.2. *p*-Orbital interactions between dipole and dipolarophile.

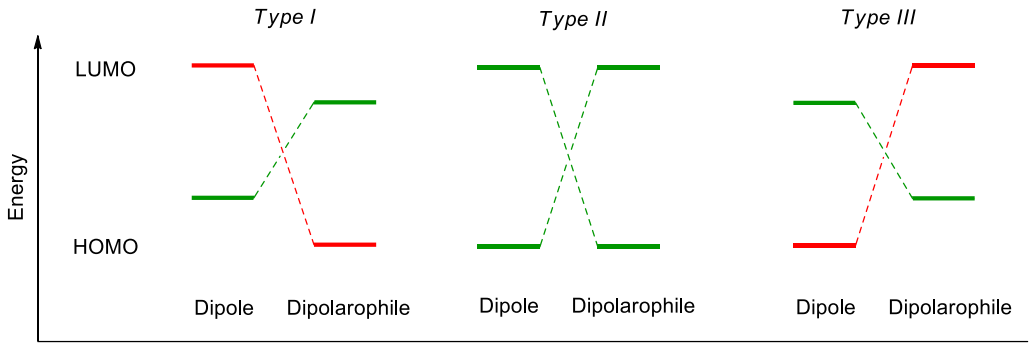

Figure 1.3. Classification of dipolar cycloadditions based on FMO interactions.

1.2. Mesoionic heterocycles

The synthesis of and with mesoionic heterocycles is arguably an old field that enjoys renaissances from time to time, given their great value as synthons toward other heterocycles and fine chemicals as well as natural products, drugs and their analogs.[1]

The concept of mesoionic heterocycle and, especially its reactivity as masked dipole, grew up from an academic curiosity to a well-consolidated subfield of heterocyclic chemistry. Historically the term mesoionic was coined by Baker and Ollis as early as the 1940s as a nickname combining "mesomeric" and "ionic".[8,9] In this context and in a strict sense, a mesoionic compound is a five-membered heterocycle that cannot be satisfactorily represented by any one Lewis structure not involving charge separation, and possessing a sextet of electrons in association with the atoms comprising the ring. That delocalization gives rise to enough stability to allow isolation in numerous cases, even though the issue of aromaticity in mesoionic rings is debatable.[1] Several resonance structures can then be drawn for a given mesoionic compound, without consensus about a preferred canonical form, each showing its dipolar character. Mesoionics can also be viewed as heterocycles of intermediate ionicity, thus echoing the universal definition of *meso* (from Greek μεσος (misos) = middle). The above definition indicates that mesoionics belong to the large family of *heterocyclic mesomeric betaines*,[11,12] but excludes explicitly six-membered rings.

It is customary to group mesoionic rings into two major types, denoted *A* and *B* (Figure 1.4), covering diazolium olate/thiolate systems to a large extent, although other systems have been introduced in recent years (*e.g.* tetrazolium derivatives),[13] including rings containing main-group heteroatoms other than O, N and S. At first glance, both types show close resemblance, being no more than positional isomers, as labels *a*, *b*, *c*, and *d* indicate atoms with one-electron contribution to the π-system, while two-electron contributions are represented by atoms *x* and *y*. This delusive appreciation can be disclosed through connectivity-matrix analysis,[12] also supported by DFT calculations,[14] which recognize further classes and subclasses of types *A* and *B* mesoionics. In short, the wide variety of mesomeric betaines should now be classified in terms of conjugated, semi-conjugated, and cross-conjugated systems. Thus, while type *A* rings are actually conjugated betaines, the calculated properties of type *B* are consistent with their classification as semi-conjugated heterocyclic betaines and show characteristics similar to those of six-membered semi-conjugated betaines. Most synthetic achievements have been conducted with the first type,

whereas the *B* series waits for further developments and explorations, as some predicted subclasses remain unknown, which may account for inherent instability, or such structures exist as the corresponding valence isomers, not yet experimentally detected.

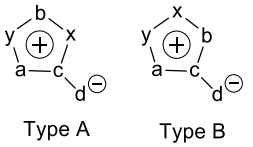

Figure 1.4. Type *A* and type *B* mesoionic rings.

As an example, Figure 1.5 shows a cyclic system with heteroatoms, sulfur and nitrogen, in positions 1 and 3 of the ring together with an exocyclic oxygen, namely a 1,3-thiazolium-4-olate, which is the type of dipole studied through this Thesis.

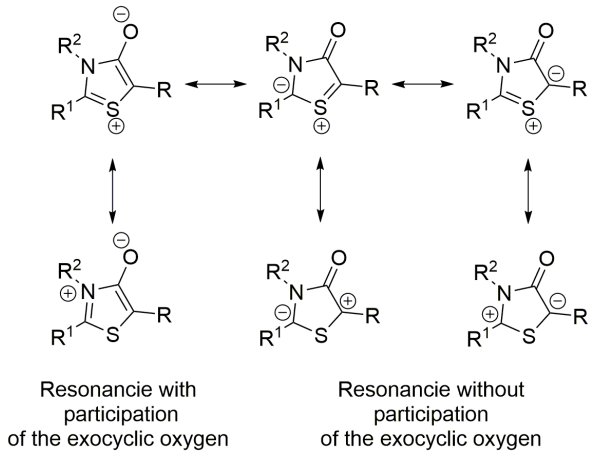

Figure 1.5. Resonance structures of a 1,4-thiazolium-4-olate.

1.3. Theoretical background

One of the most important and intriguing research topics in organic chemistry is to investigate how reactions occur, namely, the reaction mechanisms. How a bond is formed or broken, and how the tridimensional and electronic structure of a system evolves from reagents to products is a key feature for understanding the reactivity of a given molecule

and its transformation. In this context, computational chemistry has become an important tool to understand some complex systems, which are sometimes very complicated to be observed experimentally. The influence of the electronic structure on chemical reactivity was rapidly recognized with the formulation of the Schrödinger equation. All progress to date has been made possible by the rapid development in computers and software related to quantum mechanics.

One of the most important limitations in computational chemistry is the accuracy and reliability of computational methods. As a general rule arising from the computational cost, the bigger the system, the less accurate the method employed is. Consequently, less accurate results are obtained with large molecular systems, so that comparative assessment between computation and experiments is mandatory. There are several methods that differ in the mathematical approximation to resolve the Schrödinger equation. Accordingly, it is instrumental to choose the most suitable method for the system under study. The most employed classification of computational methods divides them into *ab initio*, *semi-empirical* and those based on the *density functional* (DFT).

The term *ab initio* ("from the beginning" in Latin) refers to computational methods that are based on the quantum mechanical principles without the inclusion of experimental data. These methods attempt to resolve the Schrödinger equation through mathematical approaches that average the interelectronic repulsion. This term makes it impossible to solve the Schrödinger equation for systems with more than one electron, and as a result, some mathematical approximations have been introduced to overcome that limitation.

The first and simplest *ab initio* method is the Hartree-Fock (HF),[15,16] also called *self-consistent field* method (SCF). An important limitation of the HF method is that it does not include any electron correlation, *i.e*. electron-electron repulsion. Some calculations often start with a HF method and then the electron correlation is included, such as the Post-Hartee-Fock methods. These methods are able to both predict and confirm experimental results, although they are computationally expensive.

Semiempirical methods have a similar structure than the HF calculation, regarding that they have a Hamiltionian and wavefunction as well. However, some key information is absolutely omitted. For instance, core electrons or some two-electron integrals are not taken into account. The lack of these calculations are offset by parameters that estimate the omitted information. Such parameters are taken from experimental data or *ab initio*

calculations. As a result, semiempirical calculations are much faster than those carried out with *ab initio* methods. The main disadvantage of semiempirical methods is that the above-mentioned parametrizations give erratic results, especially when the parameters are taken from systems structurally different to the molecule in question.

From its birth to date, the *Density Functional Theory* (DFT) has become a very popular and useful method to understand and compute the electron density of the ground state and its energy in molecules, clusters and solids. The high popularity of these methods is justified in terms of low computational cost, though yielding results as accurate as some *ab initio* methods. The DFT theory is an alternative procedure to other methods based on the polielectronic wavefunction. This theory, developed by Hohenberg and Kohn in 1964,[17] compute the ground state electron structure based on its electron density, ρ(r), distribution.

One of the advantages of the DFT methods is that they use the electron density to get the Coulombic repulsion integrals. The latter reduces the calculation time because the electron density (a tridimensional property) involves three coordinates. On the contrary, post-HF methods require four coordinates to define one electron, i.e. its spatial coordinates plus the spin.

Due to the size and presence, in all cases, of sulfur atoms in the molecules studied throughout this Thesis, a method based on the density functional has been chosen to carry out the computational studies. That DFT method involves the Truhlar functional M06-2X, which has demonstrated to be reliable enough for the study of non-covalent interactions and energy barriers.[18]

On the other hand, an essential point in computational chemistry is the choice of the basis set. A basis set is a set of functions used for describing the orbital shape of the atoms. At the time of approaching as much as possible to reality, the best choice would be to compute with an infinite basis set, which would allow us to obtain an exact solution. In practice, finite basis sets are employed and their choice represents a key feature for any researcher in computational chemistry. Pople's basis sets, which have been used in this work, are by far the most employed bases due to their versatility and low computational cost. In particular, this thesis has been largely conducted with the 6-311++G(d,p),[19] where each core orbital is described by a contraction of six primitive GTOs (*Gaussian-type orbitals*) and each valence orbital by three contractions, one of three primitives and two of one primitive. The inclusion of *polarized* and *diffuse functions* in the basis sets gets better

the calculations of molecular properties. *Polarized* base functions have functions with a high angular momentum for each atom, permitting a deformation of the orbital shape. The basis set 6-311++G(d,p) add *d* functions to heavier atoms than the hydrogen and *p* functions to hydrogen atoms. The *diffuse functions* are spatial extents of the valence orbitals. For instance, the 6-311++G(d,p) includes two diffuse functions, one for atoms other than hydrogen and the second for hydrogen itself. Such diffuse functions are useful to describe anions that show a high electron density in weak interactions like van der Waals bonding. The very diffuse orbitals are called Rydberg orbitals.

A significant portion of the computational work in this Thesis involves the evaluation of energy barriers, which are influenced by solvation effects. To this end, an implicit solvation method has been employed. The most employed models to simulate solvation effect assume that the molecular system is placed in a cavity surrounded by a continuum field with a dielectric constant, which are denoted by the acronym SCRF (*Self-Consistent Field Reaction*). The SCRF methods differ from each other in the cavity form and reaction field. A popular approach is the *Tomasi´s Continuum Polarized* method (PCM)[20] that defines a cavity at the join of several overlapped spheres. Herein we employed a more recent model developed by Truhlar, the SMD (*Solvent Model Density*) model.[21] The latter is based on the charge density of the solute instead of partial charges. It is suitable for estimating the solvation free energy as a difference between gas-phase energies and solvated free energies.

Nowadays some methods related to topological analysis of the electron density have become very popular owing to their ability to describe the chemical bond, like QTAIM (*Quantum Theory of Atoms in Molecules*) theory, developed by Bader.[22,23] Here, the electron density, ρ(r), is elementary, and operating on ρ(r) we obtain information about the position of atoms in a molecule and hence, the bonds connecting them. Also the so-called *Non-Covalent Interactions* (NCI),[24] which can be determined by operating on the electron density, have become extremely useful to obtain a qualitative description of non-covalent interactions like hydrogen bonding, steric repulsions, and van der Waals interactions.

Moreover, the *Natural Bond Orbital* (NBO) analysis, developed by Weinhold and coworkers,[25] constitutes a powerful tool to describe the electron distribution into atomic and molecular orbitals. It employs the monoelectronic density matrix to define the shape of the atomic orbitals in the molecular environment, thereby obtaining the electron density between two atoms. In this work the second-order perturbation theory has been employed

to calculate the donor-acceptor (bonding-antibonding) interactions in the NBO basis. This analysis is carried out by evaluating the possible interactions between filled NBO Lewis-type orbitals and unfilled NBOs (non-Lewis-type), and estimating the energetic importance of such interactions.

The global indexes within the conceptual DFT theory are also employed to predict and explain the reactivity of organic and inorganic molecules. Some of these indexes like the *electronic chemical potential* (μ), *electronegativity* (*χ*), *chemical hardness* (η) or *softness* (*S*) are calculated from the *ionization potential* (I) and *electron affinities* (A) of the molecules. By relating some of these indexes, one can assess a series of important features of chemical reactions such as electron transfer, even predicting the selectivities.

The distortion/interaction or activation strain model, developed and employed to a large extent by the groups of Houk and Bickelhaupt,[26] is another computational tool to analyze the activation energy barriers. According to this model the activation energies are the sum of the energies to distort the reactants into the geometries that they have in their transition states plus the interaction energies between the two distorted molecules, which are generally negative (i.e. stabilizing energy). The energy needed to distort the molecules is dubbed the activation strain or distortion energy. This energy is the principal contributor to the activation barrier. The transition state occurs when this activation strain is counterbalanced by the stabilizing interaction energy. This model has been applied to a vast repertoire of organic reactions, including eliminations and substitutions, cycloadditions, and several types of organometallic transformations.

In addition, in this model the activation energy ($\Delta E^{\ddagger}$) is decomposed into the distortion energies of the reactants A ($\Delta E^{\ddagger}_{strainA}$) and B ($\Delta E^{\ddagger}_{strainB}$), which give rise to the total distortion energy ($\Delta E^{\ddagger}_{strain}$), and the interaction energy between the species A and B ($\Delta E^{\ddagger}_{int}$). Figure 1.6 shows a schematic reaction between cyclopentadiene (A) and acetylene (B), and the decomposition of the activation energy ($\Delta E^{\ddagger}$) into the corresponding terms of eq. (1).

$$\Delta E^{\ddagger} = (\Delta E^{\ddagger}_{strainA} + \Delta E^{\ddagger}_{strainB}) + \Delta E^{\ddagger}_{int} = \Delta E^{\ddagger}_{strain} + \Delta E^{\ddagger}_{int} \qquad (1)$$

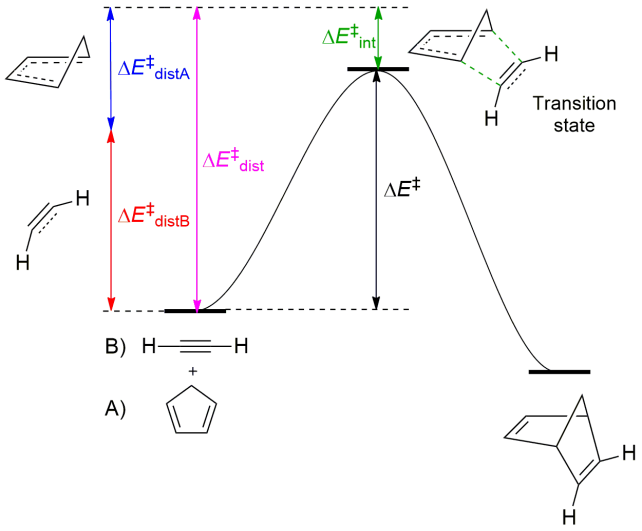

Figure 1.6. Schematic representation of the energetic decomposition ($\Delta E^{\ddagger}$) according to the distortion/interaction or activation strain model for the cycloaddition reaction between cyclopentadiene (A) and acetylene (B).

1.4. Objectives and chapters

The main goal and the longest part of this work is aimed at elucidating the effects that control the regiochemistry in the dipolar cycloadditions of rigid thioisomunchnones with all-carbon asymmetrically-substituted dipolarophiles. In some cases, the initial 1:1 cycloadducts are prone to evolve into different products, whose mechanisms of formation remain unsolved. Accordingly, another goal of this Thesis involves the computational investigation of these mechanistic pathways.

During the past decades, the QUOREX research group has widely investigated the facial stereocontrol exerted by thioisomünchnones derived from sugars, like **1** and **2**, in dipolar cycloadditions with numerous dipolarophiles. The experimental results showed that the incorporation of acyclic chains (**2**) led to modest or poor facial stereocontrol. However, when the conformational freedom of the sugar moiety is restricted, like in the case of **1,** the selectivity could be greatly enhanced. On the other hand, the hydroxyl groups of the sugar have to be protected to avoid competing side reactions, which restricts the experimental conditions and the scope of postsynthetic uses. Because of this, one of the objectives of this work was to synthesize **3** and its chiral version (**4**), which are structurally rigid and do

not come from sugars. In line with our general objectives, both the experimental and theoretical evaluation of the facial stereoselection exerted by **4** has also been carried out.

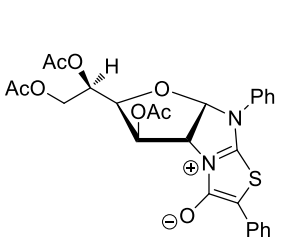

1

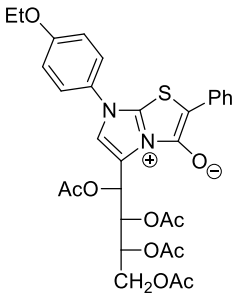

2

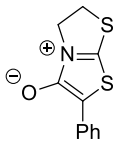

3

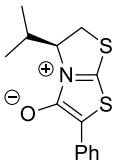

4

Likewise, though in a shorter extent, the ability of thioisomünchone (**5**), easily available from a naturally-occurring amino acid, to behave as two different masked dipoles has been investigated. Such dual reactivity has been assessed in detail by spectroscopic methods, X-ray crystallography, and theoretical analysis of the different mechanisms involved.

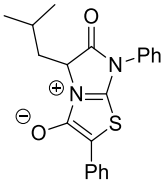

5

It is well known that sydnones, the most widely studied mesoionic dipole, have demonstrated to be useful reagents in bio-orthogonal chemistry due to their stability and selectivity in biological media. Sydnones exhibit however their own Achilles' heel in view of a low reactivity against acetylenes, thus demanding drastic conditions and preventing their general application in bio-orthogonal reactions. Bearing this drawback in mind, we have

also interrogated, through computation, the potential reactivity of alternative mesoionic dipoles, which would react faster in strained cycloadditions with typical cyclooctynes.

All results attained in this Doctoral work are gathered in Chapters 2 to 6 and summarized as follow:

Chapter 2 shows the computational and experimental analysis of 1,3-dipolar cycloadditions of mesoionic compound **3** with acetylenes. A complete regioselectivity could be observed for reactions with asymmetrically-substituted dipolarophiles and justified through the analysis of the corresponding energy barriers. The mechanistic outcome that leads to the thiazolopyridone ring is supported by our computational study. In addition, this analysis provides a rationale for the chemoselectivity detected during the evolution of the initial 1:1 cycloadducts.

Chapter 3 is actually an enlargement of the previous one. Herein the stereoelectronic effects influencing the free energy barriers of the cycloadditions with asymmetrical acetylenes, as well as solvent effects are documented. Also, a chiral thioisomünchnone (**4**) was prepared and further employed en route to optically active thiazolopyridones. This computational analysis allowed us to evaluate the stereoelectronic effects that govern the facial selection exerted by the isopropyl group of **4**. It is noteworthy that this selectivity could not be justified experimentally as the new chiral centers were lost during the *in situ* transformation of 1:1 cycloadducts.

Chapter 4 reports similar studies, although concentrating on olefins as dipolarophiles. Unlike the preceding chapter, the experimental detection of the facial stereocontrol played by **4** could be detected experimentally, as inferred from enantiomerically pure cycloadducts containing up to five chiral centers.

Chapter 5 describes the dual behavior of thioisomünchnone **5**. Its dipolar reactivity was checked against 1-phenyl-1*H*-pyrrole-2,5-dione and dimethyl (*E*)-butenedioate. As mentioned above, the dipolar duality could be corroborated by spectroscopic measurements and supported by DFT analyses.

Chapter 6 shows a computational screening of some dipolar cycloadditions of mesoionic dipoles with several cyclooctynes. This investigation aims to ascertain the key factors that control this kind cycloadditions, not only to justify previous experimental results, but also to disclose novel scenarios that may be of benefit to synthetic chemists working in the field.

1.5. Bibliography

(1) García de la Concepción, J.; Martínez, R. F.; Cintas, P. and Jiménez, J. L. In *Targets in Heterocyclic Systems: Chemistry and Properties*; Attanasi, Merino, P.; Spinelli D., Eds.; Italian Society of Chemistry: Rome, 2018; Ch 11, pp 228-253.
(2) *Exploring Chemistry with Electronic Structure Methods*; Foresman, J. B.; Frisch, A. Eds; Gaussian, Inc.: Pittsburgh, 1995.
(3) *Computational Organic Chemistry*; Bachrach, S. M., Eds.; John Wiley & Sons, Inc.: New Jersey, 2014.
(4) *Computational Chemistry: A Practical Guide for Applying Techniques to Real-World Problems*; Young. D. C., Eds.; John Wiley & Sons, Inc.: New York, 2001.
(5) (a) Baker, W.; Ollis, W. D.; Poole, V. D.; *J. Chem. Soc.* **1949**, 307-314; (b) Baker, W.; Ollis, W. D.; Poole, V. D. *J. Chem. Soc.* **1950**, 1542-1551.
(6) Sustmann, R. *Tetrahedron Lett*. **1971**, *29*, 2717-2720.
(7) Sustmann, R. *Pure Appl. Chem.* **1974**, *40*, 569-593.
(8) Baker, W.; Ollis, W. D. *Quart. Rev. (London)* **1957**, *11*, 15-29.
(9) Ollis,W. D.; Ramsden, C. A. In *Advances in Heterocyclic Chemistry*; Katritzky, A. R., Boulton, J. A.,Eds.; Academic Press: London, 1976; Vol. 19, pp. 1-122.
(10) Champagne, P. A.; Houk, K. N. *J. Org. Chem*. **2017**, *82*, 10980-10988 and references cited therein.
(11) Ollis, W. D.; Stanforth, S. P.; Ramsden, C. A. *Tetrahedron* **1985**, *41*, 2239-2329.
(12) Ramsden, C. A. *Tetrahedron* **2013**, *69*, 4146-4159.
(13) Moderhack, D. *Heterocycles* **2016**, *92*, 185-233.
(14) Oziminski,W. P.; Ramsden, C. A. *Tetrahedron* **2015**, *71*, 7191-7198.
(15) Hartree, D. R. *Proc. Cambridge Philos. Soc.* **1928**, *24*, 328-342.
(16) Fock, V. A. *Z. Phys.* **1930**, *15*, 126.
(17) Hohenberg, P.; Kohn, W. *Phys. Rev. B* **1964**, *136*, 864-871.
(18) (a) Zhao, Y.; Truhlar, D. G. *Theor. Chem. Acc.* **2008**, *120*, 215-241; (b) Zhao, Y.; Truhlar, D.G. *J. Chem. Theory Comput.* **2011**, *7*, 669-676.
(19) Francl, M. M.; Pietro, W. J.; Hehre, W. J.; Binkley, J. S.; DeFrees, D. J.; Pople, J. A.; Gordon, M. J. *J. Chem. Phys*. **1982**, *77*, 3654–3665.
(20) Tomasi, J.; Mennucci, B.;Cammi, R. *Chem. Rev.* **2005**, *8*, 2999-3094.
(21) Marenich, A. V.; Cramer,C. J:; Truhlar, D. G. *J. Phys. Chem. B*, **2009**, *18*, 6378–6396.
(22) Bader, R. F. W. *Chem. Rev.* **1991**, *91*, 893-928.
(23) Bader, R. F. W. *Atoms in Molecules a Quantum Theory*; Clarendon Press: Oxford, 1999.
(24) Johnson, E. R.; Keinan, S.; Mori-Sanchez, P.; Contreras-Garcia, J.; Cohen A. J.; Yang, W. *J. Am. Chem. Soc*. **2010**, *132*, 6498–6506.
(25) Foster J. P.; Weinhold F. *J. Am. Chem. Soc.* **1980**, *102*, 7211-7218.
(26) Bickelhaupt, F. M.; Houk, K. N. *Angew. Chem. Int. Ed*. **2017**, *56*, 10070-10086.

2. Computational insights into cycloadditions of thioisomünchnones with acetylenes: how does sulfur escape from cycloadducts?

2.1. Abstract

The spontaneous loss of sulfur or isocyanate from transient 7-thia-2-azabicyclo[2.2.1]hept-5-en-3-ones, which are initially formed by 1,3-dipolar cycloadditions of thioisomünchnones with acetylenic dipolarophiles, is the key step in the chemoselective syntheses of pyridin-2-ones or thiophenes. The way by which sulfur is released has been the subject of previous studies pointing to a concerted retro-cheletropic mechanism as a more favorable route than the alternative stepwise pathway. The latter however, is apparently prevalent for elimination of isocyanate. Working with a conformationally-restricted bicyclic thioisomünchnone that undergoes facile cycloaddition with acetylenes, sulfur elimination has now been interrogated by experiment and theoretical calculations at the M06-2X and M11 methods in combination with the 6-311++G(d,p) basis set, which unveil rather a sigmatropic shift via the intermediacy of thiirane species. These results provide new vistas and synthetic opportunities in mesoionic cycloadditions.

2.2. Introduction

Construction of densely functionalized heterocycles, and especially natural products and their analogs, by means of dipolar cycloadditions has been a fruitful area of research in recent decades.[1] Like the search for Dielsalderases, the chase of natural 1,3-dipolar cycloadditions has remained elusive until the recent finding that a prenylated flavin cofactor adopts an azomethine ylide form and plays a key role in ubiquinone biosynthesis and detoxification processes.[2,3]

Structurally exotic on their own,[4] mesoionic heterocycles, yet displaying significant aromaticity,[5] behave as masked dipoles and undergo thermal cycloadditions with a variety of dipolarophiles.[6] Thioisomünchnones (thiazol-4-ium-3-olates) emerged as a versatile family that can be harnessed in catalytic and non-catalytic routes toward numerous naturally-occurring systems.[7] Further decoration of such mesoionic rings by dialkylamino substituents gives rise to a subclass of reactive dipoles and enables the access to heterocycles not easily foreseen in cycloaddition chemistry.[8] Thioisomünchnones often react with dipolarophiles via one-step procedures which involve actually domino reactions from the non-isolated cycloadducts. A salient postcycloaddition modification is the

spontaneous sulfur extrusion that removes this element and renders up sulfur-free heterocycles, which are more suitable as drug-like candidates for in vivo studies.[9] Herein we revisit postcycloaddition through a new bicyclic thioisomünchnone that leads to novel dihydrothialozo ring-fused pyrid-2-ones.

A few years ago we reported in detail the cycloaddition of 1,3- thiazolium-4-olates with acetylenes to give pyrid-2-ones. Based on mechanistic considerations, the intermediate bicycles would have extruded sulfur by two possible routes: either a concerted retro-cheletropic process (path a) or a stepwise pathway (b) (Scheme 2.1).[10]

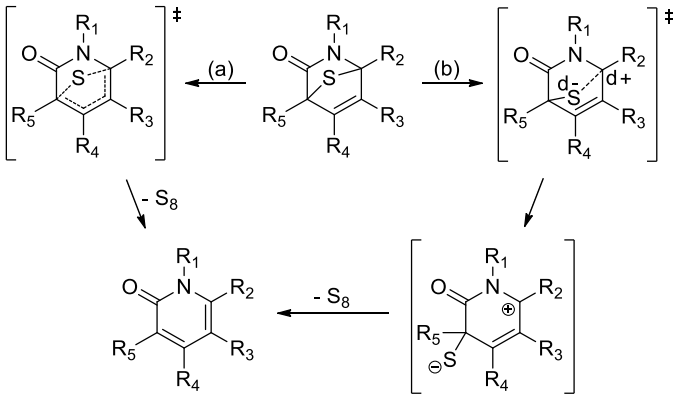

Scheme 2.1. Proposed concerted (a) and stepwise (b) mechanisms for the extrusion of sulfur from 7-thia-2-azabicyclo[2.2.1]hept-5-en-3-ones.

The concerted 1,4-retrocycloaddition has been largely invoked as the most plausible route for the extrusion of sulfur, while the stepwise mechanism is supported by the isolation of carbonothioate derivatives in the reaction of thioisomünchnones with azodipolarophiles,[11] as well as by the thionation reaction of these mesoionic dipoles with isothiocyanates (which should most likely be occurring by a stepwise pathway too).[8b-d] In this work we investigate thoroughly the loss of sulfur from 1:1 initial cycloadducts. Our results suggest that sulfur elimination takes place by a sigmatropic-type sulfur displacement followed by a 1,2-elimination from the thiirane intermediate, which has never been taken into account as working hypothesis. The computational study unravels how this elimination takes place and does proceed with high levels of selectivity, thus shedding light into an overlooked mechanistic pathway.

2.3. Results and discussion

Dihydrothiazolo[3,2-*a*]pyrid-2-one rings are privileged scaffolds that can be obtained by thioisomünchnone cycloadditions with triple bonds so long as the masked dipoles are built on a cyclic dithiocarbamate like thiazolidine-2-thione (**1**). The latter was then subjected to the well-established condensation with an a-haloacid [i.e., α-bromophenylacetic acid (**2**)], in basic medium, followed by cyclodehydration with Ac_2O/NEt_3 (1:3 ratio) (Scheme 2.2).[12] Thus, the transient thioglycolic acid derivative (**3**) evolved into a new thioisomünchnone (**4**), obtained as an orange solid.

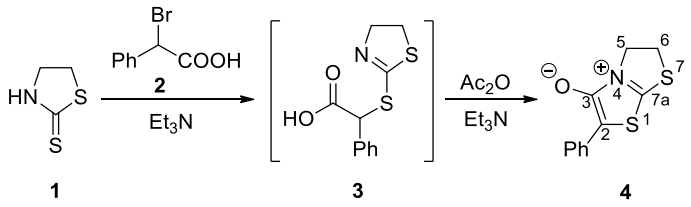

Scheme 2.2. Synthesis of 2-phenyl-5,6-dihydrothiazolo[2,3-*b*]thiazol-4-ium-3-olate (4) from thiazolidine-2-thione (**1**).

Reactions of **4** with acetylenic dipolarophiles **5**-**9** were carried out in toluene at reflux using an excess (25%) of dipolarophile. That the reaction goes to completion could be easily monitored by observing the gradual disappearance of the orange color. The solvent was removed under reduced pressure, the corresponding residues treated with diethyl ether and then recrystallized from alcohols (EtOH or MeOH), which afforded essentially pure 5-oxo-6-phenyl-3,5-dihydro-2H-thiazolo[3,2-*a*]pyridines (**15**-**19**) from the intermediate cycloadducts **10**-**14** in good overall yields (~70%). This synthesis of thiazolopyrid-5-ones in a regiospecific fashion suggests that cycloaddition of **4** with asymmetrically-substituted dipolarophiles (**6**-**9**) leads exclusively to the corresponding cycloadducts **11**-**14**, which yield spontaneously compounds **16**-**19** after sulfur extrusion (Scheme 2.3). The solid-state structure of **18** could be unambiguously elucidated by single-crystal X-ray diffraction (Figure. 2.1),[13] whereas the structure of **19** was assigned by comparison of its NMR data with those of **18**. ^{13}C NMR data of **19** do not show any significant difference with respect to

18, with the sole exception of an additional signal resonating at 60.8 ppm (attributed to the methylene carbon of the ethyl carboxylate group). Also, the structure of **17** was established on the basis of NOE enhancements that revealed the spatial proximity of H-7 (8.00 ppm) to the ortho hydrogens of phenyl group on C-6 resonating at 7.70 ppm. The structure of **16** was elucidated by com- paring its NMR data with those of **17**. ^{13}C NMR spectra of **16** and **17** were quite similar differing only by the presence of the methylene signal at 61.2 ppm in the spectrum of **17**.

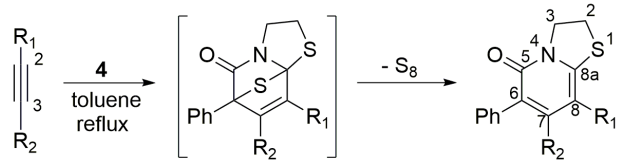

5-**9** **10**-**14** **15**-**19**

5, **10**, **15** $R^1 = R^2 = COOMe$
6, **11**, **16** $R^1 = COOMe$, $R^2 = H$
7, **12**, **17** $R^1 = COOEt$, $R^2 = H$
8, **13**, **18** $R^1 = COOMe$, $R^2 = Ph$
9, **14**, **19** $R^1 = COOEt$, $R^2 = Ph$

Scheme 2.3. Reaction of thioisomünchnone **4** with acetylenic dipolarophiles **5**-**9** leading to thiazolo[3,2-*a*]pyridine-5-ones **15**-**19**.

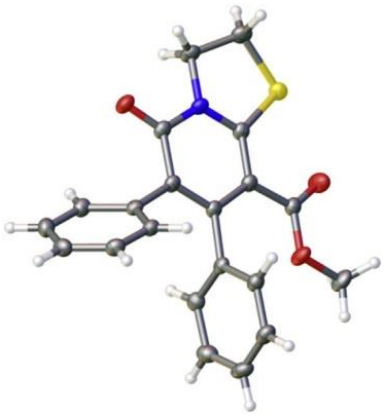

Figure 2.1. Solid-state structure of compound **18**. Ellipsoids are drawn at 50% probability.

To shed light into the reactivity of **4** against asymmetrically-substituted acetylenic dipolarophiles, we performed a computational study of the cycloaddition of 4 with methyl propiolate (**6**) using the Gaussian09 package.[14] The M06-2X[15] density functional method in conjunction with the 6-311++G(d,p) basis set[16] was selected for all the geometry optimizations and frequency analysis. Ground and transition states were characterized by none and one imaginary frequency, respectively. Solvent effects (in toluene) were included in all geometry optimizations using the SMD method.[17] To further corroborate the validity of results, all stationary points of the alternative reaction pathways were also completely reoptimized using the M11 functional plus the 6-311++G(d,p) basis set as above. Relative to other DFT methods, the accuracy of the M11 functional is particularly suitable for estimating alkyl bond dissociation energies, barrier heights, and noncovalent interaction energies.[18]

The reaction of **4** with methyl propiolate (**6**) may in principle generate two regioisomeric cycloadducts (**11** and **20**), whose sub- sequent evolution would afford thiazolo[3,2-*a*]pyridine-5-ones (**16** and **21**) by sulfur extrusion and/or thiophenes (**22** and **23**) through an isocyanate retrocycloaddition (Scheme 2.4).

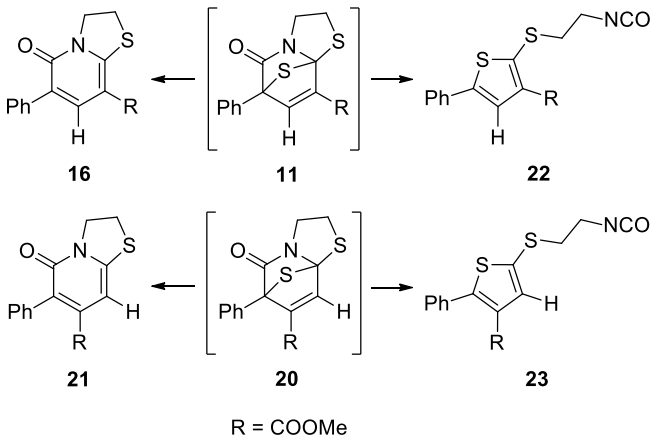

Scheme 2.4. Hypothetical conversion of cycloadducts **11** and **20** into pyridones **16** and **21** and/or thiophenes **22** and **23**, respectively.

2. Computational insights into cycloadditions of thioisomünchnones with acetylenes: how does sulfur escape from cycloadducts?

Figure 2.2 shows the reaction pathways leading to cycloadducts **11** and **20**. It should be noted that the energy barriers for either concerted (red line) (in the web version) or stepwise (black line) mechanisms differ by more than 3 kcal mol^{-1}, thus pointing to a regioselective transformation that agrees with the experimental results (see below). The free energy difference that separates $\mathbf{TS1_{11}}$ from $\mathbf{TS2_{11}}$ ($\Delta\Delta G^{\ddagger}$ = 0.79 kcal mol^{-1}) is very small and lies within the error range of DFT methods, which does not allow us to ensure that the second stage is actually the rate-determining step. This surmise was confirmed by conducting the optimization of $\mathbf{TS1_{11}}$ and $\mathbf{TS2_{11}}$ at the same level in dichloromethane and at the M06-2X/6-31+G(d) level. In addition, the geometric and energetic likeness of $\mathbf{TS1_{11}}$, $\mathbf{I_{11}}$ and $\mathbf{TS2_{11}}$ does not exclude the possibility that the allegedly stepwise mechanism takes place in a concerted manner as evidenced by further optimization performed at the MP2/6-311++G(d,p) level (Table 2.1).

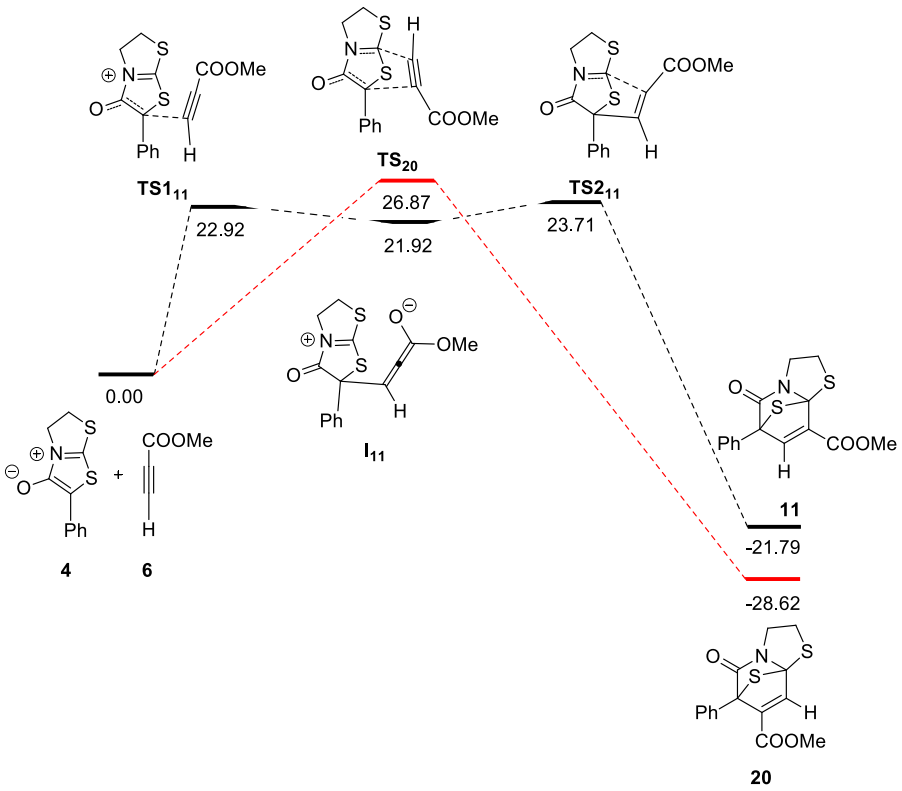

Figure 2.2. Reaction pathways leading to regioisomeric cycloadducts **11** and **20** (ΔG values are given in kcal mol^{-1}).

Table 2.1. Bond lenghts (Å) and free energy differences[a] (kcal mol^{-1}) found for saddle points **TS1$_{11}$** and **TS2$_{11}$** at several levels of theory.

Level	Structure	C_6-C_7	C_8-C_{8a}	$\Delta\Delta G^{\ddagger}$
M06-2X/6-311++G(d,p) in toluene (SMD)	**TS1$_{11}$**	1.97	3.10	-0.79
	TS2$_{11}$	1.62	2.79	
M06-2X/6-311++G(d,p) in dichloromethane (SMD)	**TS1$_{11}$**	1.99	3.16	-0.51
	TS2$_{11}$	1.62	2.74	
M06-2X/6-31+G(d) in toluene (SMD)	**TS1$_{11}$**	1.98	3.12	0.31
	TS2$_{11}$	1.62	2.78	
MP2/6-311++G(d,p) in toluene (SMD)	**TS1$_{11}$**	2.14	2.31	-----

[a]ΔG (**TS1$_{11}$**) - ΔG (**TS2$_{11}$**).

It is also worth noting that while C6-C7 and C8-C8a bond lengths in **TS1$_{11}$** are 1.97 Å and 3.10 Å, respectively [at the M06-2X/6-311++G(d,p) level in toluene], consistent with a stepwise mechanism in which the C6-C7 bond is initially formed, the lengths of those bonds (2.46 Å and 2.11 Å, respectively) in **TS$_{20}$** leading to cycloadduct **20** unveil its concerted and asynchronous nature. The same conclusion can be attained by estimating the bond orders for intermediates and transition structures involved in the formation of **11** and **20** (Table 2.2).

Table 2.2. Selected Mulliken bond orders (BO) for both intermediates and transition structures involved in the formation of **11** and **20**.

Structure	BO(C_6-C_7)	BO(C_8-C_{8a})
TS1$_{11}$	0.44	0.05
I$_{11}$	0.91	0.03
TS2$_{11}$	0.82	0.12
11	0.99	0.95
TS$_{20}$	0.22	0.38
20	0.96	0.98

Figure 2.3 and Table A2.1 shows the energy barriers of all stationary points across the reaction pathways leading to regioisomeric thiazolopyridones **16** and **21**, which would have arisen from cycloadducts **11** and **20**, respectively. Results show that, in both cases, the rate-determining step is the initial 1,3-dipolar cycloaddition (see Figure 2.2 for monitoring the formation and evolution of cycloadduct **11**). The fast evolution of **11** and **20** proceeds through energy barriers that do not exceed 20 kcal mol^{-1} to give **16** and **21**, respectively.

Both $\Delta\Delta G^{\ddagger}$ [ΔG(**TS20**) - ΔG(**TS211**) > 3 kcal mol^{-1}] and $\Delta\Delta G^{\ddagger}$ [ΔG(**21**) - ΔG(**16**) ~ 6 kcal mol^{-1}] values indicate that the formation of **16** is a kinetically and thermodynamically controlled process.

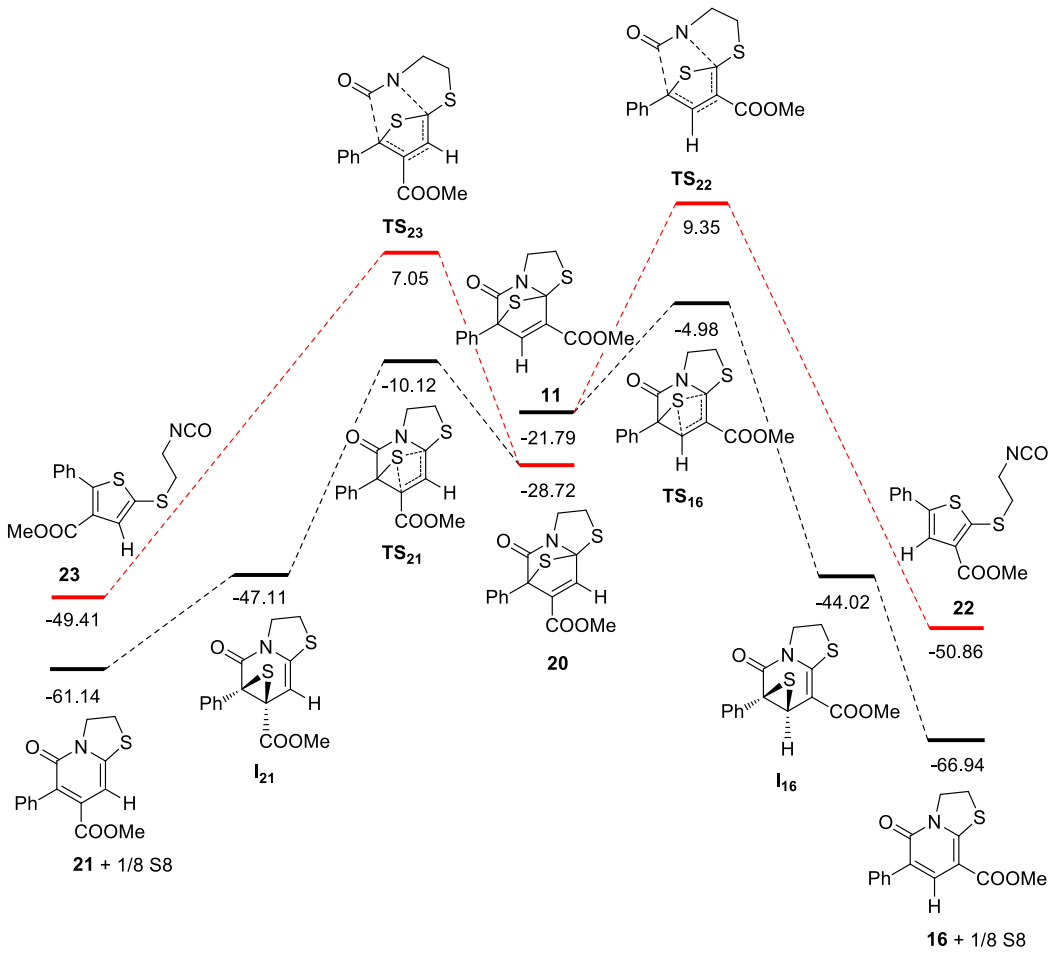

Figure 2.3. Reaction pathways leading to regioisomeric thiazolopyridones **16** and **21**, and thiophenes **22** and **23** (ΔG values are given in kcal mol^{-1}).

In order to clarify how sulfur escapes from the initial cycloadducts **11** and **20** to give the corresponding pyrid-2-ones **16** and **21**, we tried to optimize and characterize all the stationary points involved in both mechanistic pathways, i.e. the retro-cheletropic reaction (Scheme 2.1a) and the stepwise process (Scheme 2.1b). However, we were unable to

locate the transition structure corresponding to the former. Initially we assumed that the transition structure found actually (**TS_{16}**, Figure 2.2) would lead to a zwitterionic intermediate, although a further IRC analysis showed its direct conversion into thiirane **I_{16}** (Figure 2.3). So, sulfur removal appears to be consistent with an initial sulfur sigmatropic rearrangement leading to a three-membered cyclic intermediate, which has not yet been considered as mechanistic hypothesis.

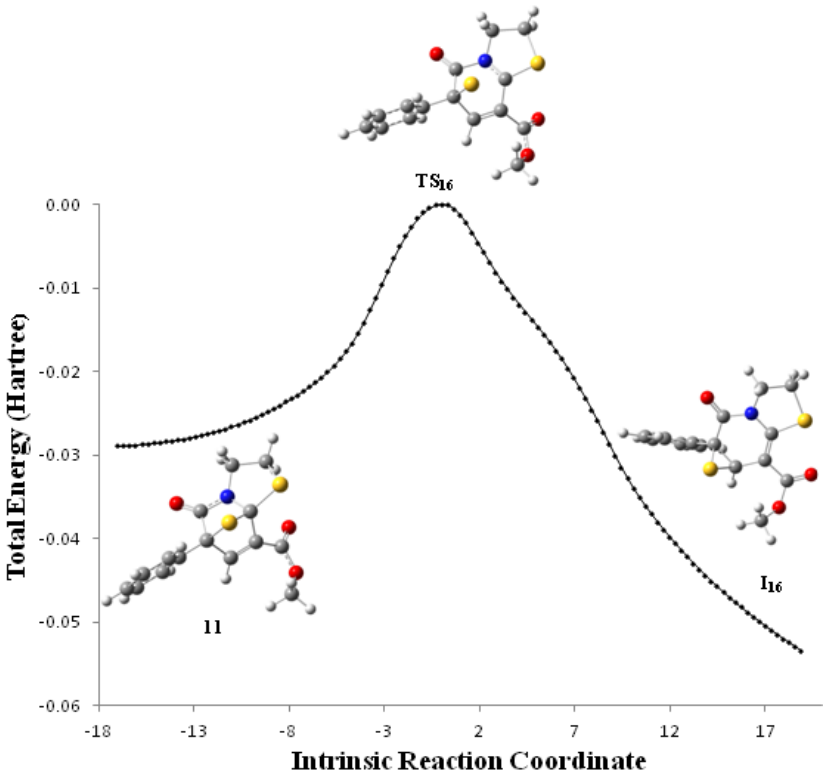

Figure 2.4. IRC of **TS_{16}** and M06-2X/6-311++G(d,p)/(SMD)-optimized structures for saddle point **TS_{16}**, thiirane **I_{16}**, and cycloadduct **11**.

It is fair to say that thiiranes are not new kids in scenarios involving sulfur elimination. Their formation and further evolution to alkenes have been postulated in previous theoretical studies [19] and explored experimentally too.[20] This suggest that the intermediate thiiranes **I_{16}** and **I_{21}** would evolve into the corresponding alkenes (namely thiazolopyridones

16 and **21**) and S8, formed by oligomerization of S2, S3 and S4 species, as evidenced by previous studies.[19]

It is well known that ring-fused thioisomünchnones do not give rise to thiophenes by reaction with acetylenes. Figure 2.3 shows that the energy gap for the intramolecular retrocycloaddition of isocyanate is 14.33 kcal mol^{-1} higher than the alternative sulfur sigmatropic rearrangement leading to the exclusive formation of **16**. Likewise, the chemoselective transformation of cycloadduct **20** into pyridone **21** has an energy barrier 17.17 kcal mol^{-1} lower than that affording thiophene **23**. Clearly, the sulfur sigmatropic rearrangement is kinetically favored relative to the retro-cycloaddition of isocyanate (Figure 2.3). Table A2.2 shows the relative energies of all stationary points leading to thiophene **22** and **23** from cycloadducts **11** and **20**, respectively. Selected bond lengths and bond orders in transition states $\mathbf{TS_{22}}$ and $\mathbf{TS_{23}}$ point to concerted, yet asynchronous, retrocycloaddition processes (Table A2.3).

Table 3 collects the relative electronic energies, enthalpies, and free energies of all stationary points located for the alternative reaction pathways of **4** and **6** optimized at the M11/6-311++G(d,p) level. These results almost mirror those previously obtained using the M06-2X functional, even although the latter magnifies the energy barriers leading to thiophene derivatives by ~1 kcal mol^{-1} and reduces on the contrary those leading to 5-oxothiazolo[3,2-*a*]pyridines by <2 kcal mol^{-1}.

In order to evaluate the influence of the dipolarophile size on the dipolar cycloaddition, the condensations of **4** with acetylene derivatives **5** and **8** have also been explored, in following the same methodology as dipolarophile **6** (Tables A4 and A5). Given the symmetrical substitution pattern of **5**, its reaction with **4** afforded only pyridone **15** (Figure A2.1). On the other hand, in the 1,3-dipolar cycloaddition of **4** with methyl phenylpropiolate (**8**), the formation of regioisomeric pyridones **18** and **24** should be taken into account (Figure A2.2). Computation at the M06-2X/6-311++G(d,p) level shows that molecular size is indeed a critical factor as the energy barriers to be overcome in the reactions with dipolarophiles **5** (ΔG_{15} = 29.28 kcal mol^{-1}) and **8** (ΔG_{18} = 26.93 kcal mol^{-1}; ΔG_{24} = 28.08 kcal mol^{-1}) are slightly higher than that of methyl propiolate (**6**) (see Addendum).

Table 2.3. Relative electronic energy (Δ*E*), enthalpy (Δ*H*), and free energy (Δ*G*) (in kcal mol^{-1})[a] of all stationary states involved in the reactions of **4** and **6** leading to 5-oxothiazolo[3,2-*a*]pyridines **16** and **21** and thiophenes **22** and **23**.

Structure	Δ*E*	Δ*H*	Δ*G*
TS1$_{11}$	9.54	9.95	24.12
I$_{11}$	5.02	6.54	22.22
TS2$_{11}$	7.51	8.38	24.01
11	-40.62	-37.74	-22.48
TS$_{16}$	-20.34	-18.32	-3.14
I$_{16}$	-62.76	-59.38	-44.25
16 + 1/8 **S$_8$**	-83.38	-79.97	-67.57
TS$_{20}$	11.62	12.09	27.44
20	-46.09	-43.39	-28.46
TS$_{21}$	-26.63	-24.65	-9.42
I$_{21}$	-66.01	-62.92	-48.57
21 + 1/8 **S$_8$**	-76.98	-73.85	-61.52
TS$_{22}$	-7.74	-6.76	8.53
22	-63.24	-60.32	-49.64
TS$_{23}$	-9.59	-8.64	6.00
23	-60.85	-58.14	-49.33

[a] Related to the electronic energy (Δ*E*), enthalpy (Δ*H*), and free energy (Δ*G*) of **4** + **6**.

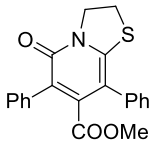

24

2.4. Conclusions

A structurally rigid 1,3-thiazolium-4-olate (**4**) can be conveniently prepared from 1,3-thiazolidine-2-thione by standard protocols of condensation with an α-haloacid and further cyclodehydration. Thermal [3+2]-cycloadditions of **4** with acetylenic dipolarophiles produce thiazolo[3,2-*a*]pyridones in good yields without isolation of the corresponding cycloadducts. The use of asymmetrically-substituted acetylenes unravels a complete regioselection where the alkoxycarbonyl group is attached to the C-8 atom of the six-membered ring. This selectivity is supported by DFT calculations [at the M06-2X and M11 methods in combination with the 6-311++G(d,p) basis set] with inclusion of solvent effects (SMD

method), which prove that the isolated regioisomers are both kinetically and thermodynamically-controlled products. Sulfur extrusion en route to pyridones does not occur through a retro-cheletropic process as usually thought, but rather by two consecutive steps, namely (a) 1,3-sigmatropic rearrangement of the sulfur atom leading to a thiirane intermediate, and (b) thermal fragmentation of the latter affording an alkene (double bond of the heterocyclic moiety). The theoretical analysis also indicates that the rate-limiting step is invariably the initial formation of cycloadducts, regardless of formation of either pyridones or thiophenes. Moreover, the six-membered heterocycle is kinetically favored relative to the intramolecular retro-cycloaddition of isocyanate that leads to thiophenes.

2.5. Experimental section

2.5.1. General methods

Solvents and reagents were purchased from commercial suppliers and used without further purification. The identity of all compounds was confirmed by their elemental analysis, high-resolution mass spectra, mp's and NMR data.

2.5.2. Computational details

All of the calculations reported in this work were carried out using the Gaussian09 package.[14] The M06-2X[15] and M11[18] density functional methods in conjunction with the 6-311++G(d,p)[16] basis set were selected for all the geometry optimizations and frequency analysis. The geometries were optimized including solvation effects in toluene, which have been estimated by the density-based self-consistent reaction field theory of bulk electrostatic, i. e. the the well-known solvation model density (SMD)[17] method that takes into account different contributions such as long-range electrostatic polarization (bulk solvent effect),[21] as well as short-range effects due to cavitation, dispersion, and solvent's structure.[22] Frequency calculations at 298.15 K on all the stationary points were carried out at the same level of theory as the geometry optimizations to ascertain the nature of the stationary points. Ground and transition states were characterized by none and one imaginary frequency, respectively. All of the relative energies shown are free energies calculated at 298.15 K with respect to the reactants. It was found that each saddle point

belonged to the reaction path by the corresponding IRC analysis (intrinsic reaction coordinate).

2.5.3. Synthetic procedures

2.5.3.1. **2-Phenyl-5,6-dihydrothiazolo[2,3-*b*]thiazol-4-ium-3-olate (4)**. A mixture of thazolidine-2-thione (**1**) (17 mmol), 2-bromo-2- phenylacetic acid (**2**) (17 mmol), triethylamine (17 mmol), and benzene (100 mL) was stirred at room temperature for 72 h. Then, the resulting triethylammonium bromide was filtered off. In order to remove dissolved salts, the solution was also passed through a silica gel [Merck®60 (400-230 mesh)] column using ethyl acetate as eluent. The solvent was evaporated to dryness to give an oily residue (3.11 g), which contained the intermediate product **3**. To this oil a mixture of acetic anhydride and triethylamine (1:3, 25 mL) was added. The mixture was softly heated for a few minutes, yielding the title compound as orange crystals, which were collected by filtration and washed with ethyl ether (1.8 g, 68%). Mp: 193-194 ºC. FTIR (KBr) ν_{max} 1579, 1493, 1431, 1364, 1139, 752, 691 cm^{-1}. ^{1}H NMR (500 MHz, $CDCl_3$) δ 7.71 (dd, 2H, *J* = 7 Hz; *J* = 1.5 Hz), 7.29-7.25 (m, 2H), 7.05-7.03 (m, 1H), 4.45 (t, 2H, *J* = 7.5 Hz), 3.98 (t, 2H, *J* = 8 Hz) ppm. ^{13}C NMR (125 MHz, $CDCl_3$) δ 156.1, 152.1, 134.2, 128.6, 124.2, 122.8, 97.9, 49.3, 36.6 ppm. Anal. Calcd for $C_{11}H_9NOS_2$: C, 56.17; H, 3.85; N, 5.95; S, 27.25. Found: C, 56.15; H, 3.98; N, 5.94; S, 27.03. 4.2.2.

2.5.3.2. **General procedure for the cycloadditions of 4 with acetylenic dipolarophiles (5-9).** A mixture of **4** (2.1 mmol), the dipolarophile (2.7 mmol), and toluene (25 mL) was heated at reflux until disappearance of the orange color (TLC analysis: ethyl acetate:hexane 1:1 v/v). The solvent was evaporated to dryness and the resulting residue was suspended in ethyl ether to yield the corresponding pyridones (**15**-**19**), which were further recrystallized from methanol or ethanol.

2.5.3.3. **Dimethyl 5-oxo-6-phenyl-3,5-dihydro-2*H*-thiazolo[3,2-*a*]pyridine- 7,8-dicarboxylate (15).** Following the general procedure, compound **15** was obtained from **4** and **5** after 2 h. Recrystallized from methanol (0.47 g, 66%) showed: Mp: 163-166 ºC. FTIR (KBr) ν_{max} 2958, 2941, 1742, 1698, 1642, 1509, 1434, 1360, 1314, 1215, 984, 699 cm^{-1}. ^{1}H NMR (400 MHz, $CDCl_3$) δ 7.37-7.28 (m, 5H), 4.58 (t, 2H, *J* = 10 Hz), 3.83 (s, 3H), 3.58 (s, 3H), 3.37 (t, 2H, *J* = 10 Hz). ^{13}C NMR (100 MHz, $CDCl_3$) δ 166.6, 164.1, 160.5, 157.7,

142.6, 132.9, 129.7, 128.3, 128.0, 125.0, 101.4, 52.5, 52.2, 51.6, 27.6 ppm. Anal. Calcd for $C_{17}H_{15}NO_5S$: C, 59.13, H, 4.36, N, 4.05, S, 9.27. Found: C, 58.75, H, 4.15, N, 4.21, S, 9.31.

2.5.3.4. **Methyl 5-oxo-6-phenyl-3,5-dihydro-2*H*-thiazolo[3,2-*a*]pyridine-8-carboxylate (16).** Following the general procedure, compound **16** was obtained from **4** and **6** after 2 h. Recrystallized from methanol (0.42 g, 70%) showed: Mp 153-154 ºC. FTIR (KBr) ν_{max} 3051, 3013, 2948, 2900, 1685, 1621, 1523, 1429, 1294, 1247, 1107, 789, 777, 693 cm^{-1}. ^1H NMR (400 MHz, $CDCl_3$) δ 8.00 (s, 1H), 7.68 (d, 2H, *J* = 7.2 Hz), 7.41 (t, 2H, *J* = 8 Hz), 7.33 (t, 1H, *J* = 7.2 Hz), 4.59 (t, 2H, *J* = 8 Hz), 3.90 (s, 3H), 3.40 (t, 2H, *J* = 8.4 Hz). ^{13}C NMR (100 MHz, $CDCl_3$) δ 165.2, 160.9, 156.1, 137.3, 135.6, 128.4, 128.3, 127.8, 125.6, 104.4, 52.2, 51.2, 27.8 ppm. Anal. Calcd for $C_{15}H_{13}NO_3S$: C, 62.71, H, 4.53, N, 4.87, S, 11.15. Found: C, 62.46, H, 4.77, N, 4.69, S, 11.24.

2.5.3.5. **Ethyl 5-oxo-6-phenyl-3,5-dihydro-2*H*-thiazolo[3,2-*a*]pyridine- 8-carboxylate (17).** Following the general procedure, compound **17** was obtained from **4** and **7** after 2 h. Recrystallized from ethanol (0.46 g, 72%) showed mp 132-133 ºC. FTIR (KBr) ν_{max} 3051, 3011, 2976, 2896, 1633, 1689, 1525, 1447, 1373, 1297, 1245, 1198, 1105, 1034, 788, 695 cm^{-1}. ^1H NMR (400 MHz, $CDCl_3$) δ 8.00 (s, 1H), 7.67-7.31 (m, 5H), 4.59 (t, 2H, *J* = 8 Hz), 4.35 (q, 2H, *J* = 6.8 Hz), 3.39 (t, 2H, *J* = 8 Hz), 1.37 (t, 3H, *J* = 7.2 Hz). ^{13}C NMR (100 MHz, $CDCl_3$) δ 164.8, 160.9, 155.8, 137.4, 135.7, 128.4, 128.2, 127.7, 125.6, 104.7, 61.2, 51.2, 27.8, 14.4. HRMS $(M+Na)^+$ Calcd for $C_{16}H_{15}O_3NNaS$: 324.0655. Found: 324.0665.0.

2.5.3.6. **Methyl 5-oxo-6,7-diphenyl-3,5-dihydro-2*H*-thiazolo[3,2-*a*] pyridine-8-carboxylate (18).** Following the general procedure, compound **18** was obtained from **4** and **8** after 24 h. Recrystallized from methanol (0.47 g, 61%) showed: Mp 177-178 ºC. FTIR (KBr) ν_{max} 3052, 3003, 2950, 1682, 1604, 1506, 1431, 1310, 1227, 704, 606 cm^{-1}. ^1H NMR (500 MHz, $CDCl_3$) δ 7.13-7.07 (m, 6H), 6.96-6.90 (m, 4H), 4.62 (t, 2H, *J* = 7.5 Hz), 3.36 (t, 2H, *J* = 7.5 Hz), 3.37 (s, 3H). ^{13}C NMR (125 MHz, $CDCl_3$) δ 166.6, 160.7, 155.4, 150.4, 138.5, 134.7, 130.8, 128.4, 127.5, 127.2, 126.9, 126.7, 106.2, 51.7, 51.6, 27.7. HRMS $(M+Na)^+$ Calcd for $C_{21}H_{17}O_3NNaS$: 386.0808. Found: 386.0821.

2.5.3.7. **Ethyl 5-oxo-6,7-diphenyl-3,5-dihydro-2*H*-thiazolo[3,2-*a*]pyridine- 8-carboxylate (19).** Following the general procedure, compound **19** was obtained from **4** and **9** after 24 h. Recrystallized from ethanol (0.44 g, 55%) showed: Mp 171-175 ºC. FTIR (KBr) ν_{max} 3059, 2978, 2934, 1884, 1606, 1558, 1503, 1393, 1250, 1222, 714, 605 cm^{-1}. ^{1}H NMR (500 MHz, $CDCl_3$) δ 7.13-7.07 (m, 6H), 6.97-6.92 (m, 4H), 4.62 (t, 2H, *J* = 8 Hz), 3.87 (q, 2H, *J* = 7 Hz), 3.70 (t, 2H, *J* = 8 Hz), 0.70 (t, 3H, *J* = 7 Hz). ^{13}C NMR (125 MHz, $CDCl_3$) δ 166.3, 160.8, 155.4, 150.5, 138.8, 134.8, 130.8, 128.5, 127.5, 127.2, 126.9, 126.7, 106.4, 60.8, 51.6, 27.7, 13.2. Anal. Calcd for $C_{22}H_{19}NO_3S$: C, 70.02, H, 5.04, N, 3.71, S, 8.48. Found: C, 69.85, H, 5.15, N, 3.91, S, 8.86.

2.6. Addendum

Table A2.1. Relative electronic energy (Δ*E*), enthalpy (Δ*H*), and free energy (Δ*G*) (in kcal mol^{-1}) of all the stationary states involved in the reaction of **4** and **6** yielding 5-oxothiazolo[3,2-a]pyridines **16** and **21**.

Structure	Δ*E*	Δ*H*	Δ*G*
4 + **6**	0.00	0.00	0.00
TS1$_{11}$	9.16	9.76	22.92
I$_{11}$	5.32	7.02	21.92
TS2$_{11}$	7.19	8.18	23.71
11	-39.75	-36.90	-21.79
TS$_{16}$	-21.53	-19.50	-4.98
I$_{16}$	-62.29	-58.92	-44.02
16 + 1/8 **S$_8$**	-83.07	-79.55	-66.94
TS$_{20}$	11.61	11.93	26.87
20	-45.78	-42.97	-28.62
TS$_{21}$	-27.74	-25.71	-10.12
I$_{21}$	-64.79	-61.47	-47.11
21 + 1/8 **S$_8$**	-76.45	-73.21	-61.14

Table A2.2. Relative electronic energy (Δ*E*), enthalpy (Δ*H*), and free energy (Δ*G*) (in kcal mol^{-1})[a] of all stationary states involved in the conversions of cycloadducts **11** and **20** into 2-((2-isocyanatoethyl)thio)thiophenes **22** and **23**.

Structure	Δ*E*	Δ*H*	Δ*G*
11	-39.75	-36.90	-21.79
TS$_{22}$	-6.67	-5.68	9.35
22	-63.57	-60.77	-50.86
20	-45.78	-42.97	-28.62
TS$_{23}$	-8.87	-8.01	7.05
23	-61.36	-58.47	-49.41

[a] Related to the electronic energy (Δ*E*), enthalpy (Δ*H*), and free energy (Δ*G*) of **4** + **6**.

Table A2.3. Selected bond lengths (Å) and Mulliken bond orders found in transition structures **TS$_{22}$** and **TS$_{23}$** optimized at the M06-2X/6-311++G(d,p) level.

Structure	Bond	Bond length	Bond order
TS$_{22}$	N4-C8a	1.86	0.47
	C5-C6	2.21	0.31
TS$_{23}$	N4-C8a	2.03	0.37
	C5-C6	2.02	0.44

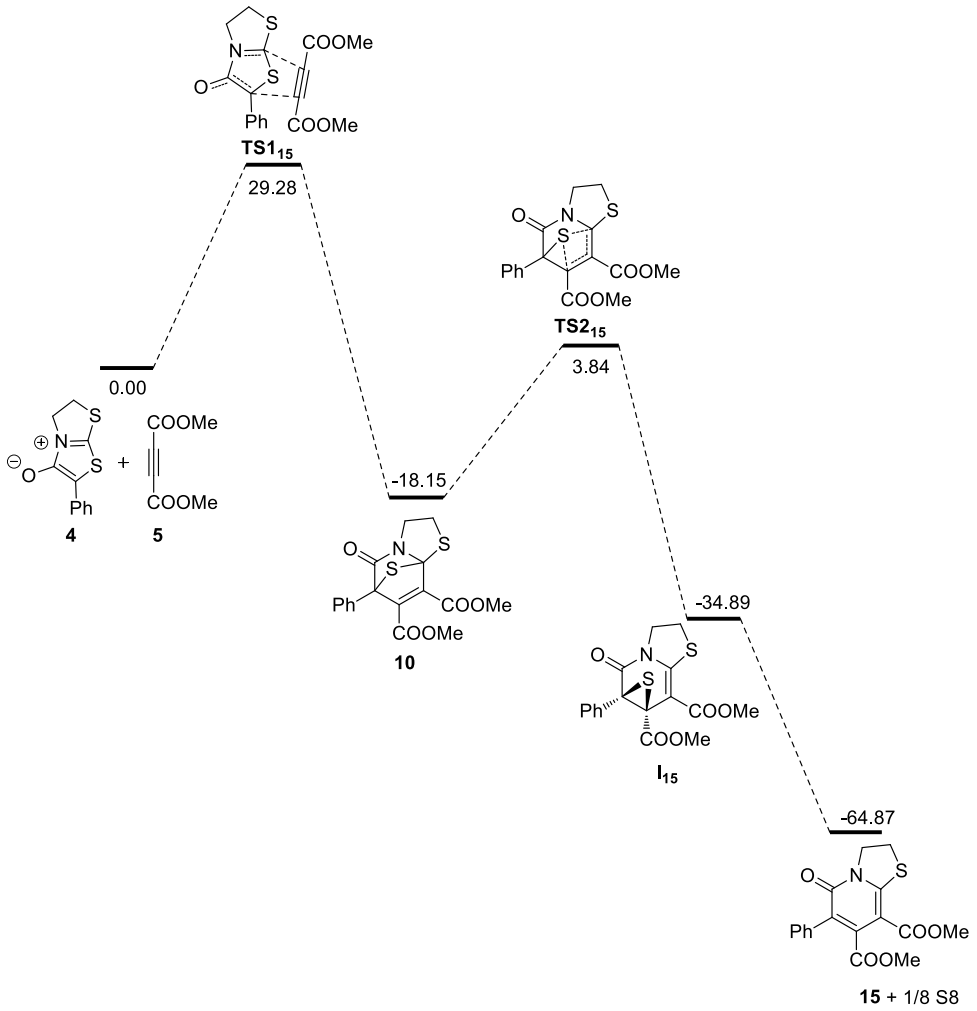

Figure A2.1. Reaction pathway leading to 5-oxothiazolo[3,2-*a*]pyridine **15** from **4** and **5** (ΔG values are given in Table A2.4).

2. Computational insights into cycloadditions of thioisomünchnones with acetylenes: how does sulfur escape from cycloadducts?

Table A2.4. Relative electronic energy (Δ*E*), enthalpy (Δ*H*), and free energy (Δ*G*) (in kcal mol^{-1}) of all stationary points involved in the reaction of **4** and **5** leading to 5-oxothiazolo[3,2-*a*]pyridine **15**.

Structure	Δ*E*	Δ*H*	Δ*G*
4 + **5**	0	0	0
TS1$_{15}$	13.68	13.87	29.28
10	-37.73	-35.23	-18.15
TS2$_{15}$	-15.18	-13.57	3.84
I$_{15}$	-54.49	-52.01	-34.89
15 + 1/8 **S$_8$**	-81.53	-78.72	-64.87

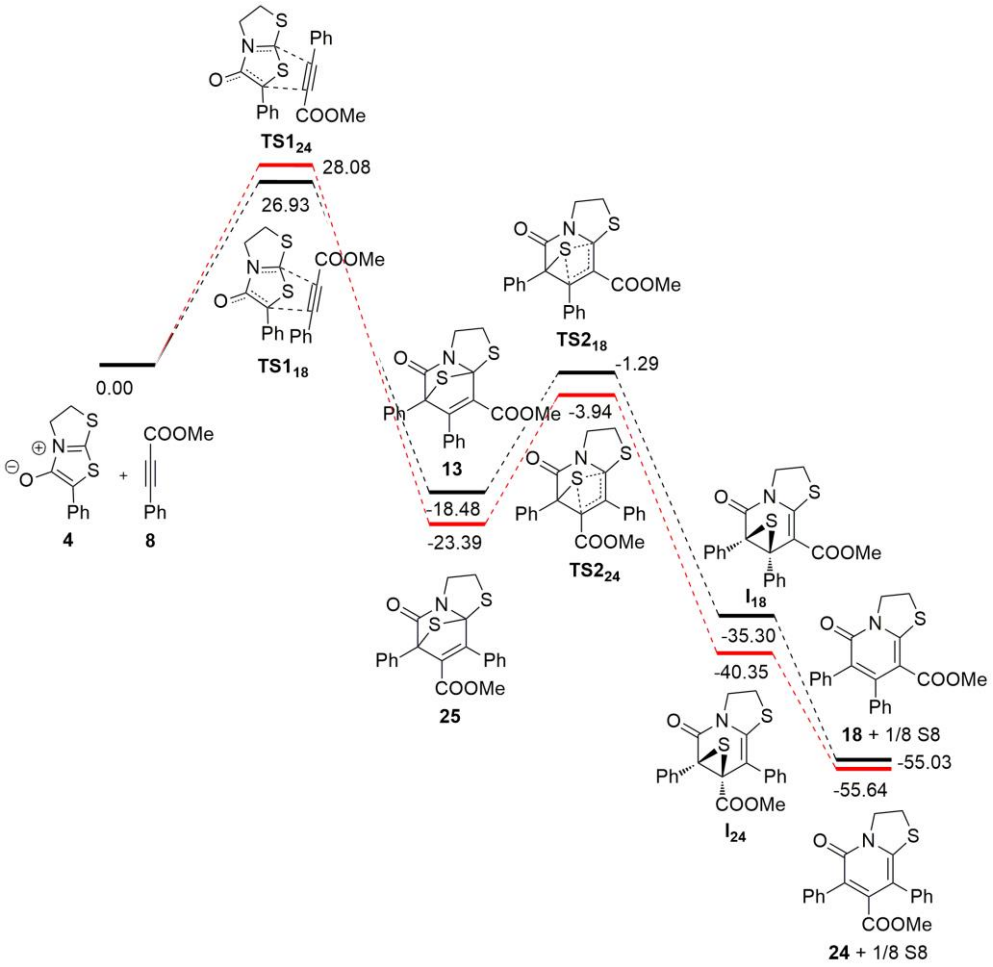

Figure A2.2. Computational analysis of regioisomeric pathways in the cycloaddition of thioisomünchnone **4** and **8** (Δ*G* values are given in Table A2.5).

Table A2.5. Relative electronic energy (Δ*E*), enthalpy (Δ*H*), and free energy (Δ*G*) (in kcal mol^{-1}) of all stationary states involved in the reaction of **4** and **8** leading to 5-oxothiazolo[3,2-*a*]pyridines **18** and **24**.

Structure	Δ*E*	Δ*H*	Δ*G*
4 + **8**	0.00	0.00	0.00
TS1$_{18}$	11.43	11.44	26.93
13	-38.17	-35.81	-18.48
TS2$_{18}$	-19.54	-18.20	-1.29
I1$_{18}$	-54.07	-51.47	-35.30
18 + 1/8 **S$_8$**	-70.76	-68.37	-55.03
TS1$_{24}$	12.03	12.34	28.08
13a	-41.81	-39.46	-23.39
TS2$_{24}$	-21.96	-20.35	-3.94
I1$_{24}$	-59.35	-56.54	-40.35
24 + 1/8 **S$_8$**	-71.31	-68.79	-55.64

2.7. Bibliography

(1) (a) *Synthetic Applications of 1,3-Dipolar Cycloaddition Chemistry toward Heterocycles and Natural* Products, (Eds. A. Padwa, W. H. Pearson), John Wiley & Sons, New York, **2002**; (b) Pellisier, H. Tetrahedron **2007**, 63, 3235-3285; (c) Suga, H.; Itoh, K. in *Methods and Applications of Cycloaddition Reactions in Organic Syntheses* (Ed.: Nishiwaki, N.), John Wiley & Sons, Inc., Hoboken, New Jersey, **2013**, pp. 175-204; (d) Hasimoto, T.; Maruoka, K. Chem. Rev. **2015**, 115, 5366-5412.

(2) (a) Payne, K. A. P.; White, M. D.; Fisher, K.; Khara, B.; Bailey, S. S.; Parker, D. Rattray, N. J. W.; Trivedi, D. K.; Goodacre, R.; Beveridge, R.; Barran, P.; Rigby, S. E. J.; Scrutton, N. S.; Hay, S.; Leys, D. *Nature* **2015**, *522*, 497-501; (b) White, M. D.; Payne, K. A. P.; Fisher, K.; Marshall, S.; Parker, D.; Rattray, N. J. W.; Trivedi, D. K.; Goodacre, R.; Rigby S. E. J.; Scrutton, N. S.; Hay, S.; Leys, D. *Nature* **2015**, *522*, 502-506.

(3) Baunach, M.; Hertweck, C. *Angew. Chem. Int. Ed*. **2015**, *54*, 12550-12552.

(4) (a) Ollis, W. D.; Ramsden, C. A. in *Advances in Heterocyclic Chemistry*, Vol. 19 (Eds. Katritzky, A. R.; Boulton, A. J.), *Academic Press*, New York, **1976**, 1-122; (b) Newton, C. G.; Ramsden, C. A. *Tetrahedron* **1982**, *38*, 2965-3011; (c) Potts, K. T. in *1,3-Dipolar Cycloaddition Chemistry*, Vol. 2 (Ed.: A. Padwa), John Wiley & Sons, New York, **1984**, pp. 1-82; (d) Ollis, W. D.; Stanforth, S. P.; Ramsden, C. A. *Tetrahedron* **1985**, *41*, 2239-2329; (e) Badami, B. V. *Resonance* **2006**, *11*, 40-48.

(5) (a) Bird, C. V.; *Tetrahedron* **1985**, *41*, 1409-1414; (b) Bird, C. W. *Tetrahedron* **1992**, *48*, 335-340; (c) Simas, A. M.; Miller, J.; de Athayade Filho, P. F. *Can. J. Chem*. **1998**, *76*, 869-872; (d) Nein, Y. I.; Morzherin, Y. Y. *Russ. Chem. Bull*. **2012**, *61*, 1111-1116; (e) Anjos, I. C.; Vasconcellos M. L. A. A.; Rocha, G. B. *Theor. Chem. Acc*. **2012**, *131*, 1-9.

(6) (a) Browne, D. L.; Harrity, P. A. *Tetrahedron* **2010**, *66*, 553-568; (b) Lopchuk, J. M.; Hughes, R. P.; Gordon, G. W. *Org. Lett*. **2013**, *15*, 5218-5221; (c) Morin, M. S.; St-Cyr, D. J.; Arndtsen, B. A.; Krenske, E. H.; Houk, K. N. *J. Am. Chem. Soc*. **2013**, *135*, 17349-17358; (d) Marco-Martínez, J.; Reboredo, S.; Izquierdo, M.; Marcos, V.; López, J. L.; Filippone, S.; Martín, N. *J. Am. Chem. Soc*. **2014**, *136*, 2897-2904; (e) Specklin, S.; Decuypere, E.; Plougastel, L.; Aliani, S.; Taran, F. *J. Org. Chem*. **2014**, *79*, 7772-7777.

(7) (a) Osterhout, M. H.; Nadler, W. R.; Padwa, A. *Synthesis* **1994**, 123-141. b) Benetti, S.; De Risi, C.; Pollini, G. P.; Zanirato, V. *Chem. Rev*. **2012**, *112*, 2129-2163; (c) Lopchuk, J. M. in *Metalation of Azoles and Related Five-Membered Ring Heterocycles* (Ed.: Gribble, G. W.), Springer, Berlin, **2012**, pp. 381-413.

(8) (a) Ávalos, M.; Babiano, R.; Cintas, P.; Jiménez, J. L.; Palacios, *Acc. Chem. Res*. **2005**, *38*, 460-468; (b) Cantillo, D.; Ávalos, M.; Babiano, R.; Cintas, P.; Jiménez, Light, M. E.; Palacios, J. C. *Org. Lett*. **2008**, *10*, 1079-1082; (c) Cantillo, D.; Ávalos, M.; Babiano, R.; Cintas, P.; Jiménez, Light, M. E.; Palacios, J. C., *J. Org. Chem*. **2009**, *74*, 3698-3705; (d) Cantillo, D.; Ávalos, M.; Babiano, R.; Cintas, P.; Jiménez, Light, M. E.; Palacios, *J. Org. Chem*. **2009**, *74*, 7644-7650; (e) Sánchez, B.; Arévalo, M. J.; Bravo, J. L.; López, I.; Light, M. E.; Silvero, G. *Austr. J. Chem*. **2009**, *62*, 356-359; (f) Sánchez, B.; López, I.; Light, M. E.; Silvero, G.; Bravo, J. L. *Eur. J. Org. Chem*. **2010**, 1648-1652.

(9) (a) Li, Q.; Mitscher, L. A.; She, L. L.; *Med. Res. Rev*. **2000**, *20*, 231-293; (b) Dragovich, P. S.; Prins, T. J.; Zhou, R.; Johnson, T. O.; Brown, E. L.; Maldonado, F. C.; Fuhrman, S. A.; Zalman, L. S.; Patick, A. K.; Matthews, D. A.; Hou, X.; Meador III, J. V.; ferre, R. A.; Worland, S. T. *Bioorg. Med. Chem. Lett*. **2002**, *12*, 733-738 (c) Parlow, J. J.; Kurumbail, R. G.; Stegeman, R. A.; Stevens, A. M.; Stallings, W. C.; South, M. S. *J. Med. Chem*. **2003**, *46*, 4696-4701; (d) Verissimo, E.; Berry, N.; Gibbons, P.; Cristiano, M. L. S.; Rosenthal, P. J.; Gut, J.; Ward, S. A.; O'Neill, P. M. *Bioorg. Med. Chem. Lett*. **2008**, *18*, 4210-4214; (e) Chorell, E.; Pinkner, J. S.; Phan, G.; Edvinsson, S.; Buelens, F.; Remaut, H.; Waksman, G. Hultgren, S. J.; Almqvist, F. *J. Med. Chem*. **2010**, *53*, 5690-5695; (f) Ali, T. E. S.; Ibrahim, M. A.; Braz, J. *Chem. Soc*. **2010**, *21*, 1007-1016.

(10) Arévalo, M. J.; Ávalos, M.; Babiano, R.; Cintas, P.; Hursthouse, M. B.; Jiménez, J. L.; Light, M. E.; López, I.; Palacios, J. C. *Tetrahedron* **2000**, *56*, 1247-1255.
(11) Arévalo, M. J.; Ávalos, M.; Babiano, R.; Cintas, P.; Hursthouse, M. B.; Jiménez, J. L.; Light, M. E.; López, I.; Palacios, J. C. *Tetrahedron Lett*. **1999**, *40*, 8675-8678.
(12) Ávalos, M.; Babiano, R.; Cabanillas, A.; Cintas, P.; Higes, F. J.; Jiménez, J. L.; Palacios, J. C. *J. Org. Chem*. **1996**, *61*, 3738-3748.
(13) Crystallographic data (excluding structure factors) for the structures in this paper have been deposited with the Cambridge Crystallographic Data Centre as supplementary publication no. CCDC-1476841.
(14) Frisch, M. J.; Trucks, G. W.; Schlegel, H. B.; Scuseria, G. E.; Robb, M. A.; Cheeseman, J. R.; Scalmani, G.; Barone, V.; Mennucci, B.; Petersson, G. A.; Nakatsuji, H.; Caricato, M.; Li, X.; Hratchian, H. P.; Izmaylov, A. F.; Bloino, J.; Zheng, G.; Sonnenberg, J. L.; Hada, M.; Ehara, M.; Toyota, K.; Fukuda, R.; Hasegawa, J.; Ishida, M.; Nakajima, T.; Honda, Y.; Kitao, O.; Nakai, H.; Vreven, T. Jr.; Montgomery J. A.; Peralta, J. E.; Ogliaro, F.; Bearpark, M.; Heyd, J. J.; Brothers, E.; Kudin, N. K.; Staroverov, V. N.; Kobayashi, R.; Normand, J.; Raghavachari, K.; Rendell, A.; Burant, J. C.; Iyengar, S. S.; Tomasi, J.; Cossi, M.; Rega, N.; Millam, J. M.; Klene, M.; Knox, J. E.; Cross, J. B.; Bakken, V.; Adamo, C.; Jaramillo, J.; Gomperts, R.; Stratmann, R. E.; Yazyev, O.; Austin, A. J.; Cammi, R.; Pomelli, C.; Ochterski, J. W.; Martin, R. L.; Morokuma, K.; Zakrzewski, V. G.; Voth, G. A.; Salvador, P.; Dannenberg, J. J.; Dapprich, S.; Daniels, A. D.; Farkas, Ö.; Foresman, J. B.; Ortiz, J. V.; Cioslowski, J.; Fox, D. J.; Gaussian 09, Revision D.01; Gaussian, Inc.: Wallingford, CT, 2009.
(15) Zhao, Y.; Truhlar, D. G. *Theor. Chem. Acc*. **2008**, *120*, 215-241.
(16) (a) Ditchfield, R.; Hehre, W. J.; Pople, J. A. *J. Chem. Phys*. **1971**, *54*, 724–728; (b) Hehre, W. J.; Ditchfield, R.; Pople, J. A.; *Mol. Phys*. **1974**, *27*, 209–214; (c) Gordon, M. S.; *Chem. Phys. Lett*. **1980**, *76*, 163–168; (d) Hariharan, P. C.; Pople, J. A. *Theor. Chem. Acc*. **1973**, *28*, 213–222; (e) Francl, M. M.; Pietro, W. J.; Hehre, W. J.; Binkley, J. S.; DeFrees, D. J.; Pople, J. A.; Gordon, M. S. *J. Chem. Phys*. **1982**, *77*, 3654–3665.
(17) (a) Marenich, A. V.; Cramer, C. J.; Truhlar, D. G. *J. Phys. Chem. B* **2009**, *113*, 4538-4543; (b) Marenich, A. V.; Cramer, C. J.; Truhlar, D. G., *J. Phys. Chem. B* **2009**, *113*, 6378-6396; (c) Ribeiro, R. F.; Marenich, A. V.; Cramer, C. J.; Truhlar, D. G. *J. Comput.-Aided Mater*. **2010**, *24*, 317-333; (d) Halim, M. A.; Shaw, D. M.; Poirier, R. A. *J. Mol. Struct. (THEOCHEM)* **2010**, *960*, 63-72; (e) G. Saielli, J. Phys. Chem. A 2010, 114, 7261-7265.
(18) Peverati, R.; Truhlar, D. G., *J. Phys. Chem. Lett.* **2011**, *2*, 2810-2817
(19) Steudel, Y.; Steudel, R.; Wong, M. W., *Chem. Eur. J*. **2002**, *8*, 217-228.
(20) Ávalos, M.; Babiano, R.; Cintas, P.; Clemente, F. R.; Gordillo, R.; Jiménez, J. L.; Palacios, J. C., *J. Org. Chem*. **2003**, *68*, 6338-6348.
(21) Tomasi, J.; Mennucci, B.; Cancès, E. *J. Mol. Struct. (THEOCHEM)* **1999**, *464*, 211-226.
(22) Liotard, D. A.; Hawkins, G. D.; Lynch, G. C.; Cramer, C. J.; Trulhar, D. G. *J. Comput. Chem.* **1995**, *16*, 422-440.

3. Assessing stereoelectronic effects in dipolar cycloadditions yielding fused thiazolopyridone rings

3.1. Abstract

We report a combined experimental and computational study on the cycloadditions of bicyclic 1,3-thiazolium-4-olates, derived from thiazolidin-2-thiones, with asymmetrically-substituted acetylenes. These results provide further mechanistic insights into the above dipolar cycloadditions and enable an unequivocal characterization by NMR spectroscopy of regiochemical patterns as previous derivatives had substituents at both C-2 (in the dipole) and C-6 (in products). Accordingly, new dihydrothiazolopyrid-2- ones have been obtained from a thioisomünchnone lacking substitution at C-2. With the aim of assessing the steric hindrance as well as the facial stereoselection induced by a bulky group on the Si face (relative to C-7a) of the mesoionic heterocycle, a chiral thioisomünchnone has also been obtained along with the resulting optically active thiazolopyridones. A computational study of these particular cycloadditions, largely based on an NBO analysis, allowed us to evaluate the influence of substituents on intermolecular steric repulsions, charge transfers, as well as solvent effects.

3.2. Introduction

Fused heterocycles comprising five- and six-membered rings, usually containing a ring-junction nitrogen, are privileged scaffolds in medicinal chemistry and such systems are frequently employed to assess and develop compound libraries and new leads.[1,2] Among them, thiazolopyridine derivatives in particular have gained some attention as potential drug candidates against different pathologies.[3,4]

The synthesis of densely functionalized heteroatom-containing rings may be accomplished by different strategies, although shortcuts often rely on [3+2]-cycloadditions as well as multicomponent reactions capable of assembling the two-unit framework in chemo- and regio-controlled fashions.[5,6] Facile and versatile elaborations harness the pentagonal core of mesoionic heterocycles, which behaving as masked allyl-type dipoles, enable further structural fusion and/or elongation with appropriate dipolarophiles, usually in metal-free protocols.[7,8] Mesoionic-based dipolar cycloadditions actually give rise to a variety of heterocyclic arrays not easily provided by conventional cycloadditions, as developed by our group over the last two decades.[9]

3. Assessing stereoelectronic effects in dipolar cycloadditions yielding fused thiazolopyridone rings

Recently, we have described the synthesis of a new fused-ring thioisomünchnone (**1**) and its 1,3-dipolar reactivity toward activated acetylenes, with a focus on the sulfur extrusion mechanism,[10] which constitutes the key step in the chemoselective syntheses of pyridin-2-ones or thiophenes from the above mesoionic rings. Despite some controversial results in the literature claiming either concerted retro-cheletropic reactions or stepwise pathways for the spontaneous loss of sulfur, or isocyanate, from the resulting monoadducts formed initially in the cycloadditions of thioisomünchnones with alkynes, that study unveiled a sigmatropic mechanism involving the intermediacy of thiirane species. Moreover, the regioselective addition of asymmetrically-substituted acetylenes to the mesoionic heterocycle (e.g. by reaction of **1** with methyl propiolate) could be corroborated by single-crystal X-ray diffractometry of compound **2** and further rationalized by DFT analysis.[10] Unfortunately, in the absence of unequivocal crystal data, the regiochemical outcome leading spontaneously to thiazolo [3,2-*a*]pyridine-5-ones cannot easily be monitored. A phenyl group at C-2 in **1**, and therefore in C-6 in **2** and its analogous, limits the diagnostic use of NMR signals to this end. To overcome this hurdle, the present study reports the synthesis and cycloadditions of an unsubstituted derivative, namely 5,6-dihydrothiazolo[2,3-*b*]thiazol-4-ium-3-olate (**3**), which not only allows the straightforward inspection of the regiochemical pattern by proton NMR, but also evaluates the influence, if any, of the substituent at C-2. Furthermore, a chiral thioisomünchnone (**15**) bearing a bulky and inert group was obtained to check, if any, the issue of facial selection. Although, as we shall see, the latter cannot be assessed from an experimental point of view, the computational study still unveils how such a facial stereodiscrimination would take place and the influence exerted by the dipolarophile's structure in particular.

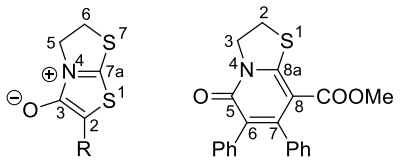

1 R = Ph
3 R = H

2

3.3. Results and discussion

3.3.1. Synthesis and structural characterization

In principle the preparation of **3** should proceed by a similar procedure to that described for the preparation of **1**, using bromoacetic acid as alkylating reagent of thiazolidine-2-thione (**4**). The intermediate thioglycolic acid, i.e. 2-[(4,5-dihydrothiazol-2-yl)thio] acetic acid (**5**) could be isolated as a white solid in good yield (>90%). However, unlike the synthesis of **1**, conventional cyclodehydration of **5** with Ac_2O/Et_3N (1:3 ratio) did not afford **3** as a stable solid. Thus, we devised a one-pot protocol that generates **3** in situ in the presence of acetylenes **6**-**8** leading to 8-alkoxycarbonyl- 5-oxo-3,5-dihydro-2H-thiazolo[3,2-*a*]pyridines (**9**-**11**) (Scheme 3.1). The above thermal cycloaddition could easily be carried out by mixing **5** and the corresponding dipolarophile (1:1.5 ratio) in CH_2Cl_2, then adding dropwise a mixture of acetic anhydride and triethylamine (1:3), and finally heated at reflux for 1 h. Chromatographic purification gave rise to compounds **9**-**11** in variable and rather modest yields (**15**-**37**%). ^{1}H NMR spectra of **10** and **11** were quite similar and showed two doublet signals at δ ~7.8 and~6.2 ppm (J = 9.5 Hz) assignable to vicinal H-6 and H-7 protons, respectively.

As mentioned in the introductory remarks, with the aim of evaluating the role of steric effects as well as the facial stereoselection induced by a bulky substituent located on the Si face (relative to C-7a) of the mesoionic heterocycle, the chiral thioisomünchnone **15** derived from (*S*)-4-isopropylthiazolidine-2-thione (**13**) and α-bromophenylacetic acid was prepared. Compound **13** has been previously obtained by reaction of (*S*)-2-amino-3-methylbutan-1-ol (**12**) with CS_2 in alkaline solution (KOH).[11] The resulting (*S*)-5-isopropyl-2-phenyl-5,6-dihydrothiazolo[2,3-*b*]thiazol-4-ium-3-olate (**15**) could be obtained by treating the mixture containing **14** (not isolated) with Ac_2O/Et_3N (Scheme 3.2).

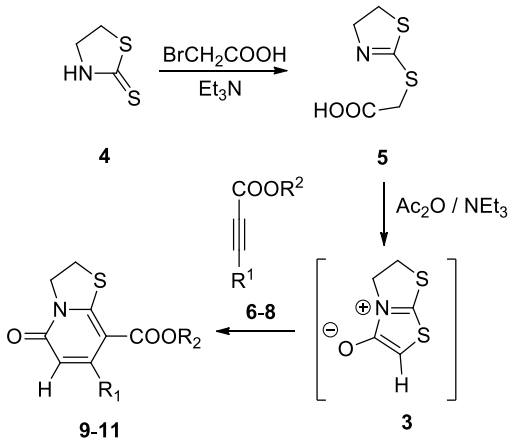

Scheme 3.1. Synthesis of thiazolo[3,2-*a*]pyridines **9**-**11** by dipolar cycloaddition of a transient dipole (**3**), generated from **5**, with acetylenes.

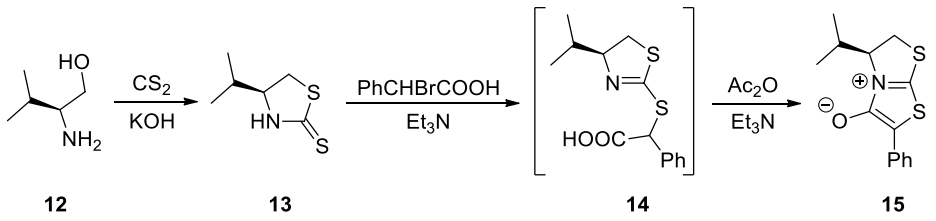

Scheme 3.2. Preparation of chiral thioisomünchnone **15**.

Reactions of **15** with dipholarophiles **6**-**8** were conducted in toluene at reflux using an excess of dipolarophile (25%) and the end point could be easily determined after the complete disappearance of the characteristic orange color of the mesoionic heterocycle (~2 h). The solvent was removed under reduced pressure and the residue treated with methanol to give pure (*S*)-3-isopropyl-5-oxo-6-phenyl-3,5-dihydro-2H-thiazolo[3,2-*a*]pyridines **16**-**18** in moderate to good overall yields (**54**-**75** %).

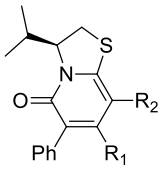

16 $R^1 = R^2 = COOMe$
17 $R^1 = H$, $R^2 = COOMe$
18 $R^1 = H$, $R^2 = COOEt$

It should be noted that inspection of crude mixtures by NMR spectroscopy prior to purification gave no evidence of any other regioisomer. Moreover, no signals accounting for the competitive formation of thiophenes or isocyanates as side products could be observed either. The modest yields of thiazolopyridones **9**-**11** in particular, as well as of **16**-**18** largely result from the thermal lability of the mesoionic dipole. Thiazolopyridone **16** enables a rapid structural elucidation by NMR and, gratifyingly compound **17** could be unambiguously characterized by single-crystal X-ray diffraction (Figure 3.1).[12]

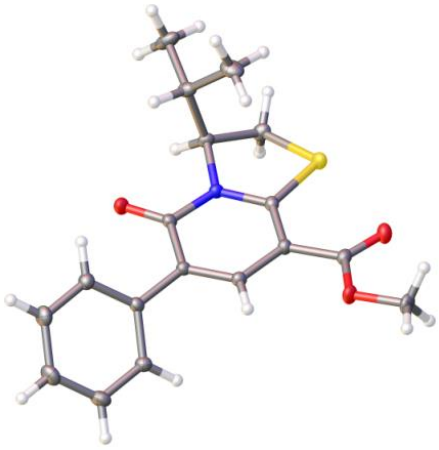

Figure 3.1. Solid-state structure of compound **17**. Ellipsoids drawn at 50% probability.

3.3.2. Mechanistic insights on the dipolar cycloaddition

As reported previously,[10] the reaction of **1** with methyl propiolate (**7**) in toluene involves initially a regiospecific stepwise 1,3-dipolar cycloaddition (rate-determining step) (Scheme 3.3). The initial cycloadduct then undergoes a 1,3-sigmatropic rearrangement to give a transient thiirane, which ultimately extrudes sulfur through a 1,2-elimination leading to pyridone **19** (for a detailed picture of the reaction pathways, see Figures A3.1-A3.3).

A comparison of the energetic profiles for the cycloadditive steps of thioisomünchnones **1** and **3** with **7**, in both toluene and CH_2Cl_2, illustrates on the one hand the influence of the substituent at the C-2 atom of the heterocyclic ring and, on the other, the effect played by the solvent on the steric course (Figure 3.2).

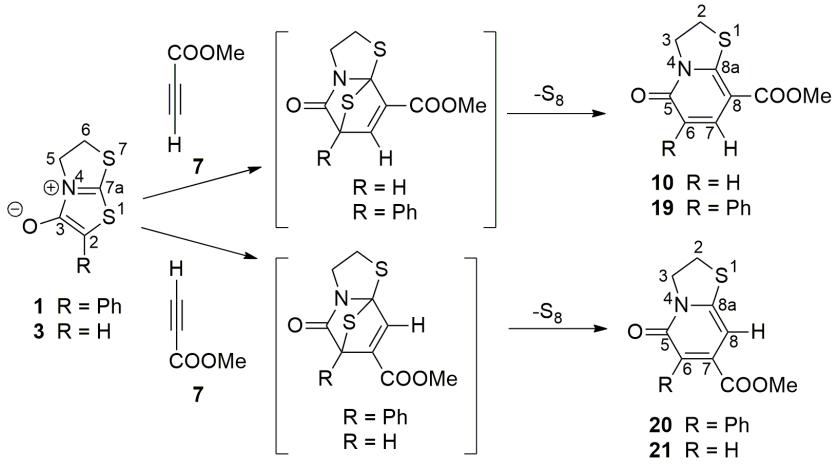

Scheme 3.3. Regiochemical approaches of methyl propiolate (**7**) to mesoionic **1** and **3**.

In every case the reaction pathways leading to **10** and **19** involve two steps with analogous stationary points (black lines in Figure 3.2). On the other hand, the alternative approaches, similar to each other as well, leading to regioisomers **20** and **21** take place through a single transition structure (red lines in Figure 3.2). At first glance, concerted pathways are disfavored with respect to stepwise cycloadditions, pointing to a regiospecific course that is consistent with our experimental results. Remarkably, reactions of **1** and **7** in both solvents are characterized by flat free energy profiles in the vicinity of transition structures [e.g., $\Delta\Delta G^{\ddagger}$(**TS2$_{19}$t-TS1$_{19}$t**) = 0.79 kcal mol^{-1} and $\Delta\Delta G$(**TS2$_{19}$t-I$_{19}$t**) = 1.79 kcal

mol^{-1}], with formation of the second C-C bond as the rate-determining step (Figure 3.2A and 3.2B).

Reactions of **3** and **7**, irrespective of the solvent too, show higher differences in their energy barriers [e.g., $\Delta\Delta G^{\ddagger}$(**TS1$_{10}$t**-**TS2$_{10}$t**) = 4.03 kcal mol^{-1} and $\Delta\Delta G$(**TS1$_{10}$t**-**I$_{10}$t**) = 6.88 kcal mol^{-1}], being now the rate-determining step the first C-C bond-forming reaction (Figure 3.2C and D). Moreover, compound **3** reacts with **7** faster than **1** in both solvents [$\Delta\Delta G^{\ddagger}$(**TS2$_{19}$t**-**TS1$_{10}$t**) = 2.85 kcal mol^{-1} and $\Delta\Delta G$(**TS2$_{19}$d**-**TS1$_{10}$d**) = 2.25 kcal mol^{-1}). These results demonstrate the influence exerted by a substituent other than hydrogen as well as solvent effects on the reactivity of thioisomünchnones and, they also agree with the higher stabilization of polar zwitterionic intermediates in CH_2Cl_2 [$\Delta\Delta G$(**I$_{19}$t**-**I$_{19}$d**) = 1.28 kcal mol^{-1} and $\Delta\Delta G$(**I$_{10}$t** e **I$_{10}$d**) = 2.41 kcal mol^{-1}]. Table 3.1 shows the energy gaps ($\Delta\Delta E$, $\Delta\Delta H$, and $\Delta\Delta G$) that separate the first saddle points of the stepwise cycloadditions from the corresponding zwitterionic intermediates, determined in both toluene and CH_2Cl_2.

Inspection of $\Delta\Delta E$, $\Delta\Delta H$ and $\Delta\Delta G$ values indicates that the stabilization of **I$_{10}$** is greater than that of **I$_{19}$** with respect to transition structures **TS1$_{10}$** and **TS1$_{19}$** in either solvent. These results show that the phenyl group linked to C-2 at the mesoionic heterocycle destabilizes the intermediate, especially as the solvent polarity increases. The major stability of **I$_{10}$** with respect to **I$_{19}$** is somewhat mirrored by the second transition structures (**TS2$_{10}$** and **TS2$_{19}$**), given the close similarity in both structure and energy between those saddle points and the corresponding zwitterionic intermediates [$\Delta\Delta G^{\ddagger}$(**TS2$_{19}$t**-**TS2$_{10}$t**) = 6.88 kcal mol-1 and $\Delta\Delta G^{\ddagger}$(**TS2$_{19}$d**-**TS2$_{10}$d**) = 7.16 kcal mol-1].

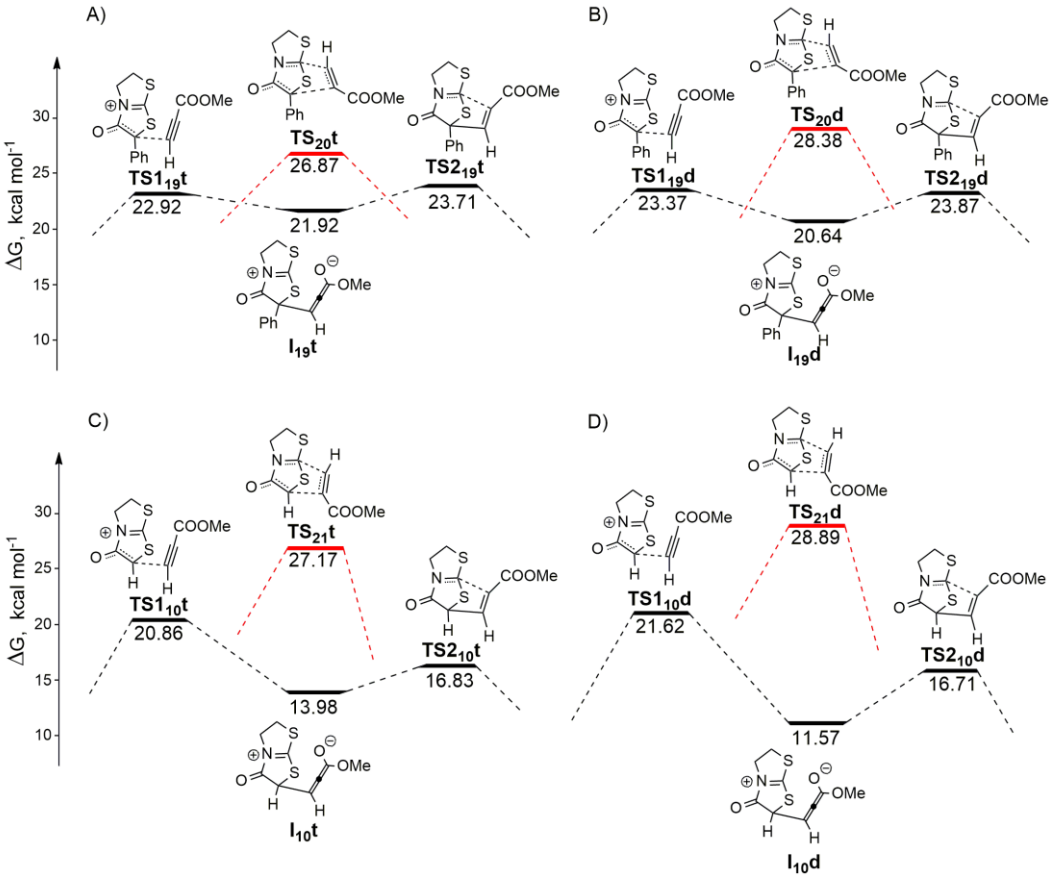

Figure 3.2. Relative free energy barriers (kcal mol^{-1}) for transition structures and intermediates involved in the 1,3-dipolar cycloadditions of **1** (A and B) and **3** (C and D) with methylpropiolate (**7**) in toluene (A and C) and CH_2Cl_2 (B and D). Black lines describe the more favored route whereas the regioisomeric pathways are depicted in red.

Table 3.1. Electronic energy, enthalpy, and free energy gaps between the first saddle point and the corresponding intermediate (in kcal mol^{-1}) for cycloadditions of **1** and **3** with **7**, in toluene and CH_2Cl_2.

Structure	ΔE^a	ΔH^a	ΔG^a	$\Delta\Delta E$	$\Delta\Delta H$	$\Delta\Delta G$
TS1$_{19}$t	9.16	9.76	22.92	3.84	2.74	1.00
I$_{19}$t	5.32	7.02	21.92			
TS1$_{19}$d	10.40	10.70	23.37	6.38	5.02	2.73
I$_{19}$d	4.02	5.68	20.64			
TS1$_{10}$t	6.68	7.32	20.86	9.05	7.59	6.88
I$_{10}$t	-2.37	-0.27	13.98			
TS1$_{10}$d	7.63	8.23	21.62	11.73	10.21	10.05
I$_{10}$d	-4.10	-1.98	11.57			

[a]Relative to reagents.

In order to understand the greater reactivity of **3** in the above cycloaddition, we performed a NSA (*natural steric analysis*)[13] for the approaches of **7** to **1** and **3** in toluene and CH_2Cl_2, which expresses the steric exchange repulsion as the energy difference due to NLMO (*natural localized molecular orbital*) orbital orthogonalization.[14] Table 3.2 shows the results obtained by comparing the total dE(i) for each TS (**TS1$_{19}$t**, **TS1$_{10}$t**, **TS1$_{19}$d**, and **TS1$_{10}$d**) with the total dE(i) values calculated when both dipolarophile and dipole fragments (**7** against dipoles **1** and **3**) are separated by a large distance (12.0 Å), in order to ensure both partners do not interact with each other. The intermolecular dE(i) values associated to the approach of **7** and **1** are higher than that of **7** with **3** (36.66 kcal mol^{-1} in toluene and 19.37 kcal mol^{-1} in CH_2Cl_2). However, as expected, the intermolecular dE(i) values are very similar for the regioisomeric concerted processes.

Table 3.2. Occupied NLMO contributions [dE(i), kcal mol^{-1}] to intermolecular steric exchange energy in transition structures **TS1$_{19}$t**, **TS1$_{10}$t**, **TS1$_{19}$d**, **TS1$_{10}$d**, and **TS$_{20}$t**, **TS$_{21}$t**, **TS$_{20}$d**, **TS$_{21}$d**.

Structure	$dE(i)_{total}$	$dE(i)_{total\ at\ 12.0\ Å}$	$\Delta dE(i)_{total}$	$\Delta\Delta dE(i)_{total}$
TS1$_{19}$t	1419.89	1256.68	163.21	36.66
TS1$_{10}$t	846.56	720.01	126.55	
TS1$_{19}$d	1385.75	1249.65	136.10	19.37
TS1$_{10}$d	837.54	720.81	116.73	
TS$_{20}$t	1448.39	1293.36	155.03	-3.18
TS$_{21}$t	903.14	744.93	158.21	
TS$_{20}$d	1444.53	1288.50	156.03	-4.50
TS$_{21}$d	904.54	744.01	160.53	

3.3.2.1. Concerted vs stepwise processes

The intermolecular steric exchange [$\Delta dE(i)_{total}$] is disfavored for the concerted cycloadditions (**TS1$_{10}$t**-**TS$_{21}$t** = -31.66 kcal mol^{-1}, **TS1$_{19}$d**-**TS$_{20}$d** = -19.93 kcal mol^{-1}, and **TS1$_{10}$d**-**TS$_{21}$d** = -43.80 kcal mol^{-1}) with the exception of **TS1$_{19}$t**-**TS$_{20}$t** (8.18 kcal mol^{-1}), thus suggesting that in this case the intermolecular steric repulsion is not responsible for a preferential stepwise process (*vide infra*).

Although structures **TS1$_{19}$t** and **TS1$_{19}$d** are quite similar, their dE(i)total values differ by 34.14 kcal mol^{-1}. In order to justify this energy difference we compared the NLMO contributions to the total steric exchanges for saddle points **TS1$_{19}$t** and **TS1$_{19}$d**. Results show a very similar orbital distribution and energy contributions, although for **TS1$_{19}$t** the LP_{C8} (for the sake of clarity, numbering is shown in Figure 3.3) contributes significantly

(26.60 kcal mol^{-1}) to dE(i)total, thus destabilizing the system. The major portion of this contribution corresponds to the interactions of LP_{C8}-σ_{C5-C6} and LP_{C8}-σ_{C6-S9} NLMO pairs (Figure 3.4).

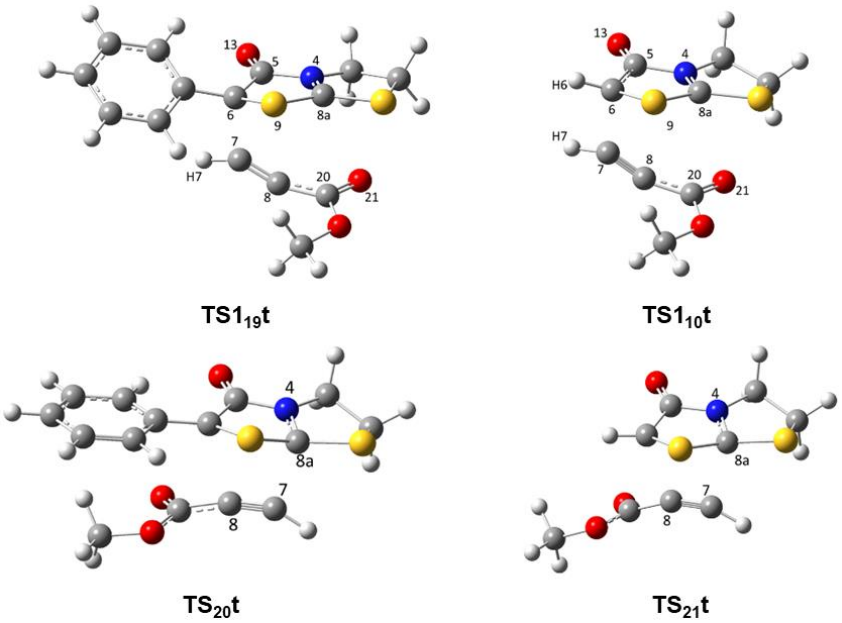

Figure 3.3. M06-2X/6-311++G(d,p)-optimized structures of **TS1$_{10}$t**, **TS1$_{19}$t**, **TS$_{20}$t**, and **TS$_{21}$t** in toluene (SMD method).

As collected in Table 3.3, the stabilization by charge transfer (CT) is always higher for the stepwise processes, especially for the reaction of the dipole **1** and **7** in toluene (521.46 kcal mol^{-1}). The highest total CT for **TS1$_{19}$t** (1847 kcal mol^{-1}) should be attributed to the methyl propiolate contribution (749.32 kcal mol^{-1}). **TS1$_{19}$t** and **TS1$_{19}$d** exhibit very similar NBO (*natural bond orbital*)[15] distribution and energy contribution to CT, though the CT of the NBO LP_{C8} stabilizes the system by 305.98 kcal mol^{-1}. In fact the highest CT value for **TS1$_{19}$t** corresponds to transfer from LP_{C8} to $\pi^*_{C20-O21}$ (170.19 kcal mol^{-1}) (Figure 3.5). The greater stabilization of **TS1$_{19}$t** provided by charge transfer would then account for a favorable process leading to **19** with respect to the concerted pathway, thereby offsetting the intramolecular steric exchange exerted by the dipolarophile.

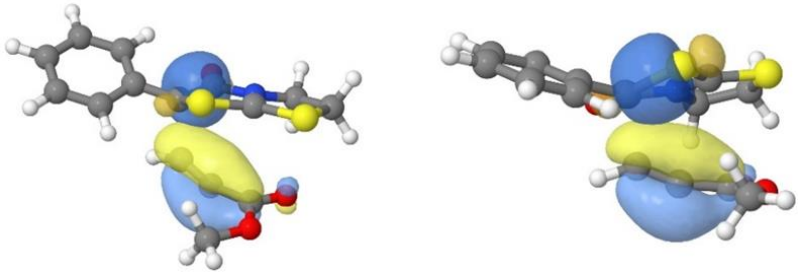

Figure 3.4. Main contributions of the NLMO LP_{C8} to steric repulsion in **$TS1_{19}t$**. Left: LP_{C8}-σ_{C5-C6} interaction; right: LP_{C8}-σ_{C6-S9} interaction.

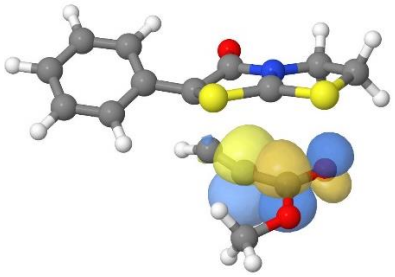

Figure 3.5. Highest CT in **$TS1_{19}t$** from NBO LP_{C8} to $\pi^*_{C20-O21}$.

The CTs from dipole to dipolarophile are greater in the saddle points of stepwise processes than those of concerted pathways. For **$TS1_{19}t$** the highest contribution corresponds to the interaction of LP_{C6} with LV_{C7} and $RY(1)_{C7}$ (23.92 and 95.45 kcal mol^{-1}, respectively). In the case of **$TS1_{19}d$** the CT goes from LP_{C6} to $\pi(2)^*_{C7-C8}$ (128.29 kcal mol^{-1}) (Figure 3.6).

For the cycloaddition of thioisomünchnone **3**, the greater contributions to CT in **$TS1_{10}t$** correspond to the interaction of π_{C6-S9} and π^*_{C6-S9} to $\pi(2)^*_{C7-C8}$ (13.03 and 98.66 kcal mol^{-1} respectively). Finally, the NBOs of **$TS1_{10}d$** are identical to those of **$TS1_{10}t$**, though with slightly lower energy values (12.40 and 90.77 kcal mol^{-1}, respectively) (Figure 3.7).

Table 3.3. Different charge transfer (kcal mol^{-1}) contributions from occupied to empty NBOs for transition structures **TS1t**, **TS1d**, **TSt** and **TSd**.

Structure	Within dipole	From dipole to dipolarophile	From dipolarophile to dipole	Within dipolarophile	Total CT	ΔCT
$TS1_{19}$t	930.62	147.8	19.95	749.32	1847.69	521.46
TS_{20}t	867.03	57.39	96.34	305.47	1326.23	
$TS1_{19}$d	945.64	163.11	15.18	306.51	1430.44	96.37
TS_{20}d	867.70	59.52	102.30	304.55	1334.07	
$TS1_{10}$t	569.23	140.94	12.2	311.56	1033.93	143.72
TS_{21}t	460.48	67.02	66.04	296.67	890.21	
$TS1_{10}$d	578.39	130.82	11.06	308.92	1029.19	126.64
TS_{21}d	464.31	69.93	70.44	297.87	902.55	

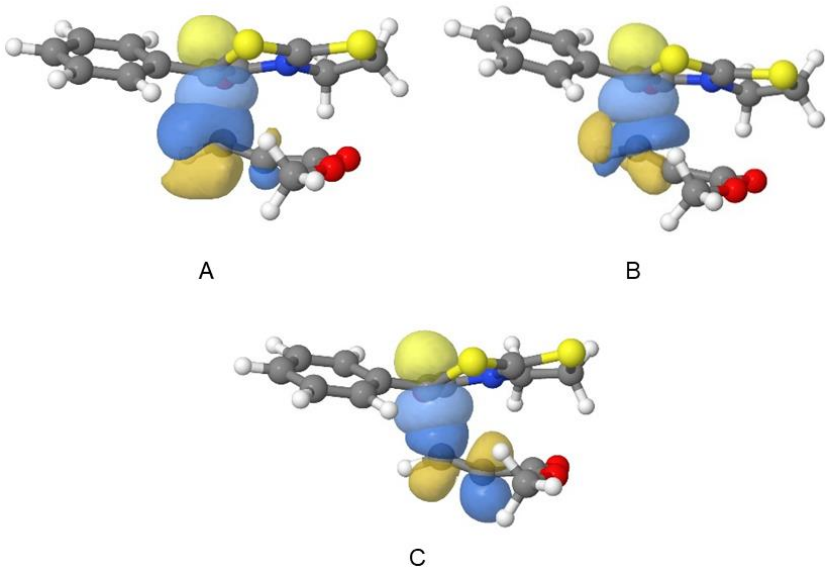

Figure 3.6. NBOs CT from LP_{C6} to LV_{C7} (A) and $RY(1)_{C7}$ (B) in **$TS1_{19}$t**, and to $\pi(2)^*_{C7\text{-}C8}$ (C) in **$TS1_{19}$d**.

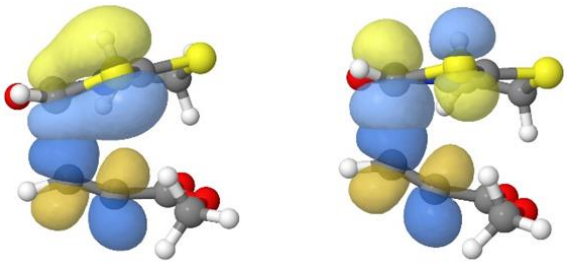

Figure 3.7. Charge transfers from NBO $\pi_{C6\text{-}S9}$ (left) and $\pi^*_{C6\text{-}S9}$ (righ) to $\pi^*_{C7\text{-}C8}$ in **TS1$_{10}$d**.

In **TS1$_{19}$t** and **TS1$_{19}$d** the major contribution involved in CT arises from the donor NBO LP_{C6}, while for **TS1$_{10}$t** and **TS1$_{10}$d** there is an important contribution from the $\pi_{C6\text{-}S9}$ orbital. Such a difference can be attributed to electron delocalization of LP_{C6} with the phenyl group in **TS1$_{19}$t** and **TS1$_{19}$d**, absent in **TS1$_{10}$t** and **TS1$_{10}$d**, for which the charge is instead delocalized with the sulfur atom. The acceptor NBO for **TS1$_{19}$d**, **TS1$_{10}$t**, and **TS1$_{10}$d** is the $\pi(2)^*_{C7\text{-}C8}$ orbital, whereas for **TS1$_{19}$t** the acceptor role is played by the empty NBOs at C7. The lack of $\pi(2)_{C7\text{-}C8}$ and $\pi(2)^*_{C7\text{-}C8}$ orbitals in **TS1$_{19}$t** could be ascribed to the high electron delocalization of LP_{C8} with the methoxycarbonyl group (Figure 3.5).

For the opposite regiochemistry, the CT from the dipolarophile to the dipole is greater than in the reverse direction. For all transition structures (**TS$_{20}$t**, **TS$_{20}$d**, **TS$_{21}$t** and **TS$_{21}$d**) the main contribution to CT goes from the $\pi(2)_{C7\text{-}C8}$ to $\pi^*_{C8a\text{-}N4}$ (65.66, 69.94, 44.25, and 47.96 kcal mol^{-1}, respectively) (Figure 3.8). All in all, these results would justify the prevalent approach of the C6-C7 bond to the C8a-C7 fragment.

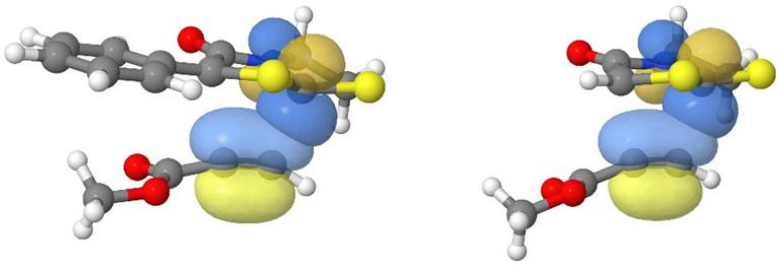

Figure 3.8. Charge transfers from NBO $\pi_{C7\text{-}C8}$ to $\pi^*_{C8a\text{-}N4}$ in **TS$_{20}$t** and **TS$_{21}$t**.

3.3.2.2. Facial stereoselection

Taking into account the chiral nature of thioisomünchnone **15**, its cycloaddition with **6** could take place by any of the two faces of the heterocycle to give the initial cycloadducts **22** and **23**. In the case of unsymmetrically-substituted alkynes such as **7** and **8**, the corresponding approaches could also occur through two different orientations, leading to cycloadducts **24**-**27** and **28**-**31**, respectively.

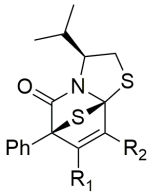

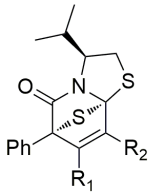

22 $R^1 = R^2 = COOMe$
24 $R^1 = H$, $R^2 = COOMe$
26 $R^1 = COOMe$, $R^2 = H$
28 $R^1 = H$, $R^2 = COOEt$
30 $R^1 = COOEt$, $R^2 = H$

23 $R^1 = R^2 = COOMe$
25 $R^1 = H$, $R^2 = COOMe$
27 $R^1 = COOMe$, $R^2 = H$
29 $R^1 = H$, $R^2 = COOEt$
31 $R^1 = COOEt$, $R^2 = H$

Figure 3.9 shows the energetic profiles for the four possible reaction channels involving the cycloaddition of thioisomünchnone **15** with **7** in toluene. Again, the regiochemistry is related to the concerted or non-concerted nature of the process, and the calculated energy barriers (Figure 3.9A) are quite similar to those previously found for the reaction of **1** and **7** (Figure 3.2A), which clearly reflects the close structural similarity of thioisomünchnones **1** and **15**.

The stepwise cycloadditions leading to thiazolopyridone **17** constitute the most favored reactions. When the dipolarophile attacks to the *Re*-2,*Re*-7a face of **15**, namely the opposite face to the isopropyl group (Figure 3.9A), the energy barrier is 5.46 kcal mol^{-1} lower than that for a concerted mechanism (red line), thereby pointing to the sole formation of cycloadduct **24**. The same happens when **7** approaches to **15** through the *Si*-2,*Si*-7a face [$\Delta\Delta G^{\ddagger}$(**TS$_{27}$**-**TS1$_{25}$**) = 4.99 kcal mol^{-1}] giving rise to cycloadduct **25**. Both cycloadducts (**24** and **25**) evolve to the same thiazolopyridone (**17**) after sulfur extrusion. Surprisingly, the interaction of **7** with the *Si*-2,*Si*-7a face of **15** (**TS1$_{25}$**) is kinetically favored (Figure 3.9B) with respect to **TS1$_{24}$** (by 1.41 kcal mol^{-1} only), a fact consistent with the poor facial

stereoselection exhibited by thioisomünchnone **15**. The lack of stereoselection could also be interpreted in geometric terms, i.e. compound **7** is rather linear-shaped and lies far to the stereodiscriminating isopropyl group in **TS1$_{25}$**.

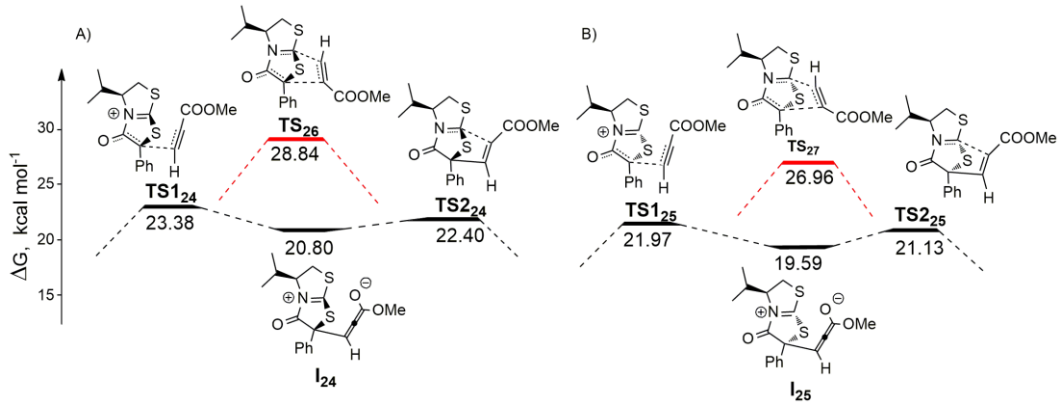

Figure 3.9. Relative free energy barriers (kcal mol^{-1}) for transition structures and intermediates involved in the regioselective approaches of **7** to the *Re*-2,*Re*-7a (Figure A) and *Si*-2,*Si*-7a (Figure B) faces of **15** in toluene. In every case, black lines denote the more favored route whereas the regioisomeric pathways are depicted in red.

In following the same methodology reported above, we performed an NSA[13] intermolecular study for both approaches of **7** to **15** (**TS1$_{24}$** and **TS1$_{25}$**). Results are given in Table 3.4.

The dE(i) values obtained for saddle points **TS1$_{24}$** and **TS1$_{25}$** indicate that the intermolecular steric exchange between the dipole and its dipolarophile is 9.22 kcal mol^{-1} lower when **7** approaches to **15** at the *Si*-2,*Si*-7a face, which contains the bulky isopropyl group, than the addition at the rear face.

Table 3.4. Occupied NLMO contributions [dE(i) in kcal mol^{-1}] to the intermolecular steric exchange energy for transition structures **TS1$_{24}$** and **TS1$_{25}$** in toluene.

Structure	dE(i)$_{total}$	dE(i)$_{total}$ at 12.0 Å	dE(i)$_{total}$ - dE(i)$_{total}$ at 12.0 Å
TS1$_{24}$	1647.12	1504.13	142.99
TS1$_{25}$	1650.30	1516.53	133.77

In order to understand the origin of these results, we performed a *natural bond critical point* analysis (NBCP).[16] The CPs are points where the gradient of the electronic density,

[∇ρ(r)], is zero, and they are characterized by three eigenvalues (λ_1, λ_2, λ_3) of the Hessian matrix of ρ(r). The CPs are identified as (r,s) according with their rank (number of nonzero eigenvalues) and signature (algebraic sum of eigenvalues signs). A (3,-1) CP in which ρ(r) diminishes in two directions and increases in the third, is a saddle point of ρ(r) found between two neighboring atoms and it defines the linkage between them (BCP). When the Laplacian of ρ(r) [$\nabla^2\rho(r)$], namely the sum of three eigenvalues (λ_1, λ_2, λ_3), is negative the electronic charge is concentrated within the region of the BCP which is characteristic of covalent or polarized bonds, namely a shared layer interaction. However, a positive $\nabla^2\rho(r)$ corresponds to a charge leakage area, characteristic of a closed shell interaction. In the transition structure **TS1$_{25}$** the calculated distance between the carbonyl oxygen of **7** (O21 in Figure 3.10) and the nearest methyl hydrogen of **15** (H11 in Figure 3.10) is 2.60 Å, and the eigenvalues of the Hessian matrix are λ_1 = 0.0403, λ_2 = -0.0067, and λ_2 = -0.0068.

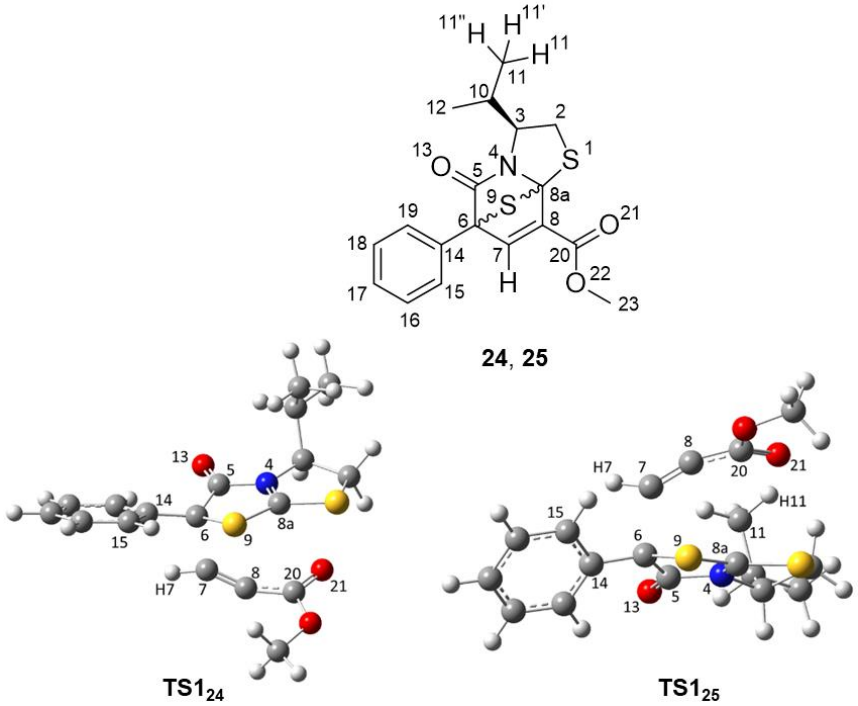

Figure 3.10. M06-2X/6-311++G(d,p)-optimized structures of **TS1$_{24}$** and **TS$_{25}$** in toluene (SMD method).

Accordingly, this CP is identified to be a first-order saddle point [(3,- 1)]. The magnitudes of ρ(r) and $\nabla^2\rho(r)$ for the aforementioned CP are quite small (0.0085 and 0.0268 au, respectively), pointing a weak interaction, and the positive value of $\nabla^2\rho(r)$ suggests a closed shell interaction. The NLMO contributions to ρ(r) and $\nabla^2\rho(r)$ for this BCP are shown in Table 3.5.

Table 3.5. NLMO contributions to ρ(**r**) and $\nabla^2\rho(\mathbf{r})$ for the $BCP_{O21\text{-}H11}$ in **TS1$_{25}$**

NLMO	% ρ(r)	$\nabla^2\rho(r)$ (au)
$LP(1)_{O21}$	15.90%	0.0058
$LP(2)_{O21}$	33.50%	0.0061
$\sigma_{C11\text{-}H11}$	45.50%	0.0125
$\sigma_{C11\text{-}H11'}$	2.80%	0.0004

The correlation (in percentage) of such NLMOs with their parent localized NBOs is extremely high, all over 98.8%, which points to a high electron localization at these NLMOs. The charge transfer (CT) energy between these NBOs goes from the first lone pair of the O21 atom to the $\sigma^*_{C11\text{-}H11}$ orbital (0.21 kcal mol^{-1}) and from the second pair of the same oxygen atom to the $\sigma^*_{C11\text{-}H11}$ and $\sigma^*_{C11\text{-}H11'}$ orbitals (0.34 and 0.10 kcal mol^{-1}, respectively). Overall, these interactions stabilize the system and their total value (0.65 kcal mol^{-1}) can be interpreted in terms of a weak van der Waals interaction.

Table 3.6 shows the steric interactions of occupied NLMOs of methyl propiolate (**7**) with the isopropyl group of **15** in **TS1$_{25}$**. Again these steric interactions are very small [$\sum dE(i,j)$ = 3.61 kcal mol^{-1}], thus proving that the isopropyl group does not destabilize the system by steric repulsions, at least to an appreciable extent. Since this alkyl group does not appear to be responsible for the greater stability of **TS1$_{25}$**, we then considered the saddle point moiety in which both transition structures (**TS1$_{24}$** and **TS1$_{25}$**) match, namely formation of the C6-C7 bond (Table 3.7).

Both BCPs C6-C7 in **TS1$_{24}$** and **TS1$_{25}$** are very similar with small values for ρ(r) and $\nabla^2\rho(r)$. However $\nabla^2\rho(r)$ is positive for **TS1$_{24}$**, and therefore indicative of a closed shell interaction, while it is negative for **TS1$_{25}$**, which corresponds to a shared layer interaction. Table 3.8 shows the NLMO contributions to ρ(r) and $\nabla^2\rho(r)$ for these BCPs.

Table 3.6. Steric exchange energies (in kcal mol^{-1}) for i,j NLMOs of **7** with the isopropyl group of **15** in **TS1$_{25}$**.

NLMO(i)	NLMO(j)	dE(i,j)
LP(1)$_{O21}$	$\sigma_{C11-H11}$	0.0304
	$\sigma_{C11-H11'}$	-0.0134
LP(2)$_{O21}$	$\sigma_{C11-H11}$	-0.0545
	$\sigma_{C11-H11'}$	0.0183
	$\sigma_{C11-H11''}$	-0.0219
π_{C7-C8}	$\sigma_{C11-H11}$	-0.023
	$\sigma_{C11-H11'}$	0.0168
	$\sigma_{C11-H11''}$	-0.1014
		ΣdE(i,j) = -0.1487

Table 3.7. Bond lengths, Hessian eigenvalues of ρ(**r**), ρ(**r**) and $\nabla^2\rho$(**r**) for BCPs of incipient bonds C6-C7 in **TS1$_{24}$** and **TS1$_{25}$**.

Structure	BCP	Bond lenght (Å)	Eigenvalues of Hessian of ρ(**r**)			ρ(**r**) (au)	$\nabla^2\rho$(**r**) (au)
TS1$_{24}$	BCP$_{C6-C7}$	1.94	0.2483	-0.1192	-0.1264	0.0976	0.0027
TS1$_{25}$	BCP$_{C6-C7}$	1.93	0.2529	-0.1241	-0.1306	0.0999	-0.0018

Table 3.8. NLMO contributions to ρ(**r**) and $\nabla^2\rho$(**r**) for the BCP$_{C6-C7}$ of **TS1$_{24}$** and **TS1$_{25}$**.

Structure	NLMO	% ρ(**r**)	$\nabla^2\rho$(**r**) (au)
TS1$_{24}$	LP$_{C6}$	92.3	-0.1390
TS1$_{25}$	LP$_{C6}$	93.1	-0.1448

Clearly, in both TSs the largest contributor to ρ(r) in such BCPs is the LP$_{C6}$ orbital, and the corresponding $\nabla^2\rho$(r) values suggest that the electron densities are highly localized in those NLMOs; or in other words, they reflect the nucleophilic character of the carbon atom in question, which is slightly higher in **TS1$_{25}$**. The low correlation percentage of these NLMOs with their parent localized NBOs (57.86% for **TS1$_{24}$** and 57.33% for **TS1$_{25}$**) suggests a significant level of electron delocalization, which in turn justifies a high charge transfer (CT) efficiency between these NBOs and the closer empty NBOs (see Table A3.4).

The total stabilization energy by CT ascribed to the lone pair that initiates the nucleophilic attack is higher for **TS1$_{25}$** than that for **TS1$_{24}$** (33.10 kcal mol^{-1}). The delocalization between the heterocycle and the alkyne reagent is quite similar for both

saddle points (only 4.76 kcal mol^{-1} higher in energy for **TS1$_{24}$**), albeit electron delocalization of the LP$_{C6}$ orbital with the phenyl group is higher in **TS1$_{25}$** (31.04 kcal mol^{-1}) than in **TS1$_{24}$** (1.53 kcal mol^{-1}). Likewise, electron delocalization of LP$_{C6}$ with the Rydberg orbitals of C6, C5, S9, and C14 is somewhat higher in **TS1$_{25}$** (21.85 kcal mol^{-1}) than in **TS1$_{24}$** (13.19 kcal mol^{-1}). Together these data account for a preferential cycloaddition of **7** to **15** on the *Si*-2,*Si*-7a face of the latter (**TS1$_{25}$**).

Table 3.3 showed that for **TS1$_{19}$t** a high charge transfer takes place in the dipolarophile fragment (749.32 kcal mol^{-1}). For **TS1$_{24}$** and **TS1$_{25}$** these values are quite similar (735.03 and 799.72 kcal mol^{-1}). In fact, the most important contribution to CT is given by the interaction of LP$_{C8}$ to π*$_{C20\text{-}O21}$ with energy values of 157.91 and 190.07 kcal mol^{-1} for **TS1$_{24}$** and **TS1$_{25}$**, respectively, exactly the same as for **TS1$_{19}$t**. Also, Table A3.4 shows the CT from the donor NBO LP$_{C6}$ to LV$_{C7}$ and RY(1)$_{C7}$ for **TS1$_{24}$** and **TS1$_{25}$**. In such interactions the orbital participation is identical to those shown in Figure 3.6A and 3.6B for **TS1$_{19}$t**, and the corresponding CT values are quite similar as well. In short, transition structure **TS1$_{19}$t** has the same orbital distribution and almost identical energy values as those of **TS1$_{24}$** and **TS1$_{25}$**, all of them optimized in toluene.

3.4. Conclusions

Two structurally rigid thioisomünchnone dipoles (**3** and **15**) have been prepared by condensation of α-haloacids with thiazolidin-2-thiones (**4** and **13**) under basic conditions. The mesoionic dipole **3** was generated in situ and then trapped with acetylenes, thus providing a one-pot route to novel 8-alkoxycarbonyl-5-oxo-3,5-dihydro-2H-thiazolo[3,2-*a*]pyridines (**9**-**11**). The structural characterization of products derived from asymmetrically substituted dipolarophiles could be successfully accomplished through NMR spectroscopy due to the vicinal disposition of hydrogen atoms at C-6 and C-7 of the heterocycles. Cycloadditions conducted with chiral thioisomünchnone **15** afforded optically active products, namely (*S*)-3-isopropyl-5-oxo-6-phenyl-3,5-dihydro-2H-thiazolo[3,2-*a*]pyridines **16**-**18**, whose structural characterization could be achieved by comparing their spectroscopic data to those of **17**, the latter being unequivocally elucidated by single-crystal X-ray diffraction. In all cases, the use of asymmetrically-substituted dipolarophiles proceeded with complete regioselectivity.

The experimental results have been corroborated by a detailed DFT study, at the M06-2X/6-311++G(d,p) level of theory, with inclusion of solvents effects (through the SMD model) in toluene and CH_2Cl_2. All cycloadditions involving methyl propiolate (**7**) giving rise to the regioisomer isolated experimentally are stepwise processes, while an opposite orientation of the dipolarophile turned out to be a concerted mechanism. Data collected in Figure 3.2 show that a phenyl group at C-2 of the mesoionic dipole lead to higher energy barriers for these cycloadditions. All concerted transformations are disfavored, a fact that can be rationalized in terms of intermolecular steric repulsions during the dipole-dipolarophile interaction, which are indeed greater for all concerted pathways with the sole exception of **TS1$_{19}$t**. This behavior is well counterbalanced by a large stabilization due to charge transfer in **TS1$_{19}$t** of the LP_{C8} (in the dipolarophile's fragment), thereby accounting for a stepwise pathway too. Moreover, this behavior for **TS1$_{19}$t** can also be inferred from a comparative analysis with transition structures **TS1$_{24}$** and **TS1$_{25}$**, which have also been optimized in toluene and exhibit an almost identical orbital distribution to **TS1$_{19}$t**.

It is known that most common 1,3-dipolar cycloadditions can be interpreted as Sustmann type I processes involving a nucleophilic attack from the dipole to the dipolarophile. This kind of cycloadditions is consistent with stepwise cycloadditions studied herein, for which the nucleophilic addition involves the C-6 atom of the dipole and the C-7 atom of the dipolarophile. Data gathered for the opposite orientation of **7** suggest that the nucleophilic attack goes from C-7 of the dipolarophile to C-8a of the dipole, thus becoming a Sustmann type III cycloaddition. The saddle points **TS1$_{24}$** and **TS1$_{25}$** correspond to the approach of **7** to both faces of chiral thioisomünchnone **15**. Subsequent comparative analyses of intermolecular steric repulsions for the above TSs have ultimately proven that the isopropyl group does not exert a marked steric repulsion; in fact there is actually a minor stabilization by charge transfer.

3.5. Experimental section

3.5.1. General methods

Solvents and reagents were purchased from commercial suppliers and used without further purification. The identity of all compounds was confirmed by their elemental analysis, high resolution mass spectra, mps, and NMR data.

3.5.2. Computational details

All calculations reported in this work were carried out using the Gaussian09 package.[17] The M06-2X[18] density functional method in conjunction with the 6-311++G(d,p)[19] basis set were selected for all the geometry optimizations and frequency analysis. The geometries were optimized including solvation effects in toluene and CH_2Cl_2, which have been determined by the density-based selfconsistent reaction field theory of bulk electrostatic, i.e., the wellknown solvation model density (SMD)[20] method that takes into account different contributions such as long-range electrostatic polarization (bulk solvent effect). Frequency calculations at 298.15 K on all the stationary points were carried out at the same level of theory as the geometry optimizations to ascertain the nature of the stationary points. Ground and transition states were characterized by none and one imaginary frequency, respectively. NSA (*natural steric analysis*),[13] which evaluates the occupied NLMO contributions [dE(i)], NBCP (*natural bond critical point analysis*)[16] and CT (charge transfer) analysis were all carried out with the NBO 6.0 package.[21] Main orbital [NBO[15] (*natural bond orbital*) and NLMO[14] (*natural localized molecular orbital*)] interactions have been represented with the Jmol software.[22] All of the relative energies shown are free energies calculated at 298.15 K with respect to the reagents.

3.5.3. Synthetic procedures

3.5.3.1. **2-((4,5-Dihydrothiazol-2-yl)thio)acetic acid (5).** To a solution of thiazolidine-2-thione (**4**) (8.4 mmol) in CH_2Cl_2 and bromoacetic acid (8.4 mmol) was added triethylamine and the mixture was stirred a room temperature for 72 h. Then, the resulting triethylammonium bromide was filtered off. In order to remove dissolved salts the, the solution was also passed through a silica gel [Merck 60 (400-230 mesh)] column using ethyl acetate as eluent. The solvent was evaporated to dryness to give a white solid (91%). Mp 125-126 ºC. FTIR (KBr) ν_{max} 3002, 2957, 2786, 2365, 1885, 1710, 1557, 1388, 1317, 1186, 1036, 895, 678, 656, 447 cm^{-1}. ^1H NMR (500 MHz, $CDCl_3$) δ 4.25 (t, 2H, *J* = 8.0 Hz), 3.71 (s, 2H), 3.56 (t, 2H, *J* = 8.0 Hz) ppm. ^{13}C NMR (125 MHz, $CDCl_3$) δ 173.6, 169.1, 61.8, 36.5, 35.4 ppm. Anal. Calcd for $C_5H_7NO_2S_2$: C, 33.90; H, 3.95; N, 7.91; S, 36.16. Found: C, 34.11; H, 4.12; N, 7.83; S, 36.26.

3.5.3.2. **(*S*)-5-Isopropyl-2-phenyl-5,6-dihydrothiazolo[2,3-*b*]thiazol-4-ium-3-olate (15).** A mixture of (*S*)-4-isopropylthiazolidine-2-thione (**13**) (23 mmol), 2-bromo-2-phenylacetic acid (23 mmol), and triethylamine (23 mmol) in benzene (50 mL) was stirred at room temperature for 72 h. The resulting precipitate of triethylammonium bromide was filtered off. To remove dissolved salts the solution was also passed through a silica gel [Merck 60 (400-230 mesh)] column using ethyl acetate as eluent. The solvent was evaporated to dryness to give an oily residue (5.4 g), which contained the intermediate thioglycolic acid **14**. To this oil a mixture of triethylamine an acetic anhydride (3:1, 40 mL) was added. The mixture was softly heated for a few minutes, yielding the title compound as orange crystals which were collected by filtration and washed with diethyl ether (50%). Mp 190-192 ºC. $[\alpha]_D$ 177.8º (c 5.1, CH_2Cl_2). FTIR (KBr) ν_{max} 3052, 3023, 2961, 2917, 2864, 1645, 1504, 1495, 1443, 1189, 754, 697, 687 cm^{-1}. ^1H NMR (500 MHz, $CDCl_3$) δ 7.74 (dd, 2H, *J* = 1.0 Hz, *J* = 8.5 Hz), 7.29 (dd, 2H, *J* = 7.5 Hz, *J* = 8.0 Hz), 7.05 (m, 1H), 4.91 (m, 1H), 4.11 (dd, 1H, *J* = 9.0 Hz, *J* = 11.0 Hz), 3.77 (dd, 1H, *J* = 2.5 Hz, *J* = 11.5 Hz), 2.98 (m, 1H), 1.09 (d, 3H, *J* = 7.0 Hz), 0.95 (d, 3H, *J* = 7.0 Hz) ppm. ^{13}C NMR (125 MHz, $CDCl_3$) δ 156.1, 152.6, 134.3, 128.6, 124.1, 122.71, 97.4, 67.3, 36.3, 29.3, 19.0, 15.7 ppm. Anal. Calcd for $C_{14}H_{15}NOS_2$: C, 60.65; H, 5.42; N, 5.05; S, 23.10. Found: C, 60.51; H, 5.37; N, 5.02; S, 22.70.

3.5.3.3. **Cycloadditions of 3 with acetylenic dipolarophiles 6-8. General procedure A.** To a mixture of **5** (2.8 mmol) and the dipolarophile (4.2 mmol) in CH_2Cl_2 (20 mL) were

added acetic anhydride and triethylamine (1:3, 3 mL) and the reaction mixture was heated at reflux for 1 h (TLC analysis: ethyl acetate:hexane 2:1 v/v). The products were isolated by column chromatography on silica gel [Merk 60 (400-230 mesh)] using ethyl acetate and hexane (1:1 and 2:1) as eluents. The solvent was removed to dryness and the residue was treated with diethyl ether to give the thiazolopyridones **9**-**11**, which were further recrystallized from ethyl acetate.

3.5.3.4. **Cycloadditions of 15 with acetylenic dipolarophiles 6-8. General Procedure B.** A mixture of **15** (1.4 mmol), the dipolarophile (1.8 mmol), and toluene (25 mL) was heated at reflux until the disappearance of the orange color (TLC analysis: ethyl acetate:hexane 1:2 v/v). The solvent was evaporated to dryness and the resulting residue was suspended in methanol or ethanol to yield the corresponding pyridones (**16**-**18**), which were further recrystallized from ethyl acetate.

3.5.3.5. **Dimethyl 5-oxo-3,5-dihydro-2*H*-thiazolo[3,2-*a*]pyridine-7,8-dicarboxylate (9).** Following the general procedure A, compound **9** was obtained from **3** and **6** after 1 h. Recrystallized from ethyl acetate (15%) had mp 131-135 ºC. FTIR (KBr) ν_{max} 3463, 3019, 2958, 1737, 1693, 1651, 1442, 1265, 1143, 1056, 986, 839, 786 cm^{-1}. ^{1}H NMR (500 MHz, $CDCl_3$) δ 6.24 (s, 1H), 4.53 (t, 2H, *J* = 8.0 Hz), 3.88 (s, 3H), 3.83 (s, 3H), 3.38 (t, 2H, *J* = 8.0 Hz) ppm. ^{13}C NMR (125 MHz, $CDCl_3$) δ 167.0, 164.0, 160.4, 158.9, 145.0, 113.5, 101.6, 52.8, 52.4, 50.9, 27.7 ppm. Anal. Calcd for $C_{11}H_{11}NO_5S$: C, 49.07; H, 4.10; N, 5.20; S, 12.00. Found: C, 48.90; H, 4.21; N, 5.27; S, 12.04.

3.5.3.6. **Methyl 5-oxo-3,5-dihydro-2*H*-thiazolo[3,2-*a*]pyridine-8-carboxylate (10).** Following the general procedure A, compound **10** was obtained from **3** and **7** after 1 h. Recrystallized from ethyl acetate (37%). Mp 170-174 ºC. FTIR (KBr) ν_{max} 3052, 2988, 2951, 1687, 1659, 1508, 1435, 1298, 1206, 1124, 1020, 834, 781 cm^{-1}. ^{1}H NMR (500 MHz, $CDCl_3$) δ 7.82 (d, 1H, *J* = 9.5 Hz), 6.24 (d, 1H, *J* = 9.5 Hz), 4.56 (t, 3H, *J* = 7.5 Hz), 3.83 (t, 2H, *J* = 7.5 Hz), 3.87 (s, 3H), 3.37 (t, 2H, *J* = 8.0 Hz) ppm. ^{13}C NMR (125 MHz, $CDCl_3$) δ 165.1, 161.9, 157.6, 139.5, 114.2, 104.5, 52.1, 50.6, 27.6 ppm. Anal. Calcd for $C_9H_9NO_3S$: C, 51.17, H, 4.29, N, 6.63, S, 15.18. Found: C, 51.12, H, 4.22, N, 6.60, S, 15.29.

3.5.3.7. **Ethyl 5-oxo-3,5-dihydro-2*H*-thiazolo[3,2-a]pyridine-8-carboxylate (11).** Following the general procedure A, compound **11** was obtained from **3** and **8** after 1 h. Recrystallized from ethyl acetate (32%). Mp 112-115 ºC. FTIR (KBr) ν_{max} 2958, 2925, 2854, 1697, 1640, 1511, 1443, 1412, 1293, 1128, 1035, 823, 778, 589 cm^{-1}. ^{1}H NMR (400 MHz, $CDCl_3$) δ 7.84 (d, 1H, *J* = 9.6 Hz), 6.25 (d, 1H, *J* = 9.2 Hz), 4.52 (t, 2H, *J* = 8.0 Hz), 4.33 (q, 2H, *J* = 7.2 Hz), 3.37 (t, 2H, *J* = 8.0 Hz), 1.37 (t, 3H, *J* = 7.2 Hz) ppm. ^{13}C NMR (100 MHz, $CDCl_3$) δ 164.6, 162.0, 157.3, 139.6, 114.1, 104.8, 61.2, 50.6, 27.6, 14.4 ppm. Anal. Calcd for $C_{10}H_{11}NO_3S$: C, 53.32, H, 4.92, N, 6.22, S, 14.23. Found: C, 53.12, H, 4.89, N, 6.21, S, 14.09.

3.5.3.8. **(*S*)-Dimethyl 3-isopropyl-5-oxo-3,5-dihydro-2*H*-thiazolo[3,2-*a*]pyridine-7,8-dicarboxylate (16).** Following the general procedure B, compound **16** was obtained from **15** and **6** after 2 h. Recrystallized from ethyl acetate (56%). Mp 151-153 ºC. $[\alpha]_D$ 276.7º (*c* 5.2, CH_2Cl_2). FTIR (KBr) ν_{max} 2954, 2868, 1740, 1694, 1652, 1511, 1437, 1365, 1315, 1234, 1212, 1176, 716, 703, 537 cm^{-1}. ^{1}H NMR (500 MHz, $CDCl_3$) δ 7.32 (m, 5H), 5.17 (m, 1H), 3.83 (s, 3H), 3.57 (s, 3H), 3.48 (dd, 1H, *J* = 9.0 Hz, *J* = 11.5 Hz), 3.17 (dd, 1H, *J* = 1.5 Hz, *J* = 12.0 Hz), 2.58 (m, 1H), 0.99 (dd, 6H, *J* = 7.0 Hz, *J* = 15.5 Hz) ppm. ^{13}C NMR (125 MHz, $CDCl_3$) δ 166.8, 164.2, 160.3, 158.2, 142.4, 133.2, 129.7, 128.2, 128.0, 125.1, 100.8, 68.5, 52.4, 52.2, 29.3, 28.3, 19.4, 16.4 ppm. Anal. Calcd for $C_{20}H_{21}NO_5S$: C, 62.00, H, 5.46, N, 3.62, S, 8.28. Found: C, 61.86, H, 5.61, N, 3.70, S, 7.93.

3.5.3.9. **(*S*)-Methyl 3-isopropyl-5-oxo-3,5-dihydro-2*H*-thiazolo[3,2-*a*]pyridine-8-carboxylate (17).** Following the general procedure B, compound **17** was obtained from **15** and **7** after 2 h. Recrystallized from ethyl acetate (74%). Mp 155-157 ºC. $[\alpha]_D$ 361.2º (*c* 6.1, CH_2Cl_2). FTIR (KBr) ν_{max} 3052, 3032, 2995, 2962, 2868, 1696, 1640, 1520, 1446, 1425, 1367, 1301, 1237, 1182, 1104, 1015, 788, 703, 592 cm^{-1}. ^{1}H NMR (500 MHz, $CDCl_3$) δ 8.01 (s, 1H), 7.68 (m, 2H), 7.40 (m, 2H), 7.32 (m, 1H), 5.22 (m, 1H), 4.35 (m, 2H), 3.49 (dd, 1H, *J* = 9.0 Hz, *J* = 11.5 Hz), 3.19 (dd, 1H, *J* = 1,5 Hz, *J* = 12.0 Hz), 2.64 (m, 1H), 1.37 (t, 3H, *J* = 7.0 Hz) 1.03 (d, 3H, *J* = 7.0 Hz), 0.94 (d, 3H, *J* = 7.0 Hz) ppm. ^{13}C NMR (125 MHz, $CDCl_3$) δ 165.3, 160.6, 156.6, 137.2, 135.8, 128.4, 128.2, 127.7, 125.6, 103.8, 68.0, 52.0, 29.3, 28.3, 19.4, 16.3 ppm. Anal. Calcd for $C_{18}H_{19}NO_3S$: C, 65.63, H, 5.81, N, 4.25, S, 9.73. Found: C, 65.58, H, 5.79, N, 4.22, S, 9.55.

3.5.3.10. **(*S*)-Ethyl 3-isopropyl-5-oxo-6-phenyl-3,5-dihydro-2*H*-thiazolo[3,2-*a*]pyridine-8-carboxylate (18).** Following the general procedure B, compound **18** was obtained from **15** and **8** after 2 h. Recrystallized from ethyl acetate (64%). Mp 108-111 ºC. $[\alpha]_D$ 326.2º (*c* 5.4, CH_2Cl_2). FTIR (KBr) ν_{max} 3065, 2961, 2935, 2873, 1694, 1639, 1596, 1521, 1445, 1395, 1303, 1255, 1237, 1168, 1102, 1035, 777, 700, 597, 542 cm^{-1}. ^1H NMR (500 MHz, $CDCl_3$) δ 8.02 (s, 1H), 7.68 (m, 2H), 7.41 (t, 2H, *J* = 7.0 Hz), 7.33 (m, 1H), 4.35 (m, 2H) 3.49 (dd, 1H, *J* = 9.0 Hz, *J* = 11.5 Hz), 3.20 (dd, 1H, *J* = 1.0 Hz, *J* = 11.5 Hz), 2.64 (m, 1H), 1.37 (t, 3H, *J* = 7.0 Hz), 1.03 (d, 3H, *J* = 7.0 Hz), 0.95 (d, 3H, *J* = 7.0 Hz) ppm. ^{13}C NMR (125 MHz, $CDCl_3$) δ 164.9, 160.6, 156.4, 137.3, 135.8, 128.5, 128.2, 127.7, 125.6, 104.2, 68.0, 61.2, 29.3, 28.3, 19.4, 16.4, 14.4 ppm. Anal. Calcd for $C_{19}H_{21}NO_3S$: C, 66.45, H, 6.16, N, 4.08, S, 9.34. Found: C, 66.39, H, 6.14, N, 3.97, S, 9.30.

3.6. Addendum

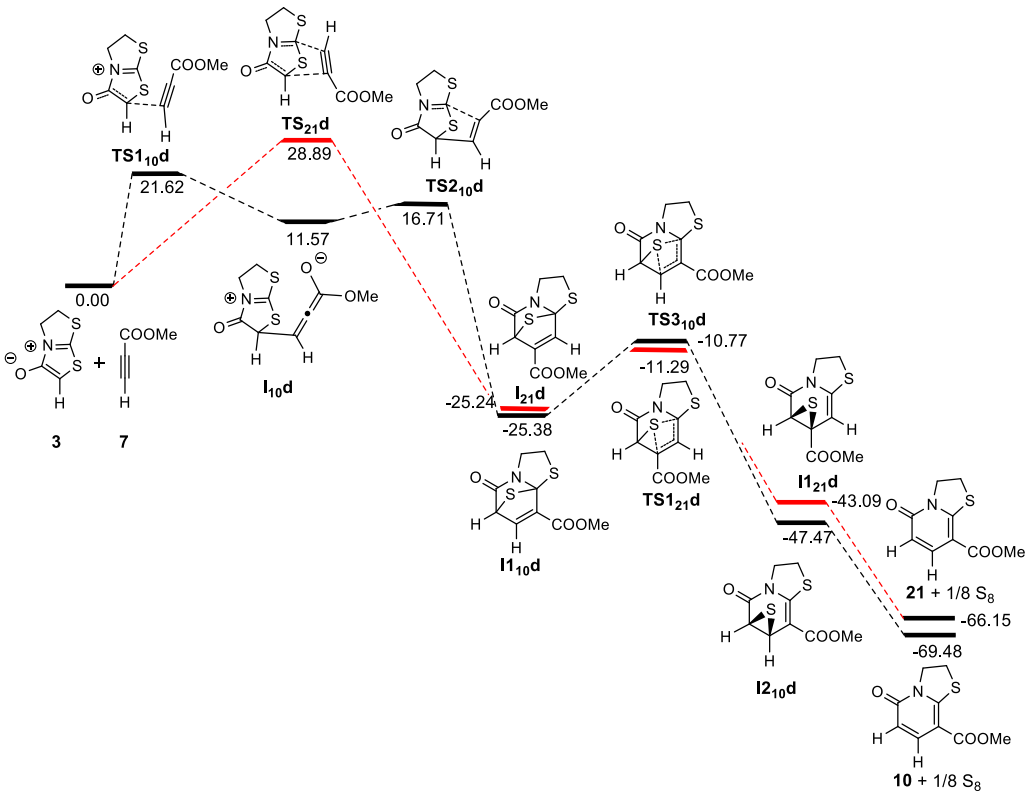

Figure A3.1. Reaction pathways leading to regioisomeric cycloadducts **I1$_{10}$d** and **I$_{21}$d**, and its subsequent conversion into pyridones **10** and **21** respectively in dichloromethane. (ΔG values are given in kcal mol^{-1})

Table A3.1. Relative electronic energy (Δ*E*), enthalpy (Δ*H*), and free energy (Δ*G*) (in kcal mol^{-1}) of all stationary points involved in the reactions of **3** and **7** leading to 5-oxothiazolo[3,2-*a*]pyridines **10** and **21**.

Structure	ΔE	ΔH	ΔG
3 + **7**	0.00	0.00	0.00
TS1$_{10}$d	7.63	8.23	21.62
I$_{10}$d	-4.10	-1.98	11.57
TS2$_{10}$d	1.12	2.22	16.71
I1$_{10}$d	-43.60	-40.46	-25.38
TS3$_{10}$d	-28.11	-25.60	-10.77
I1$_{10}$d	-65.54	-61.96	-47.47
10 + 1/8 **S$_8$**	-85.09	-81.78	-69.98
TS$_{21}$d	15.30	15.58	28.89
I$_{21}$d	-43.78	-40.55	-25.24
TS1$_{21}$d	-29.12	-26.64	-11.29
I1$_{21}$d	-61.20	-57.54	-43.09
21 + 1/8 **S$_8$**	-81.53	-78.17	-66.15

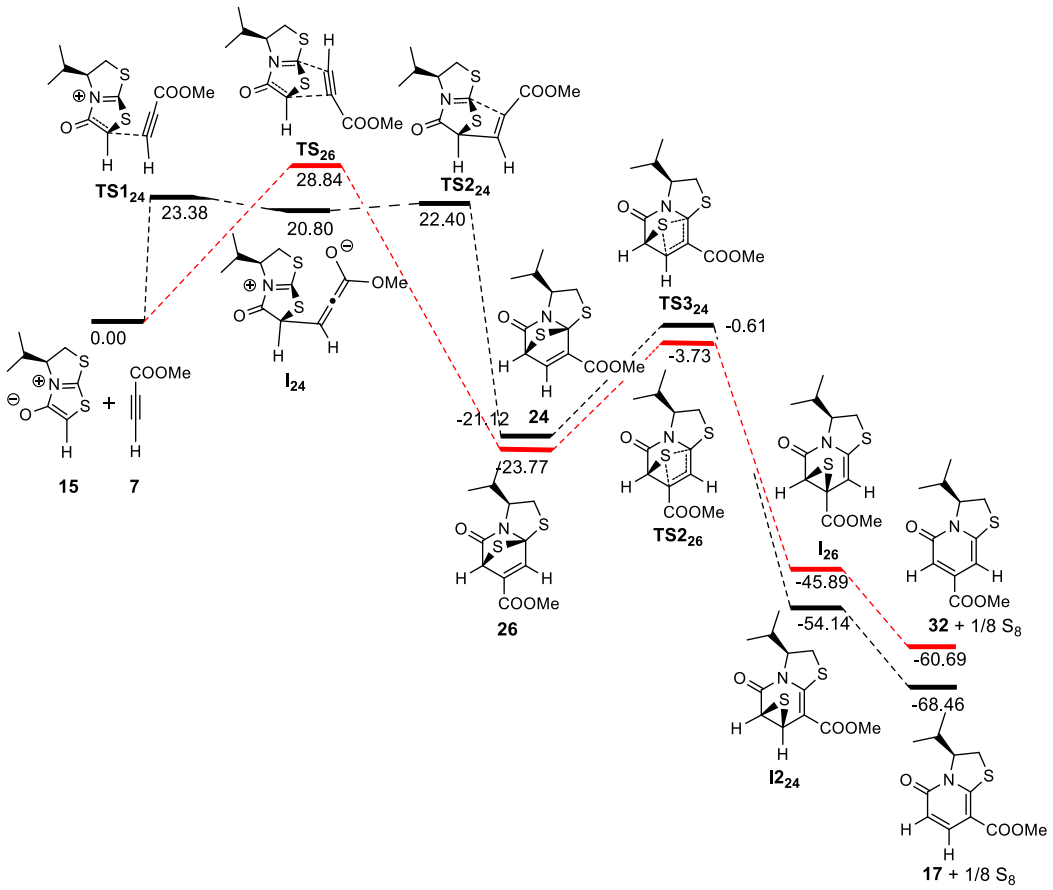

Figure A3.2. Reaction pathways leading to regioisomeric cycloadducts **24** and **26**, and its subsequent conversion into pyridones **17** and **32** respectively in toluene. (ΔG values are given in kcal mol^{-1}).

Table A3.2. Relative electronic energy (Δ*E*), enthalpy (Δ*H*), and free energy (Δ*G*) (in kcal mol^{-1}) of all stationary points involved in the *re*-2,*re*-7a approach of **15** and **7** leading to 5-oxothiazolo[3,2-*a*]pyridines **17** and **32**.

Structure	ΔE	ΔH	ΔG
15 + **7**	0.00	0.00	0.00
TS1$_{24}$	7.58	8.38	23.38
I$_{24}$	3.90	5.63	20.80
TS2$_{24}$	5.69	6.42	22.40
24	-39.70	-37.04	-21.12
TS3$_{24}$	-18.95	-16.88	-0.61
I2$_{24}$	-63.47	-60.09	-45.14
17 + 1/8 **S$_8$**	-84.26	-81.01	-68.46
TS$_{26}$	12.29	12.65	28.84
26	-43.40	-41.46	-23.77
TS2$_{26}$	-22.47	-20.49	-3.73
I$_{26}$	-64.36	-60.89	-45.89
32 + 1/8 **S$_8$**	-77.63	-74.28	-60.69

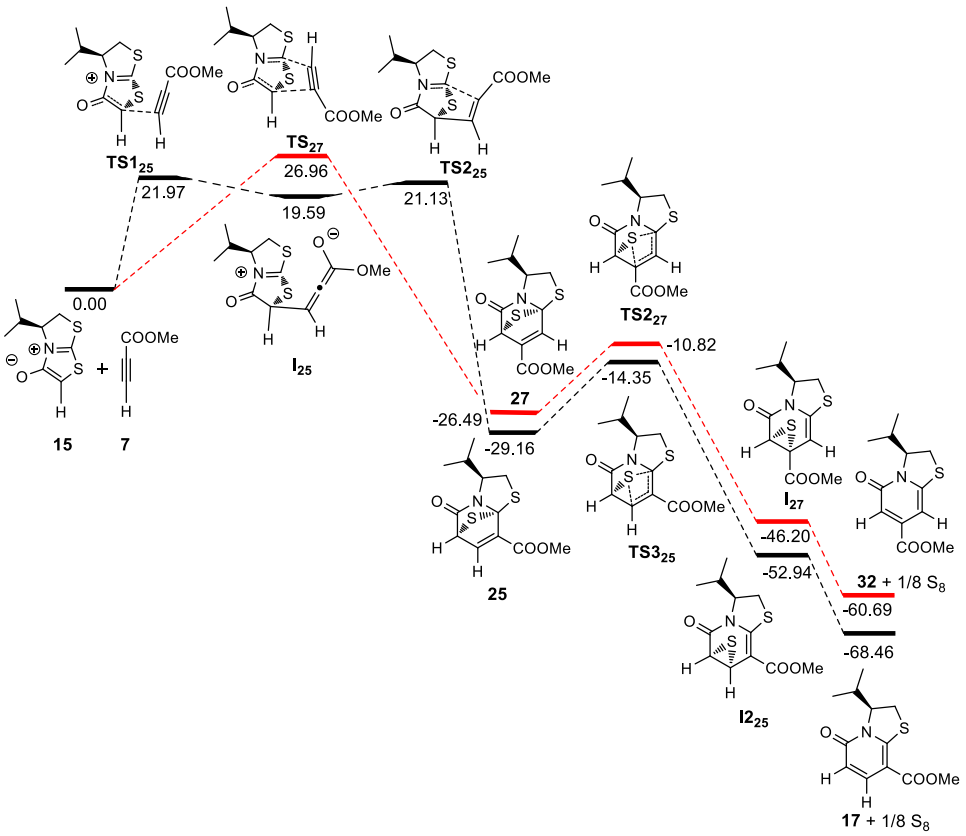

Figure A3.3. Reaction pathways leading to regioisomeric cycloadducts **25** and **27**, and its subsequent conversion into pyridones **17** and **32** respectively in toluene. (ΔG values are given in kcal mol^{-1}).

Table A3.3. Relative electronic energy (Δ*E*), enthalpy (Δ*H*), and free energy (Δ*G*) (in kcal mol^{-1}) of all stationary points involved in the *si*-2,*si*-7a approach of **15** and **7** leading to 5-oxothiazolo[3,2-*a*]pyridines **17** and **32**.

Structure	ΔE	ΔH	ΔG
15 + **7**	0.00	0.00	0.00
TS1$_{25}$	6.91	7.35	21.97
I$_{25}$	3.11	4.78	19.59
TS2$_{25}$	4.25	5.17	21.13
25	-47.19	-44.52	-29.16
TS3$_{25}$	-32.16	-30.06	-14.35
I2$_{25}$	-72.04	-68.38	-52.94
17 + 1/8 **S$_8$**	-84.26	-81.01	-68.46
TS$_{27}$	11.18	11.65	26.96
27	-45.09	-41.92	-26.49
TS2$_{27}$	-28.83	-26.72	-10.82
I$_{27}$	-64.18	-61.19	-46.20
32 + 1/8 **S$_8$**	-77.63	-74.28	-60.69

Table A3.4. CT energies (in kcal mol^{-1}) between donor LP_{C6} and acceptor NBOs for structural fragments of **7** and **15** in **TS1$_{24}$** and **TS1$_{25}$**.

Structure	Donor	Acceptor	E
TS1$_{24}$	LP_{C6}	σ^*_{C5-C6}	1.35
		σ^*_{C5-O13}	3.41
		π^*_{C5-O13}	58.72
		$\sigma^*_{C14-C15}$	1.53
		$RY(3)_{C5}$	1.8
		$RY(3)_{C6}$	1.63
		$RY(5)_{C6}$	0.87
		$RY(6)_{C6}$	1.12
		$RY(15)_{C6}$	0.89
		$RY(1)_{S8}$	4.7
		$RY(1)_{C14}$	1.02
		$RY(3)_{C14}$	2.22
		$RY(7)_{C14}$	0.57
		ΣE	**79.83**
		LV_{C7}	25.41
		σ^*_{C7-C8}	1.39
		σ^*_{C7-H7}	0.96
		σ^*_{C8-C20}	0.73
		$\pi^*_{C20-O21}$	0.17
		$RY(1)_{C7}$	102.13
		$RY(2)_{C7}$	0.09
		$RY(3)_{C7}$	3.19
		$RY(4)_{C7}$	0.41
		$RY(5)_{C7}$	0.12
		$RY(7)_{C7}$	0.08
		$RY(10)_{C7}$	0.06
		$RY(15)_{C7}$	0.05
		$RY(16)_{C7}$	0.61
		$RY(3)_{C8}$	0.12
		$RY(5)_{C8}$	0.18
		$RY(6)_{C8}$	0.27
		$RY(7)_{C8}$	0.16
		$RY(15)_{C8}$	0.05
		$RY(1)_{H7}$	0.08
		$RY(4)_{H7}$	0.06
		ΣE	**136.32**
		ΣE_{total}	**216.15**

Structure	Donor	Acceptor	E
TS1$_{25}$	LP_{C6}	σ^*_{C5-C6}	1.57
		σ^*_{C5-O13}	4.59
		π^*_{C5-O13}	58.64
		$\sigma^*_{C14-C15}$	1.83
		$\pi^*_{C14-C15}$	24.18
		$\sigma^*_{C14-C16}$	5.03
		$RY(1)_{C5}$	0.76
		$RY(3)_{C5}$	2.38
		$RY(7)_{C5}$	1.17
		$RY(8)_{C5}$	0.67
		$RY(3)_{C6}$	0.61
		$RY(4)_{C6}$	1.61
		$RY(5)_{C6}$	1.6
		$RY(8)_{C6}$	1.27
		$RY(10)_{C6}$	1.1
		$RY(13)_{C6}$	0.5
		$RY(15)_{C6}$	1.17
		$RY(16)_{C6}$	1.36
		$RY(1)_{S9}$	4.02
		$RY(3)_{S9}$	0.58
		$RY(3)_{C14}$	2.42
		$RY(6)_{C14}$	0.63
		ΣE	**117.69**
		LV_{C7}	23.92
		σ^*_{C7-C8}	1.17
		σ^*_{C7-H7}	1.04
		σ^*_{C8-C20}	0.7
		$\pi^*_{C20-O21}$	0.19
		$RY(1)_{C7}$	98.2
		$RY(2)_{C7}$	0.1
		$RY(3)_{C7}$	3.03
		$RY(4)_{C7}$	0.53
		$RY(5)_{C7}$	0.25
		$RY(6)_{C7}$	0.07
		$RY(9)_{C7}$	0.21
		$RY(11)_{C7}$	0.05
		$RY(16)_{C7}$	0.73
		$RY(1)_{H7}$	0.07
		$RY(4)_{C8}$	0.37
		$RY(5)_{C8}$	0.06
		$RY(6)_{C8}$	0.23
		$RY(8)_{C8}$	0.09
		$RY(9)_{C20}$	0.14
		$RY(11)_{C20}$	0.08
		$RY(12)_{C20}$	0.24
		$RY(13)_{C20}$	0.09
		ΣE	**131.56**
		ΣE_{total}	**249,25**

3.7. Bibliography

(1) Taylor, R. D.; MacCoss, M.; Lawson, A. D. G. *J. Med. Chem.* **2014**, *57*, 5845-5859.
(2) Vaquero, J. J.; Alvarez-Builla, J. In *Modern Heterocyclic Chemistry*; Alvarez-Builla, J., Vaquero, J. J., Barluenga, J., Eds.; Wiley-VCH, Weinheim, 2011; Vol. 4, Ch. 22, pp. 1989-2070.
(3) Pinto, D. J. P.; Smallheer, J. M.; Cheney, D. L.; Knabb, R. M.; Wexler, R. R. *J. Med. Chem.* **2010**, *53*, 6243-6274.
(4) Shi, F.; Li, C.; Xia, M.; Miao, K.; Zhao, Y.; Tu, S.; Zheng, W.; Zhang, G.; Ma, N. *Bioorg. Med. Chem. Lett.* **2009**, *19*, 5565-5568.
(5) (a) *Synthetic Applications of 1,3-Dipolar Cycloaddition Chemistry toward Heterocycles and Natural Products*; Padwa, A., Pearson, W. H., Eds.; John Wiley & Sons: New York, 2002; (b) Pellisier, H. *Tetrahedron* **2007**, 63, 3235-3285; (c) Suga, H.; Itoh, K. In *Methods and Applications of Cycloaddition Reactions in Organic Syntheses*; Nishiwaki, N., Ed.; John Wiley & Sons, Inc.: Hoboken, New Jersey, 2013; pp. 175-204; (d) Hasimoto, T.; Maruoka, K. *Chem. Rev.* **2015**, 115, 5366-5412; (e) *Science of Synthesis: Houben-Weyl Methods of Molecular Transformations*; Danheiser, R. L., Ed.; Georg Thieme: Stuttgart, 2014; Vol. 23: Compounds with Four and Three Carbon-Heteroatom Bonds, pp. 461-462.
(6) Candeias, N. R.; Branco, L. G.; Gois, P. M. P.; Afonso, C. A. M.; Trindade, A. F. *Chem. Rev.* **2009**, *109*, 2703-2802.
(7) (a) Ollis, W. D.; Ramsden, C. A. In *Advances in Heterocyclic Chemistry*; Katritzky, A. R.; Boulton, A. J., Eds.; *Academic Press*: New York, 1976; Vol. 19, pp. 1-122; (b) Newton, C. G.; Ramsden, C. A. *Tetrahedron* **1982**, *38*, 2965-3011; (c) Potts, K. T. In *1,3-Dipolar Cycloaddition Chemistry*; Padwa, A., Ed.; John Wiley & Sons: New York, 1984; Vol. 2, pp. 1-82; (d) Ollis, W. D.; Stanforth, S. P.; Ramsden, C. A. *Tetrahedron* **1985**, *41*, 2239-2329; (e) Badami, B. V. *Resonance* **2006**, *11*, 40-48.
(8) (a) Osterhout, M. H.; Nadler, W. R.; Padwa, A. *Synthesis* **1994**, 123-141; (b) Benetti, S.; De Risi, C.; Pollini, G. P.; Zanirato, V. *Chem. Rev*. **2012**, *112*, 2129-2163; (c) Lopchuk, J. M. In *Metalation of Azoles and Related Five-Membered Ring Heterocycles*; Gribble, G. W., Ed.; Springer: Berlin, 2012; pp. 381-413.
(9) (a) Ávalos, M.; Babiano, R.; Cintas, P.; Jiménez, J. L.; Palacios, *Acc. Chem. Res*. **2005**, *38*, 460-468 and references cited therein; (b) Cantillo, D.; Ávalos, M.; Babiano, R.; Cintas, P.; Jiménez, Light, M. E.; Palacios, J. C. *Org. Lett*. **2008**, *10*, 1079-1082; (c) Cantillo, D.; Ávalos, M.; Babiano, R.; Cintas, P.; Jiménez, Light, M. E.; Palacios, J. C., *J. Org. Chem*. **2009**, *74*, 3698-3705; (d) Cantillo, D.; Ávalos, M.; Babiano, R.; Cintas, P.; Jiménez, Light, M. E.; Palacios, *J. Or. Chem*. **2009**, *74*, 7644-7650; (e) Sánchez, B.; Arévalo, M. J.; Bravo, J. L.; López, I.; Light, M. E.; Silvero, G. *Austr. J. Chem*. **2009**, *62*, 356-359; (f) Sánchez, B.; López, I.; Light, M. E.; Silvero, G.; Bravo, J. L. *Eur. J. Org. Chem*. **2010**, 1648-1652.
(10) García de la Concepción, J.; Ávalos, M.; Babiano, R.; Cintas, P.; Jiménez, J. L.; Light, M. E.; Palacios, J. C. *Tetrahedron* **2016**, *72*, 4665-4670.
(11) Delaunay D.; Toupet L.; Le Corre M. *J. Org. Chem*. **1995**, *60*, 6604-6607.
(12) Crystallographic data (excluding structure factors) for the structures in this paper have been deposited with the Cambridge Crystallographic Data Centre as supplementary publication no. CCDC-1519821.
(13) (a)J. K. Badenhoop and F. Weinhold. *J. Chem. Phys.* **1997**, *107*, 5406-5421, 5422-5432 (b) *Int. J. Quantum Chem.* **1999**, *72*, 269-280.
(14) A. E. Reed and F. Weinhold. *J. Chem. Phys*. **1985**, *83*, 1736-1740.
(15) J. P. Foster and F. Weinhold. *J. Am. Chem. Soc*. **1980**, *102*, 7211-7218.
(16) F. Weinhold, *J. Comput. Chem.* **2012**, *33*, 2440-2449.
(17) Frisch, M. J.; Trucks, G. W.; Schlegel, H. B.; Scuseria, G. E.; Robb, M. A.; Cheeseman, J. R.; Scalmani, G.; Barone, V.; Mennucci, B.; Petersson, G. A.; Nakatsuji, H.; Caricato, M.; Li, X.; Hratchian, H. P.; Izmaylov, A. F.; Bloino, J.; Zheng, G.; Sonnenberg, J. L.; Hada, M.; Ehara, M.; Toyota, K.; Fukuda, R.; Hasegawa, J.; Ishida, M.; Nakajima, T.; Honda, Y.; Kitao,

O.; Nakai, H.; Vreven, T. Jr.; Montgomery J. A.; Peralta, J. E.; Ogliaro, F.; Bearpark, M.; Heyd, J. J.; Brothers, E.; Kudin, N. K.; Staroverov, V. N.; Kobayashi, R.; Normand, J.; Raghavachari, K.; Rendell, A.; Burant, J. C.; Iyengar, S. S.; Tomasi, J.; Cossi, M.; Rega, N.; Millam, J. M.; Klene, M.; Knox, J. E.; Cross, J. B.; Bakken, V.; Adamo, C.; Jaramillo, J.; Gomperts, R.; Stratmann, R. E.; Yazyev, O.; Austin, A. J.; Cammi, R.; Pomelli, C.; Ochterski, J. W.; Martin, R. L.; Morokuma, K.; Zakrzewski, V. G.; Voth, G. A.; Salvador, P.; Dannenberg, J. J.; Dapprich, S.; Daniels, A. D.; Farkas, Ö.; Foresman, J. B.; Ortiz, J. V.; Cioslowski, J.; Fox, D. J.; Gaussian 09, Revision D.01; Gaussian, Inc.: Wallingford, CT, 2009.

(18) Zhao, Y.; Truhlar, D. G. *Theor. Chem. Acc*. **2008**, *120*, 215-241.

(19) (a) Ditchfield, R.; Hehre, W. J.; Pople, J. A. *J. Chem. Phys*. **1971**, *54*, 724–728. (b) Hehre, W. J.; Ditchfield, R.; Pople, J. A. *Mol. Phys*. **1974**, *27*, 209–214. (c) Gordon, M. S.; *Chem. Phys. Lett*. **1980**, *76*, 163–168. (d) Hariharan, P. C.; Pople, J. A. *Theor. Chem. Acc*. **1973**, *28*, 213–222. (e) Francl, M. M.; Pietro, W. J.; Hehre, W. J.; Binkley, J. S.; DeFrees, D. J.; Pople, J. A.; Gordon, M. S. *J. Chem. Phys*. **1982**, *77*, 3654–3665.

(20) (a) Marenich, A. V.; Cramer, C. J.; Truhlar, D. G. *J. Phys. Chem. B.* **2009**, *113*, 4538-4543. (b) Marenich, A. V.; Cramer, C. J.; Truhlar, D. G., *J. Phys. Chem. B* **2009**, *113*, 6378-6396. (c) Ribeiro, R. F.; Marenich, A. V.; Cramer, C. J.; Truhlar, D. G. *J. Comput.-Aided Mater*. **2010**, *24*, 317-333. (d) Halim, M. A.; Shaw, D. M.; Poirier, R. A. *J. Mol. Struct*. **2010**, *960*, 63-72. (e) G. Saielli, *J. Phys. Chem. A.* **2010**, *114*, 7261-7265.

(21) E. D. Glendening, J, K. Badenhoop, A. E. Reed, J. E. Carpenter, J. A. Bohmann, C. M. Morales, C. R. Landis, and F. Weinhold, Theoretical Chemistry Institute, University of Wisconsin, Madison (2013).

(22) http://www.jmol.org/

4. Mechanistic and Synthetic Studies of 1,3-Dipolar Cycloadditions of Bicyclic Thioisomünchnones with Olefinic Bonds. A Computational Rationale Focused on Donor-Acceptor Interactions

4.1. Abstract

This paper describes a mechanistic study, in the interplay of experiment and theory, on the cycloadditions of a bicyclic mesoionic 1,3-dipole versus a series of representative symmetrical (1-phenyl-1*H*-pyrrole-2,5-dione and dimethyl maleate) and asymmetrical [(*E*)-(2-nitrovinyl)benzene, acrylonitrile, and but-3-en-2-one] olefinic dipolarophiles. These results allow a comparative analysis with monocyclic dipoles and open further avenues to structurally diversified heteroatom-rich rings. The unichiral version of the bicyclic dipole leads to adducts containing up to five chiral centers, whose formation proceeds with high levels of facial stereoinduction in reactions involving bulky dipolarophiles. The second and largest part of this study provides a theoretical interrogation on the pericyclic mechanism with DFT-methods [M06-2X/6-311G++(d,p) In order to get further mechanistic insights, we have also explored charge transfers between reaction partners using an NBO analysis, which satisfactorily justifies the stereochemical outcome.

4.2. Introduction

1,3-Dipolar cycloadditions represent an indispensable synthetic tool to construct five- and six-membered rings in an expeditious fashion and often with high levels of regio- and stereoselection.[1] This assembly exploits a wide range of unsaturated dipolarophiles in conjunction with some reactive dipoles, which usually exhibit a remarkable orthogonality to other functional groups. As a result, this family of pericyclic reactions has found interesting applications in biological studies[2,3] and materials design.[4]

The search for reactive, yet functionalized, dipoles capable of building-up complex structures with stereocontrol is still a must. Mesoionics, once considered exotic ionic structures and showing significant electron delocalization, are always an appropriate choice given their versatility and facile supply of polyheteroatomic arrangements in one-pot condensations.[5,6] The use of mesoionics is however limited by the steps required to obtain such heterocycles and the intrinsic stability of the structure, thus avoiding side reactions en route to high-yielding synthesis of the target products.[7]

For many years we have been interested in the design of mesoionic dipoles and their utility in heterocycle synthesis with a focus on stereocontrolled strategies.[8] Explorations

with a modified 1,3-thiazolium-4-olate (usually nicknamed thioisomünchnone) bearing a dialkylamino group constituted a watershed as the latter exerted a pivotal stereoelectronic effect enabling the preparation of hitherto unknown heterocycles by conventional dipolar cycloadditions.[6b]

While most thioisomünchnones undergo dipolar cycloadditions with alkenes to provide stable bridged cycloadducts, which eventually fragment into pyrid-2-ones by a stepwise elimination of hydrogen sulfide, other thioisomünchnones give rise to dihydrothiophenes when reacted with β-nitrostyrenes.[9,10] Although the structural diversity in heterocyclic build-up represents a plus in mesoionics-based cycloadditions, an additional advantage of these heterocyclic dipoles is the simplified assembly of multiple fused rings, present in natural compounds and drugs, as the resulting cycloadducts might be prevented from subsequent ring opening. A conformationally-restricted mesoionic dipole as starting material would enable such decorations so long as little or no chemical evolution takes place subsequently. In recent studies, we have reported the preparation and 1,3-dipolar reactivity against substituted acetylenes of 2-phenyl-5,6-dihydrothiazolo[2,3-*b*]thiazol-4-ium-3-olate (**1**),[11] and an enantiomerically pure version (**2**), easily generated from a chiral amino alcohol,[12] which afford pyridin-2-one derivatives. We describe here the extension of their reactivity toward five well-established dipolarophiles (**3**-**7**). Prompted by the potential significance of these synthetic pursuits, our quantum calculations aimed at elucidating the reaction pathways and energy landscape now dig deep to dissecting the electron distribution and orbital contribution at the saddle points, which allows a more precise rationale of the mechanism and interpretation of orbital control in dipolar cycloadditions.

4.3. Results and discussion

4.3.1. Synthesis and reactivity

The dipolar reactivity of 2-phenyl-5,6-dihydrothiazolo[2,3-*b*]thiazol-4-ium-3-olate (**1**) against symmetrically-substituted [1-phenyl-1*H*-pyrrole-2,5-dione (**3**) and dimethyl maleate (**4**)] and asymmetrically-substituted [(*E*)-(2-nitrovinyl)benzene (**5**), acrylonitrile (**6**), and but-3-en-2-one (**7**)] olefinic dipolarophiles (Figure 4.1) has been thoroughly investigated, leading to 1:1-cycloadducts that readily incorporate a polyheteroatomic core. Some

reactions involving asymmetrical dipolarophiles (*vide infra*) have proven to be highly stereoselective and completely regioselective.

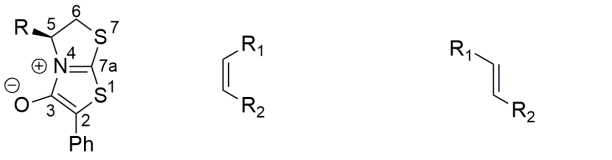

1 R = H
2 R = ^{i}Pr
3 R^1, R^2 = CON(Ph)CO
4 R^1 = R^2 = CO_2Me
5 R^1 = NO_2; R^2 = Ph
6 R^1 = CN; R^2 = H
7 R^1 = COMe; R^2 = H

Figure 4.1. Structures of the thioisomünchnones **1** and **2** and the dipolarophiles employed in this work (**3**-**7**).

The reaction of **1** and **3**, conducted in CH_2Cl_2 solution at room temperature, afforded after 24 h a mixture of the 6,8-diphenyldihydro-2*H*-6,9*b*-epithiopyrrolo[3,4-*c*]thiazolo[3,2-*a*]pyridine-5,7,9(3*H*,8*H*,9a*H*)-triones **8** and **9**, which was stable enough to be purified and isolated by crystallization in moderate yields (43% and 28%, respectively). These adducts could not be separated, however, when the reaction was carried out in toluene at reflux, as the latter evolved into a complex mixture. As we shall see later, the formation under such conditions of a fluorescent product, detected by TLC analysis, is noteworthy.

Crystals of cycloadducts **8** and **9**, suitable for X-ray diffraction analysis, could be obtained by recrystallization and slow evaporation, and their unequivocal structures are shown in Figure 4.2.

^{1}H and ^{13}C NMR analysis are consistent with such structures and some signals possess also diagnostic value, thereby aiding the elucidation and structural correlations in these polycyclic system. The *exo* H-6a and H-9a protons of **8** show downfield shifts (4.55 and 4.30 ppm, respectively) relative to the corresponding *endo*-hydrogens of **9** (4.30 and 4.08 ppm, respectively). Moreover, the coupling constant $J_{6a,9a}$ (8.5 Hz for **8** and 7.0 Hz for **9**) allows a valuable inspection of the stereochemical course (*vide infra*).

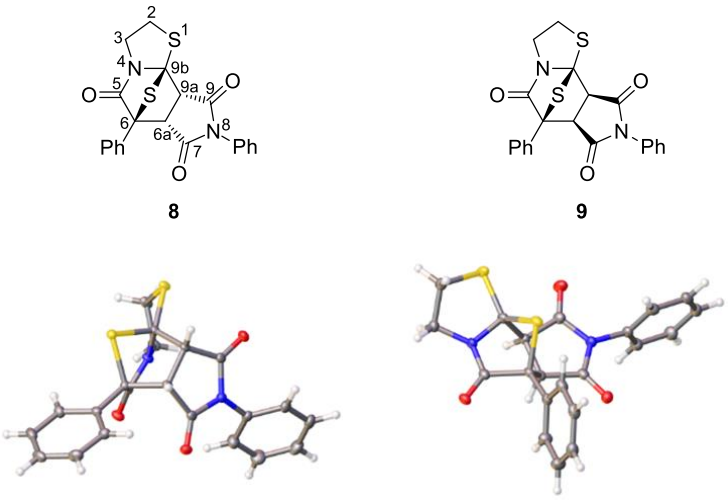

Figure 4.2. Structures **8** and **9** and its solid-state structures (X-ray diffractometry). Ellipsoids are shown at 50% probability.

As mentioned previously, a mixture of cycloadducts **8** and **9** heated in refluxing toluene in the presence of silica gel as catalyst afforded a fluorescent *tricyclic* pyrid-2-one (**10**). This substance could further be purified by crystallization and isolated in 54% yield.

By refluxing in toluene a mixture of **1** and **4** for 4 h, which was subsequently cooled to room temperature, the *exo* cycloadduct dimethyl 5-oxo-6-phenylhexahydro-6,8a-epithiothiazolo[3,2-*a*]pyridine-7,8-dicarboxylate (**11**) crystallized spontaneously (71% yield). Its structure was unambiguously determined by X-ray diffraction analysis (Figure 4.3). In contrast, the minor *endo* cycloadduct **12** could not be isolated. The *endo* H-7 and H-8 protons of **11** appeared as two doublets at 4.11 and 3.74 ppm ($J_{7,8}$ 9.0 Hz).

When cycloadduct **11** was heated at reflux in toluene for prolonged time (80 h) with silica gel as heterogeneous catalyst, a new fluorescent compound appeared in the reaction mixture, whose structure was tentatively assigned to dimethyl 5-oxo-6-phenyl-3,5-dihydro-2*H*-thiazolo[3,2-*a*]pyridine-7,8-dicarboxylate (**13**). Unfortunately, all attempts to get this substance in pure form failed.

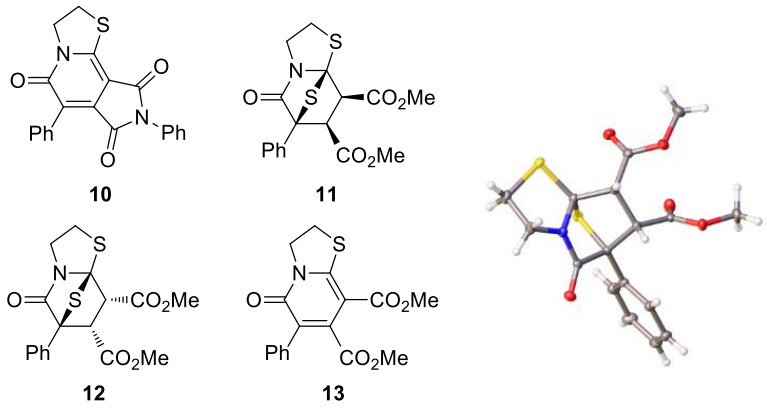

Figure 4.3. Structures of **10**-**13** and crystal structure of cycloadduct **11** depicted at 50% ellipsoid probability.

Although the cycloaddition of **1** with non-symmetrical alkenes (**5**-**7**) would afford four cycloadducts in every case, the reaction of **1** and **5** (1:1.5 molar ratio) in CH_2Cl_2 at room temperature for 72 h selectively gave rise to 8-nitro-6,7-diphenyltetrahydro-6,8a-epithiothiazolo[3,2-*a*]pyridin-5(6*H*)-one (**14**) in 63% yield, whose structure could be verified by single crystal X-ray diffraction (Figure 4.4). The *endo* H-7 and *exo* H-8 protons of **14**, which resonated as two doublets ($J_{7,8}$ 4.5 Hz) at 4.54 and 5.78 ppm, respectively, correlated well (HSQC experiment) with the corresponding peaks of C-7 (57.0 ppm) and C-8 (97.8 ppm) carbon atoms, while the C-6 and C-8a bridgehead carbon atoms resonated at 77.3 and 86.2 ppm, respectively.

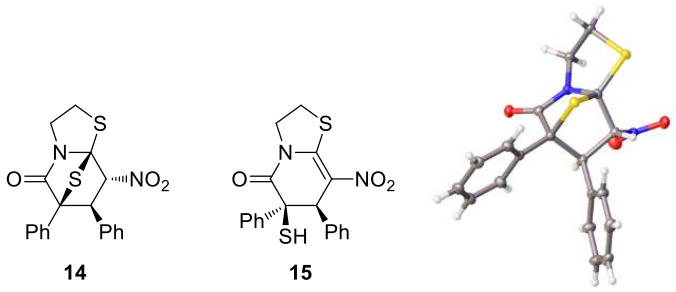

Figure 4.4. Structures **14** and **15** and crystal structure of cycloadduct **14** depicted at 50% ellipsoid probability.

A solution of **14** in CH_2Cl_2 kept at room temperature for several days led to the formation of 6-mercapto-8-nitro-6,7-diphenyl-6,7-dihydro-2*H*-thiazolo[3,2-*a*]pyridin-5(3*H*)-one (**15**) (52% yield). This conversion was essentially complete within 19 h by refluxing a solution of **14** in CH_2Cl_2 containing silica gel. Two singlet signals at 2.33 ppm and 5.33 ppm, attributale to the SH and H-7 protons respectively, along with chemical shifts characteristic of C-6, C-7, C-8, and C-8a carbon atoms (60.0, 50.5, 126,4, and 154,4 ppm, respectively) confirmed the structure of **15**.

The cycloaddition of **1** with acrylonitrile (**6**) was carried out at room temperature using the dipolarophile itself as solvent. After 24 h the mixture was quenched and two major cycloadducts could be isolated by column chromatography in low yield (18 and 20% for **16** and **17** respectively). Suitable crystals for X-ray diffraction analysis allowed us to identify them as 5-oxo-6-phenylhexahydro-6,8*a*-epithiothiazolo[3,2-*a*]pyridine-8-carbonitriles **16** and **17** (Figure 4.5).

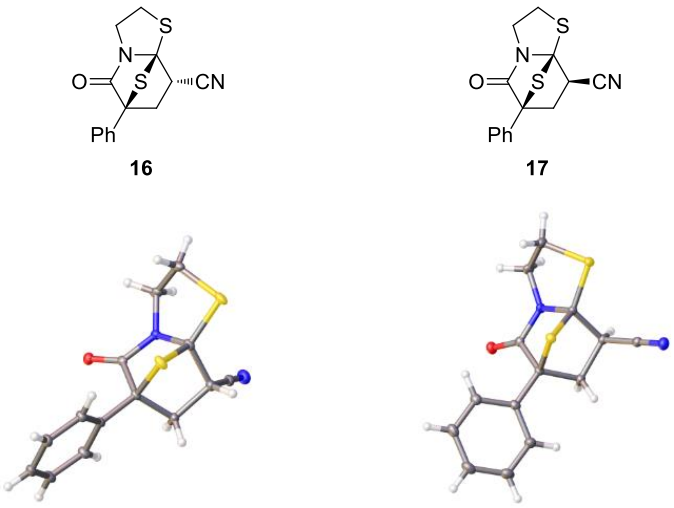

Figure 4.5. Structures of **16** and **17** and its crystal structures. Ellipsoids are shown at 50% probability.

The more relevant difference observed in the ^{1}H NMR spectra of **16** and **17** correspond to the chemical shifts of their H-8 protons that appeared as double doublets at 3.96 ppm (**16**) and 3.56 pm (**17**). Also, the coupling constants measured in such signals (J = 4.0 and 10.0 Hz for **16** and J = 3.5 Hz and 8.0 Hz for **17**) have diagnostic value.

On refluxing for 30 min a mixture containing **1** and but-3-en-2-one (**7**), compound **18**, 8-acetyl-6-[(3-oxobutyl)thio]-6-phenyl-6,7-dihydro-2*H*-thiazolo[3,2-*a*]pyridin-5(3*H*)-one, could be isolated in 32% yield. Again, adequate crystals for X-ray diffractometry revealed the unambiguous structure shown in Figure 4.6. The formation of **18** can be judiciously rationalized in terms of a conjugate addition involving the non-isolated thiol **19** plus an additional molecule of but-3-en-2-one.

The *exo* cycloadduct **20** could also be isolated from the reaction mixture by column chromatography in 22% yield. Its ^{1}H NMR spectrum indicated that the H-8 proton resonates at lower field (4.99 ppm) than the corresponding H-8 protons of **16** and **17**. Moreover, its coupling constants are smaller than those measured in the proton spectrum of **17** (J = 2.5 Hz and 6.5 Hz).

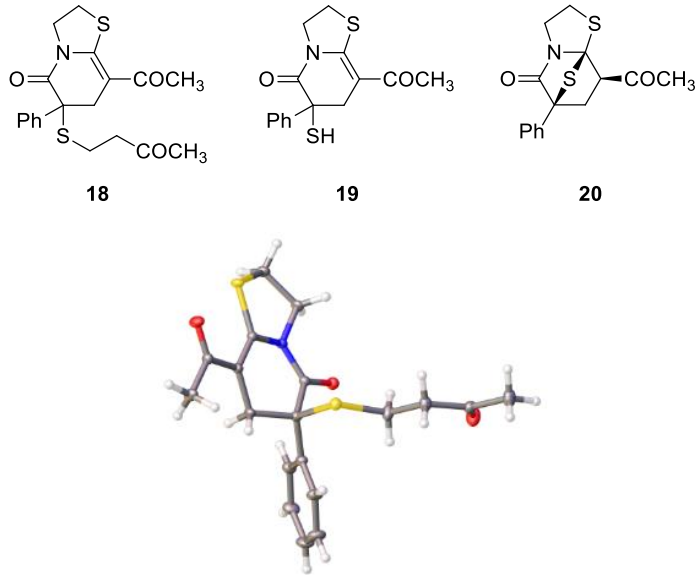

Figure 4.6. Structures **18**-**20** and solid-state structure of compound **18**. Thermal ellipsoids are shown at 50% probability.

In a recent computational study we have shown that the size of the dipolarophile is a key feature in facial stereocontrol as inferred from an isopropyl group attached to *unichiral*[13] thioisomünchnone **2**.[12] To prove this concept further, this work now enlarges the scope of cycloadditions of **2** with other bulky dipolarophiles like **3** and **5**. The cycloaddition of **2** with

1-phenyl-1*H*-pyrrole-2,5-dione (**3**) was performed under the same conditions described above for the reaction of **1** and **3**. In this case the TLC analysis of the reaction crude showed the formation of several products, however, only the enantiomerically pure *exo*-cycloadducts **21** and **22** could be isolated by fractionated crystallization in 72% and 15% yield, respectively. Once again, single-crystal X-ray analysis proved to be instrumental in structural elucidation and Figure 4.7 shows the solid-state structure of (3*S*,6*R*,6*aR*,9*aS*,9*bR*)-3-isopropyl-6,8-diphenyldihydro-2*H*-6,9*b*-epithiopyrrolo[3,4-*c*]thiazolo[3,2-*a*]pyridine-5,7,9(3H,8H,9*a*H)-trione (**22**). Its ^{1}H and ^{13}C NMR data were quite similar to those of **21**. Thus, ^{1}H NMR spectra of **21** and **22** showed doublet signals at ~4.1 ppm (H-6a) and ~3.8 ppm (H-9a) with coupling constants ($J_{6a,9a}$ = 7.0 Hz) identical to those found in the ^{1}H NMR spectrum of **9**.

As described before for the transformation of **11** into **13**, cycloadducts **21** and **22** were converted in refluxing toluene containing silica gel into enantiopure (*S*)-3-isopropyl-6,8-diphenyl-2,3-dihydropyrrolo[3,4-*c*]thiazolo[3,2-*a*]pyridine-5,7,9(8*H*)-trione (**23**) in 37 % yield.

On the other hand, the chiral dipole **2** reacted with (*E*)-(2-nitrovinyl)benzene (**5**) (1:1.1 ratio) in CH_2Cl_2 at room temperature for 30 h, to give (3*S*,6*S*,7*R*,8*R*,8*aS*)-3-isopropyl-8-nitro-6,7-diphenyltetrahydro-6,8*a*-epithiothiazolo[3,2-*a*]pyridin-5(6*H*)-one (**24**) in 78% yield. However, starting from a 1:1.5 (dipole:dipolarophile) ratio a mixture of **24** (33%) and the thioether derivative **25** (22%) was isolated after 48 h. The origin of the latter might reasonably be interpreted by spontaneous breakage of the C_{8a}-S bond in **24** followed by nucleophilic addition of the SH group of **26** on the *Si* face of an extra molecule of **5**, as discussed above for the reaction of **1** with but-3-en-2-one (**7**). Moreover, the structure of **25** was determined by X-ray diffraction analysis (Figure 4.8).

In order to demonstrate unequivocally that cycloadduct **24** arises from the reaction of **2** and **5**, a solution of **24** and **5** (1:1 molar ratio) was stirred in CH_2Cl_2 for five days, leading to a complex mixture from which only the Michael-type adduct **25** could be isolated. Furthermore, a solution of **24** in refluxing CH_2Cl_2 in the presence of silica gel for 72 h did not afford thiol **26**; instead compound **25** was isolated again, thereby revealing that retro-cycloaddition of **24** releases the dipolarophile, which reacts then with **24** to give **25**. These results clearly evidence the role of bulky dipolarophiles in stereocontrolled cycloadditions with a chiral thioisomünchnone such as **2**.

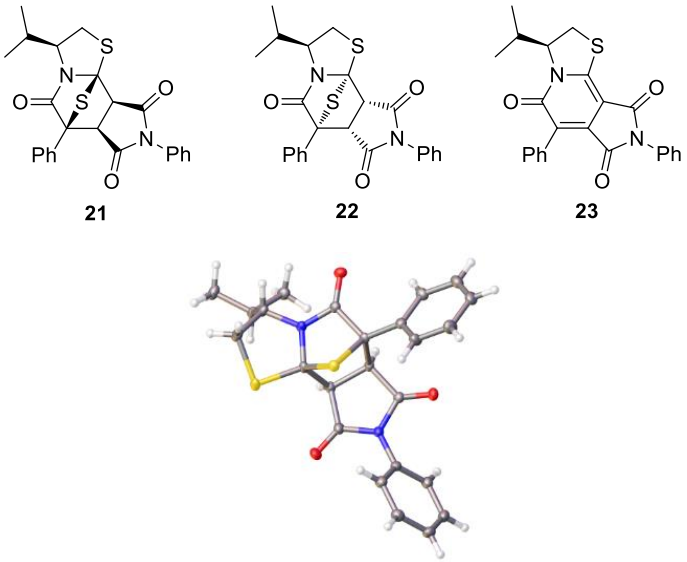

Figure 4.7. Structures **21**-**23** and crystal structure of **22** with thermal ellipsoids at 50% probability.

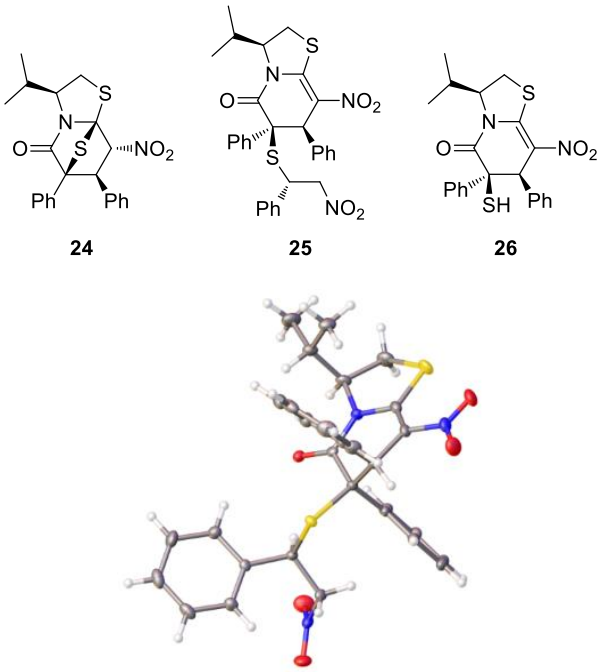

Figure 4.8. Structures **24**-**26** and crystal structure of **25** with thermal ellipsoids depicted at 50% probability.

4.3.2. Computational analysis

Firstly, we have addressed the influence exerted by dipolarophiles on the 1,3-dipolar cycloadditions of thioisomünchnone **1** with compounds **3**-**7**. All the reactions were simulated at the M06-2X/6-311++G(d,p) level using the continuous solvation model (SMD) in the solvent employed experimentally. Accordingly, the reactions with 1-phenyl-1*H*-pyrrole-2,5-dione (**3**) and (*E*)-(2-nitrovinyl)benzene (**5**) were simulated in CH_2Cl_2, whereas the reaction with dimethyl maleate (**4**) was evaluated in toluene. Because of the reactions with acrylonitrile (**6**) and but-3-en-2-one (**7**) were carried out under neat conditions using such dipolarophiles as solvents, their role was simulated computationally by means of 2-propanol and *N*,*N*-dimethylacetamide, respectively.

The reactions of **1** with symmetrical dipolarophiles **3** and **4** are highly concerted processes that could lead to *endo* cycloadducts **8** and **12** and/or to their *exo* isomers **9** and **11**, respectively. Both *endo* and *exo* approaches of **3** to thioisomünchnone **1** are characterized by very similar energy barriers. This small energy difference clearly accounts for the experimental isolation of both diastereomers (Figure 4.9, left). In stark contrast, the reaction of **1** with **4** is more selective (Figure 4.9, right) and formation of diastereomer **11**, experimentally isolated, constitutes the most favorable process.

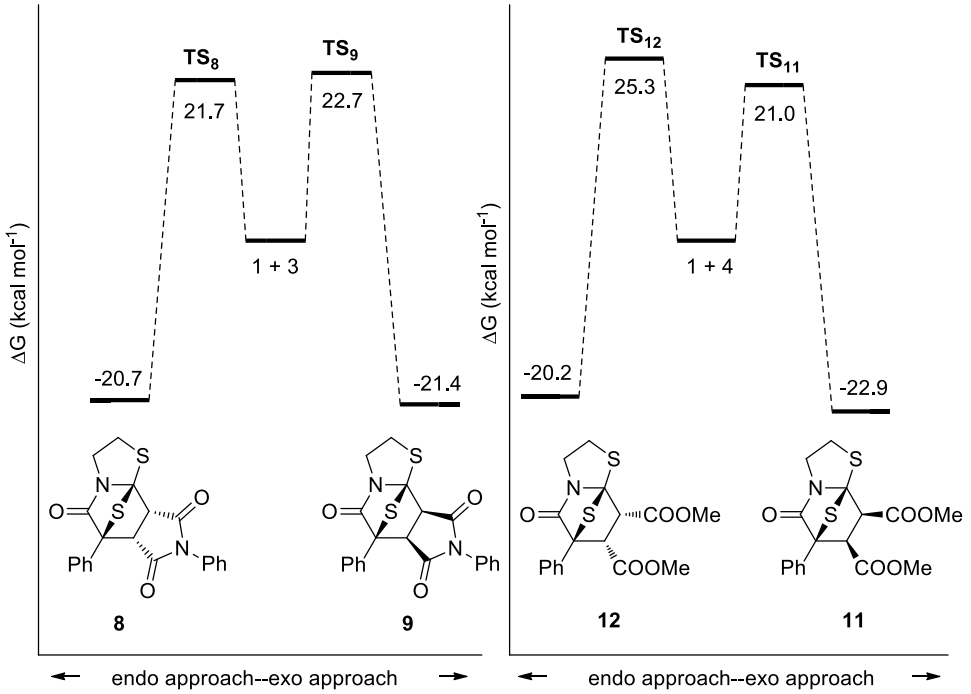

Figure 4.9. Relative free energy values (Δ*G*, kcal mol^{-1}) of all stationary points involved in both *endo* and *exo* approaches of **1** to **3** and **4**, calculated at the M06-2X/6-311++G(d,p) level in CH_2Cl_2 for **3** and toluene for **4** (SMD).

In order to understand the enhanced reactivity of dimethyl maleate (**4**) during its *exo* approach to dipole **1** (**TS$_{11}$**), we compared the main NBO (*natural bond orbital*)[14] interactions of the four saddle points **TS$_8$**, **TS$_9$**, **TS$_{11}$**, **TS$_{12}$**. Figures 4.10 and 4.11 shows the optimized geometries of such saddle points together with the two main orbital interactions for each structure. The most concerted cycloadditions were found for 1-phenyl-1*H*-pyrrole-2,5-dione (**3**), whereas the cycloadditions with dimethyl maleate are slightly more asynchronous. The donation process (from dipole to dipolarophile) in the four saddle points involves the same orbitals [LP_{C2} of the dipole as donor and the π* of the dipolarophile as acceptor], where the strongest interaction corresponds to **TS$_{12}$** and the weakest one to **TS$_{11}$**. On the other hand, the back-donation interactions for saddle points **TS$_8$**, **TS$_9$** and **TS$_{12}$** are weaker than the corresponding donation processes and involve the same orbitals as well, namely the π orbital of the dipolarophile as donor and the $\pi^*_{C7a\text{-}N4}$ of the dipole as

acceptor. The behavior is reversed in the most favored approach of dimethyl maleate (**TS_{11}**), for which the back-donation is markedly higher than the opposite interaction, where the acceptor orbital is the empty lone pair of the C7a carbon atom (LV_{C7a}).

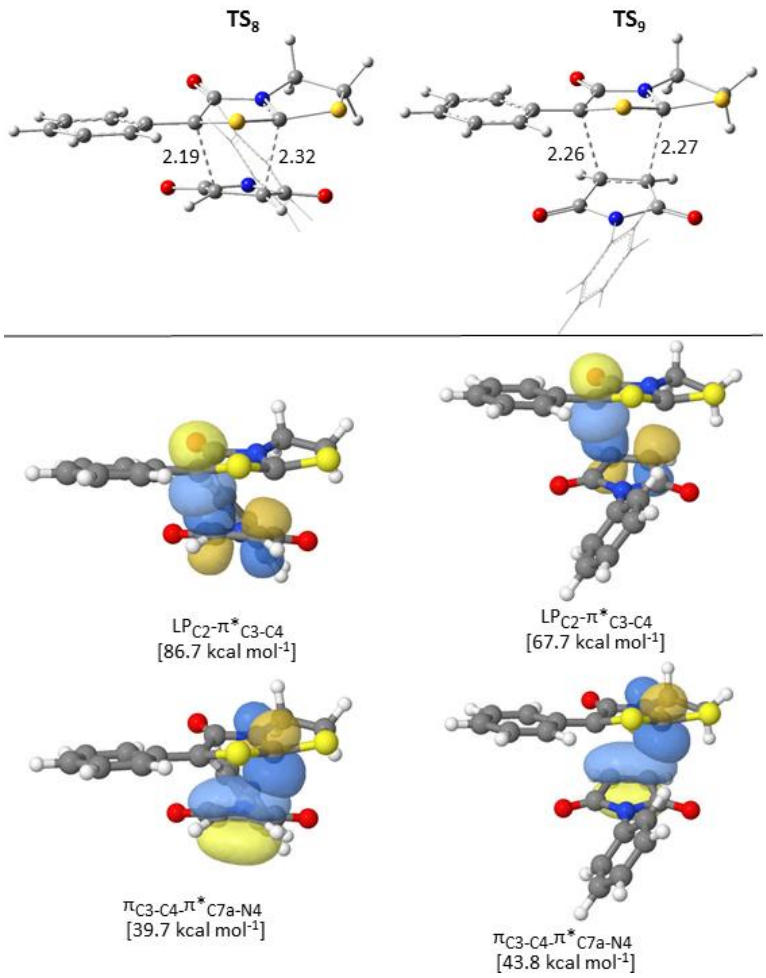

Figure 4.10. Optimized geometries of saddle points **TS_8** and **TS_9** at the M06-2X/6-311++G(d,p)-level in CH_2Cl_2 (SMD). Bond distances are given in angstroms. The highest values of charge transfer found in the four saddle points are given in kcal mol^{-1}.

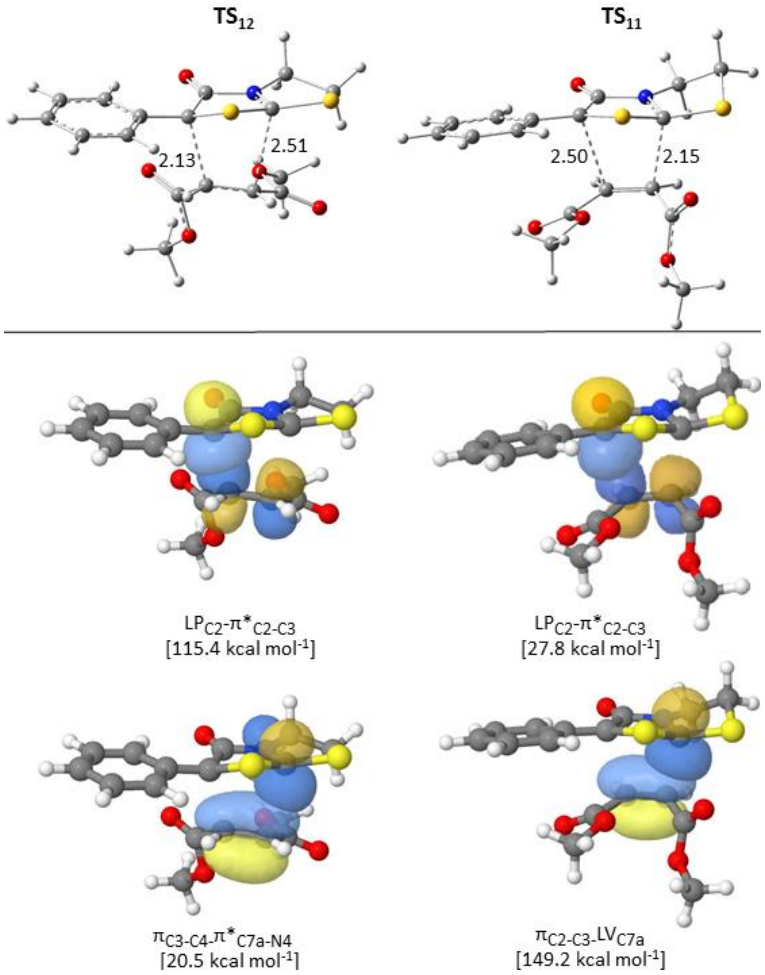

Figure 4.11. Optimized geometries of saddle points **TS$_{11}$** and **TS$_{12}$** at the M06-2X/6-311++G(d,p)-level in toluene (SMD). Bond distances are given in angstroms. The highest values of charge transfer found in the four saddle points are given in kcal mol^{-1}.

As noted in our preceding synthetic analysis, the reaction of **1** with unsymmetrical dipolarophiles (**5**-**7**) would afford up to four cycloadducts in every case: **14** and **27**-**29** from [(*E*)-(2-nitrovinyl)benzene (**5**); **16**, **17**, **30**, and **31** from acrylonitrile (**6**); and **20** and **32**-**34** from but-3-en-2-one (**7**).

Figure 4.12 shows the free energy barriers for the four competitive approaches of **1** and **5** in CH_2Cl_2. The results indicate that cycloadducts **14** and **27** should be generated through

a two-step mechanism whose first stage is the rate-limiting step. This stepwise mechanism is energetically favored with respect to the concerted mechanism leading to regioisomers **28** and **29**. The formation of **14** is kinetically favored with respect to that of **27** by ~3 kcal mol^{-1}, in good agreement with experimental results.

The characterization of zwitterionic intermediates in cycloaddition reactions, like $\mathbf{I_{14}}$ and $\mathbf{I_{27}}$, have been found recently.[15] Herein, in the reaction with (*E*)-(2-nitrovinyl)benzene (**5**), the high electron withdrawing power owing to the nitro group allows to concentrate a high electron charge and stabilizes the intermediates. The electrostatic potential maps of these two zwitterionic intermediates can be seen in Figure 4.12, where the electron density is highly localized in the nitro groups.

The four approaches of acrylonitrile (**6**) to thioisomünchnone **1** are concerted cycloadditions, albeit they proceed with different levels of asynchronicity (Figure 4.13). Thus, the formation of cycloadducts **30** and **31** occurs through more concerted pathways than the rest, although they are also energetically disfavored, pointing to a regioselective cycloaddition, in close mimicry to the cycloaddition of **1** and **5**.

The most asynchronous saddle point ($\mathbf{TS_{16}}$) is practically as stable as its diastereomer $\mathbf{TS_{17}}$ ($\Delta\Delta G^{\ddagger}$ 0.66 kcal mol^{-1}), thereby suggesting a non-diastereoselective cycloaddition as it was demonstrated experimentally.

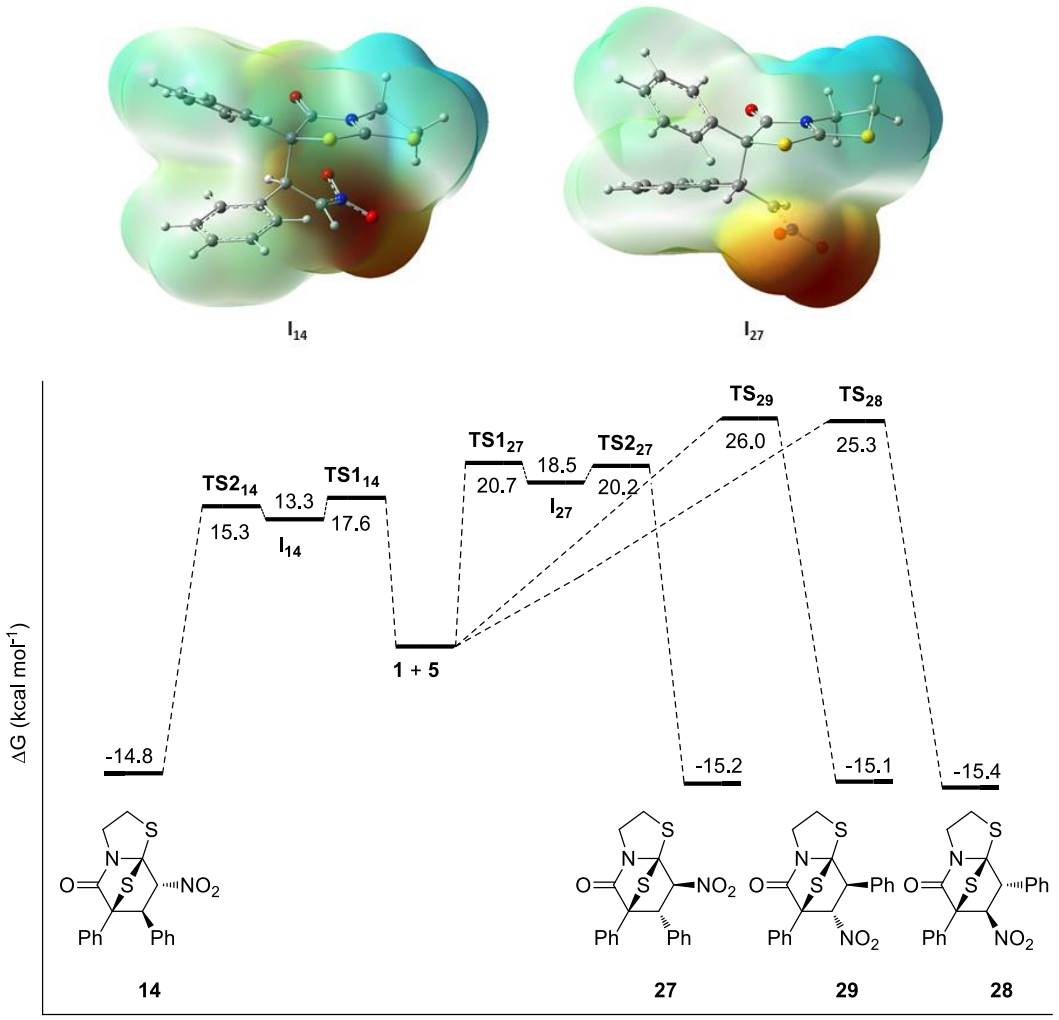

Figure 4.12. Relative free energy values (Δ*G*, kcal mol^{-1}) of all stationary points involved in the four possible reaction channels of **1** and **5** calculated at the M06-2X/6-311++G(d,p) level in CH_2Cl_2 (SMD method) (left). Elestrostatic potential maps for zwitterionic intermediates **I_{14}** and **I_{27}** (right).

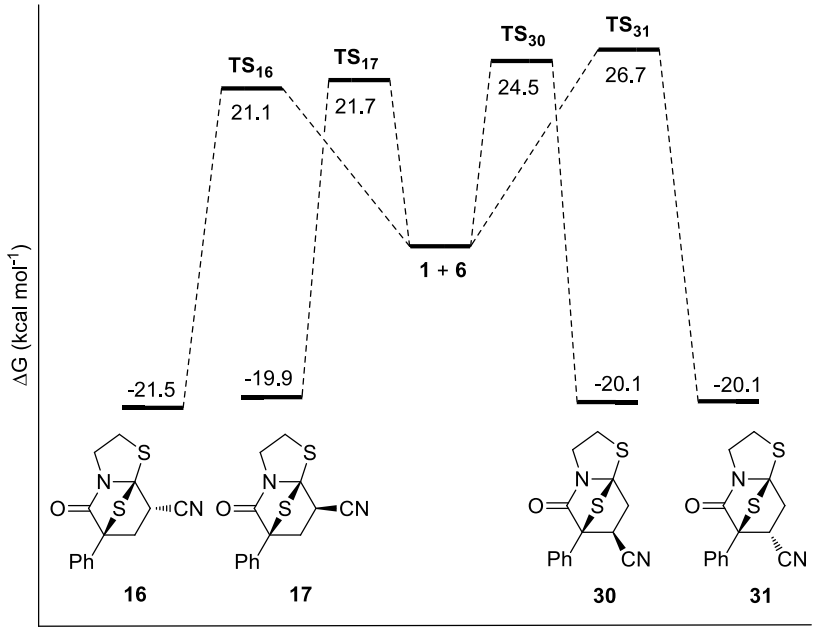

Figure 4.13. Relative free energy values (Δ*G*, kcal mol^{-1}) of all stationary points involved in the four possible reaction channels of **1** and **6** calculated at the M06-2X/6-311++G(d,p) level in *N*,*N*-dimethylacetamide (SMD method).

The energy landscape of the four reaction channels of **1** with but-3-en-2-one (**7**) (Figure 4.14) is likewise similar to those previously described for the cycloaddition with acrylonitrile (Figure 4.13). The reaction is regioselective because the more asynchronous saddle points (**TS$_{20}$** and **TS$_{32}$**) are more favored than their regioisomers **TS$_{33}$** and **TS$_{34}$**, although the calculated $\Delta\Delta G^{\ddagger}$ [$\Delta G^{\ddagger}$(**TS$_{20}$**) - $\Delta G^{\ddagger}$(**TS$_{32}$**) < 1 kcal mol^{-1}] value would justify the lack of diastereoselectivity and the formation of both cycloadducts (**20** and **32**) in similar ratio. Moreover, this finding suggests that the formation of thioether **18** should most likely arise from the evolution of cycloadducts **20** and **32**.

Our computational study shows that the cycloadditions of asymmetrical dipolarophiles **5**, **6** and **7** with **1** are regioselective. Moreover, the *endo* approaches for this regiochemistry are favored, albeit to a lesser extent. In order to explain this selectivity we have compared the main orbital interactions present in the saddle points **TS1$_{14}$**, **TS$_{16}$** and **TS$_{32}$** (*endo* approaches of dipolarophiles **5**-**7** to dipole **1**) with those of the opposite regiochemistry, namely **TS$_{29}$**, **TS$_{31}$** and **TS$_{34}$**. Such geometries along with the main orbital interactions are

gathered in Figures 4.15, 4.16 and 4.17. The most favored approaches proceeding through **TS1$_{14}$**, **TS$_{16}$** and **TS$_{32}$** exhibit a high charge transfer in the direction dipole-dipolarophile, whereas the corresponding back-donation is irrelevant. On the other hand, the less favored attacks occurring through **TS$_{29}$**, **TS$_{31}$** and **TS$_{34}$** exhibit a similar behavior to those of **TS$_{11}$** (see Figure 4.11), where the back-donation dictates the charge transfer process.

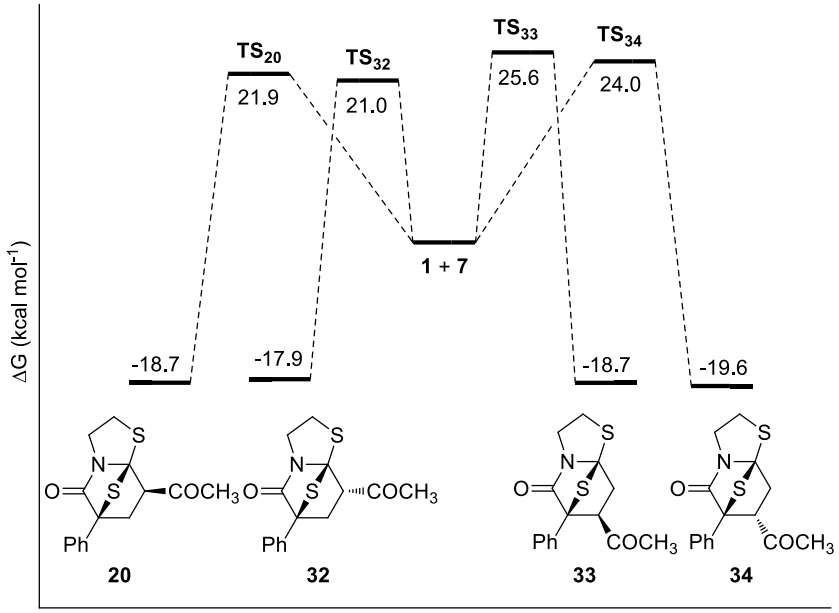

Figure 4.14. Relative free energy values (Δ*G*, kcal mol^{-1}) of all stationary points involved in the four possible approaches of **1** and **7** calculated at the M06-2X/6-311++G(d,p) level in 2-propanol (SMD method).

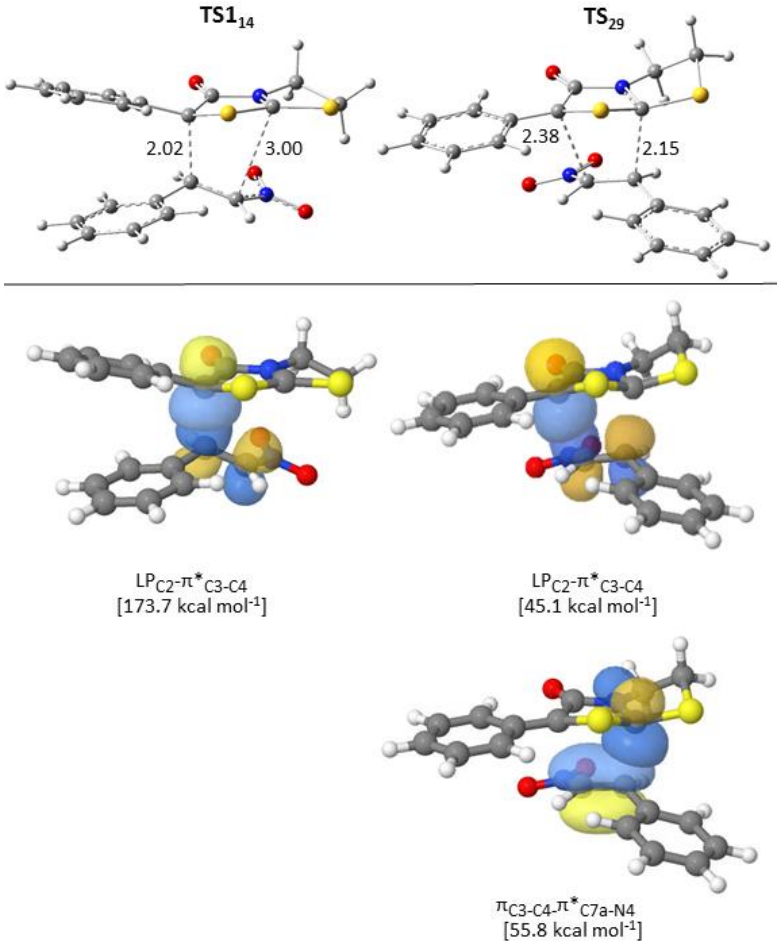

Figure 4.15. Optimized geometries for saddle points **TS1$_{14}$** and **TS$_{29}$** at the M06-2X/6-311++G(d,p)-level in CH_2Cl_2 (SMD). Bond distances are given in angstroms. The highest values of charge transfer found in the four saddle points are given in kcal mol^{-1}.

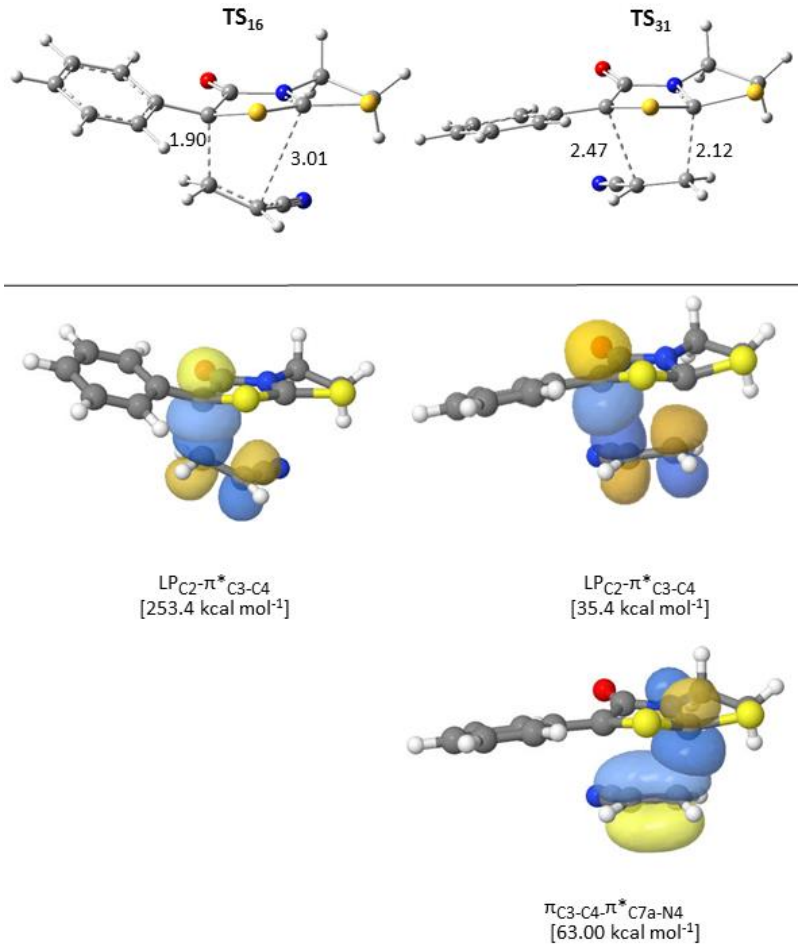

Figure 4.16. Optimized geometries for saddle points **TS_{16}** and **TS_{31}** at the M06-2X/6-311++G(d,p)-level *N*,*N*-dimethylacetamide (SMD). Bond distances are given in angstroms. The highest values of charge transfer found in the four saddle points are given in kcal mol^{-1}.

It is worth pointing out that although the formation of **16** and **32** are concerted cycloadditions, the geometry of their saddle points **TS_{16}** and **TS_{32}** is quite similar to that of **$TS1_{14}$**, which corresponds to a stepwise process. Furthermore, the interaction energy is even higher for the cycloaddition with acrylonitrile (**TS_{16}**) (see Figures 4.15, 4.16 and 4.17).

The IRC (intrinsic reaction coordinate) analyses for saddle points **TS_{16}** and **TS_{32}** show a caldera-like region with a pronounced depression of the energy gradient. The geometries for such structures are quite similar to **$TS2_{14}$**, which corresponds to the second saddle point of the stepwise cycloaddition of **1** with (*E*)-(2-nitrovinyl)benzene (**5**). Also the back-donation courses are similar both in orbital composition and interaction energies. In this case the lowest charge transfer was obtained in the cycloaddition with acrylonitrile (**6**) (Figure 4.18).

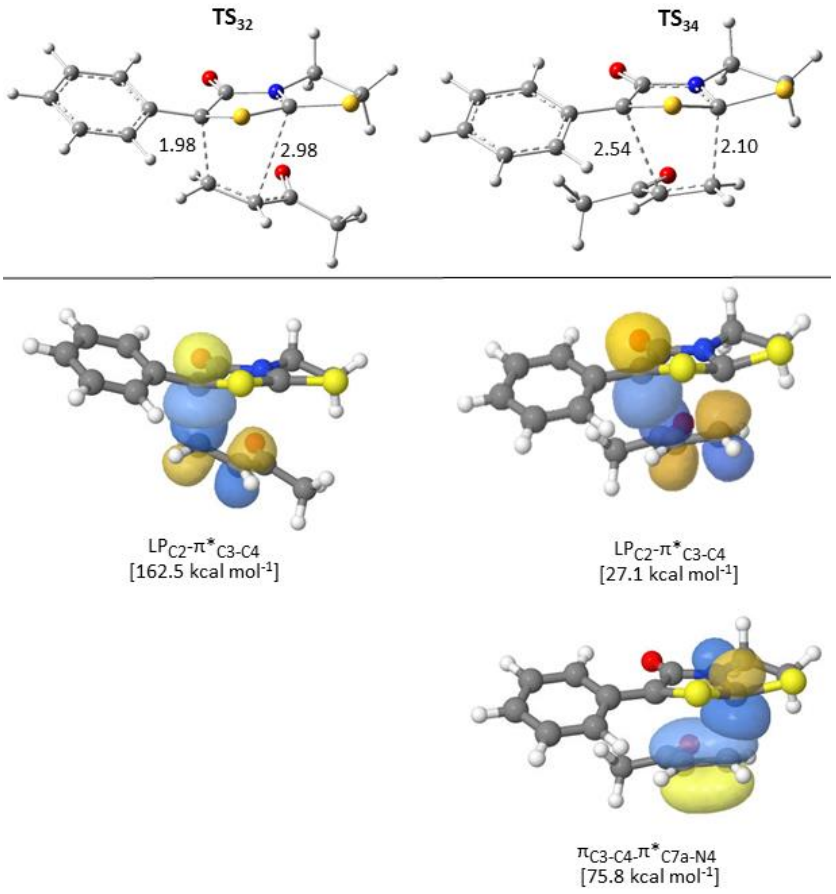

Figure 4.17. Optimized geometries for saddle points **TS_{32}** and **TS_{34}** at the M06-2X/6-311++G(d,p)-level in 2-propanol (SMD). Bond distances are given in angstroms. The highest values of charge transfer found in the four saddle points are given in kcal mol^{-1}.

In order to assess the facial stereocontrol induced by the chiral thioisomünchnone (**2**) with the bulkiest symmetrical and asymmetrical dipolarophiles employed in this work (**3** and **5**), we have considered the formation of all the possible diastereomers, i.e. up to four in the cycloaddition with 1-phenyl-1*H*-pyrrole-2,5-dione (**21**, **22**, **35**, and **36**) and up to eight with (*E*)-(2-nitrovinyl)benzene (**24**, and **37**-**43**).

Figure 4.19 shows the energy barriers for the four approaches of **2** and **3**, leading to cycloadducts **21**, **22**, **35**, and **36**. The *exo*-approaches of **3** to the 2-*Re*,7a-*Re* and 2-*Si,7a*-*Si* faces of **2** would afford **21** and **22**, respectively, through the corresponding saddle points $\mathbf{TS_{21}}$ and $\mathbf{TS_{22}}$, whereas **35** and **36** would form, via $\mathbf{TS_{35}}$ and $\mathbf{TS_{36}}$, as a result of the *endo*-approaches of **3** to the 2-*Re*,7a-*Re* and 2-*Si,7a*-*Si* faces of **2**. All cycloadditions are very concerted processes and the free energies computed for $\mathbf{TS_{21}}$, $\mathbf{TS_{22}}$ and $\mathbf{TS_{35}}$ are similar to those found for $\mathbf{TS_8}$ and $\mathbf{TS_9}$ (Figure 4.9). The highest energy barrier corresponds to the formation of the *endo* cycloadduct **36**, where the approach of the 1*H*-pyrrole-2,5-dione ring lies near the isopropyl group ($\mathbf{TS_{36}}$) exerting a marked steric effect. However, the isopropyl group does not affect significantly the *exo* approach of **3** to the same face (2-*Si,7a*-*Si*) of the mesoionic ring ($\mathbf{TS_{22}}$) (*vide infra*), a fact which manifests itself in a lower energy barrier and explains the isolation of cycloadduct **22**.

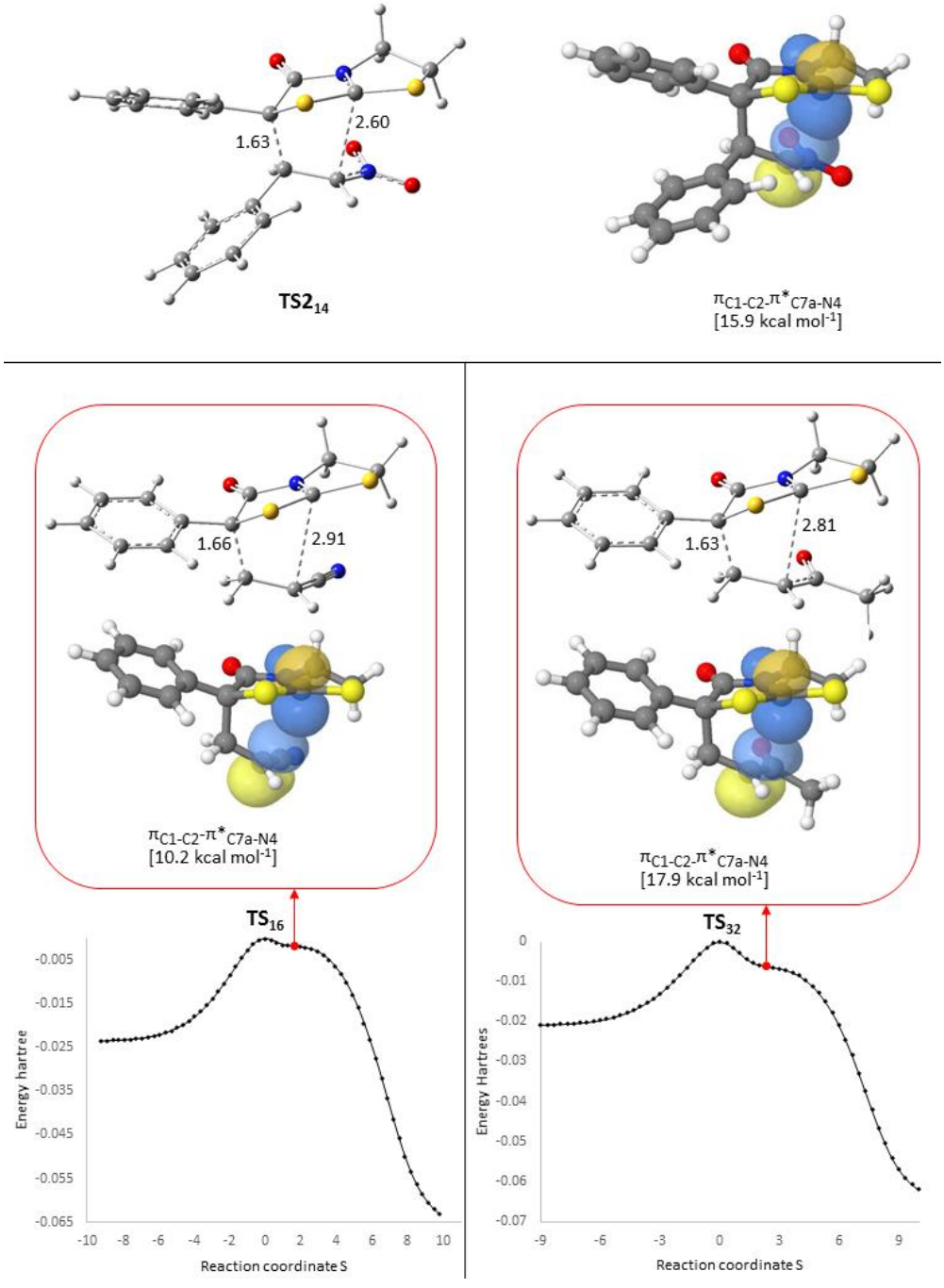

Figure 4.18. IRC analyses for saddle points **TS$_{16}$** (left) and **TS$_{32}$** (middle). The geometries for the lowest gradient in the caldera-type region are depicted as well together with NBO interactions during the back-donation. The optimized geometry for **TS2$_{14}$** at the M06-2X/6-311++G(d,p)-level in CH_2Cl_2 (SMD) and the back-donation interaction are shown on the right.

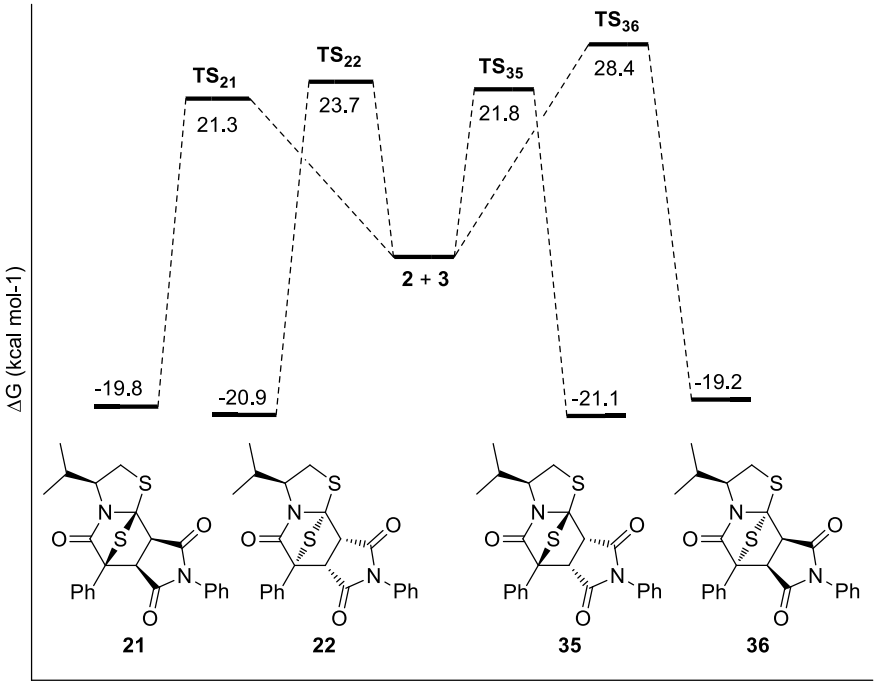

Figure 4.19. Relative free energy values (Δ*G*, kcal mol^{-1}) of all stationary points involved in the *endo* and *exo* approaches of **2** and **3** calculated at the M06-2X/6-311++G(d,p) level in CH_2Cl_2 (SMD method).

A suitable algorithm for depicting, in qualitative form, the non-covalent interactions exerted by the bulky isopropyl group involves the use of the RDG (reduced density gradient)[16] function, whose 3D representation (reduced gradient multiplied by the sign of the second Hessian eigenvalue of the electron density plotted versus the electron density) allows an eye-catching visualization of the zones where such weak interactions take place. Figure 4.20 shows the 3D plots of the steric and Van der Waals interactions experienced by the isopropyl group during the approach of **3** to thioisomünchnone **2** through the 2-*Si,7a-Si* face (**TS$_{22}$** and **TS$_{36}$**). As shown in this Figure, the 1*H*-pyrrole-2,5-dione ring lies far from the isopropyl group in the *exo* approach (**TS$_{22}$**) and the small steric repulsion is offset by the Van der Waals interaction. This situation mismatches the graphical plot for **TS$_{36}$** where the imide ring lies in close proximity to the isopropyl group and the Van der Waals interactions do not offset such a substantial steric hindrance.

The energy gaps associated to the reaction of **2** with (*E*)-(2-nitrovinyl)benzene (**5**) are collected in Figures 4.21 and 4.22. Pathways involving the approach of **5** to the 2-*Re*,7a-*Re* face of **2** (Figure 4.21) are more favored processes than the corresponding approaches to the 2-*Si,7a-Si* face (Figure 4.22), thus highlighting the facial selection exerted by the isopropyl group on a bulky dipolarophile like **5**. Notably, the reaction channels facing carbon atoms C-2 and C-7a of **2** with C-2 and C-1 of **5**, respectively, are stepwise processes whereas the reaction pathways with the opposite regiochemistry are concerted, albeit energetically less favored, processes. Stepwise cycloadditions involving the 2-*Re*,7a-*Re* face of **2** have free energy barriers similar to those shown in Figure 11, while the processes involving the 2-*Si*,7a-*Si* face are somewhat less favorable from an energy viewpoint.

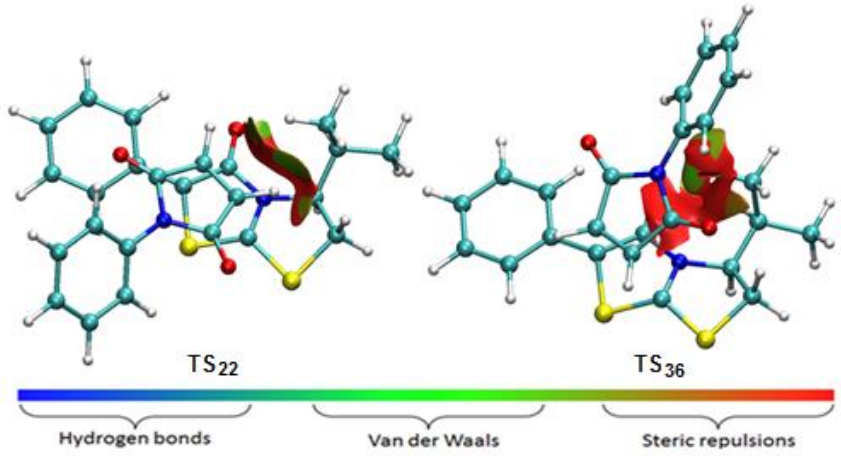

Figure 4.20. 3D Plots of the reduced density gradient (RDG) *versus* the electron density. Results are shown for the geometries of the transition structures **TS$_{22}$** and **TS$_{36}$** optimized at the M062X/6-311++g(d,p) level in CH_2Cl_2 (SMD).

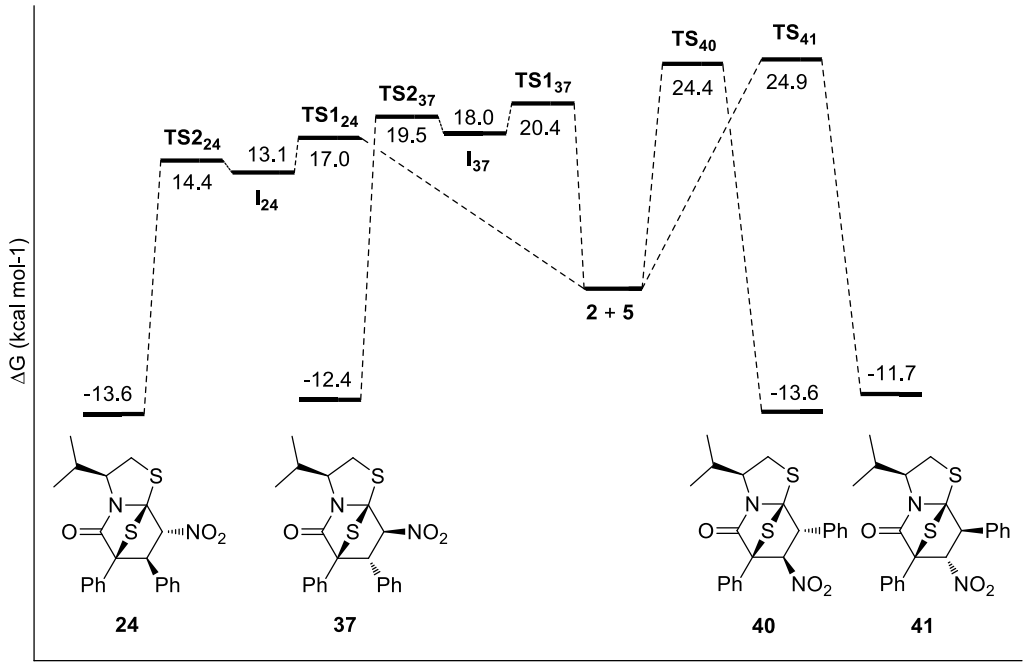

Figure 4.21. Relative free energy values (Δ*G*, kcal mol^{-1}) of all stationary points involved in the four approaches of **5** to the 2-*Re*,7a-*Re* face of **2** calculated at the M06-2X/6-311++G(d,p) level in CH_2Cl_2 (SMD method).

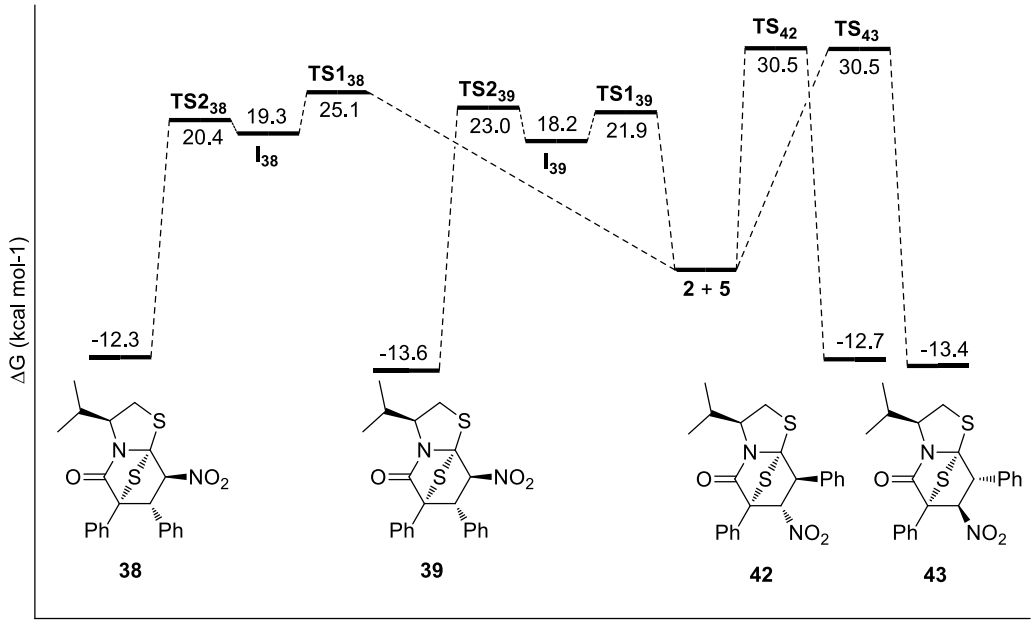

Figure 4.22. Relative free energy values (Δ*G*, kcal mol^{-1}) of all stationary points involved in the four approaches of **5** to the 2-*Si*,7a-*Si* face of **2** calculated at the M06-2X/6-311++G(d,p) level in CH_2Cl_2 (SMD method).

Among the cycloadditions computationally studied, the reaction of dipole **2** with (*E*)-(2-nitrovinyl)benzene appears to be the most selective process and predicts the formation of only one cycloadduct (**24**), thus corroborating the experimental results.

In order to gain further insight into the facial stereocontrol exerted by the isopropyl group of the chiral thioisomünchnone **2** in a quantitative manner, we employed the distortion/interaction model to quantify the distortion energies of the reactants when they approach both, to the 2-*Re*,7a-*Re* and 2-*Si*,7a-*Si* faces of **2**. The distortion/interaction or activation strain model have been widely employed for explaining reactivity in cycloaddition reactions, and to justify the selectivity of some dipolar cycloadditions.[17]

Figure 4.23 shows the distortion energies of the dipole (red) dipolarophiles (blue), interaction energies (green) and activation energies (black) for the saddle points calculated in the reactions of the dipole **2** with **3** (above) and **5** (below). The results obtained for the reaction with the 1-phenyl-1*H*-pyrrole-2,5-dione (**3**) shows that the distortion energies of the dipoles mirror the free energy barriers depicted in Figure 4.19, where the values for the transition structures $\mathbf{TS_{21}}$, $\mathbf{TS_{22}}$ and $\mathbf{TS_{35}}$ are quite similar each other. On the other hand, the saddle point $\mathbf{TS_{36}}$, which correspond with the *endo* approach of **3** to the 2-*Si*,7a-*Si* face of **2** shows a higher distortion energy.

The distortion energy of the dipole for the reaction with (*E*)-(2-nitrovinyl)benzene (**5**) also match with the free energy barriers obtained (Figures 4.21 and 4.22). The saddle points corresponding to the concerted cycloadditions show that the approach of **5** to the 2-*Si*,7a-*Si* face of **2** ($\mathbf{TS_{42}}$ and $\mathbf{TS_{43}}$) gives higher values of $\Delta G^{\ddagger}$ and distortion energy of the dipole than the approach of **5** to the 2-*Re*,7a-*Re* face of **2** ($\mathbf{TS_{40}}$ and $\mathbf{TS_{41}}$).

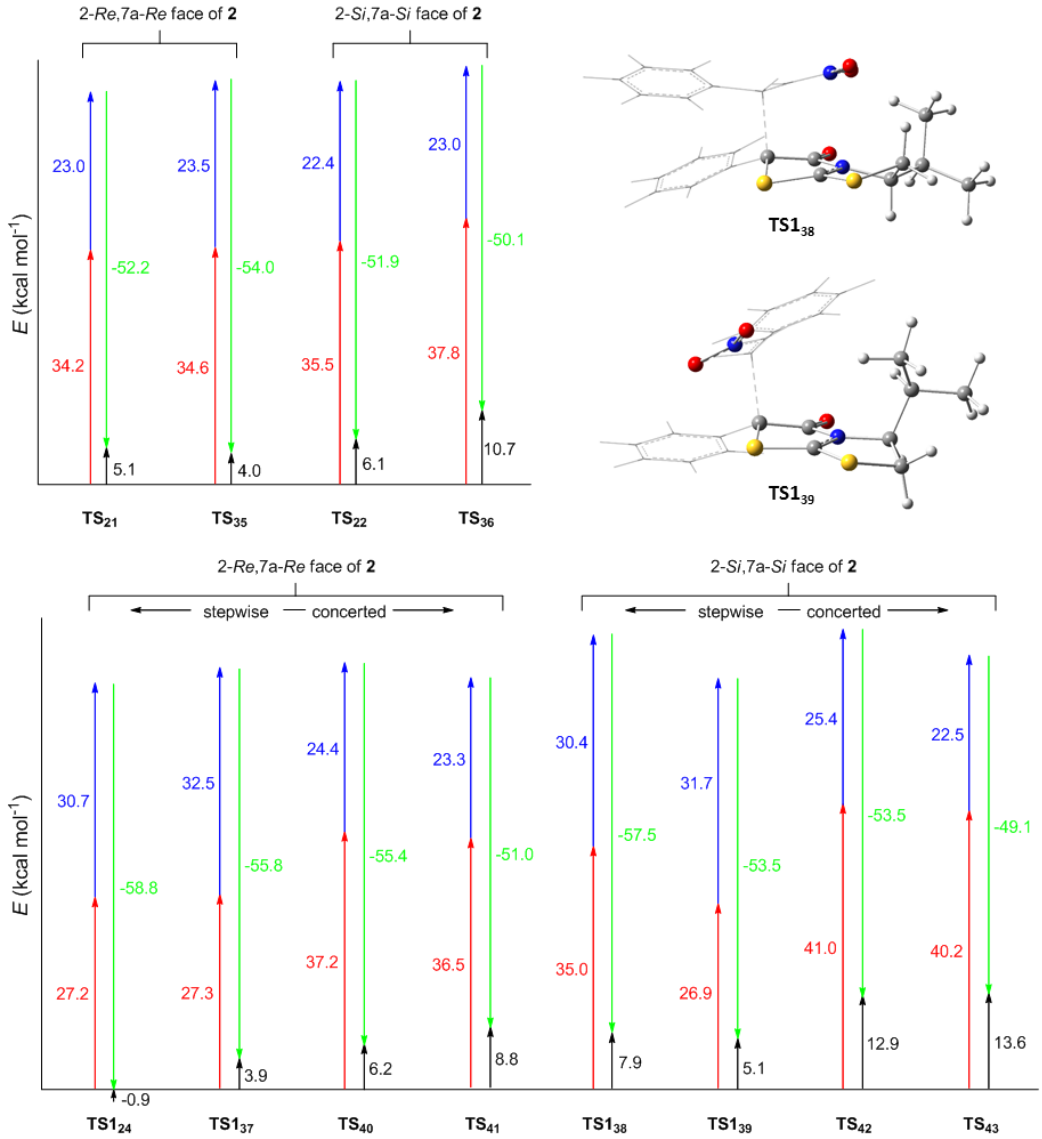

Figure 4.23. Distortion energies of the dipole (red) dipolarophiles (blue), interaction energies (green) and activation energies (black) for the reactions of the chiral thioisomünchnone **2** with the dipolarophiles **3** (above) and **5** (below). Optimized structures of the saddle points **TS1$_{38}$** and **TS1$_{39}$** at the M06-2X/6-311++G(d,p) level in CH_2Cl_2 (SMD method). For clarity the backbone of the dipole and the nitro group have been represented with balls and the rest of the molecules with wireframe.

On the other hand, the results obtained for the stepwise processes mirror to those of the reaction with 1-phenyl-1*H*-pyrrole-2,5-dione (**3**), where the *exo* approach of the dipolarophile to the 2-*Si*,7a-*Si* face of **2** (**TS1$_{39}$**) gives similar distortion energy of the dipole to those obtained for the approach to the contrary face (2-*Re*,7a-*Re*) (**TS1$_{24}$** and **TS1$_{37}$**). These differences in the distortion energy of the dipole for **TS1$_{38}$** and **TS1$_{39}$** can be visualized in Figure 4.23, where the *endo* approach of **5** to **2** in **TS1$_{38}$** makes the dipole to distort due to the proximity of the isopropyl to the nitro group.

We have noted previously that the reaction of thioisomünchnone **1** led to a thioether derivative (**18**) when reacted with but-3-en-2-one (**7**)**.** This behavior could also be detected in the reaction between the chiral dipole **2** and (*E*)-(2-nitrovinyl)benzene (**5**), where the enantiomerically pure thioether **25** comes, unequivocally, from the *endo* cycloadduct (**24**). Compound **25** could then be generated by conjugate addition of thiolate **45** or thiol **26** to one additional molecule of **5**. The intermediacy of **26** would require the abstraction of H-8 by the sulfur atom attached to C-6 in **45** (Scheme 4.1). Cycloadduct **14** could evolve in a similar way, although compound **46** was not detected experimentally.

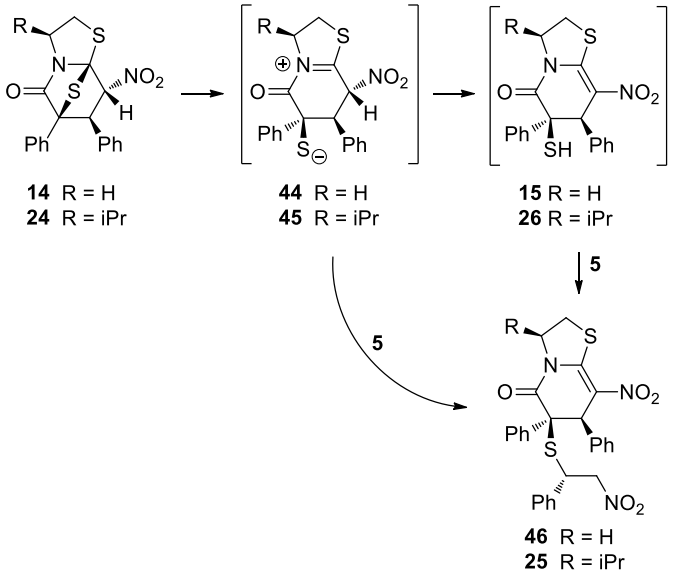

Scheme 4.1. Possible transformations of cycloadducts **14** and **24** to yield thiols **15** and **26** or thioethers **46** and **25**.

Figure 4.24 shows the reaction pathways for the formation of thiols **15** and **26** from cycloadducts **14** and **24**, respectively. The conjugate addition of the second unit of (*E*)-(2-nitrovinyl)benzene (**5**) could take place either by reaction of thiols **15** and **26** or thiolates **44** and **45**. The markedly higher stability of thiols relative to that of thiolates [even isolable in one case (**15**)], and the fact that **44** and **45** must be stronger nucleophiles, suggests that the formation of **15** and **26** would take place through the intermediacy of **44** and **45**. The reaction profiles depicted in Figure 4.24 show that, even though the energy barriers involved in the formation of **15** and **26** are identical, the rate-limiting step and the relative stability of the zwitterionic intermediates **44** and **45** is different. Accordingly, if these intermediates were formed, the average life of **45** should be higher than that of **44**, which would account for the subsequent reaction of **45** with another molecule of (*E*)-(2-nitrovinyl)benzene to give the cycloadduct **25**.

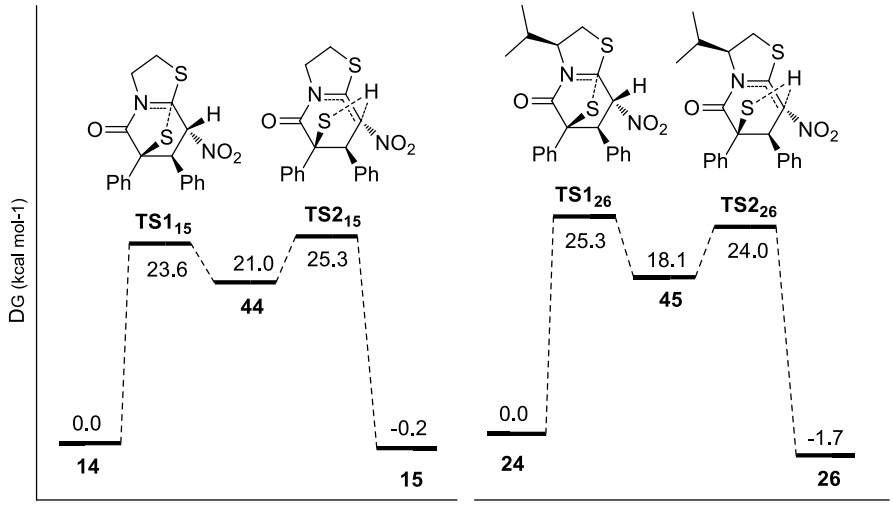

Figure 4.24. Relative free energy values (Δ*G*, kcal mol^{-1}) of all stationary points involved in the transformation of **14** and **24** into thiols **15** and **26**, respectively, calculated at the M06-2X/6-311++G(d,p) level in CH_2Cl_2 (SMD method).

4.4. Conclusions

The reactivity of 2-phenyl-5,6-dihydrothiazolo[2,3-b]thiazol-4-ium-3-olate (**1**) against symmetrical [1-phenyl-1*H*-pyrrole-2,5-dione (**3**) and dimethyl maleate (**4**)] and asymmetrical [(*E*)-(2-nitrovinyl)benzene (**5**), acrylonitrile (**6**), and but-3-en-2-one (**7**)] olefinic dipolarophiles, as well as and the unichiral version (**2**) with **3** and **5** have been investigated in detail. The cycloaddition of **1** with 1-phenyl-1*H*-pyrrole-2,5-dione (**3**) was not diastereoselective, which contrasts to the situation with dimethyl maleate (**4**), from which only the *exo* cycloadduct (**11**) was obtained. The reactions with unsymmetrically-substituted dipolarophiles (**5**-**7**) were found to be completely regioselective. The isopropyl group of the unichiral thioisomünchnone **2** dictates a marked facial stereocontrol against bulky dipolarophiles like **3** and **5**, giving rise to enantiomerically-pure cycloadducts. Computational results at the M062-X/6-311++G(d,p) level with inclusion of solvent effects (SMD model) have demonstrated that these kinetically-controlled 1,3-dipolar cycloadditions are concerted transformations of varied synchronicity with the sole exception of (*E*)-(2-nitrovinyl)benzene (**5**), which takes place by a stepwise mechanism with the characterization of zwitterionic intermediates that evolve to the most favored regioisomers. A natural bond orbital (NBO) analysis of molecular interactions at the saddle points reveals that cycloadditions with symmetrical dipolarophiles are favored when back-donation (electron flux from dipolarophile to dipole) overcomes the donation effect. On the contrary, when this situation occurs with asymmetrical dipolarophiles, the resulting cycloadditions are disfavored, i.e. such saddle points lead to the non-observed regioisomers. However, the transition structures evolving into the favored regioisomers exhibit strong donation processes. Analysis of the energy barriers for unichiral thioisomünchnone **2** show in general a pronounced facial stereoselection, which agrees with the distortion energy of the dipole.

4.5. Experimental section

4.5.1. General methods

Solvents and reagents were purchased from commercial suppliers and used without further purification. The identity of all compounds was confirmed by their elemental analyses,

melting points, NMR and crystallographic data. Optical rotations were measured using a Na lamp ($[\alpha]_D$ values at λ = 589 nm).

4.5.2. Computational details

All the geometries were optimized by the density functional theory (DFT) with the M06-2X[18] in combination with 6-311++G(d,p)[19] basis set and were performed with Gaussian09 program package[20]. The geometries were optimized including solvation effects in toluene and dichloromethane, which have been estimated by the well-established solvation model density (SMD)[21] method that takes into account different contributions such as long-range electrostatic polarization (bulk solvent effect). The IRC analysis (intrinsic reaction coordinate) for the cycloadditions involving compound **1** demonstrate that each saddle point belongs to the reaction path. Ground and transition structures were characterized by none and one imaginary frequency, respectively. All the relative energies shown are free energies calculated at 298.15 K with respect to the reagents. The orbital interaction in the saddle points and the geometries of the low-gradient region in caldera-type areas were carried out with the NBO 6.0 package[22] and visualized with Jmol.[23]

4.5.3. Synthetic procedures

4.5.3.1. **6,8-Diphenyldihydro-2*H*-6,9*b*-epithiopyrrolo[3,4-*c*]thiazolo[3,2-*a*]pyridine-5,7,9(3*H*,8*H*,9a*H*)-trione (9).** A mixture of **1** (7 mmol) and **3** (10.5 mmol) in CH_2Cl_2 (80 mL) was kept at room temperature for 24 h until the disappearance of the orange color of the mesoionic heterocycle (**1**). The solution was concentrated at reduced pressure (rotary evaporator) affording crystals of the *exo* cycloadduct (**9**) (28%). Mp 220-221 ºC; IR (KBr) ν_{max} 3060, 2934, 2358, 1707, 1497, 1445, 1380, 1260, 1186, 752, 695 cm^{-1}; ^1H NMR ($CDCl_3$, 500 MHz): δ 7.43-7.21 (m, 10H), 4.20-4.17 (m, 1H), 4.08 (d, *J* = 7.0 Hz, 1H), 3.88 (d, *J* = 7.0 Hz, 1H), 3.50-3.39 (m, 2H), 3.29-3.23 (m, 1H) ppm; ^{13}C NMR ($CDCl_3$, 125 MHz): δ 172.1, 171.5, 170.9, 131.3, 130.2, 129.1, 129.0, 128.9, 128.6, 128.3, 126.2, 87.2, 75.0, 60.0, 51.3, 46.5, 33.5 ppm. Anal. Calcd for $C_{21}H_{16}N_2O_3S_2$: C, 61.75; H, 3.95; N, 6.86; S, 15.70. Found: C, 61.57; H, 3.98; N, 6.72; S, 15.83.

4.4.3.2. **6,8-Diphenyldihydro-2*H*-6,9*b*-epithiopyrrolo[3,4-*c*]thiazolo[3,2-*a*]pyridine-5,7,9(3*H*,8*H*,9a*H*)-trione (8).** After filtration of compound **9**, the resulting solution was evaporated to dryness under reduced pressure to give a solid residue, which consisted of a mixture of **8** and **9**. That solid was recrystallized from ethyl acetate yielding the *endo* cycloadduct (**8**) (43%). Mp 227-229 ºC; IR (KBr) ν_{max} 3058, 2973, 2929, 2879, 1778, 1714, 1493, 1378, 1333, 1213, 1187, 760, 730, 691 cm^{-1}; ^{1}H NMR ($CDCl_3$, 500 MHz): δ 7,77 (d, *J* = 7.0 Hz, 2H), 7.44-7.37 (m, 6H), 7.16 (d, *J* = 7.0 Hz, 2H), 4.56 (d, *J* = 8.5 Hz, 1H), 4.30 (d, *J* = 8.5 Hz, 2H), 4.20-4.17 (m, 1H), 3.47-3.34 (m, 3H) ppm; ^{13}C NMR ($CDCl_3$, 125 MHz): δ 170.8, 170.3, 169.7, 131.3, 131.1, 129.2, 129.2, 129.1, 129.04, 128.4, 126.4, 86.2, 72.9, 59.0, 54.1, 46.6, 34.1 ppm. Anal. Calcd for $C_{21}H_{16}N_2O_3S_2$: C, 61.75; H, 3.95; N, 6.86; S, 15.70. Found: C, 61.63; H, 4.01; N, 6.80; S, 15.91.

4.5.3.3. **6,8-Diphenyl-2,3-dihydropyrrolo[3,4-*c*]thiazolo[3,2-*a*]pyridine-5,7,9(8*H*)-trione (10).** A mixture of cycloadducts **8** and **9** (0.5 g) in toluene (300 mL) containing silica gel [Merck 60 (400-230 mesh)] (3 g) was stirred at reflux for 72 h until the disappearance of both cycloadducts (TLC analysis: ethyl acetate:hexane 1:2 v/v). The silica gel was removed by filtration and washed with acetone until formation of a colorless solution. The solvent was removed under reduced pressure giving a solid, which was suspended in ethyl acetate yielding solid thiazolopyridone **10** that was further recrystallized from ethyl acetate (54%). Mp 195-196 ºC; IR (KBr) ν_{max} 3023, 1754, 1709, 1654, 1586, 1363, 1137, 1098, 766, 690 cm^{-1}; ^{1}H NMR ($CDCl_3$, 500 MHz): δ 7.50-7.34 (m, 10H), 4.48 (t, *J* = 8.0 Hz, 2H), 3.49 (t, *J* = 8.0 Hz, 2H) ppm; ^{13}C NMR ($CDCl_3$, 125 MHz): δ 164.0, 163.7, 161.7, 149.4, 134.3, 131.1, 130.0, 129.6, 128.8, 128.6, 127.8, 127.3, 126.5, 126.0, 101.6, 50.4, 28.6 ppm. Anal. Calcd for $C_{21}H_{14}N_2O_3S$: C, 67.37, H, 3.77; N, 7.48; S, 8.56. Found: C, 67.24; H, 3.81; N, 7.40; S, 8.70.

4.5.3.4. **Dimethyl 5-oxo-6-phenylhexahydro-6,8*a*-epithiothiazolo[3,2-*a*]pyridine-7,8-dicarboxylate (11).** A mixture of **1** (2.6 mmol) and **4** (3.8 mmol) in toluene (50 mL) was stirred at reflux during 4 h until the disappearance of the orange color of the mesoionic heterocycle (**1**). The solution was allowed to cool at room temperature, affording crystals of the *exo* cycloadduct **11** (71%). Mp 185-187 ºC; IR (KBr) ν_{max} 3452, 3406, 3034, 2946, 2880, 2835, 2361, 1742, 1716, 1447, 1354, 1217, 1159, 1058, 965, 949, 844, 748, 697; cm^{-1}; ^{1}H NMR ($CDCl_3$, 500 MHz): δ 7.36-7.27 (m, 5H), 4.19-4.16 (m, 1H), 4.11 (d, 1H, *J* = 9.0 Hz), 3.74 (d, 1H, *J* = 9.0 Hz), 3.69 (s, 3H), 3.36-3.33 (m, 2H), 3.24 (s, 3H), 3.12-3.08

(m, 1H). ^{13}C NMR ($CDCl_3$, 125 MHz): δ 171.6, 169.7, 168.6, 131.1, 128.7, 128.3, 128.1, 86.0, 74.1, 63.0, 55.2, 52.3, 51.8, 45.7, 32.9 ppm. Anal. Calcd for $C_{17}H_{17}NO_5S_2$: C, 53.81; H, 4.52; N, 3.69; S, 16.90. Found: C, 53.78; H, 4.49; N, 3.71; S, 17.15.

4.5.3.5. **8-Nitro-6,7-diphenyltetrahydro-6,8*a*-epithiothiazolo[3,2-*a*]pyridin-5(6*H*)-one (14)**. A mixture of **1** (2.12 mmol) and (*E*)-(2-nitrovinyl)benzene (**5**) (3.21 mmol) in CH_2Cl_2 (25 mL) was kept at room temperature for 72 h until the disappearance of the orange color of the mesoionic heterocycle (**1**). The solvent was evaporated to dryness affording a solid residue that was treated with ethyl acetate yielding the title compound, which could be obtained in pure form by recrystallization from ethyl acetate (63%). Mp 204-205 ºC; IR (KBr) ν_{max} 3414, 3064, 3036, 2994, 2934, 2881, 1719, 1550, 1366, 1332, 939, 860, 775, 741, 702, 694, 609 cm^{-1}; ^{1}H NMR ($CDCl_3$, 500 MHz): δ 7.28-7.30 (m, 2H), 7.03-7.12 (m, 6H), 7.03-7.05 (m, 2H), 5.78 (d, *J* = 4.5 Hz, 1H), 4.54 (d, *J* = 5.0 Hz, 1H), 4.25 (m, 1H), 3.47 (m, 2H), 3.29 (m, 1H) ppm; ^{13}C NMR ($CDCl_3$, 125 MHz): δ 171.1, 135.7, 131.0, 128.5, 128.4, 128.4, 128.3, 128.2, 128.0, 97.8, 86.1, 77.2, 56.0, 46.2, 33.9. Anal. Calcd for $C_{19}H_{16}N_2O_3S_2$: C, 59.35, H, 4.19; N, 7.29; S, 16.68. Found: C, 59.22; H, 4.18; N, 7.25; S, 16.79.

4.5.3.6. **6-Mercapto-8-nitro-6,7-diphenyl-6,7-dihydro-2*H*-thiazolo[3,2-*a*]pyridin-5(3*H*)-one (15).** To a solution of compound **14** (0.2 g) in CH_2Cl_2 (30 mL) was added silica gel [Merck 60 (400-230 mesh)] (3 g) and the mixture was stirred at reflux for 19 h until the disappearance of **14** (TLC analysis: ethyl acetate:hexane 1:2 v/v). The silica gel was removed by filtration and washed with dichloromethane until a colorless solution resulted. The solvent was removed under reduced pressure giving rise to thiol **15**, which was crystallized from diethyl ether on standing (52%). Mp 213-214 ºC; IR (KBr) ν_{max} 3059, 2941, 2892, 2558, 1695, 1578, 1446, 1300,1234, 1186, 721, 697 cm^{-1}; ^{1}H NMR ($CDCl_3$, 500 MHz): δ 7.33-7.43 (m, 8H), 7.22-7.24 (m, 2H), 5.33 (s, 1H), 4.70-4.75 (m, 1H), 4.14-4.20 (m, 1H), 3.15-3.25 (m, 2H), 2.33 (s, 1H) ppm; ^{13}C NMR ($CDCl_3$, 125 MHz): δ 168.1, 154.7, 139.3, 135.8, 129.4, 129.1, 129.0, 128.8, 128.7, 126.9, 125.3, 60.0, 50.5, 50.1, 28.6. Anal. Calcd for $C_{19}H_{16}N_2O_3S_2$: C, 59.35, H, 4.19; N, 7.29; S, 16.68. Found: C, 59.27; H, 4.15; N, 7.28; S, 16.80.

4.5.3.7. **5-Oxo-6-phenylhexahydro-6,8*a*-epithiothiazolo[3,2-*a*]pyridine-8-carbonitrile (16).** Compound **1** (2.98 mmol) was dissolved in acrylonitrile (**6**) (20 mL) and kept at room temperature for 24 h until the disappearance of the orange color of **1**. The *endo* cycloadduct

16 was isolated by column chromatographic (ethyl acetate:petroleum ether 1:5 v/v) and recrystallized from ethyl acetate (18%). Mp 134-135 ºC; IR (KBr) ν_{max} 3422, 3058, 3031, 2826, 2874, 2237, 1717, 1598, 1445, 1360, 1332, 1261, 1185, 1112, 978, 927, 794, 765, 708 697, 673, 574, 501, 457 cm^{-1}; ^1H NMR ($CDCl_3$, 500 MHz): δ 7.45-7.36 (m, 5H), 4.20-4.16 (m, 1H), 3.97-3.95 (dd, 1H, *J* = 4 Hz, *J* = 10 Hz), 3.71-3.65 (m, 1H), 3.51-3.43 (m, 2H), 3.21-3.17 (dd, 1H, *J* = 10 Hz, *J* = 13 Hz), 3.05-3.01 (dd, 1H, *J* = 4 Hz, *J* = 13 Hz). ppm; ^{13}C NMR ($CDCl_3$, 125 MHz): δ 171.7, 132.8, 129.0, 128.7, 127.9, 117.9, 87.1, 71.4, 46.4, 44.5, 40.9, 34.5. Calcd for $C_{14}H_{12}N_2OS_2$: C, 58.31; H, 4.19; N, 9.71; S, 22.24. Found: C, 58.27; H, 4.21; N, 9.68; S, 22.07.

4.5.3.8. **5-Oxo-6-phenylhexahydro-6,8*a*-epithiothiazolo[3,2-*a*]pyridine-8-carbonitrile (17).** In following the same methodology as for *endo* cycloadduct **16**, the *exo* cycloadduct was recrystallized from ethyl acetate. (20%). Mp 157-158 ºC; IR (KBr) ν_{max} 3409, 3059, 2936, 2884, 2243, 1800, 1718, 1595, 1444, 1363, 1299, 1218, 1151, 1070, 989, 938, 844, 702, 626, 558, 491 cm^{-1}; ^1H NMR ($CDCl_3$, 500 MHz): δ 7.45-7.38 (m, 5H), 4.18-4.11 (m, 1H), 3.57-3.55 (dd, 1H, *J* = 3.5 Hz, *J* = 8 Hz), 3.51-3.43 (m, 2H), 3.34-3.29 (m, 1H), 3.18-3.14 (dd, 1H, *J* = 8 Hz, *J* = 13 Hz), 3.03-3.00 (dd, 1H, *J* = 4 Hz, *J* = 13 Hz). ppm; ^{13}C NMR ($CDCl_3$, 125 MHz): δ 172.0, 132.6, 129.0, 128.7, 128.0, 118.9, 88.3, 71.3, 46.1, 45.8, 41.5, 34.2. Calcd for $C_{14}H_{12}N_2OS_2$: C, 58.31; H, 4.19; N, 9.71; S, 22.24. Found: C, 58.25; H, 4.22; N, 9.69; S, 22.10.

4.5.3.9. **8-Acetyl-6-((3-oxobutyl)thio)-6-phenyl-6,7-dihydro-2H-thiazolo[3,2-*a*]pyridin-5(3*H*)-one (18).** Compound **1** (4.26 mmol) was dissolved in but-3-en-2-one (**7**) (20 mL) and heated at reflux for 30 minutes, until the disappearance of the orange color of **1**. The solution was evaporated to dryness and the residue was dissolved in warm ethyl acetate. After cooling to room temperature the tittle compound crystallized as a white solid (32%). Mp 182-183 ºC; IR (KBr) ν_{max} 3338, 2980, 2879, 2829, 1705, 1678, 1639, 1518, 1372, 1248, 1202, 1125, 985, 849, 706, 588, 461 cm^{-1}; ^1H NMR ($CDCl_3$, 500 MHz): δ 7.54-7.53 (d, 2H, *J* = 7.5 Hz), 7.40-7.37 (t, 2H, *J* = 7.5 Hz), 7.32-7.29 (t, 1H, *J* = 7.5 Hz), 4.26-4.23 (t, 2H, *J* = 7.5 Hz), 3.24-3.20 (d, 1H, *J* = 16.5 Hz), 3.19-3.10 (m, 2H), 3.05-3.02 (d, 1H, *J* = 16.5 Hz), 2.66-2.63 (t, 2H, *J* = 6.5 Hz), 2.56-2.53 (t, 2H, *J* = 6.5 Hz), 2.21 (s, 3H), 2.07 (s, 3H). ppm; ^{13}C NMR ($CDCl_3$, 125 MHz): δ 205.9, 193.5, 167.0, 151.8, 138.3, 128.5, 127.8, 127.5, 105.7, 56.9, 47.9, 42.3, 39.2, 29.7, 28.0, 27.1, 23.9. Anal. Calcd for $C_{19}H_{21}NO_3S_2$: C, 60.77; H, 5.64; N, 3.73; S, 17.08. Found: C, 60.62; H, 5.72; N, 3.65; S, 16.78.

4.5.3.10. **8-Acetyl-6-phenyltetrahydro-6,8*a*-epithiothiazolo[3,2-*a*]pyridin-5(6*H*)-one (20).** From the reaction mixture of **1** and **7**, the *exo* cycloadduct **20** could be isolated by column chromatography (ethyl acetate:petroleum ether 1:5 v/v). Recrystallized from ethyl acetate (22%) had mp 178-179 ºC; IR (KBr) ν_{max} 3344, 3083, 2943, 2889, 1686, 1640, 1442, 1374, 1347, 1115, 950, 925, 842, 749, 628 cm^{-1}; ^1H NMR ($CDCl_3$, 500 MHz): δ 7.45-7.43 (dd, 2H, *J* = 1.5 Hz y *J* = 8.5 Hz), 7.34-7.29 (m, 3H), 5.00-4.98 (dd, 1H, *J* = 2.5 Hz, *J* = 6.5 Hz), 4.28-4.21 (m, 1H), 4.05-3.99 (m, 1H), 3.52-3.48 (dd, 1H, *J* = 2.5Hz, *J* = 16.5 Hz), 3.16-3.09 (m, 2H), 3.03-2.99 (m, 1H), 2,29 (s, 3H) ppm; ^{13}C NMR ($CDCl_3$, 125 MHz): δ 194.84, 166.02, 135.69, 134.65, 128.66, 128.51, 127.35, 94.59, 59.78, 48.57, 33.86, 30.13, 28,26. Anal. Calcd for $C_{15}H_{15}NO_2S_2$: C, 58.99, H, 4.95; N, 4.59; S, 21.00. Found: C, 58.73; H, 5,11; N, 4.48; S, 19.85.

4.5.3.11. **(3*S*,6*S*,6*aS*,9*aR*,9*bS*)-3-Isopropyl-6,8-diphenyldihydro-2*H*-6,9*b*-epithio-pyrrolo-[3,4-*c*]thiazolo[3,2-*a*]pyridine-5,7,9(3*H*,8*H*,9*aH*)-trione (21).** A mixture of **2** (2.2 mmol) and **3** (3.3 mmol) in CH_2Cl_2 (80 mL) was kept at room temperature for 24 h until the disappearance of the orange color of the mesoionic heterocycle (**2**). The solvent was evaporated to dryness under reduced pressure and the resulting residue was dissolved in ethyl acetate. Further addition of petroleum ether (6 mL) resulted in crystals of the title compound (72%). Mp 221-223 ºC; $[\alpha]_D$ 52.3º (c 4.6 CH_2Cl_2); IR (KBr) ν_{max} 3477, 3063, 3034, 2962, 2873, 1781, 1704, 1596, 1498, 1375, 1195, 751, 694 cm^{-1}; ^1H NMR ($CDCl_3$, 500 MHz): δ 7.35-7.44 (m, 8H), 7.20-7.23 (m, 2H) 4.02 (d, *J* = 7 Hz, 1H), 3.98-4.00 (m, 1H), 3.84 (d, *J* = 7 Hz, 1H), 3.36 (dd, *J* = 8.5 Hz, *J* = 11.5 Hz, 1H), 3.24 (q, 1H, *J* = 5.5 Hz), 2.94-3.01 (m, 1H), 1.01 (d, *J* = 7.5 Hz, 1H), 0.91 (d, *J* = 6.5 Hz, 3H) ppm; ^{13}C NMR ($CDCl_3$, 125 MHz): δ 171.9, 171.0, 169.9, 131.4, 130.6, 129.10, 129.0, 128.9, 128.7, 128.2, 126.2, 88.0, 66.2, 60.6, 50.6, 33.5, 26.6, 20.2, 16.1. Anal. Calcd for $C_{24}H_{22}N_2O_3S_2$: C, 63.98, H, 4.92; N, 6.22; S, 14.23. Found: C, 63.87; H, 4.90; N, 6.18; S, 14.40.

4.5.3.12. **(3*S*,6*R*,6*aR*,9*aS*,9*bR*)-3-Isopropyl-6,8-diphenyldihydro-2*H*-6,9*b*-epithio-pyrrolo[3,4-*c*]thiazolo[3,2-*a*]pyridine-5,7,9(3*H*,8*H*,9*aH*)-trione (22).** After filtration of compound **21**, the resulting solution was evaporated to dryness under reduced pressure giving a solid that was dissolved in diethyl ether, crystallizing subsequently a mixture of cycloadduct **22** and **2**. Further recrystallization from diethyl ether afforded pure **22** (15%). Mp 223-224 ºC; $[\alpha]_D$ 18.7º (c 5.2 CH_2Cl_2); IR (KBr) ν_{max} 3476, 3065, 3033, 2967, 2936, 2901, 2872, 1781, 1713, 1596, 1495, 1388, 1189, 772, 753, 694 cm^{-1}; ^1H NMR ($CDCl_3$, 500

MHz): δ 7.34-7.43 (m, 8H), 7.21-7.23 (m, 2H) 4.12 (d, *J* = 7 Hz, 1H), 3.96 (dd, *J* = 6.0 Hz, *J* = 9.5 Hz, 1H), 3.87 (d, *J* = 6.5 Hz, 1H), 3.50 (q, *J* = 6.0 Hz, 1H), 3.18 (d, *J* = 12.0 Hz, 1H), 2.00-2.10 (m, 1H), 1.03 (d, *J* = 6.5 Hz, 3H), 0.97 (d, *J* = 6.5 Hz, 3H) ppm. ^{13}C NMR ($CDCl_3$, 125 MHz): δ 172.3, 172.1, 170.8, 131.4, 130.4, 129.1, 129.0, 128.9, 128.7, 128.3, 126.2, 87.5, 74.6, 65.3, 60.3, 51.3, 36.0, 31.1, 19.9, 19.7. Anal. Calcd for $C_{24}H_{22}N_2O_3S_2$: C, 63.98, H, 4.92; N, 6.22; S, 14.23. Found: C, 63.90; H, 4.94; N, 6.20; S, 14.37.

4.5.3.13. **(*S*)-3-Isopropyl-6,8-diphenyl-2,3-dihydropyrrolo[3,4-*c*]thiazolo[3,2-*a*]pyridine-5,7,9(8*H*)-trione (23).** In following the same procedure as for **10**, the title compound was isolated after reaction completion (48 h). Recrystallization from diethyl ether gave the pure compound in 37% yield. Mp 222-223 ºC; $[\alpha]_D$ 255.7º (c 5.4 CH_2Cl_2); IR (KBr) ν_{max} 3454, 3060, 3022, 2965, 2929, 2880, 1758, 1713, 1642, 1371, 1111, 767, 693, 620 cm^{-1}; ^{1}H NMR ($CDCl_3$, 500 MHz): δ 7.50-7.52 (m, 2H), 7.35-7.45 (m, 8H) 5.12-5.15 (m, 1H), 3.65 (dd, J_1 = 9.0 Hz, J_2 = 11.5 Hz, 1H), 3.40 (dd, *J* = 1.5 Hz, *J* = 11.5 Hz, 1H), 2.63-2.70 (m, 1H), 1.10 (d, *J* = 7.0 Hz, 3H), 0.99 (d, *J* = 7.0 Hz, 3H) ppm; ^{13}C NMR ($CDCl_3$, 125 MHz): δ 164.4, 164.2, 162.0, 150.2, 134.5, 131.6, 130.5, 130.1, 129.1, 128.9, 128.1, 127.6, 126.9, 126.3, 101.5, 68.0, 29.5, 29.2, 19.4, 16.2. Anal. Calcd for $C_{24}H_{20}N_2O_3S$: C, 69.21, H, 4.84; N, 6.73; S, 7.70. Found: C, 69.39; H, 4.90; N, 6.49; S, 7.89.

4.5.3.14. **(3*S*,6*S*,7*R*,8*R*,8*aS*)-3-Isopropyl-8-nitro-6,7-diphenyltetrahydro-6,8*a*-epithiothiazolo[3,2-*a*]pyridin-5(6*H*)-one (24).** A mixture of **2** (3.6 mmol) and **5** (4 mmol) in CH_2Cl_2 (45 mL) was kept at room temperature for 30 h, the solvent was removed under reduced pressure, and the resulting crude was suspended in diethyl ether yielding compound **24**, which was recrystallized from diethyl ether (78%). Mp 137-139 ºC; $[\alpha]_D$ 382.6º (c 5.2 CH_2Cl_2); IR (KBr) ν_{max} 3399, 3060, 3032, 3009, 2960, 2896, 2873, 1709, 1555, 1374, 1361, 1324, 1276, 697 cm^{-1}; ^{1}H NMR ($CDCl_3$, 500 MHz): δ 7.26-7.30 (m, 2H), 7.10-7.20 (m, 8H) 5.70 (d, *J* = 4.5 Hz, 1H), 4.44 (d, *J* = 4.5 Hz, 1H), 4.14-4.17 (m, 1H), 3.35 (dd, *J* = 7.0 Hz, *J* = 11 Hz, 1H), 3.26 (dd, *J* = 5.5 Hz, *J* = 11.5 Hz, 1H) 2.92-2.96 (m, 1H), 0.98 (dd, *J* = 2.0 Hz, *J* = 7.0 Hz, 6H) ppm; ^{13}C NMR ($CDCl_3$, 125 MHz): δ 169.6, 135.6, 131.2, 128.5, 128.3, 128.2, 127.9, 100.2, 87.0, 78.9, 65.1, 55.9, 34.0, 27.4, 19.8, 15.9. Anal. Calcd for $C_{22}H_{22}N_2O_3S_2$: C, 61.95, H, 5.20; N, 6.57; S, 15.03. Found: C, 61.85; H, 5.22; N, 6.43; S, 15.28.

4.5.3.15. **(3*S*,6*S*,7*R*,8*R*)-3-Isopropyl-8-nitro-6-((*R*)-2-nitro-1-phenylethyl)thio)-6,7-diphenyltetrahydro-2*H*-thiazolo[3,2-*a*]pyridin-5(3H)-one (25).** In following the same procedure as for **24**, although using a different molar ratio of the starting materials, 1:1.5 (**2**:**5**), the title compound was isolated after reaction completion (48 h). The solvent was evaporated under reduced pressure, and further addition of diethyl ether resulted in crystals of compound **24** in 33% yield. The filtrate was evaporated under reduced pressure and the crude was dissolved in methanol crystallizing **25** in 22% yield. Mp 189-191 ºC; $[\alpha]_D$ 26.7º (c 5.1 CH_2Cl_2); IR (KBr) ν_{max} 3407, 3060, 3030, 2967, 1705, 1581, 1551, 1455, 1376, 1311, 1215, 1191, 696 cm^{-1}; ^1H NMR ($CDCl_3$, 500 MHz): δ 7.51 (d, *J* = 7.5 Hz, 2H), 7.44 (t, *J* = 7.5 Hz,2H), 7.35-7.40 (m, 3H), 7.27-7.30 (m, 3H), 7.14-7.22 (m, 5H), 5.47 (s, 1H), 5.04-5.10 (m, 1H), 4.60 (dd, *J* = 4.5 Hz, *J* = 11.5 Hz, 1H), 4.30 (dd, *J* = 11.5 Hz, *J* = 13.0 Hz, 1H), 3.25 (dd, *J* = 8.5 Hz, *J* = 12.0 Hz, 1H), 3.16 (dd, *J* = 4.5 Hz, *J* = 13.0 Hz, 1H), 3.05 (dd, *J* = 1.0 Hz, *J* = 12.0 Hz, 1H), 2.60-2.64 (m, 1H), 1.1 (d, *J* = 6.5 Hz, 3H), 1.00 (d, *J* = 7.0 Hz, 3H) ppm; ^{13}C NMR ($CDCl_3$, 125 MHz): δ 168.3, 155.7, 137.2, 136.6, 134.5, 129.9, 129.6, 128.9, 128.8, 128.1, 127.5, 126.5, 126.2, 78.1, 67.7, 63.2, 49.0, 45.6, 30.8, 29.2, 19.8, 17.0. Anal. Calcd for $C_{30}H_{29}N_3O_5S_2$: C, 62.59, H, 5.08; N, 7.30; S, 11.14. Found: C, 62.42; H, 5.03; N, 7.21; S, 11.30.

4.5.3.16. **Transformation of 24 into 25 catalyzed by silica gel.** A mixture of **24** (1.95 mmol) and silica gel (10 g) in CH_2Cl_2 (100 mL) was heated at reflux for 72 h. TLC monitoring (ethyl acetate:hexane 1:3 v/v) revealed that the initial cycloadduct did not disappear completely. The catalyst was removed by filtration and washed with CH_2Cl_2 until formation of a colorless solution. The solvent was removed under reduced pressure giving a solid residue, which was suspended in diethyl ether and led to compound **25** (5%).

4.5.3.17. **Transformation of 24 into 25 in the presence of (*E*)-(2-nitrovinyl)benzene (5).** A solution of cycloadduct **24** and (*E*)-(2-nitrovinyl)benzene (**5**) in CH_2Cl_2 (molar ratio 1:1) was stirred for five days. TLC analysis (ethyl acetate:hexane 1:3 v/v) showed the formation of a new compound, which was purified by preparative TLC and had spectroscopic data identical to a pure sample of **25**.

4.5. Bibliography

(1) (a) *Synthetic Applications of 1,3-Dipolar Cycloaddition Chemistry Toward Heterocycles and Natural Products*; Padwa, A., Pearson, W. H., Eds.; John Wiley & Sons: New York, 2002; (b) Pellisier, H. *Tetrahedron* **2007**, 63, 3235-3285; (c) Suga, H.; Itoh, K. In *Methods and Applications of Cycloaddition Reactions in Organic Syntheses*; Nishiwaki, N., Ed.; John Wiley & Sons, Inc.: Hoboken, New Jersey, 2013; pp. 175-204; (d) Hasimoto, T.; Maruoka, K. *Chem. Rev.* **2015**, *115*, 5366-5412; (e) Singh, M. S.; Chowdhury, S.; Koley, S. *Tetrahedron* **2016**, *72*, 1603-1644.

(2) (a) Prescher, J. A.; Bertozzi, C. R. *Nat. Chem. Biol.* **2005**, *1*, 13-21; (b) Lutz, J. F.; Zarafshani, Z. *Adv. Drug Deliv. Res.* **2008**, *60*, 958-970; (c) Narayan, R.; Potowski, M.; Jia, Z. J.; Antonchick, A. P.; Waldmann, H. *Acc. Chem. Res.* **2014**, *47*, 1296-1310.

(3) For studies on natural dipolar cycloadditions: a) Payne, K. A. P.; White, M. D.; Fisher, K.; Khara, B.; Bailey, S. S.; Parker, D. Rattray, N. J. W.; Trivedi, D. K.; Goodacre, R.; Beveridge, R.; Barran, P.; Rigby, S. E. J.; Scrutton, N. S.; Hay, S.; Leys, D. *Nature* **2015**, *522*, 497-501. b) White, M. D.; Payne, K. A. P.; Fisher, K.; Marshall, S.; Parker, D.; Rattray, N. J. W.; Trivedi, D. K.; Goodacre, R.; Rigby S. E. J.; Scrutton, N. S.; Hay, S.; Leys, D. *Nature* **2015**, *522*, 502-506.

(4) (a) Xi, W.; Scott, T. F.; Kloxin, C. J.; Bowman, C. N. *Adv. Funct. Mater.* **2014**, *24*, 2572-2590; (b) Delaittre, G.; Guimard, N. K.; Barner-Kowollik, C. *Acc. Chem. Res.* **2015**, *48*, 1296-1307; (c) Yan, W.; Seifermann, S. M.; Pierrat, P.; Brase, S. *Org. Biomol. Chem.* **2015**, *13*, 25-54.

(5) For classical and comprehensive reviews on mesoionic structures and reactions of mesoionic dipoles: (a) Ollis, W. D.; Ramsden, C. A. In *Advances in Heterocyclic Chemistry*; Katritzky, A. R.; Boulton, A. J., Eds.; *Academic Press*: New York, 1976; Vol. 19, pp. 1-122; (b) Newton, C. G.; Ramsden, C. A. *Tetrahedron* **1982**, *38*, 2965-3011; (c) Potts, K. T. In *1,3-Dipolar Cycloaddition Chemistry*; Padwa, A., Ed.; John Wiley & Sons: New York, 1984; Vol. 2, pp. 1-82; (d) Ollis, W. D.; Stanforth, S. P.; Ramsden, C. A. *Tetrahedron* **1985**, *41*, 2239-2329; (e) Osterhout, M. H.; Nadler, W. R.; Padwa, A. *Synthesis* **1994**, 123-141.

(6) For recent reviews and treatments on mesoionics-based chemistry: (a) Gribble, G. W. In *Synthetic Applications of 1,3-Dipolar Cycloaddition Chemistry Toward Heterocycles and Natural Products*; Padwa, A., Pearson, W. H., Eds.; John Wiley & Sons: New York, 2002; pp. 681-753; (b) Ávalos, M.; Babiano, R.; Cintas, P.; Jiménez, J. L.; Palacios, J. C. *Acc. Chem. Res.* **2005**, *38*, 460-468; c) Lopchuk, J. M. In *Metalation of Azoles and Related Five-Membered Ring Heterocycles*; Gribble, G. W., Ed.; Springer: Berlin, 2012; pp. 381-413.

(7) For recent and representative examples involving different mesoionic heterocycles: (a) Browne, D. L.; Harrity, P. A. *Tetrahedron* **2010**, *66*, 553-568; (b) Lopchuk, J. M.; Hughes, R. P.; Gordon, G. W. *Org. Lett*. **2013**, *15*, 5218-5221; (c) Morin, M. S.; St-Cyr, D. J.; Arndtsen, B. A.; Krenske, E. H.; Houk, K. N. *J. Am. Chem. Soc*. **2013**, *135*, 17349-17358; (d) Marco-Martínez, J.; Reboredo, S.; Izquierdo, M.; Marcos, V.; López, J. L.; Filippone, S.; Martín, N. *J. Am. Chem. Soc*. **2014**, *136*, 2897-2904; (e) Specklin, S.; Decuypere, E.; Plougastel, L.; Aliani, S.; Taran, F. *J. Org. Chem*. **2014**, *79*, 7772-7777; (f) Erguven, H.; Leitch, D. C.; Keyzer, E. N.; Arndtsen, B. A. *Angew. Chem. Int. Ed.* **2017**, *56*, 6078-6082.

(8) For recent examples: (a) Cantillo, D.; Ávalos, M.; Babiano, R.; Cintas, P.; Jiménez, J. L.; Light, M. E.; Palacios, J. C. *Org. Lett*. **2008**, *10*, 1079-1082; (b) Cantillo, D.; Ávalos, M.; Babiano, R.; Cintas, P.; Jiménez, J. L.; Light, M. E.; Palacios, J. C. *J. Org Chem*. **2009**, *74*, 3698-3705; (c) Cantillo, D.; Ávalos, M.; Babiano, R.; Cintas, P.; Jiménez, J. L.; Light, M. E.; Palacios, J. C. *J. Org. Chem*. **2009**, *74*, 7644-7650; (d) Cantillo, D.; Ávalos, M.; Babiano, R.; Cintas, P.; Jiménez, J. L.; Light, M. E.; Palacios, J. C.; Rodríguez, V. *Org. Biomol. Chem*. **2010**, *8*, 7644-7650; (e) Cantillo, D.; Ávalos, M.; Babiano, R.; Cintas, P.; Jiménez, J. L.; Light, M. E.; Palacios, J. C. *J. Org. Chem*. **2014**, *79*, 4201-4205.

(9) Ávalos, M.; Babiano, R.; Cabanillas, A.; Cintas, P.; Diánez, M. J.; Estrada, M. D.; Jiménez, J. L.; López-Castro, A.; Palacios, J. C.; Garrido, S. P. *J. Chem. Soc. Chem. Commun.* **1995**, 2213-2214.
(10) Ávalos, M.; Babiano, R.; Cabanillas, A.; Cintas, P.; Higes, F. J.; Jiménez, J. L.; Palacios, J. C. *J. Org. Chem.* **1996**, *61*, 3738-3748.
(11) García de la Concepción, J.; Ávalos, M.; Babiano, R.; Cintas, P.; Jiménez, J. L.; Palacios, J. C. and Light, M. E. *Tetrahedron* **2016**, *72*, 4665-4670.
(12) García de la Concepción, J.; Ávalos, M.; Babiano, R.; Cintas, P.; Jiménez, J. L.; Palacios, J. C. and Light, M. E. *Tetrahedron* **2017**, *73*, 1551-1560.
(13) In stereochemical language, chemists often allude to "homochiral" and/or "chiral non-racemic", which may engender considerable puzzling, as neither of them denote strictly enantiomerically pure samples. The latter in particular is to be discouraged (see: Eliel, E. L.; Wilen, S. H. *Stereochemistry of Organic Compounds*; John Wiley & Sons: New York, 1994; p. 5), as enantioenriched samples of varied purity lie in this terminology. The term *unichiral*, introduced by Gal, and scarcely employed so far, is a useful and clever alternative that denotes single chirality and hence enantiomerically pure. See: (a) Gal, J. *Enantiomer* **1998**, *3*, 263-273; (b) Gal, J. *Chirality* **2011**, *23*, 647-659. Unless otherwise specified, we use through this paper the terms unichiral and enantiopure as synonymous.
(14) Foster, J. P.; Weinhold, F. J. *J. Am. Chem. Soc*., **1980**, *102*, 7211-7218.
(15) Yang, Y. F.; Yu P.; Houk, K. N. *J. Am. Chem. Soc*., **2017**, *139*, 18213-18221.
(16) Johnson, E. R.; Keinan, S.; Mori-Sanchez, P.; Contreras-Garcia, J.; Cohen, A. J.; Yang, W. *J. Am. Chem. Soc.* **2010**, *132*, 6498-6506.
(17) Lin, B.;Yu, P.; He C. Q.; Houk, K. N. *Bio. Med. Chem*. **2016**, *24*, 4787-4790
(18) (a) Zhao, Y.; Truhlar, D. G. *Theor. Chem. Acc*. **2008**, *120*, 215-241. (b) Zhao, Y.; Truhlar, D. G. *Acc. Chem. Res*. **2008**, *41*, 157-167.
(19) McGrath, M. P.; Radom, L. *J. Chem. Phys*. **1991**, *94*, 511-516.
(20) Frisch, M. J.; Trucks, G. W.; Schlegel, H. B.; Scuseria, G. E.; Robb, M. A.; Cheeseman, J. R.; Scalmani, G.; Barone, V.; Mennucci, B.; Petersson, G. A.; Nakatsuji, H.; Caricato, M.; Li, X.; Hratchian, H. P.; Izmaylov, A. F.; Bloino, J.; Zheng, G.; Sonnenberg, J. L.; Hada, M.; Ehara, M.; Toyota, K.; Fukuda, R.; Hasegawa, J.; Ishida, M.; Nakajima, T.; Honda, Y.; Kitao, O.; Nakai, H.; Vreven, T.; Montgomery Jr., J. A.; Peralta, J. E.; Ogliaro, F.; Bearpark, M.; Heyd, J. J.; Brothers, E.; Kudin, K. N.; Staroverov, V. N.; Kobayashi, R.; Normand, J.; Raghavachari, K.; Rendell, A.; Burant, J. C.; Iyengar, S. S.; Tomasi, J.; Cossi, M.; Rega, N.; Millam, J. M.; Klene, M.; Knox, J. E.; Cross, J. B.; Bakken, V.; Adamo, C.; Jaramillo, J.; Gomperts, R.; Stratmann, R. E.; Yazyev, O.; Austin, A. J.; Cammi, R.; Pomelli, C.; Ochterski, J. W.; Martin, R. L.; Morokuma, K.; Zakrzewski, V. G.; Voth, G. A.; Salvador, P.; Dannenberg, J. J.; Dapprich, S.; Daniels, A. D.; Farkas, Ö; Foresman, J. B.; Ortiz, J. V.; Cioslowski, J.; Fox, D. J. Gaussian 09, Revision D.01; Gaussian, Inc.: Wallingford, CT, 2009.
(21) Marenich, A. V.; Cramer, C. J.; Truhlar, D. G. *J. Phys. Chem. B* **2009**, *113*, 6378-6396.
(22) Glendening, E. D.; Badenhoop, J. K.; Reed, A. E.; Carpenter, J. E.; Bohmann, J. A. Morales, C. M.; Landis, C. R.; Weinhold, F. Theoretical Chemistry Institute, University of Wisconsin, Madison (2013).
(23) http://www.jmol.org/

5. On the dual reactivity of a Janus-type mesoionic dipole: experiments and theoretical validation

5.1. Abstract

A mesoionic bicycle, easily synthesized from a proteinogenic amino acid, L-leucine, behaves as both thiazolium-olate and diazolium-olate dipoles, as unveiled by its dipolar cycloadditions. This chameleonic reactivity has been thoroughly interpreted by dissecting the mechanistic landscape aided by the distortion-interaction model.

5.2. Introduction

The concept of dual reactivity, by which single molecules may exhibit complementary and often opposing roles, allows for elegant and divergent synthetic strategies, which would otherwise require multiple reagents or pathways. This vast concept is well exemplified by tautomeric species and umpolung effects of the classical carbonyl reactivity.[1] More recent and specific development include new catalysts with dual reactivity,[2] ambivalent reaction conditions,[3] and chameleonic behaviors shown by simple reagents like acetylenes, oximes, hydrides, and even water.[4]

Given the enormous versatility of [3+2]-cycloaddition reactions en route to highly-functionalized heterocycles present in natural products and pharmaceuticals,[5] 1,3-dipoles by virtue of their bielectronic character might be susceptible of opposing reactivities. However, to our knowledge the dipolar duality has not yet been achieved and most dipoles follow invariably well-established reactivity patterns. Among cyclic dipoles, mesoionic heterocycles were once postulated to exist in equilibrium with their uncharged valence tautomers, but trapping of such species remains largely elusive. Some alkylated 1,3-thiazolium-4-olates (dubbed thioisomünchnones), however, appear to equilibrate with non-dipolar tautomers that react as mild nucleophiles in the presence of strong electrophiles.[6]

5.3. Results and discussion

Clearly, the possibility of detecting dual reactivity hinges on dipoles prone to tautomeric equilibria. Herein we show the proof of principle with a bicyclic ring-fused thioisomünchnone (**3**), which can easily be obtained in a few steps from the naturally-occurring amino acid L-leucine (**1**), via the intermediacy of its hydantoin **2** (Figure 5.1, top).[7]

Compound **3** shows the expected masked dipole at the C2-S1-C7a fragment, namely a 1,4-thiazolium-3-olate. Proton transfer, however, from C5 to C2 would render a different mesoionic ring (**4**: 4,7-diazolium-6-olate; Figure 5.1, middle), where the masked dipole is now located across the C5-N4-C7a bonds. This kind of dipoles has received little attention, although a recent study has demonstrated its synthetic utility by reaction with acetylenes.[8] The unequivocal identity of **3** can be inferred from its spectroscopic data. In particular, a triplet signal resonating at 5.03 ppm can be reliably assigned to the hydrogen atom at the C5 atom. Clearly, the term "Janus" (i.e. "two faces") is appropriate and eye-catching to denote the dual reactivity of this mesoionic heterocycle. A dipolarophile could intercept either of them (**3** and **4**), so long as such dipoles equilibrate in solution. To check this surmise, compound **3** was reacted with two representative and reactive alkenes, such as 1-phenyl-1*H*-pyrrole-2,5-dione (**5**) and dimethyl (*E*)-butenedioate (**6**). These cycloadditions were heated in toluene using a professional MW oven (2.45 GHz), thereby enabling accurate control of both power and temperature for 1h. Although complex mixtures were detected by TLC analyses, the resulting products evolving from the dipolar cycloaddition could be isolated by crystallization (diethyl ether) from the reaction mixture. The dipolar cycloaddition of **3** with **5** gave rise to the *endo* cycloadduct **7** in 45% yield. Gratifyingly, crystals of the latter suitable for X-ray diffraction were grown by slow evaporation and allowed us its unequivocal structural elucidation (Figure 5.1, bottom). In a previous study, it has been shown the marked facial control exerted by a bulky alkyl group in the dipole,[9] a fact corroborated by the present result as well. The cycloaddition with **6** was likewise conducted as described above and a different dihydropyrrole structure (**8**) could be isolated in 24% yield. Both NMR (showing the lack of a CH_4O fragment) and elemental analysis were inconsistent with the expected cycloadduct (with molecular formula $C_{27}H_{26}N_2O_6S$). Again, X-ray diffractometry was rewarding enough to confirm the unambiguous solid-state structure of **8** (Figure 5.1, bottom). The formation of the latter cannot be rationalized if one assumes the cycloaddition of **6** with a 1,4-thiazolium-3-olate moiety, but rather with its chameleonic transformation into 4,7-diazolium-6-olate. Scheme 5.1 outlines a mechanistic proposal, where the formation of **8** would proceed through the generation of cycloadduct **9** by a ring-opening pathway that we shall discuss in detail later.

To understand the differential reactivity of dipoles **3** and **4** against compounds **5** and **6**, we performed a full computational study at the ONIOM(M06-2X/6-311++G(d,p):M06-2X/6-31G) level of theory[10-12] using the Gaussian09 package.[13] Furthermore, to reproduce the

experimental conditions, all calculations were carried out in toluene (SMD model)[14] at 373.1 K. A distortion/interaction (D/I) model was employed to assess the origin of the reactivity of the dipolar cycloadditions. The D/I model has proven to be a useful tool to predict and justify the reactivity of mesoionic dipoles.[15,16]

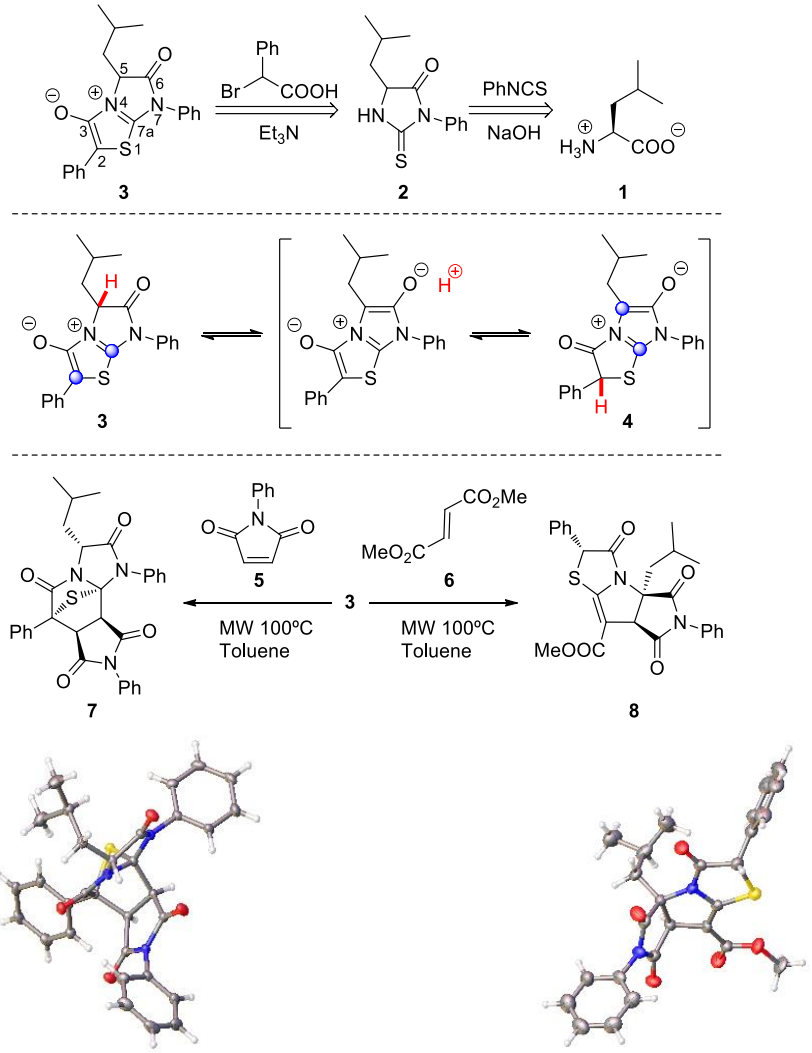

Figure 5.1. Retrosynthetic route for the preparation of 5-isobutyl-6-oxo-2,7-diphenyl-6,7-dihydro-5*H*-imidazo[2,1-*b*]thiazol-4-ium-3-olate (**3**) (top). Equilibrium between mesoionic heterocycles **3** and **4** (middle). Reactions of thioisomünchnone **3** with dipolarophiles 5 and **6** leading to the *endo* cycloadduct **7** and dihydropyrrole **8**, respectively. X-ray structures of **6** (left) and **7** (right) shown at 50% ellipsoid probability (bottom).

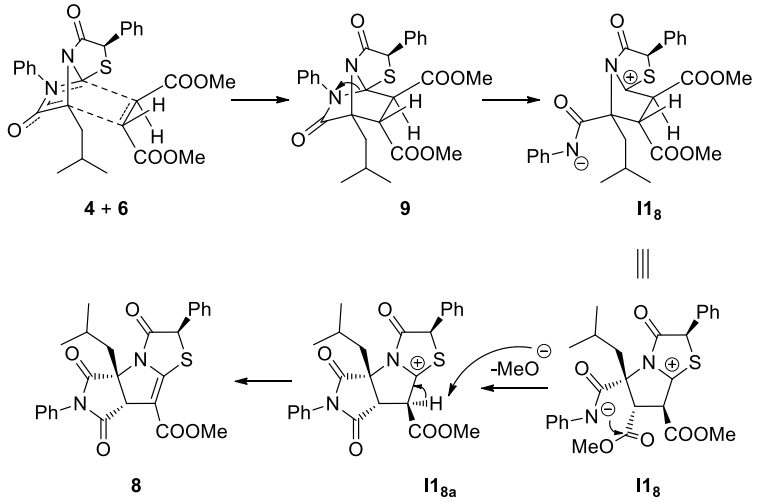

Scheme 5.1. Tentative mechanism for the formation of **8**.

Figure 5.2 top shows the optimized geometries of the reactants where the ball and wireframe representations correspond to high- and low-level calculations, respectively. In addition and, given the inherent chirality provided by L-leucine, the formation of all the possible diastereomers during the approaches of **5** (or **6**) to dipoles **3** and **4** were taken into consideration as well. This analysis affords up to four cycloadducts from each pair of reactants. Although the mesoionization protocol resulted in extensive racemization yielding compounds **3** and **4** as essentially racemic mixtures, the remaining computation focused on the (*R*)-configured enantiomer to assess the facial stereocontrol exerted by both the isobutyl group of **3** and the phenyl group of **4**. It is noteworthy the greater relative stability of dipole **3** with respect to **4** by 6.7 kcal mol^{-1}. A topological analysis of electron density[17] of both mesoionic rings show very similar results electron density [ρ(r)] and Laplacian of the electron density [$\nabla^2\rho(r)$] in their five bond critical points (BCP) and ring critical points (RCP), which point to similar reactivity as dipoles (see Figure 5.2 bottom).

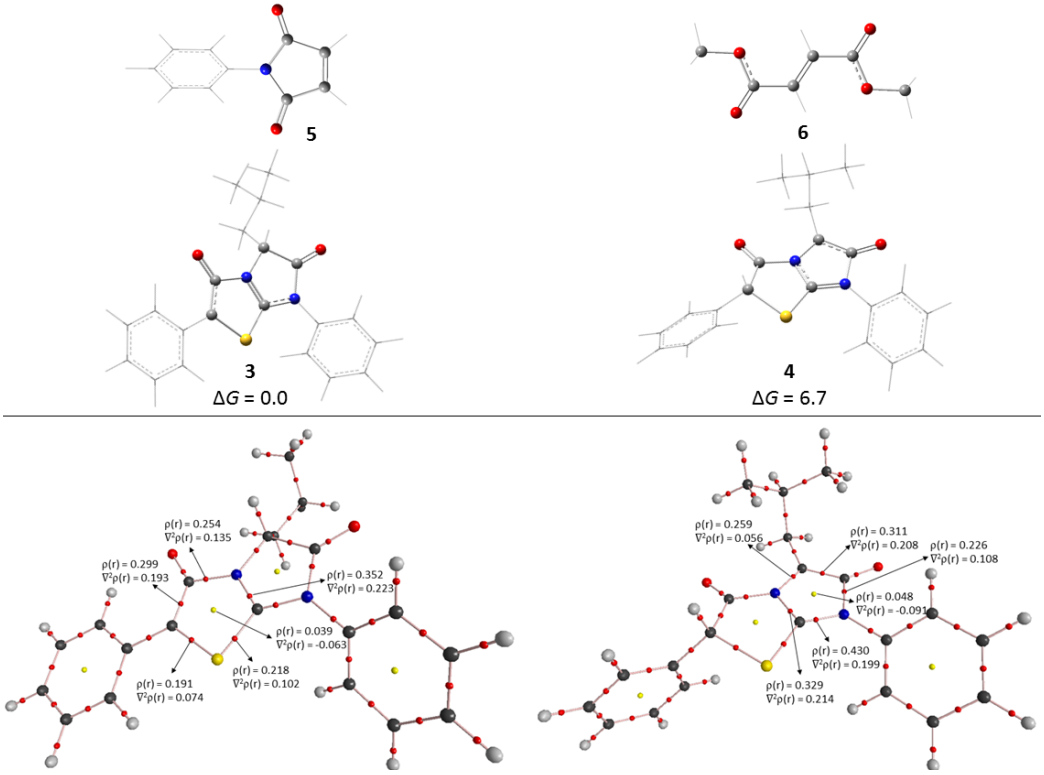

Figure 5.2. Optimized geometries of dipoles **3** and **4** and dipolarophiles **5** and **6** at the ONIOM(M06-2X/6-311++G(d,p):M06-2X/6-31G) level of theory in toluene (SMD) at 373.1 K. Ball and wireframe representations correspond to high- and low-level calculations, respectively. Relative free energy values of **3** and **4** are given in kcal mol^{-1} (top). Laplacian of the electron density [$\nabla^2\rho(r)$] and electron density [$\rho(r)$] values for the critical points of the thazolium-olate (left) and diazolium-olate (right) rings (bottom).

Figures 5.3 and 5.4 show the computed reaction pathways for dipolarophiles **5** and **6** *versus* dipoles **3** (top) and **4** (bottom). The energy barriers for the reactions between **4** and **5** are lower than those estimated for the cycloadditions with the thiazolium-olate dipole (**3**). The enhanced reactivity of the diazolium-olate tautomer (**4**) is consistent with a higher interaction energy wit compound **5** (see Figure 5.5, top).

The less favored approaches of **3** to **5** correspond to the formation of *exo* cycloadducts **10** and **11**. The geometries of the corresponding saddle points $\mathbf{TS1_{11}}$ and $\mathbf{TS_{10}}$ are quite similar, and although the formation of **11** proceeds by a stepwise process, the structure of $\mathbf{TS_{10}}$ is characteristic of a very asynchronous cycloaddition. Both saddle points ($\mathbf{TS1_{11}}$ and $\mathbf{TS_{10}}$) shows a pronounced steric hindrance caused by the phenyl group linked to N7 in

dipole **3**, which prevents close contacts between dipole and dipolarophile (Figure 5.6) which translates into a high distortion energy of the dipolarophile.

Likewise, the less favored cycloadditions of **5** with the diazolium-olate (**4**) correspond to either stepwise (**TS1$_{15}$**) or asynchronous (**TS$_{13}$**) cycloadditions, which lead however to *endo* cycloadducts **13** and **15**. The phenyl group at the N7 position exhibits a strong π-π stacking interaction with the phenyl group of **4**. Once again, such an interaction moves the dipolarophile away moiety from the dipole moiety (Figure 5.6), thus increasing the distortion energy of the dipolarophile.

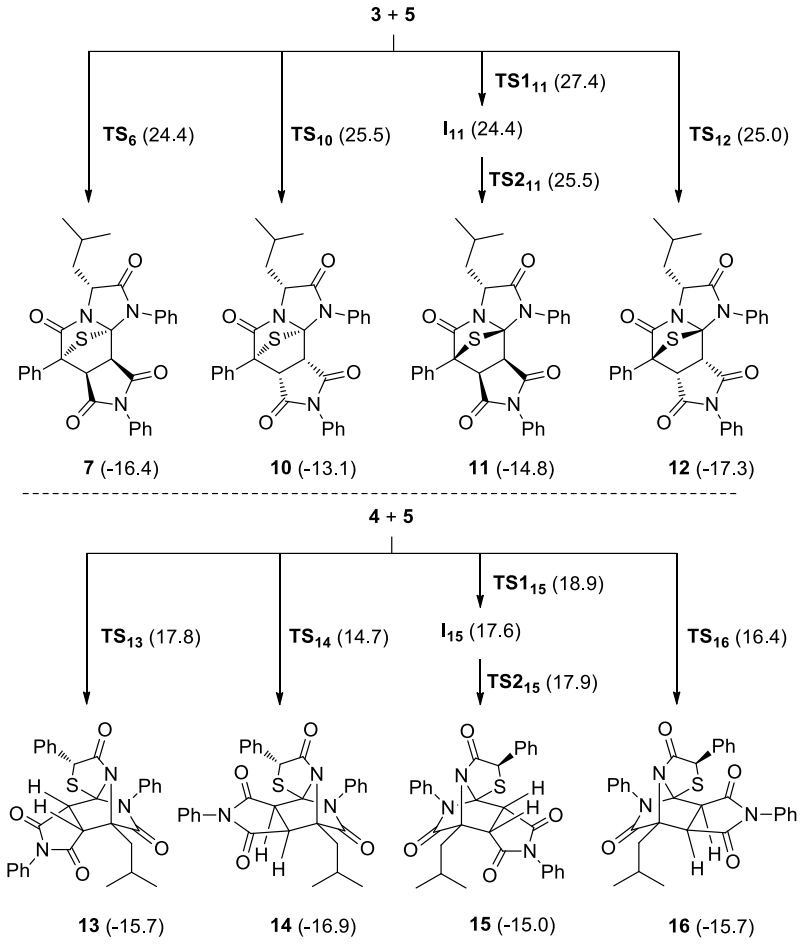

Figure 5.3. Computed free energy barriers for the reaction of dipolarophile **5** with dipoles **3** (above) and **4** (below) at the ONIOM(M06-2X/6-311++G(d,p):M06-2X/6-31G) level, in toluene (SMD) at 373.1 K. Energy values are given in kcal mol^{-1}.

In following the above-mentioned computational procedure, the free energy barriers for the reaction channels of **6** to dipoles **3** and **4** are collected in Figure 5.4. All the approaches of **6** to the diazolium-olate dipole (**4**) show very similar energy barriers, albeit slightly higher for the saddle points involving the approach of **6** to the 5-*Si*,8-*Si* face of **4** (**TS_{23}** and **TS_9**), which show in that case a little increase in distortion energy of the dipole (Figure 5.5, bottom).

As mentioned, the product isolated by reaction of **4** and **6**, i.e. dihydropyrrole **8**, arises from cycloadduct **9**, whose formation is not favored, from both kinetic and thermodynamic viewpoints. These data support the complex reaction mixture obtained experimentally.

On the other hand, the reaction with the thiazolium-olate dipole (**3**) suggests that formation of cycloadduct **18** is strongly disfavored with respect to those of **17**, **19** and **20**. The corresponding saddle point that led to that cycloadduct (**TS_{18}**) shows a high total distortion energy and a low interaction energy, as expected, the phenyl group linked to the N7 atom in **3** hinders sterically one of the methyl carboxylate fragments of **6** (Figure 5.7). Like the cycloadditions with **5**, the results obtained for **6** point clearly to an enhanced reactivity of the diazolium-olate dipole relative to its thiazolium-olate counterpart. However, in this case, the increased reactivity is associated with a lower distortion energy of the dipole. This difference accounting for the dual reactivity of dipoles **3** and **4** with **5** and **6** does also suggest a significant influence of the structure of dipolarophiles on the energetic profile.

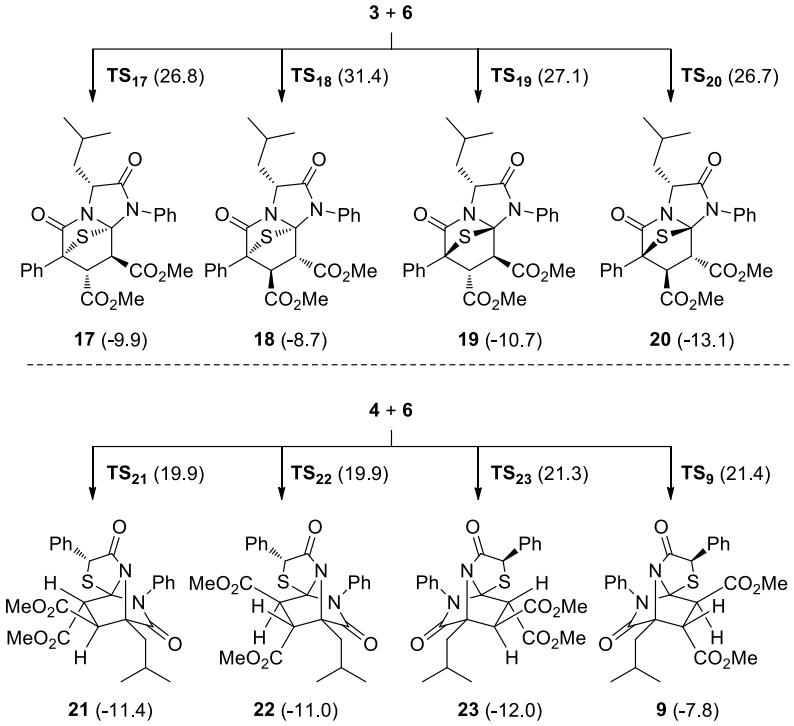

Figure 5.4. Computed free energy barriers for the reaction of dipolarophile **6** with dipoles **3** (above) and **4** (below) at the ONIOM(M06-2X/6-311++G(d,p):M06-2X/6-31G) level, in toluene (SMD) at 373.1 K. Energy values are given in kcal mol^{-1}.

Figure 5.8 shows the calculated reaction pathway leading to **8** via the intermediacy of cycloadduct **9**. Fragmentation of the latter alleviates ring strain yielding $\mathbf{I1_8}$ through the corresponding saddle point $\mathbf{TS1_8}$. This kind of ring opening has been previously described for reactions of thioisomünchnones with alkenes.[18] This path would then be followed by attack of the nitrogen atom in zwitterionic intermediate $\mathbf{I1_8}$ to the methyl carboxylate group ($\mathbf{TS2_8}$) giving rise to a tetrahedral intermediate ($\mathbf{I2_8}$). The latter evolves directly to a neutral and stable intermediate ($\mathbf{I3_8}$). In this transition state ($\mathbf{TS3_8}$), the leaving group (methoxide) attacks directly to the carbonium ion and both bond breaking at the pyrrolidinedione ring and bond-forming step occur in a concerted manner. Lastly, $\mathbf{TS4_8}$ corresponds to the concerted elimination of methanol giving product **8**. The free energy profile of this elimination is consistent with a high thermodynamic control during the conversion of cycloadduct **9** into **8**.

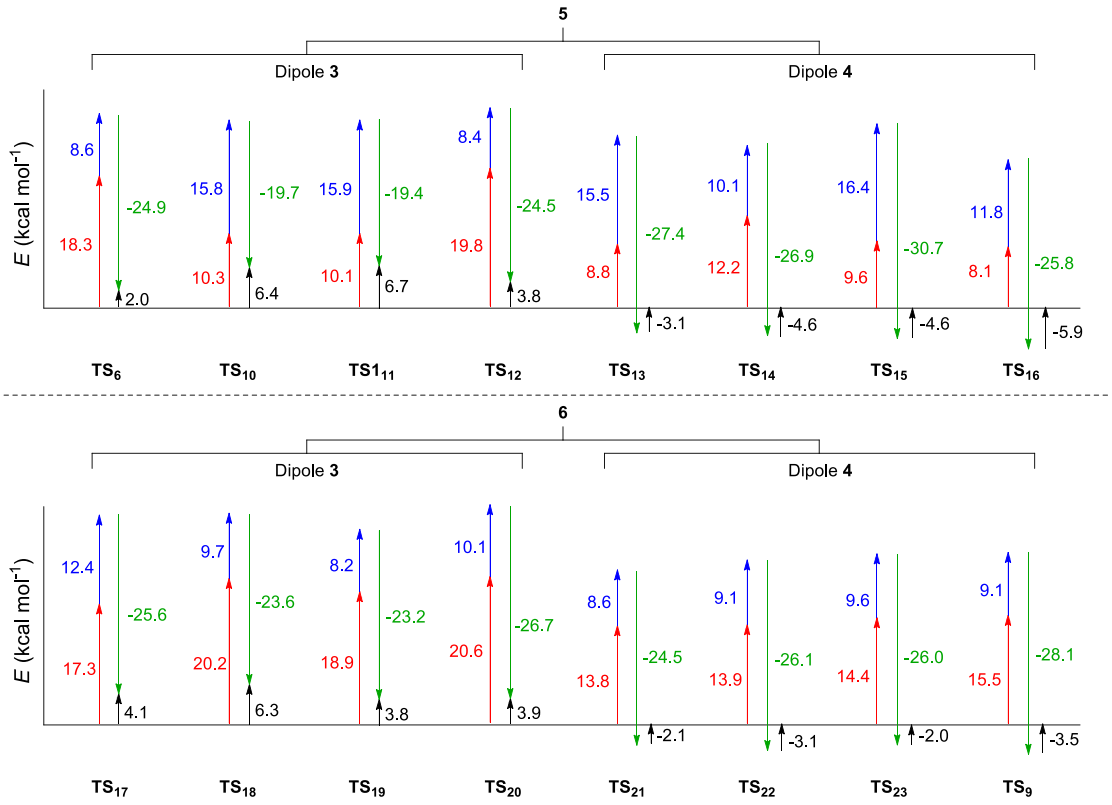

Figure 5.5. Distortion energies of dipoles (red), dipolarophiles (blue), interaction energies (green) and activation energies (black) for the reactions of dipoles **3** and **4** with dipolarophiles **5** (top) and **6** (bottom).

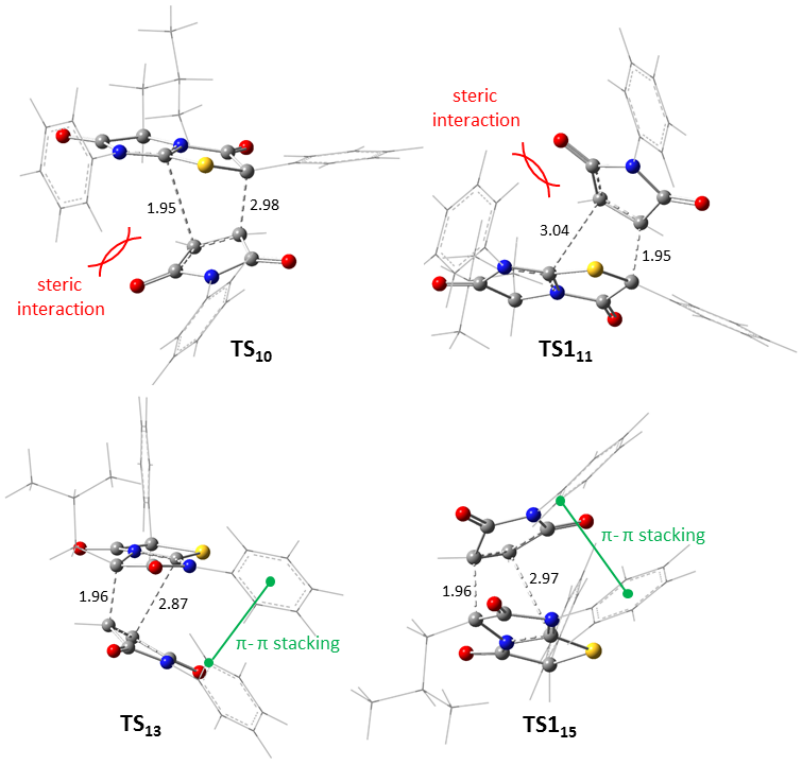

Figure 5.6. Optimized geometries of **TS$_{10}$**, **TS1$_{11}$**, **TS$_{13}$** and **TS1$_{15}$** at the ONIOM(M06-2X/6-311++G(d,p):M06-2X/6-31G) level of theory in toluene (SMD) at 373.1 K.

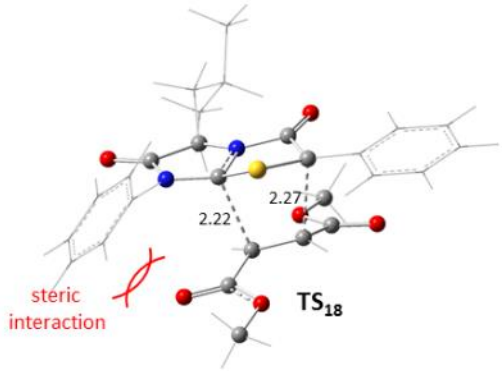

Figure 5.7. Optimized geometry of **TS$_{18}$** at the ONIOM(M06-2X/6-311++G(d,p):M06-2X/6-31G) level of theory in toluene (SMD) at 373.1 K.

Moreover, this computational study shows that the reactions of dipoles **3** and **4** with **5** are controlled by the dipolarophile distortion, caused to a significant extent by the phenyl group linked to N7 of the dipole, which exerts both π-π stacking and steric interactions with **5**. The stereochemical outcome with **6** depends however on the dipole. Thus, the less favored cycloaddition with dipole **3** combines high total distortion energy plus low interaction energy, while the reaction with **4** is controlled by the distortion of the dipole. In a nutshell, dipole **4** appears to be more reactive than **3**, as inferred from a higher interaction energy with the dipolarophiles evaluated. In addition, all the cycloaddition reactions of compound **5** are thermodynamically favored with respect to those of **6** (see Figures 6.3 and 6.4). Finally, the cycloadduct (**9**) that evolves into dihydropyrrole **8** is the most unstable species formed in the reaction between **4** and **6**. A further look at the reaction profile depicted in Figure 5.8 also indicates that the formation of **8** is largely driven by thermodynamically control.

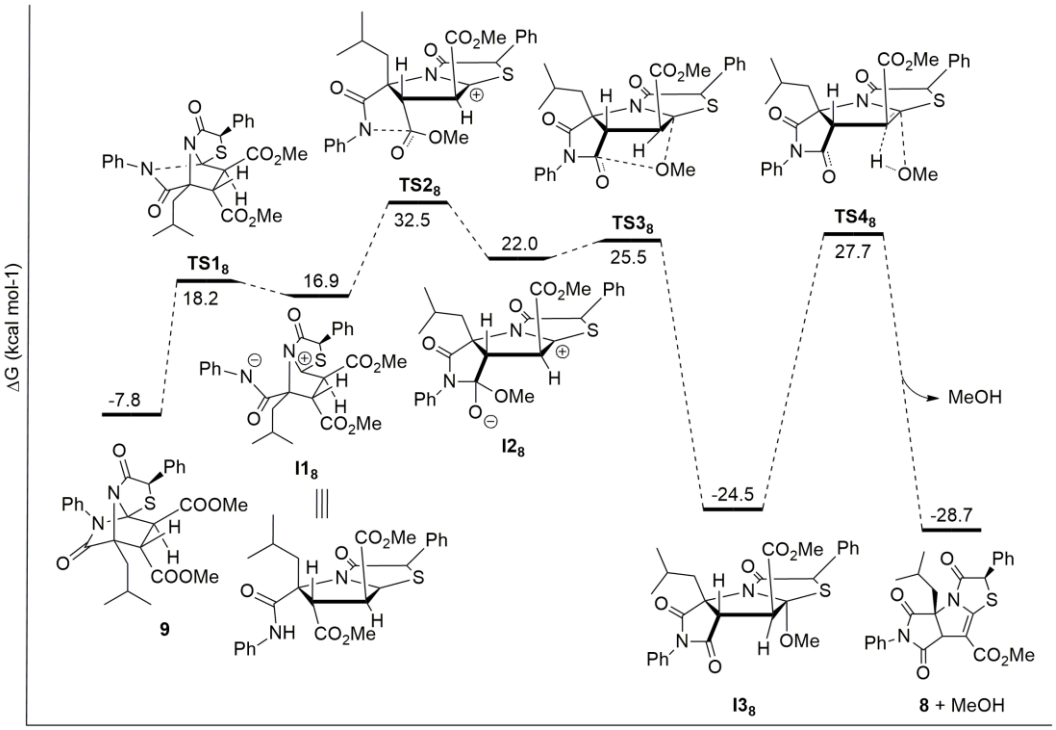

Figure 5.8. Reaction pathway leading to dihydropyrrole **8** from cycloadduct **9**. Free energy values are given in kcal mol^{-1}.

5.4. Conclusions

In conclusion, we disclose for the first time the anomalous behavior of a Janus-type mesoionic dipole susceptible of dual reactivity owing to proton transfer between two atom positions, giving access to divergent structures. Although this ditopic character has been shown against a couple of dipolarophiles, these preliminary results have been explained by theoretical calculations and the principle can be exploited to fine-tune the dipoles to further the scope of novel [3+2] cycloadditions.

5.5. Experimental section

5.5.1. General methods

Solvents and reagents were purchased from commercial suppliers and used without further purification. The identity of all compounds was confirmed by their elemental analyses, melting points, NMR and crystallographic data. The cycloaddition reactions were conducted in a professional microwave oven (Milestone Ethos Touch Control MW reactor) using a non-sealed flask. All NMR data were recorded in $CDCl_3$ solutions (500 MHz for ^{1}H and 125 MHz for ^{13}C). FT-IR spectra were registered in the 4000-6000 cm^{-1} range in KBr disks. Elemental microanalyses were performed by SAIUEx at the University of Extremadura.

5.5.2. Computational details

All calculations reported in this work were carried out using the Gaussian09 package.[13] For all the geometry optimizations and frequency analysis the two-layer ONIOM10 method was employed with the M06-2X[11] density functional method in conjunction with the 6-311++G(d,p) and 6-31G basis sets[12] for high- and for low-level, respectively. The geometries were optimized including solvation effects in toluene, which have been determined by the density-based self-consistent reaction field theory of bulk electrostatic, i.e., the well-known solvation model density (SMD)[14] method that takes into account different contributions such as long-range electrostatic polarization (bulk solvent effect). Frequency at 373.1 K on all the stationary points were carried out at the same level of

theory as the geometry optimizations to ascertain the nature of the stationary points. Ground and transition states were characterized by none and one imaginary frequency, respectively. All of the relative energies shown are free energies calculated at 373.1 K with respect to the reagents. IRC calculations were carried out for the most asynchronous cycloadditions in order to ensure the saddle points were connected with the corresponding minimums, and the saddle points involved in the formation of **8**. Topological analysis of the electron density for dipoles **3** and **4** was carried out with the AIM2000 software at M06-2X/6-311++G(d,p)//ONIOM(M06-2X/6-311++G(d,p):M06-2X/6-31g)-level of theory.

5.5.3. Synthetic procedures

5.5.3.1. Compound **2** was synthetized following previous procedures (80% yield)[7a] and showed spectroscopic properties identical to those of an authentical sample.[7b]

5.5.3.2. **5-Isobutyl-6-oxo-2,7-diphenyl-6,7-dihydro-5*H*-imidazo[2,1-*b*]thiazol-4-ium-3-olate (3).** To a stirred solution of **2** (10 mmol) and 2-bromo-2-phenylacetic acid (10 mmol) in benzene or toluene (60 mL) was added dropwise triethylamine (10 mmol). The mixture was heated at reflux for 15 h. The solution was cooled at room temperature and the resulting crystals of triethylammonium bromide were filtered off. The solution was washed with water (5 x 30 mL) and brine (1 x 30 mL). The organic layer was dried over $MgSO_4$, filtered and evaporated to dryness to give a light orange foam, which was dried under vacuum. To this residue acetic anhydride (7 mL) was added dropwise under stirring followed by triethylamine (21 mL), and the resulting solution was kept at room temperature for 5-10 minutes. Then cold diethyl ether was added, which gave rise to the spontaneous crystallization of the mesoionic heterocycle (**3**) that was collected by filtration and washed with diethyl ether (40% yield). Mp 196-198 ºC. IR (KBr) ν_{max} 3499, 3055, 3019, 2963, 2952, 2867, 1755, 1624, 1586, 1497, 1425, 1330, 1129, 749, 690 cm^{-1}. ^1H NMR (500 MHz, $CDCl_3$) δ 7.70- 6.99 (m, 10H), 5.03 (t, *J* = 8.0 Hz, 1H), 2.33 (t, *J* = 6.8 Hz, 2H), 2.20-2.10 (m, 1H), 1.01 (d, *J* = 8.0 Hz, 6H) ppm. ^{13}C NMR (125 MHz, $CDCl_3$) δ 171.4, 154.2, 153.6, 134.0, 130.9, 130.3, 129.7, 128.6, 123.7, 123.6, 122.3, 99.9, 87.4, 61.7, 37.7, 24.5, 22.7, 22.2 ppm. Anal. Calcd for $C_{21}H_{20}N_2O_2S$: C, 69.20, H, 5.53; N, 7.69; S, 8.80. Found: C, 69.17, H, 5.51; N, 7.68; S, 8.87.

5.5.3.3. **General procedure for the synthesis of compounds 7 and 8.** A suspension of the mesoionic heterocycle **3** (1.0 mmol) and the dipolarophile (**5** or **6**) (1.25 mmol) in

toluene (5 mL) was heated in a MW oven (300 W) for 8 min until reaching a plateau of 100 ºC and then it was kept at that temperature for 12 min (three cycles). The solvent was removed under reduced pressure and the residue was treated with diethyl ether, which afforded crystals of the resulting product (either **7** or **8**).

5.5.3.4. **3-Isobutyl-1,6,8-triphenyldihydro-6,9b-epithioimidazo[1,2-*a*]pyrrolo[3,4-*c*]-pyridine-2,5,7,9(1*H*,3*H*,8*H*,9a*H*)-tetraone (7).** Recrystallized from ethanol (45 % yield). Mp 261-263 ºC. IR (KBr) ν_{max} 3473, 3093, 3065, 3036, 2956, 2935, 2913, 2869, 2360, 1749, 1717, 1597, 1499, 1387, 1361, 1200, 1153, 753, 695 cm^{-1}. ^{1}H NMR (500 MHz, $CDCl_3$) δ 7.80-7.16 (m, 15H), 4.36 (d, *J* = 8.5 Hz, 1H), 4.24 (m, 1H), 4.22 (d, *J* = 8.5 Hz, 1H), 2.19-2.10 (m, 3H), 0.99 (t, 6H) ppm. ^{13}C NMR (125 MHz, $CDCl_3$) δ 170.3, 170.2, 170.0, 168.1, 132.8, 130.9, 130.0, 129.4, 129.3, 129. 2, 128.5, 127.1, 126.3, 92.1, 71.3, 57.1, 56.0, 52.1, 37.3, 24.5, 23.5, 21.9 ppm. Anal. Calcd for $C_{31}H_{27}N_3O_4S$: C, 69.25, H, 5.06; N, 7.82; S, 5.96. Found: C, 69.19, H, 5.02; N, 7.80; S, 6.07.

5.5.3.5. **Methyl 4*a*-isobutyl-3,5,7-trioxo-2,6-diphenyl-3,4*a*,5,6,7,7*a*-hexahydro-2*H*-pyrrolo[3',4':4,5]pyrrolo[2,1-*b*]thiazole-8-carboxylate (8).** Recrystallized from dichloromethane/ethanol (24 % yield). Mp 212-214 ºC. IR (KBr) ν_{max} 3485, 3430, 3076, 3028, 2958, 2871, 2365, 2198, 2100, 1955, 1883, 1726, 1683, 1591, 1500, 1242, 746, 698 cm^{-1}. ^{1}H NMR (500 MHz, $CDCl_3$) δ 7.50-7.26 (m, 10H), 5.39 (s, 1H), 4.56 (s, 1H), 3.86 (s, 3H), 2.56 (dd, J = 11.6 Hz, J = 4.8 Hz, 1H), 2.26 (dd, J = 11.6 Hz, J = 6.4 Hz, 1H), 1.82 (m, 1H), 1.02 (d, J = 5.2 Hz, 3H), 0.97 (d, J = 5.2 Hz, 3H) ppm. ^{13}C NMR (125 MHz, $CDCl_3$) δ 171.9, 171.4, 167.3, 164.2, 156.7, 134.4, 131.2, 129.2, 129.2, 129.0, 128.4, 126.2, 97.4, 71.4, 57.6, 55.6, 51.9, 38.5, 24.9, 23.6, 23.1. Anal. Calcd for $C_{26}H_{24}N_2O_5S$: C, 65.53, H, 5.08; N, 5.88; S, 6.73. Found: C, 65.48, H, 5.07; N, 5.85; S, 6.85.

5.6. Bibliography

(1) (a) *Tautomerism: Concepts and Applications In Science and Technology*; Antonov, L. Eds.; ; Wiley-VCH: Weinheim, 2016. (b) Brehme, R.;Enders, D.;Fernandez, R.;Lassaletta. J. M. *Eur. J. Org. Chem.*, **2007**, 5629-5660. (c) Tanaka, F.; Barbas, C. F. III. In *Enantioselective Organocatalysis: Reactions and Experimental Procedures*; Dalko, P. I., Eds. Wiley-VCH: Weinheim, 2007, Ch. 2, pp 19-55.

(2) (a) Shin, K.; Ryu, J.; Chang, S. *Org. Lett.,* **2014**, *16*, 2022-2025. (b) Loftus, I. M.; White, J. K.; Albani, B. A.; Kohler, L.; Kodanco, J. J.;. Thummel, R. P.; Dunbar, K. R.; Turro, C. *Chem. Eur. J.,* **2016**, *22*, 3704-3708. (c) Causero, A.; Elsen, H.;Ballmann, G.; Escalona A.; Harder, S. *Chem. Comm*. **2017**, *53*, 10386-10389. (d) Widera, A.; Kaifer, E.; Wadepohl, H.; Himmel, H-. J. *Chem. Eur. J.* **2018**, *24*, 1209-1216.

(3) Buzzetty, L.; Prieto, A.; Roy, S. R.; Melchiorre, P. *Angew. Chem. Int. Ed*. **2017**, *56*, 15039-15043.

(4) (a) Izquierdo, C.; Esteban, F.; Parra, A.; Alfaro, R.; Alemán, J.; Fraile, A.; García Ruano, J. L. *J. Org. Chem.* **2014**, *79*, 10417-10433. (b) Trofimov, B. A.; Schmidt, E. Y. *Acc. Chem. Res*., **2018**, 51, 1117-1130. (c) Merino, P.; Chiacchio, M. A.; Legnani, L.; Delso, I.; Tejero, T. *Org. Chem. Front.* **2017**, *4*, 1541-1554. (d) Mao, Y.; Liu, Y.; Hu, Y.; Wang, L.; Zhang, S.; Wang, W. *ACS Catal.* **2018**, *8*, 3016-3020. (e) Sadhukhan, S.; Baire, B. *Adv. Synth. Catal.* **2018**, *360*, 298-304.

(5) (a) *Synthetic Applications of 1,3-Dipolar Cycloaddition Toward Heterocycles and Natural Products*: Padwa, A.; Pearson, W. F., Eds; John Wiley & Sons: New York, 2002. (b) Pellisier, H. *Tetrahedron*, **2007**, *63*, 3235-3285. (c) Suga, H.; Itoh, K. In *Methods and Applications of Cycloaddition Reactions in Organic Synthesis;* Nishiwaki, N., Eds.; John Wiley & Sons: Hoboken, NJ, 2013, pp. 175-204.

(6) Ávalos, M.; Babiano, R.; Cintas, P.; Díaz, J. L.; Jiménez, J. L.; López, I.; Palacios, J. C. *Eur. J. Org. Chem.* **2004**, 2805-2811.

(7) (a) Wolfe, D. M.; Schreiner, P. R. *Synthesis*. **2007**, *13*, 2002-2008. (b) Sundaram, G. S. M.; Venkatesh, C.; Ila, H.; Junjappa, H. *Synlett*, **2007**, *2*, 251-254.

(8) Erguven, H.; Leitch, D. C.; Keyzer, E. N.; Arndtsen, B. A. *Angew. Chem. Int. Ed*. **2017**, *56*, 6078-6082.

(9) García de la Concepción, J.; Ávalos, M.; Cintas, P.; Jiménez, J. L.; Light, M. E. *Org. Biomol. Chem.* **2018**, *16*, 3438-3452.

(10) (a) Dapprich, S.; Komáromi, I.; Byun, K. S.; Morokuma, K.; Frisch, M. J. *J. Mol. Struct. (Theochem).* **1999**, *461-462*, 1-21. (b) Maseras, F.; Morokuma, K. *J. Comp. Chem*. **1995**, *16*, 1170-1179. (c) Froese, R. D.; Morokuma, K. In *The Encyclopedia of Computational Chemistry*; Schleyer, P. v. R.; Allinger, N. L.; Clark, T.; Gasteiger, J.; Kollman, P. A.; Schaefer, H. F. III; Schreiner, P. R., Eds. John Wiley & Sons: Chichester, 1998, pp. 167-183.

(11) (a) Zhao, Y.; Truhlar, D. G. *Theor. Chem. Acc*. **2008**, *120*, 215-241. (b) Zhao, Y.; Truhlar, D. G. *Acc. Chem. Res*. **2008**, *41*, 157-167.

(12) (a) Ditchfield, R.; Hehre, W. J.; Pople, J. A. *J. Chem. Phys*. **1971**, *54*, 724–728. (b) Hehre, W. J.; Ditchfield, R.; Pople, J. A. *Mol. Phys*. **1974**, *27*, 209–214. (c) Gordon, M. S.; *Chem. Phys. Lett*. **1980**, *76*, 163–168. (d) Hariharan, P. C.; Pople, J. A. *Theor. Chem. Acc*. **1973**, *28*, 213–222. (e) Francl, M. M.; Pietro, W. J.; Hehre, W. J.; Binkley, J. S.; DeFrees, D. J.; Pople, J. A.; Gordon, M. S. *J. Chem. Phys*. **1982**, *77*, 3654–3665.

(13) Frisch, M. J.; Trucks, G. W.; Schlegel, H. B.; Scuseria, G. E.; Robb, M. A.; Cheeseman, J. R.; Scalmani, G.; Barone, V.; Mennucci, B.; Petersson, G. A.; Nakatsuji, H.; Caricato, M.; Li, X.; Hratchian, H. P.; Izmaylov, A. F.; Bloino, J.; Zheng, G.; Sonnenberg, J. L.; Hada, M.; Ehara, M.; Toyota, K.; Fukuda, R.; Hasegawa, J.; Ishida, M.; Nakajima, T.; Honda, Y.; Kitao, O.; Nakai, H.; Vreven, T.; Montgomery Jr., J. A.; Peralta, J. E.; Ogliaro, F.; Bearpark, M.; Heyd, J. J.; Brothers, E.; Kudin, K. N.; Staroverov, V. N.; Kobayashi, R.; Normand, J.; Raghavachari, K.; Rendell, A.; Burant, J. C.; Iyengar, S. S.; Tomasi, J.; Cossi, M.; Rega,

N.; Millam, J. M.; Klene, M.; Knox, J. E.; Cross, J. B.; Bakken, V.; Adamo, C.; Jaramillo, J.; Gomperts, R.; Stratmann, R. E.; Yazyev, O.; Austin, A. J.; Cammi, R.; Pomelli, C.; Ochterski, J. W.; Martin, R. L.; Morokuma, K.; Zakrzewski, V. G.; Voth, G. A.; Salvador, P.; Dannenberg, J. J.; Dapprich, S.; Daniels, A. D.; Farkas, Ö; Foresman, J. B.; Ortiz, J. V.; Cioslowski, J.; Fox, D. J. Gaussian 09, Revision D.01; Gaussian, Inc.: Wallingford, CT, 2009.

(14) Marenich, A. V.; Cramer, C. J.; Truhlar, D. G. *J. Phys. Chem. B* **2009**, *113*, 6378-6396.

(15) Ávalos, M.; Babiano, R.; Bravo, J. L.; Cintas, P.; Jiménez, J. L.; Palacios, J. C.; Silva, M. A. *J. Org. Chem.* **2000**, *65*, 6613-6619.

(16) Houk, K. N.; Champagne, P. A. *J. Org. Chem*. **2017**, *82*, 10980-10988.

(17) Bader, R. F. W. Atoms in Molecules: A Quantum Theory, Oxford University Press, Oxford, 1990.

(18) Ávalos, M.; Babiano, R.; Cabanillas, A.; Cintas, P.; Higes, F. J.; Jiménez, J. L.; Palacios, J. C. *J. Org. Chem.* **1996**, *61*, 3738-3748.

6. Computational Screening of New Orthogonal Metal-Free Dipolar Cycloadditions of Mesomeric Betaines

6.1. Abstract

Computational strategies have gained increasing impact in the *de novo* design of large molecular sets targeted to a desired application. Herein, DFT-assisted theoretical analyses of cycloadditions, involving mesoionic dipoles and strained cycloalkynes, unveil a series of unexplored mesomeric betaines as vastly superior candidates for orthogonal applications. Thus, isosydnones; thiosydnones; and a sixmembered homolog, 6-oxo-1,3-oxazinium-4-olate, exhibit enhanced reactivity with respect to sydnone, which is the archetypal mesoionic ring employed so far in orthogonal chemistry. These compounds were found by assessing energy barriers and transition structures, which are largely governed by electron fluxes from dipolarophile to dipole and noncovalent interactions. Charge-transfer analysis also accounts for previous experimental and theoretical results gathered in the literature, and provides a rationale for further substitution variations. The above naked dipoles release only CO_2 as a byproduct through retro-Diels–Alder of the resulting cycloadducts. These results should invite practitioners to look at such underestimated dipoles and could also help to minimize the number of experiments.

6.2. Introduction

The interplay between the tunable and selective characteristics of ligation reactions harnessing the use of orthogonal pairs, whereby any modification in one pair does not cause any effect onto the other,[1] has resulted in the rapid development of bioorthogonal chemistry, aimed at dissecting life processes with exogenous chemical modifications.[2] Although the Cu(I)-catalyzed azide-alkyne cycloaddition represents the paradigmatic example of so-called click reactions, the cytotoxicity of Cu(I) ions hinders its application in living systems, a drawback shared by other metal-catalyzed couplings, which do not meet the stringent requirements of *in vivo* monitoring. Metal-free versions, the strain-promoted azide-alkyne cycloaddition in particular, have improved the biocompatibility of ligation protocols,[3] thereby enlarging successfully the scope of traditional conjugation reactions.[4] Dipoles other than azides, such as nitrones,[5] diazo compounds,[6] and sydnones[7] have been employed in orthogonal cycloadditions as well. Sydnones (1,2,3-oxadiazolium-5-olates), which belong to the wide family of masked dipole heterocycles,[8] are willing partners against

alkynes, yet requiring harsh thermal conditions, leading to pyrazoles. The use of strained cycloalkynes affords milder protocols and, in fact the cycloaddition of *N*-phenylsydnone and bicyclononyne (BCN) was the first bioorthogonal application of a mesoionic compound.[7a] Further improvements have been introduced since, especially by Taran and coworkers, who have described fast click cycloadditions with fluorosydnones.[7b-d]

In most cases, however, the direct and often the only direct way to probe the characterization of orthogonal cycloadditions is through experimentation, which leads invariably to trial and error, as such processes may take place through high-energy barriers, being in addition quite sensitive to solvent and substituent effects. Some successful *a posteriori* theoretical analysis, including predictive behaviors too, have been recently reported for strained cycloadditions including mesoionic dipoles as well.[9] Taking advantage of our studies on computation-aided reactivity of mesoionic heterocycles, we herein provide a theoretical analysis of dipolar cycloadditions of structurally simple mesoionic rings, which unveiled the potential use of mesomeric betaines, yet unexplored in orthogonal chemistry, as superior dipoles in click cycloadditions, thus guiding further experimental pursuits.

6.3. Results and discussion

Our preliminary toehold was to examine the reactivity of phenyl azide (**2**) toward a series of representative unsubstituted mesoionic dipoles (**3**-**7**) against cyclooctyne, thereby making it possible a comparative analysis. To this end, calculations were performed at the M06-2X hybrid functional[10] in conjunction with the 6-311++G(d,p) basis set,[11] and modeling bulk solvation in water[12] under ambient conditions (298 K and 1 atm). Results depicted in Figure 6.1 show that reactivity follows the order: phenyl azide (**2**) < sydnone (**3**) < thioisomünchnone (**4**) < münchnone (**5**) < isomünchnone (**6**) < 1,3-oxathiolium-5-olate (**7**). Regarding mesoionic dipoles, the preceding order indicates that the more exothermic cycloaddition reactions also have lower barriers. Inspection of the corresponding saddle points evidences that all the cycloadditions proceed by concerted mechanisms leading to highly strained cycloadducts **8**-**13**.

It is well known that most mesoionic-based intermediate cycloadducts are not stable enough and undergo facile retro-Diels-Alder reactions that render aromatic heterocycles. Accordingly, cycloadducts **9**, **11**, and **13** would extrude carbon dioxide to yield pyrazole, pyrrole, and thiophene rings, respectively.

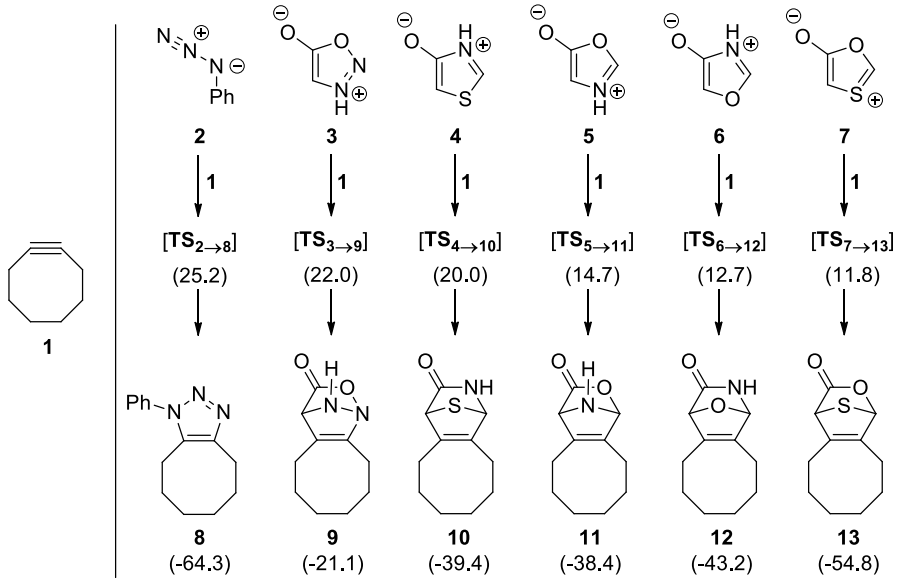

Figure 6.1. Free energy values (in kcal mol^{-1}) for the concerted cycloadditions of dipoles **2**-**7** with cyclooctyne (**1**) at the M06-2X/6-311++G(d,p) level in water (SMD).

Cycloadduct **10** could evolve into either thiophene or pyridin-2-one derivatives by extrusion of isocyanate or sulfur, respectively. Finally, compound **12** should release easily an isocyanate fragment to give a furan-containing bicycle. Since a pre-requisite for reactions to be bioorthogonal is the absence of toxic by-products, the extrusion of isocyanate or sulfur prevents the use of heterocycles **4** and **6** in such applications. On the contrary, the facile elimination of carbon dioxide from cycloadducts **9**, **11**, and **13** make them potentially biocompatible as CO_2 signaling has been identified in mechanisms of cell signal transduction.[13] On the other hand, münchnones and thiomünchnones, which exhibit enhanced reactivity toward alkynes, are not usually stable and must be generated *in situ* by means of toxic reagents (acetic anhydride, trifluoroacetic anhydride or carbodiimides), thus discouraging their *in vivo* application still further. Having the above drawbacks in mind, we turned the attention to isostructural variations of the sydnone skeleton looking for the desirable CO_2-release from the corresponding cycloadducts. Data retrieved from older literature[14] indicate that isosydnones (**14**), thiosydnones (**15**), and 6-oxo-1,3-oxazinium-4-olates (**16**) exhibit reactivity as dipoles against dipolarophiles and, in line with mesoionics **3**, **5**, and **7**, their resulting cycloadducts (Figure 6.2) from strained alkynes would extrude

CO_2. It is worth pointing out that, although all mesoionics belong to the general class of mesomeric betaines, six-membered rings are no longer circumscribed to mesoionic structures. Moreover, on the basis of recent connectivity-matrix analysis and DFT calculations,[15] most type-A mesoionics (which include sydnones and other common mesoionic dipoles) are actually conjugated betaines, rather than semi-conjugated or cross-conjugated systems comprising both five- and six-membered heterocycles. Clearly, the six-membered counterparts, mesoionic 1,3-oxazinium-4-olates remain unexplored in orthogonal chemistry. Such systems undergo cycloadditions with some heterocumulenes, although metastable, but isolable, rings may also rearrange to both acyclic and cyclic structures.[16]

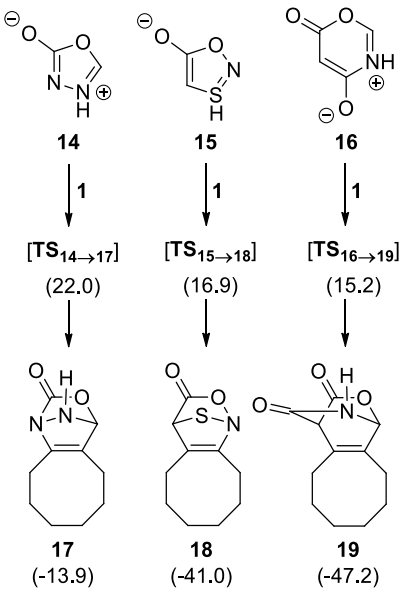

Figure 6.2. Free energy values (in kcal mol^{-1}) for the concerted cycloadditions of dipoles **14**-**16** with cyclooctyne (**1**) at the M06-2X/6-311++G(d,p) level in water (SMD).

Computational analysis shows again that cycloadditions of **14**-**16** with cyclooctyne are concerted processes characterized by lower free energy barriers than the one calculated for the equivalent cycloaddition with sydnone **3** (Figures 6.2, 6.3 and 6.4). Also, the corresponding transition structures show a greater asynchronicity, especially in the case of

dipoles **16** and **14**, than those of **3** and **15**, i.e. when carbon replaces nitrogen at the electrophilic terminus of the dipole. Furthermore, the retro-Diels-Alder processes by which cycloadducts **9** and **17**-**19** extrude carbon dioxide (Figure A6.1) exhibit lower free energy barriers than the initial 1,3-dipolar cycloadditions, which account for rate-determining steps in all cases.

As these cycloadditions are kinetically controlled processes, further insight into the factors controlling the reaction outcome could be extracted from an in-depth analysis of structures $\mathbf{TS_{3\rightarrow9}}$, $\mathbf{TS_{14\rightarrow17}}$, $\mathbf{TS_{15\rightarrow18}}$ and $\mathbf{TS_{16\rightarrow19}}$. To assess both the electron flux direction and charge transfer (CT), we calculated, by the FMO approximation,[17d] the chemical potential ($\mu = \partial E/\partial N$) and chemical hardness ($\eta = \partial^2 E/\partial N^2$) of distorted geometries of reactants at their saddle points. Charge transfer values were obtained by relating the chemical potential ($\mu = \partial E/\partial N$) of the fragments with respect to their chemical hardness ($\eta = \partial^2 E/\partial N^2$), while donation and back donation features were estimated by relating the *I* (ionization potential) and *A* (electron affinity) values of the fragments.[17a-c] Such calculations were performed at the above-mentioned M06-2X method, but removing the diffuse functions [6-311G(d,p)] because the *A* values become essentially zero when adding such functions to the basis sets.[17d] The *I* and *A* values were also computed by the finite difference method (FD) (see Addendum). All these data gathered in Tables 6.1 and 6.2 are given in eV. For the sake of clarity, the most relevant data collected in Tables 6.1 and 6.2 are shown in Figures 6.3 and 6.4 as well, thus helping further understanding. Likewise, the main interactions arising from FMO overlappings have also been displayed.

The chemical potentials of dipoles **3** and **14**-**16** (Table 6.2 and Figures 6.3 and 6.4), are lower than that of cyclooctyne, thereby indicating the main electron flux moves in all cases from dipolarophile (d) to dipole (D). The net charge transfer (highlighted in yellow) at the saddle points increases as the energy barrier decreases, with the sole exception of the cycloaddition of **16**, whose *I* value (7.44 eV) is the lowest of the four dipoles. By decomposing the net CT into donation (green values in Figures 6.3 and 6.4) and back donation (depicted in blue), the former follows the same trend as net CTs whereas back donation values decreases as the energy barrier decreases. This trend is slightly reversed for **16** owing to the *I* contribution. In addition, the HOMO-LUMO energy gaps for the distorted dipoles (D) and dipolarophile (d) at the four saddle points fully agree with HOMO(d)–LUMO(D) controlled processes. Accordingly, the HOMO(d)–LUMO(D) gap does illustrate well the CT donation, while the HOMO(D)–LUMO(d) gap mirrors that of CT back

donation. Not least, the low HOMO(d)-LUMO(D) gap calculated for the cycloaddition of **16** evidences the greatest reactivity of that dipole.

Table 6.1. FMO energies and HOMO-LUMO gaps values for the distorted fragments of saddle points **$TS_{3\rightarrow9}$**, **$TS_{14\rightarrow17}$**, **$TS_{15\rightarrow18}$** and **$TS_{16\rightarrow19}$** calculated by the FMO method at the M06-2X/6-311G(d,p) level (all data given in eV).

Saddle points	Fragments	Frontier Molecular Orbitals		HOMO-LUMO gaps	
		HOMO	LUMO	$LUMO_d$-$HOMO_D$	$LUMO_D$-$HOMO_d$
$TS_{3\rightarrow9}$	Sydnone (**3**)	-7.78	-1.61	8.67	6.46
	Cyclooctyne (**1**)	-8.07	0.89		
$TS_{14\rightarrow17}$	Isosydnone(**14**)	-7.91	-1.86	9.06	6.26
	Cyclooctyne (**1**)	-8.12	1.15		
$TS_{15\rightarrow18}$	Thiosydnone (**15**)	-8.20	-2.86	9.34	5.21
	Cyclooctyne (**1**)	-8.07	1.14		
$TS_{16\rightarrow19}$	Betaine(**16**)	-7.44	-2.94	8.80	5.19
	Cyclooctyne (**1**)	-8.13	1.36		

Table 6.2. Ionization potentials (I), electron affinities (A), chemical potentials (μ), chemical hardness (η) and total charge transfer (ΔN_{tot}), charge donation (ΔN_{don}) and back-donation ($\Delta N_{back\text{-}donated}$) values for the distorted fragments of saddle points **$TS_{3\rightarrow9}$**, **$TS_{14\rightarrow17}$**, **$TS_{15\rightarrow18}$** and **$TS_{16\rightarrow19}$** calculated by the FMO method at the M06-2X/6-311G(d,p) level (all data given in eV).

Saddle points	Fragments	I	A	μ	η	ΔN_{tot}	$\Delta N_{back\text{-}donanted}$	ΔN_{don}
$TS_{3\rightarrow9}$	Cyclooctyne (**1**)	7.78	1.61	-4.69	6.17	0.073	-0.214	0.286
	Sydnone (**3**)	8.07	-0.89	-3.59	8.95			
$TS_{14\rightarrow17}$	Cyclooctyne (**1**)	7.91	1.86	-4.89	6.05	0.092	-0.204	0.296
	Isosydnone(**14**)	8.12	-1.15	-3.48	9.26			
$TS_{15\rightarrow18}$	Cyclooctyne (**1**)	8.20	2.86	-5.53	5.34	0.142	-0.179	0.321
	Thiosydnone(**15**)	8.07	-1.14	-3.46	9.21			
$TS_{16\rightarrow19}$	Cyclooctyne (**1**)	7.44	2.94	-5.19	4.51	0.129	-0.186	0.314
	Betaine(**16**)	8.13	-1.36	-3.38	9.49			

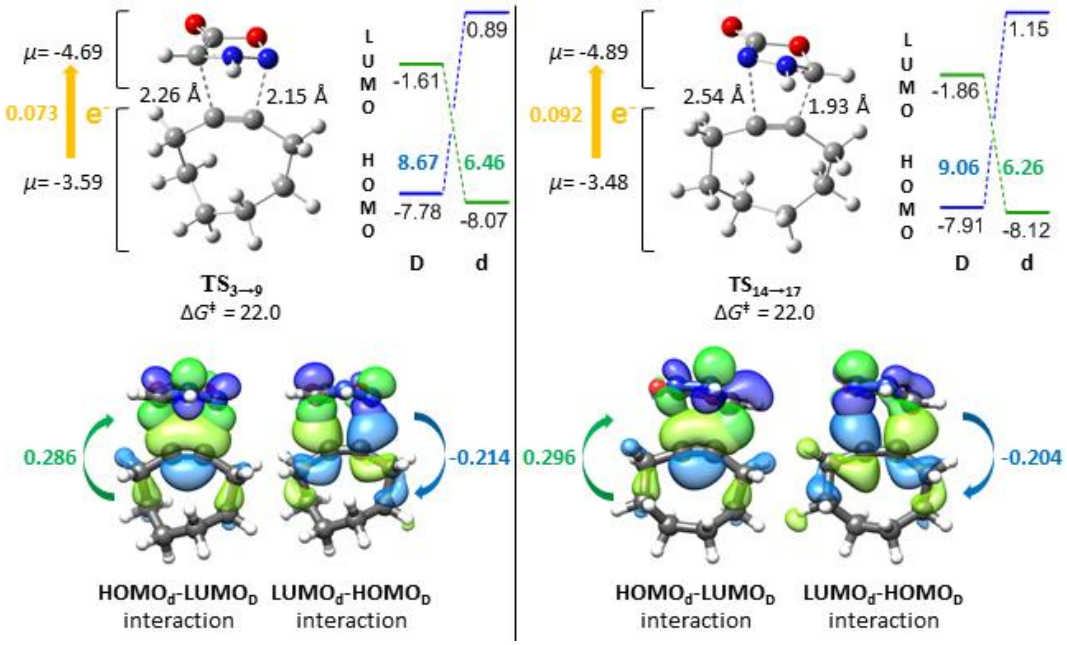

Figure 6.3. Saddle points (**TS$_{3\rightarrow9}$** and **TS$_{14\rightarrow17}$**) optimized-geometries for the reaction between dipoles **3** and **14** and cyclooctyne (**1**) at the M06-2X/6-311++G(d,p)-level in water (SMD) (free energies are given in kcal mol^{-1}). Chemical potential (μ) values of the distorted fragments, net charge transfer (in yellow), donation (in green), and back donation (in blue) were calculated at the M06-2X/6-311G(d,p) level through the FMO approximation and are given in eV. FMO energies and energy gaps were determined at the same level (the "D" and "d" symbols are referred to the dipole and dipolarophile, respectively).

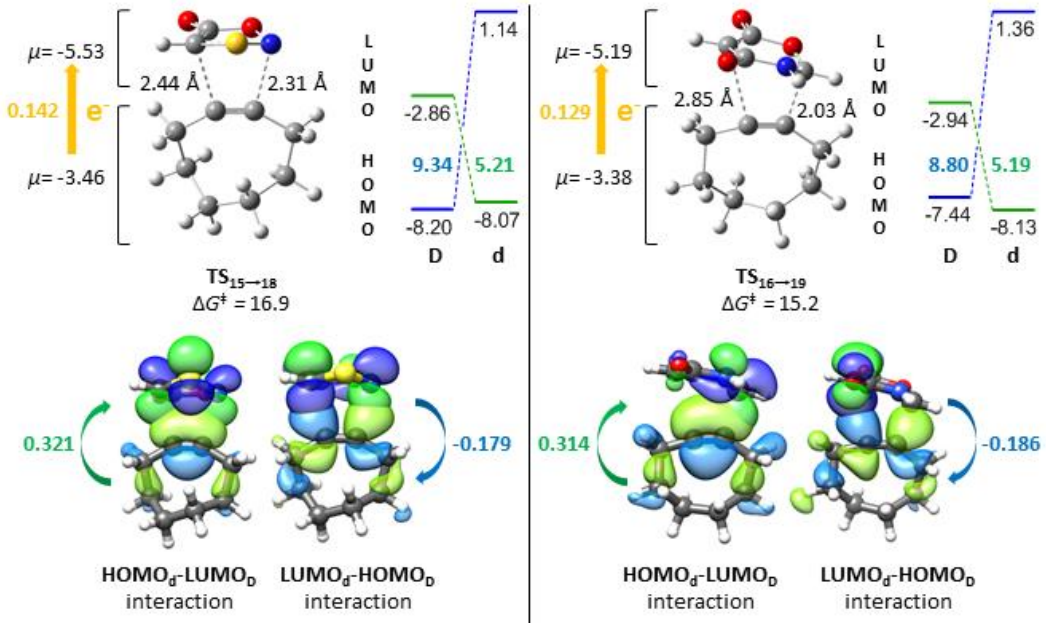

Figure 6.4. Saddle points (**TS$_{15\rightarrow18}$** and **TS$_{16\rightarrow19}$**) optimized-geometries for the reaction between dipoles **15** and **16** and cyclooctyne (**1**) at the M06-2X/6-311++G(d,p)-level in water (SMD) (free energies are given in kcal mol^{-1}). Chemical potential (μ) values of the distorted fragments, net charge transfer (in yellow), donation (in green), and back donation (in blue) were calculated at the M06-2X/6-311G(d,p) level through the FMO approximation and are given in eV. FMO energies and energy gaps were determined at the same level (the "D" and "d" symbols are referred to the dipole and dipolarophile, respectively).

The above results showing how the electron flux arrow goes from cyclooctyne to the dipole, allow us to rationalize previous computational and experimental studies. Thus, the poor reactivity of some cyclooctynes, like DIFO (**28**), against *N*-phenylsydnone,[9c] should reasonably be ascribed to the presence of electron-withdrawing fluorine atoms near the triple bond in the dipolarophile unit, which minimize the electron flux. Conversely, methyl groups near the triple bond exert the opposite effect, giving rise to the ultrafast click cycloaddition reported for *N*-phenylfluorosydnone (**20**) and TMTH (**26**).[7b] Notably, there appears to be a synergetic effect that benefits from both the presence of fluorine atoms at the dipole moiety and the positive inductive effect exerted by four methyl groups in cyclooctyne **26**. Recently, kinetic studies involving the cycloaddition of 3,4-disubstituted sydnones with highly strained cyclooctynes have shown how the presence of a

trifluoromethyl group in *N*-phenylsydnone led to a remarkable rate enhancement (by 2-fold).[18] This result overcomes the challenging isolation of fluorosydnones and evidences again the importance of electron-withdrawing substituents at the mesoionic dipole, which favor the dominating electron transfer from dipolarophile to dipole.

Furthermore, our computational analysis took us to replace the C-H bonds in dipoles **3**, **14** and **16** by C-F counterparts and the unsubstituted N-H groups by *N*-Ph linkages, giving rise to dipoles **20**, **21** and **23** (Figure 6.5). For thiosydnone **15**, capable of accommodating only one substituent, model compound **22** bears an additional phenyl group, as a fluorine atom at that position would result in an inefficient dipole for biorthogonal application (i.e. unable to be linked to a biomolecule or fluorophore unit).

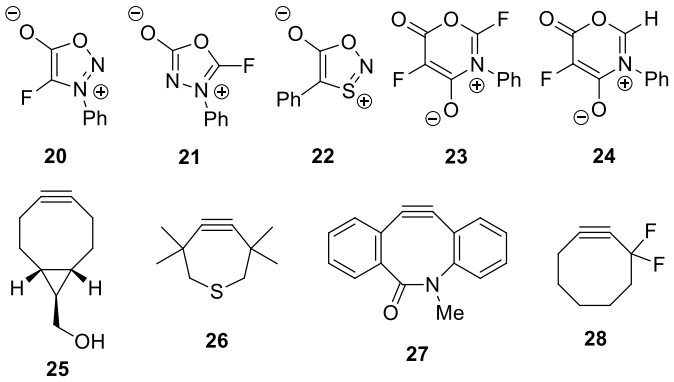

Figure 6.5. Reactive dipoles (**20**-**24**) and cyclooctynes **25**-**27** checked in the *in silico* study.

As expected, the reactions of fluoroderivatives **20**, **21** and **23** with cyclooctyne (**1**) (Table 6.3) are much faster than those shown for dipoles **3**, **14**-**16** (Figures A6.3 and A6.4). The energy barrier decreases by 7.2 kcal mol^{-1} in the case of sydnone **20**, 8.7 kcal mol^{-1} for **21**, 5.4 kcal mol^{-1} for **23**, and just 1.9 kcal mol^{-1} for 4-phenylthiosydnone (**22**). The latter represents the least reactive dipole against cyclooctyne (**1**) (see Table 6.3), a fact that together with the lack of structural diversity make it unsuitable for orthogonal chemistry. Accordingly, dipole **22** was ruled out for further explorations of reactivity toward cyclooctynes. For comparative assessments with fluorosydnone **20**, we screened the cycloadditions of dipoles **21** and **23** against BCN (**25**), TMTH (**26**), and BARAC (**27**). BCN has been widely employed in bioorthogonal cycloadditions with sydnones, whereas

BARAC and TMTH have proven to be the most reactive strained dipolarophiles toward sydnones. The three cycloalkynes bear electron-withdrawing groups far enough from the reactive site and, hence (-I) effects should not be expected. On the other hand, saturated structures (**25** and **26**), leaving aside the triple bond will hardly be able to delocalize charge. On the contrary, the four methyl groups in **26**, near the triple bond, exert a notable (+I) effect that lowers significantly the energy barriers as predicted by our analysis, thereby increasing the corresponding reaction rates.[7b,9c]

Table 6.3 shows the corresponding barriers and free energies for the above-mentioned cycloadditive processes involving fluorodipoles **20**, **22**-**24** against cyclooctynes **1**, **25**-**27**. It should be noted that cycloaddition with BARAC (**27**) affords two regioisomers, i.e. the process is not regiospecific, albeit one of them is slightly favored (see Figure A6.8).

Table 6.3. Free energy differences among saddle points and cycloadducts with respect to their reagents in kcal mol^{-1} for the cycloadditions of fluorodipoles **20**, **21**, **23** and **24** with dipolarphiles **1**, **25**-**27**, as well as between *N*-phenylthiosydnone (**22**) with cyclooctyne (**1**).

		1	**25**	**26**	**27**[a]
20	$\Delta G^{\ddagger}$	14.8	16.4	11.2	10.0
	ΔG	-33.5	-30.4	-35.7	-43.2
21	$\Delta G^{\ddagger}$	13.3	15.3	13.7	12.0
	ΔG	-25.7	-22.3	-25.4	-37.6
22	$\Delta G^{\ddagger}$	15.0	---	---	---
	ΔG	-39.7	---	---	---
23	$\Delta G^{\ddagger}$	9.8	11.0	9.3	10.6
	ΔG	-61.3	-53.3	-50.0	-71.9
24	$\Delta G^{\ddagger}$	10.2	12.5	8.4	9.6
	ΔG	-57.5	-49.1	-51.8	-69.1

[a] Both energy barriers and free energies shown for BARAC refer to those of the prevalent regioisomer.

Surprisingly, the cycloadditions of **20**, **21**, and **23** with BCN (**25**) are slightly slower than with cyclooctyne. In the search for a rationale, these results led us to carry out the same analysis developed in Tables 6.1 and 6.2 and Figures 6.3 and 6.4 for the reactions of **20**, **21**, and **23** with both BCN and cyclooctyne (Figures A6.3-A6.6). The resulting data showed that the dipolar cycloadditions of **20** and **21** with BCN (**25**) involve more CT donation (from dipolarophile to dipole) and lower $HOMO_d$-$LUMO_D$ gaps than in the reaction with cyclooctyne. This behavior is reversed for **23** and BCN (**25**), where lower CT donation is accompanied by a greater $HOMO_d$-$LUMO_D$ gap. Nevertheless, this comparative analysis of TSs alone does not justify the lower reactivity of the three dipoles against BCN (**25**). A

subsequent analysis of non-covalent interactions (NCI)[19] for the transition structures of cycloadditions involving **20**, **21**, and **23** with cyclooctyne (**1**) and BCN (**25**) (see Table 6.4 and figures therein where green and red colors highlight van der Waals and steric interactions, respectively) reveal that a slight increase in steric interactions for BCN in the calculated isosurfaces also translates into a slight rise in the energy barriers relative to cyclooctyne.

Table 6.4. 3D-Plots of the reduced density gradient (RDG) *versus* the electron density (ρ) multiplied by the sign of the second Hessian eigenvalue [(λ_2)ρ], with an isosurface value of 0.5 for the saddle points optimized-geometries in reactions involving cyclooctyne (**1**) and BCN (**25**) with dipoles **20**, **21** and **23**.

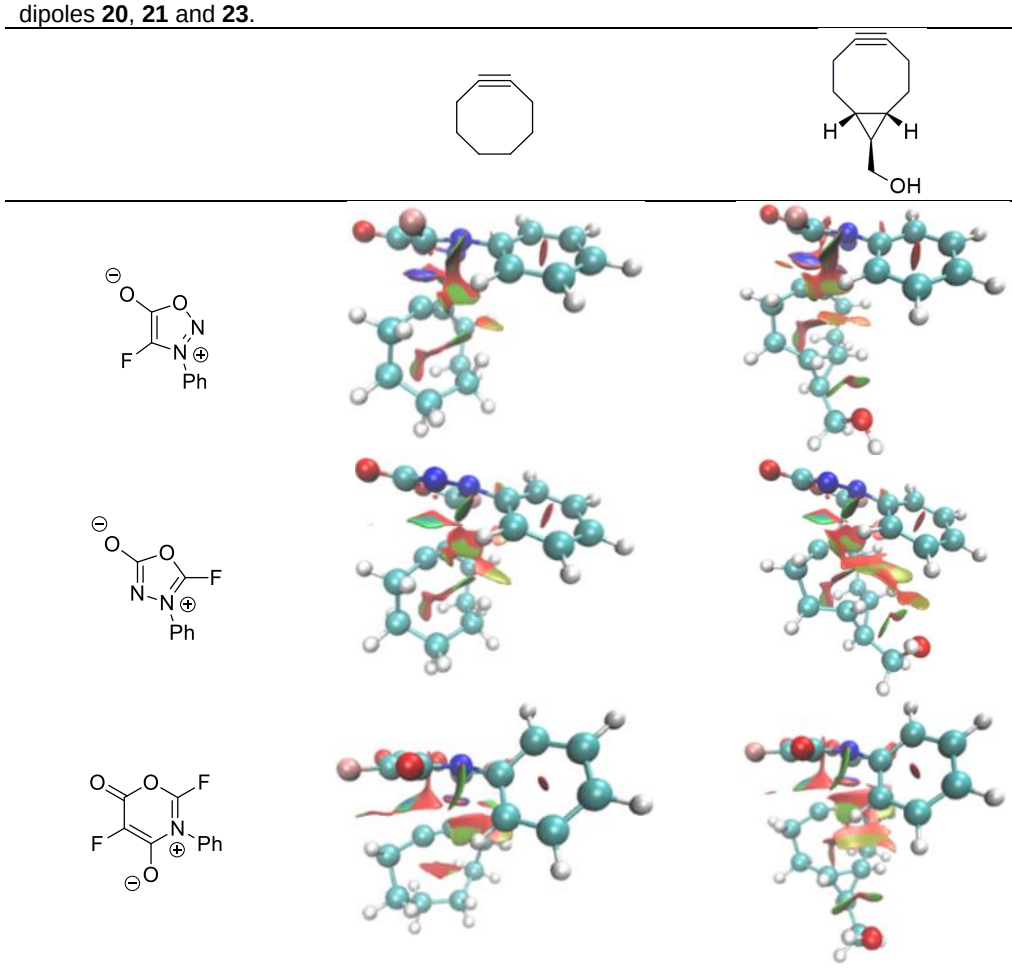

While the reactivity of **21** and **23** toward TMTH (**26**) and cyclooctyne (**1**) is quite similar ($\Delta\Delta G^{\ddagger}$ ~0.5 kcal mol^{-1}), the energy barrier for the cycloaddition of **20** with TMTH is lower (by *ca*. 3.5 kcal mol^{-1}) than the one calculated *versus* cyclooctyne (see Table 6.3). This unexpected lack of reactivity of **21** and **23** against TMTH is due to steric interaction occurring between the fluorine atom at C-2 of **21** and **23** (i.e. the acceptor carbon of dipoles) and the methyl groups of TMTH (see Figure 6.6). Actually the replacement of the fluorine atom at C-2 of **23** by hydrogen (betaine **24**) causes a drop to 8.4 kcal mol^{-1} in the energy barrier (Table 6.3). That substitution in dipole **21** makes it useless because elimination of its electron withdrawing group would raise the energy barriers, as it happens in the case of **22**.

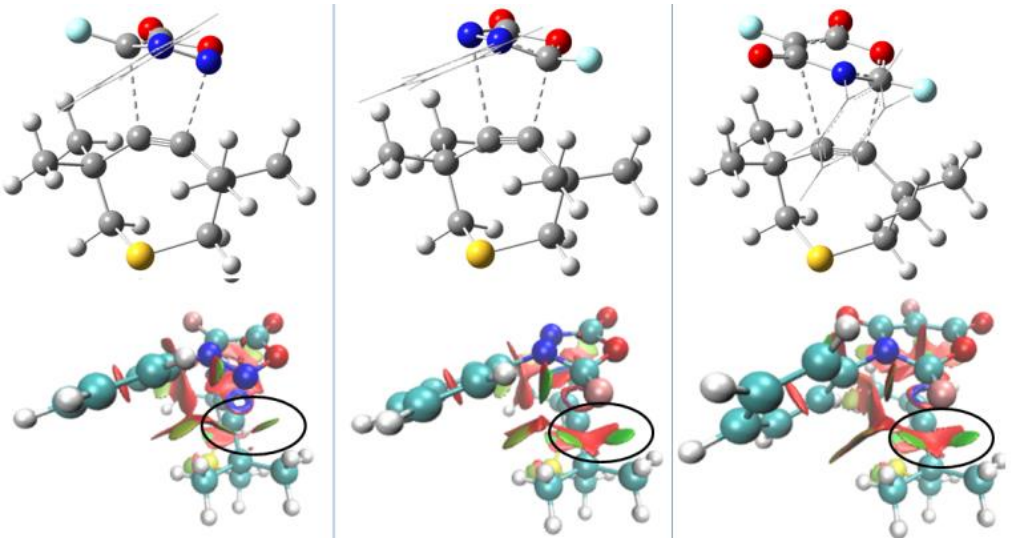

Figure 6.6. Optimized geometries of the saddle points for cycloaddition reactions between TMTH (**26**) and dipoles **20**, **21**, and **23** (left to right) (up) and their 3D plots of the reduced density gradient (RDG) *versus* the electron density (ρ) multiplied by the sign of the second Hessian eigenvalue [(λ_2)ρ], with an isosurface value of 0.5 (down). For clarity the phenyl groups of upper figures have been represented with wireframe.

As pointed out before, the cycloadditions of **20**, **21**, and **23** with BARAC (**27**) were not regioselective at all (Figure A6.8). The reactivities of those three dipoles were similar and followed the order: isosydnone **21** < betaine **23** < sydnone **20** for the most favored regioisomeric approach (see Table 6.3). When the reaction was computed for **24**, the energy barrier diminished by ~1 kcal mol^{-1} relative to that calculated for **23** (Figure 6.7),

thereby confirming the fluorine atom at that position exerts a mild steric hindrance in line with the cycloaddition involving TMTH as dipolarophile.

Moreover, data summarized in Table 6.3 are consistent with a poorer reactivity of the monofluoro-substituted betaine **24** with cyclooctyne (**1**) and BCN (**25**) relative to its difluoro counterpart **23**. Thus, while the presence of a F-atom at C-2 causes some steric repulsion when **23** approaches both TMTH (**26**) and BARAC (**27**), the halogen atom has little influence on the cycloadditions with cyclooctyne (**1**) and BCN (**25**). Apparently, the corollary that follows from these observations is that hydrogen atoms on sp^3-hybridized carbon atoms contiguous to the triple bond do not cause any significant steric hindrance. In addition, in cases devoid of steric interactions, the influence exerted by two electron-withdrawing F-atoms in **23** is indeed remarkable with respect to the presence of only one fluorine atom (as in **24**), thus affording slightly lower barriers for the former.

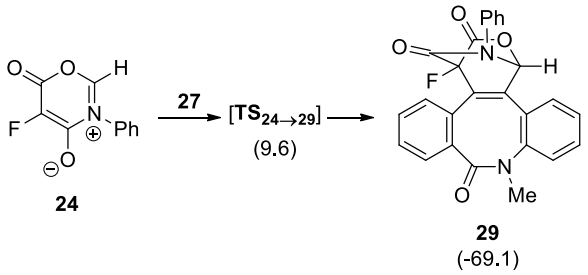

Figure 6.7. Computed free energy barrier for the reaction between the conjugated mesomeric betaine **24** *versus* BARAC (**27**) at the M06-2X/6-311++G(d,p)-level in water (SMD), leading to cycloadduct **29**. Free energies are given in kcal mol-1 (values in parentheses).

6.4. Conclusions

To sum up, this computational study shows some key, often overlooked, features of mesoionic dipoles to be valuable synthons in orthogonal chemistry, unearthing novel and unexplored candidates, and yielding explanatory insights into reactivity based on charge-transfer analysis and non-covalent interactions at the saddle points. Notably, sydnone, the first and widely employed mesoionic heterocycle for orthogonal cycloadditions with strained cycloalkynes appears to be the less reactive dipole. Other mesomeric betaines, like isosydnones and thiosydnones would be superior to that end. A six-membered homolog,

namely 6-oxo-1,3-oxazinium-4-olate and its fluoroderivatives fulfill the ingredients required for orthogonal and/or bioconjugate labeling in terms of low-energy thermal barriers and absence of toxic or unwanted side products other than CO_2.

6.5. Experimental section

6.1.1. Computational details

All the geometries were optimized by the density functional theory (DFT) with the M06-2X in combination with 6-311++G(d,p) basis set as implemented in the Gaussian09 program package[20]. The geometries were optimized including solvation effects in water, with the aim of simulating the *in vivo* environment, which have been estimated by the well-established solvation model density (SMD) method that takes into account different contributions such as long-range electrostatic polarization (bulk solvent effect). Ground and transition structures were characterized by none and one imaginary frequency, respectively. All the relative energies shown are free energies calculated at 298.15 K with respect to the reagents. The ionization potential (*I*) and electron affinity (*A*) calculations were performed through the FMO approximation and finite differences method, at the M06-2X/6-311G(d,p) level for the distorted geometries of the reactants at the saddle points. Diffuse functions were removed because *A* values are essentially zero when adding diffuse function to the basis sets. The visualization of the frontier molecular orbitals interactions were carried out with the Chimera software.[21] The reduced density gradient (RDG) representation was calculated with the Multiwfn software[22] and visualized with VMD.[23]

The ionization potentials (*I*) and electron affinities (*A*) have been calculated by the FMO theory, whereby the ionization potential is approximated to the negative value of the HOMO energy ($I \sim -E_{HOMO}$) and the electron affinity is related to the LUMO energy ($A \sim -E_{LUMO}$). These data have also been estimated through the finite difference method, which takes into account the electronic energies of the cationic (E_{N-1}) and anionic (E_{N-1}) forms of the starting reagents with their distorted geometries at the saddle points. *N* denotes the number of electrons of a given system.

$$I = E_{N-1} - E \qquad (1)$$

$$A = E - E_{N+1} \qquad (2)$$

The chemical potential ($\mu = \partial E/\partial N$) and the chemical hardness ($\eta = \partial^2 E/\partial N^2$) were calculated in terms of the ionization potential (*I)* and the electron affinity (*A*) as follows:

$$\mu = -\frac{1}{2}(I + A) \qquad (3)$$

$$\eta = I - A \qquad (4)$$

In order to calculate the net charge transfer at the saddle points, one has to consider that the number of electrons (*N*) in the chemical system is conserved, so the total charge transfer is given by:

$$\Delta N_D = \frac{\mu_d - \mu_D}{\eta_d + \eta_D} = -\Delta N_d \qquad (5)$$

were ΔN_D and ΔN_d are the amount of charge transferred by the species D (dipole) and d (dipolarophile), respectively. By substituting equations 3 and 4 into eq. 5, the latter can express both donation and back-donation processes as follows:

$$\Delta N_D^{nuc} = \frac{I_D - A_d}{2(\eta_d + \eta_D)} = -\Delta N_d^{ele} \qquad (6)$$

and

$$\Delta N_D^{ele} = \frac{A_D - I_d}{2(\eta_d + \eta_D)} = -\Delta N_d^{nuc} \qquad (7)$$

were ΔN_D^{ele} and ΔN_D^{nuc} denote the electrophilic and nucleophilic channels in the total amount of charge transfer:

$$\Delta N_D = \Delta N_d^{nuc} + \Delta N_d^{ele} = -\Delta N_d \qquad (8)$$

6.6. Addendum

Table A6.1. Electronic energies (in Hartrees) of the cation (E_{N-1}), the anion (E_{N+1}) and the neutral (E_N) geometries of the distorted fragments of saddle points **TS$_{3\rightarrow9}$**, **TS$_{14\rightarrow17}$**, **TS$_{15\rightarrow18}$** and **TS$_{16\rightarrow19}$**, calculated at the M06-2X/6-311G(d,p) level.

Saddle points	Fragments	Electronic energies		
		E_N	E_{N-1}	E_{N+1}
TS$_{3\rightarrow9}$	Sydnone (**3**)	-337.1998773	-336.8663432	-337.2162048
	Cyclooctyne (**1**)	-311.9221633	-311.5880229	-311.8509642
TS$_{14\rightarrow17}$	Isosydnone(**14**)	-337.2407976	-336.9037866	-337.2639765
	Cyclooctyne (**1**)	-311.9252395	-311.5857951	-311.8452908
TS$_{15\rightarrow18}$	Thiosydnone (**15**)	-680.0263584	-679.6820215	-680.0890084
	Cyclooctyne (**1**)	-311.9250109	-311.5905422	-311.8452908
TS$_{16\rightarrow19}$	Betaine(**16**)	-434.5436715	-434.2308844	-434.6110210
	Cyclooctyne (**1**)	-311.9275047	-311.5869814	-311.8406329

Table A6.2. Ionization potentials (I), electron affinities (A), chemical potentials (μ), chemical hardness (η) and total charge transfer (ΔN_{tot}), charge donation (ΔN_{don}) and back-donation ($\Delta N_{back\text{-}donated}$) values of the distorted fragments of saddle points **TS$_{3\rightarrow9}$**, **TS$_{14\rightarrow17}$**, **TS$_{15\rightarrow18}$** and **TS$_{16\rightarrow19}$**, calculated by the finite difference method at the M06-2X/6-311G(d,p) level.

Saddle points	Fragments	I	A	μ	η	ΔN_{tot}	$\Delta N_{back\text{-}donated}$	ΔN_{don}
TS$_{3\rightarrow9}$	Sydnone (**3**)	9.08	0.44	-4.76	8.63	0.060	-0.220	0.280
	Cyclooctyne (**1**)	9.09	-1.94	-3.58	11.03			
TS$_{14\rightarrow17}$	Isosydnone(**14**)	9.17	0.63	-4.90	8.54	0.070	-0.216	0.284
	Cyclooctyne (**1**)	9.24	-2.18	-3.53	11.41			
TS$_{15\rightarrow18}$	Thiosydnone (**15**)	9.37	1.70	-5.54	7.67	0.110	-0.195	0.305
	Cyclooctyne (**1**)	9.10	-2.17	-3.47	11.27			
TS$_{16\rightarrow19}$	Betaine(**16**)	8.51	1.83	-5.17	6.68	0.090	-0.203	0.297
	Cyclooctyne (**1**)	9.27	-2.36	-3.45	11.63			

Table A6.3. FMO energies and HOMO-LUMO gaps for the distorted fragments of saddle points **TS$_{20\rightarrow A5}$**, **TS$_{21\rightarrow A6}$**, **TS$_{23\rightarrow A8}$** calculated by the FMO method at the M06-2X/6-311G(d,p) level in eV.

Saddle points	Fragments	Frontier Molecular Orbitals		HOMO-LUMO gaps	
		HOMO	LUMO	$LUMO_d$-$HOMO_D$	$LUMO_D$-$HOMO_d$
TS$_{20\rightarrow A5}$	Sydnone (**20**)	-7.58	-1.79	8.64	6.28
	Cyclooctyne (**1**)	-8.08	1.05		
TS$_{21\rightarrow A6}$	Isosydnone(**21**)	-7.86	-1.86	9.03	6.20
	Cyclooctyne (**1**)	-8.07	1.17		
TS$_{23\rightarrow A8}$	Betaine(**23**)	-7.36	-2.77	8.78	5.36
	Cyclooctyne (**1**)	-8.12	1.42		

Table A6.4. Ionization potentials (I), electron affinities (A), chemical potentials (μ), chemical hardness (η) and total charge transfer (ΔN_{tot}), charge donation (ΔN_{don}) and back-donation ($\Delta N_{back\text{-}donated}$) values for the distorted fragments of saddle points **TS$_{20\rightarrow A5}$**, **TS$_{21\rightarrow A6}$**, **TS$_{23\rightarrow A8}$** calculated by the FMO method at the M06-2X/6-311G(d,p) level in eV.

Saddle points	Fragments	I	A	μ	η	ΔN_{tot}	$\Delta N_{back\text{-}donanted}$	ΔN_{don}
TS$_{20\rightarrow A5}$	Sydnone (**20**)	7.58	1.79	-4.69	5.79	0.079	-0.211	0.289
	Cyclooctyne (**1**)	8.08	-1.05	-3.51	9.13			
TS$_{21\rightarrow A6}$	Isosydnone(**21**)	7.86	1.86	-4.86	6.00	0.093	-0.204	0.296
	Cyclooctyne (**1**)	8.07	-1.17	-3.45	9.24			
TS$_{23\rightarrow A8}$	Betaine(**23**)	7.36	2.77	-5.06	4.59	0.121	-0.189	0.311
	Cyclooctyne (**1**)	8.12	-1.42	-3.35	9.55			

Table A6.5. Electronic energies (in Hartrees) of the cation (E_{N-1}), the anion (E_{N+1}) and the neutral (E_N) geometries of the distorted fragments of saddle points **TS$_{20\rightarrow A5}$**, **TS$_{21\rightarrow A6}$** and **TS$_{23\rightarrow A8}$** calculated at the M06-2X/6-311G(d,p) level.

Saddle points	Fragments	Electronic energies		
		E_N	E_{N-1}	E_{N+1}
TS$_{20\rightarrow A5}$	Sydnone (**20**)	-667.4349524	-667.1226697	-667.4709970
	Cyclooctyne (**1**)	-311.9241349	-311.5895698	-311.8469919
TS$_{21\rightarrow A6}$	Isosydnone(**21**)	-667.4943225	-667.1702878	-667.5343600
	Cyclooctyne (**1**)	-311.9235540	-311.5896273	-311.8425166
TS$_{23\rightarrow A8}$	Betaine(**23**)	-864.0111436	-863.7071364	-864.0843766
	Cyclooctyne (**1**)	-311.9283877	-311.5874160	-311.8393673

Table A6.6. Ionization potentials (I), electron affinities (A), chemical potentials (μ), chemical hardness (η) and total charge transfer (ΔN_{tot}), charge donation (ΔN_{don}) and back-donation ($\Delta N_{back\text{-}donated}$) values of the distorted fragments of saddle points **TS$_{20\rightarrow A5}$**, **TS$_{21\rightarrow A6}$** and **TS$_{23\rightarrow A8}$** calculated by the finite difference method at the M06-2X/6-311G(d,p) level.

Saddle points	Fragments	I	A	μ	η	ΔN_{tot}	$\Delta N_{back\text{-}donated}$	ΔN_{don}
TS$_{20\rightarrow A5}$	Sydnone (**20**)	8.50	0.98	-4.74	7.52	0.066	-0.217	0.283
	Cyclooctyne (**1**)	9.10	-2.10	-3.50	11.20			
TS$_{21\rightarrow A6}$	Isosydnone(**21**)	8.82	1.09	-4.95	7.73	0.080	-0.210	0.290
	Cyclooctyne (**1**)	9.09	-2.21	-3.44	11.29			
TS$_{23\rightarrow A8}$	Betaine(**23**)	8.27	1.99	-5.13	6.28	0.095	-0.203	0.297
	Cyclooctyne (**1**)	9.28	-2.42	-3.43	11.70			

Table A6.7. FMO energies and HOMO-LUMO gaps for the distorted fragments of saddle points **TS20→A9**, **TS21→A10**, **TS23→A11** calculated by the FMO method at the M06-2X/6-311G(d,p) level in eV.

Saddle points	Fragments	Frontier Molecular Orbitals		HOMO-LUMO gaps	
		HOMO	LUMO	$LUMO_d$-$HOMO_D$	$LUMO_D$-$HOMO_d$
TS20→A9	Sydnone (**20**) BCN (**25**)	-7.57 -7.94	-1.78 1.24	8.81	6.15
TS21→A10	Isosydnone(**21**) BCN (**25**)	-7.89 -8.06	-2.02 1.16	9.06	6.04
TS23→A11	Betaine(**23**) BCN (**25**)	-7.38 -8.07	-2.59 1.31	8.69	5.48

Table A6.8. Ionization potentials (I), electron affinities (A), chemical potentials (μ), chemical hardness (η) and total charge transfer (ΔN_{tot}), charge donation (ΔN_{don}) and back-donation ($\Delta N_{back\text{-}donated}$) values for the distorted fragments of saddle points **TS20→A9**, **TS21→A10**, **TS23→A11** calculated by the FMO method at the M06-2X/6-311G(d,p) level in eV.

Saddle points	Fragments	I	A	μ	η	ΔN_{tot}	$\Delta N_{back\text{-}donanted}$	ΔN_{don}
TS20→A9	Sydnone (**20**) BCN (**25**)	7.57 7.94	1.78 -1.24	-4.68 -3.35	5.79 9.18	0.089	-0.206	0.294
TS21→A10	Isosydnone(**21**) BCN (**25**)	7.89 8.06	2.02 -1.16	-4.96 -3.45	5.87 9.23	0.100	-0.200	0.300
TS23→A11	Betaine(**23**) BCN (**25**)	7.38 8.07	2.59 -1.31	-4.99 -3.38	4.79 9.38	0.113	-0.193	0.307

Table A6.9. Electronic energies (in Hartrees) of the cation (E_{N-1}), the anion (E_{N+1}) and the neutral (E_N) geometries of the distorted fragments of saddle points **TS20→A9**, **TS21→A10**, **TS23→A11** calculated by the finite difference method at the M06-2X/6-311G(d,p) level.

Saddle points	Fragments	Electronic energies		
		E_N	E_{N-1}	E_{N+1}
TS20→A9	Sydnone (**20**) BCN (**25**)	-667.4338082 -464.5218346	-667.1218771 -464.1938467	-667.4694263 -464.4391736
TS21→A10	Isosydnone(**21**) BCN (**25**)	-667.4913847 -464.5210245	-667.1662853 -464.1885171	-667.5378411 -464.4440394
TS23→A11	Betaine(**23**) BCN (**25**)	-864.0156237 -464.5230669	-863.7105245 -464.1903495	-864.0818602 -464.4424097

Table A6.10. Ionization potentials (I), electron affinities (A), chemical potentials (μ), chemical hardness (η) and total charge transfer (ΔN_{tot}), charge donation (ΔN_{don}) and back-donation ($\Delta N_{back\text{-}donated}$) values of the distorted fragments of saddle points **TS$_{20\rightarrow A9}$**, **TS$_{21\rightarrow A10}$**, **TS$_{23\rightarrow A11}$** calculated by the finite difference method at the M06-2X/6-311G(d,p) level.

Saddle points	Fragments	I	A	μ	η	ΔN_{tot}	$\Delta N_{back\text{-}donated}$	ΔN_{don}
TS$_{20\rightarrow A9}$	Sydnone (**20**)	8.49	0.97	-4.73	7.52	0.074	-0.213	0.287
	BCN (**25**)	8.93	-2.25	-3.34	11.17			
TS$_{21\rightarrow A10}$	Isosydnone(**21**)	8.85	1.26	-5.06	7.58	0.084	-0.208	0.292
	BCN (**25**)	9.05	-2.09	-3.48	11.14			
TS$_{23\rightarrow A11}$	Betaine(**23**)	8.30	1.80	-5.05	6.50	0.091	-0.204	0.296
	BCN (**25**)	9.05	-2.19	-3.43	11.25			

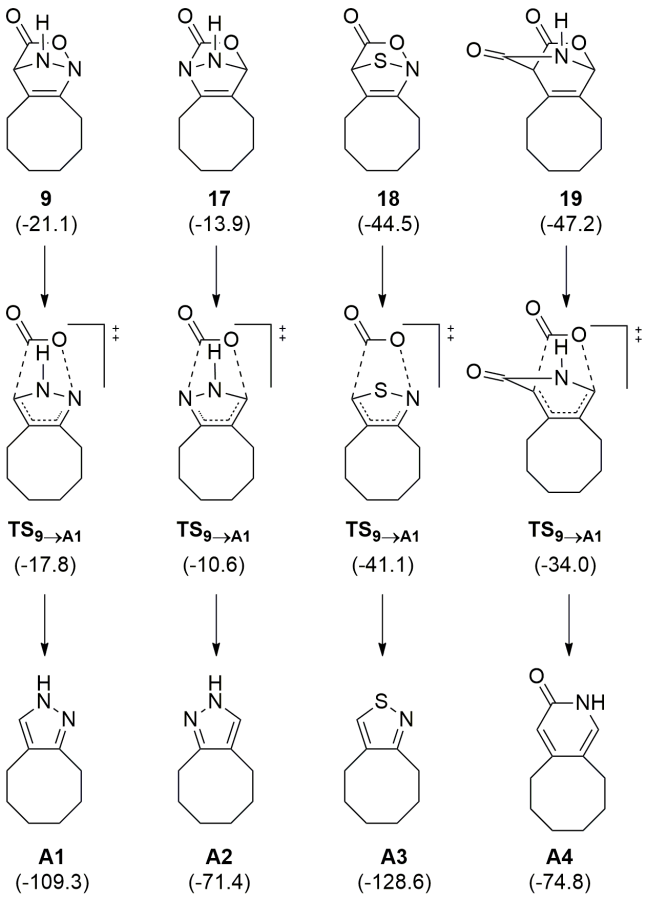

Figure A6.1. Computed free energy barriers for the retro Diels-Alder cycloaddition going from the intermediate cycloadducts **9** and **17**-**19** to the corresponding heterocycles **A1**-**A4** at the M06-2X/6-311++G(d,p)-level in water (SMD). Free energies are given in kcal mol^{-1} (values in parentheses).

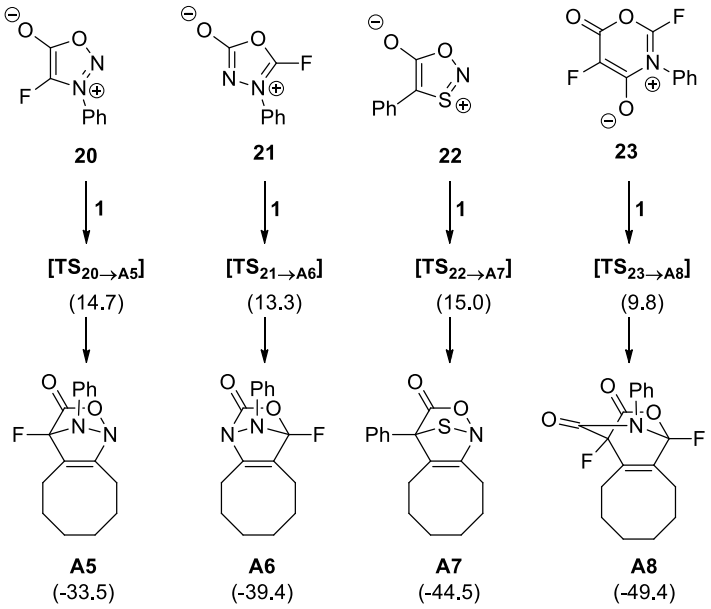

Figure A6.2. Computed free energy barriers for the reactions between dipoles **20**-**23** *versus* cyclooctyne at the M06-2X/6-311++G(d,p)-level in water (SMD), giving rise to cycloadducts **A5**-**A8**. Free energies are given in kcal mol^{-1} (values in parentheses).

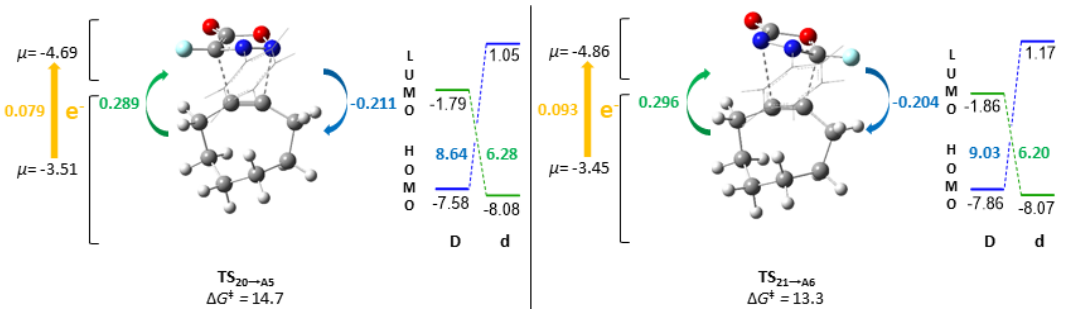

Figure A6.3. Saddle points (**TS$_{20\rightarrow A5}$** and **TS$_{21\rightarrow A6}$**) optimized-geometries for the reaction between dipoles **20** and **21** and cyclooctyne at the M06-2X/6-311++G(d,p)-level in water (SMD) (free energies are given in kcal mol^{-1}). Chemical potential (μ) values of the distorted fragments, net charge transfer (in yellow), donation (in green), and back donation (in blue) values are calculated at the M06-2X/6-311G(d,p)-level through the FMO approximation and given in eV. FMO energies and energy gaps are calculated at the same level of theory (the symbols “D” and “d” refer to the dipole and dipolarophile respectively). For clarity, the phenyl groups have been represented with wireframe.

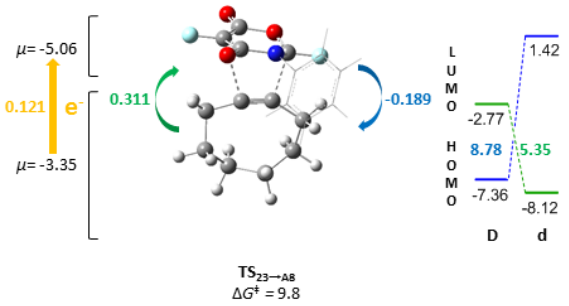

Figure A6.4. Saddle point (**TS$_{23\rightarrow A8}$**) optimized-geometrie for the reaction between dipole **23** and cyclooctyne at the M06-2X/6-311++G(d,p)-level in water (SMD) (free energy are given in kcal mol^{-1}). Chemical potential (μ) values of the distorted fragments, net charge transfer (in yellow), donation (in green), and back donation (in blue) values are calculated at the M06-2X/6-311G(d,p)-level through the FMO approximation and given in eV. FMO energies and energy gaps are calculated at the same level of theory (the symbols “D” and “d” refer to the dipole and dipolarophile respectively). For clarity, the phenyl groups have been represented with wireframe.

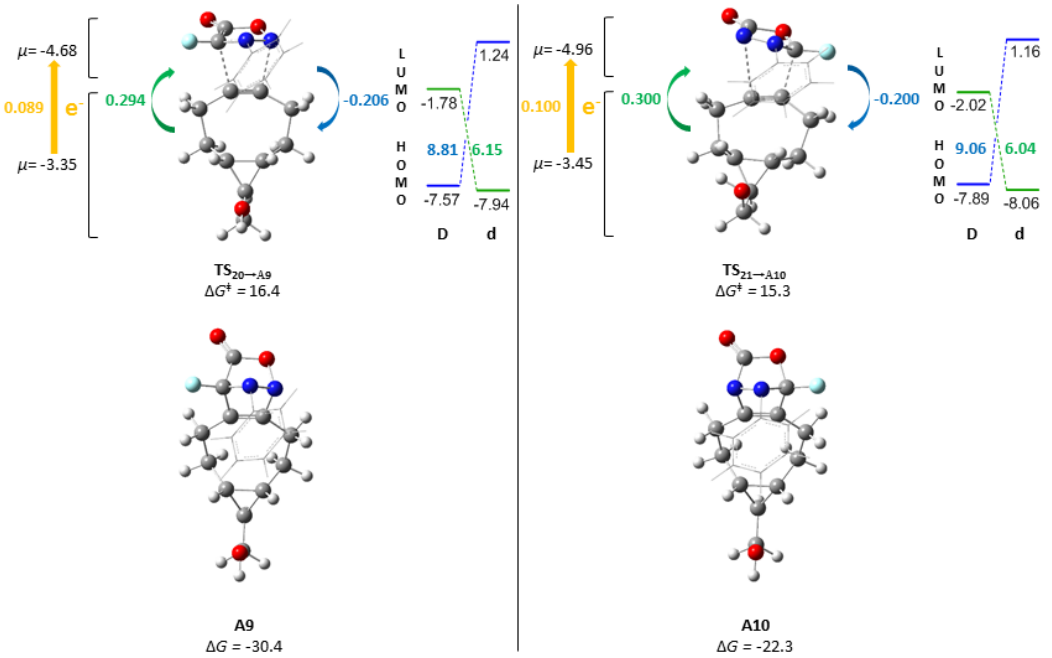

Figure A6.5. Saddle points (**TS$_{20\rightarrow A9}$** and **TS$_{21\rightarrow A10}$**) and cycloadducts (**A9** and **A10**) optimized-geometries for the reaction between dipoles **20** and **21** and BCN at the M06-2X/6-311++G(d,p)-level in water (SMD) (free energies are given in kcal mol^{-1}). Chemical potential (μ) values of the distorted fragments, net charge transfer (in yellow), donation (in green), and back donation (in blue) values are calculated at the M06-2X/6-311G(d,p)-level through the FMO approximation and given in eV. FMO energies and energy gaps are calculated at the same level of theory (the symbols “D” and “d” refer to the dipole and dipolarophile respectively). For clarity the phenyl groups have been represented with wireframe.

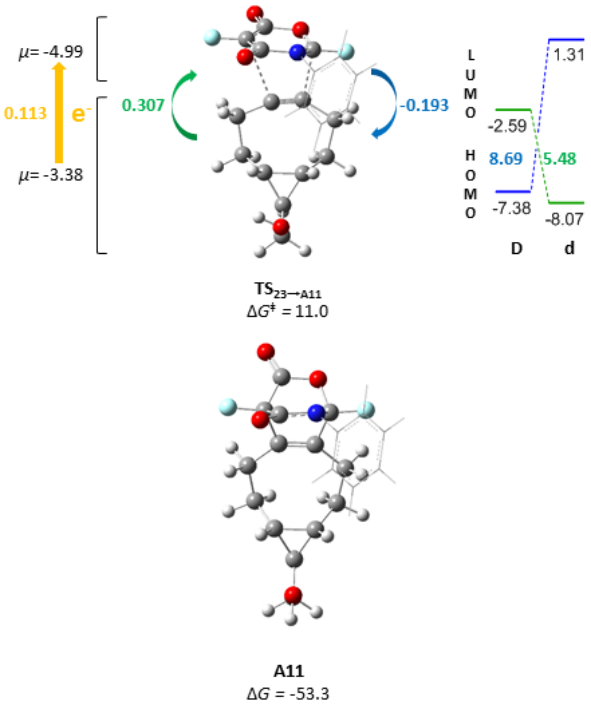

Figure A6.6. Saddle point (**TS$_{23\rightarrow A11}$**) and cycloadduct (**A11**) optimized-geometries for the reaction between dipole **23** and BCN at the M06-2X/6-311++G(d,p)-level in water (SMD) (free energies are given in kcal mol^{-1}). Chemical potential (μ) values of the distorted fragments, net charge transfer (in yellow), donation (in green), and back donation (in blue) values are calculated at the M06-2X/6-311G(d,p)-level through the FMO approximation and given in eV. FMO energies and energy gaps are calculated at the same level of theory (the symbols “D” and “d” refer to the dipole and dipolarophile respectively). For clarity the phenyl groups have been represented with wireframe.

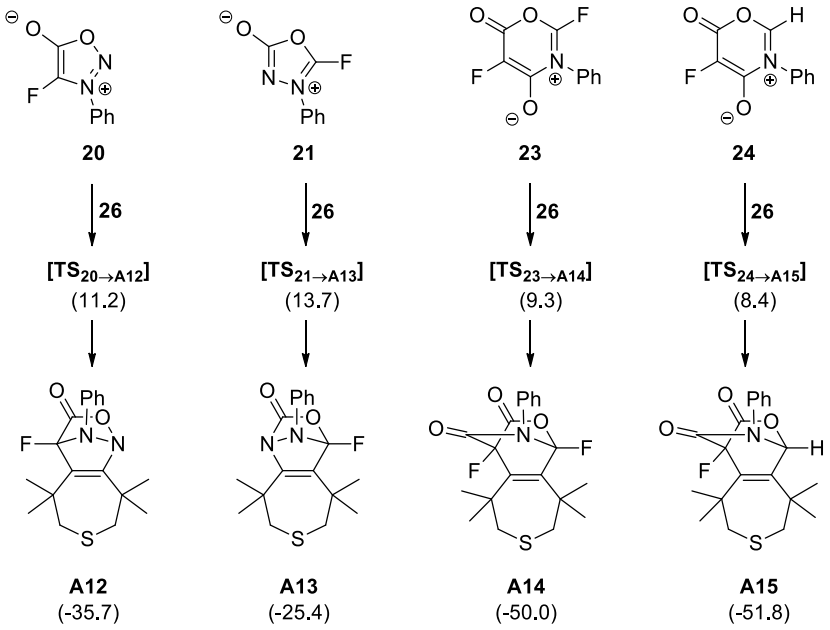

Figure A6.6. Computed free energy barriers for the reactions between dipoles **20**, **21**, **23** and **24** *versus* TMTH (**26**) at the M06-2X/6-311++G(d,p)-level in water (SMD), yielding cycloadducts **A12**-**A15**. Free energies are given in kcal mol^{-1} (values in parentheses).

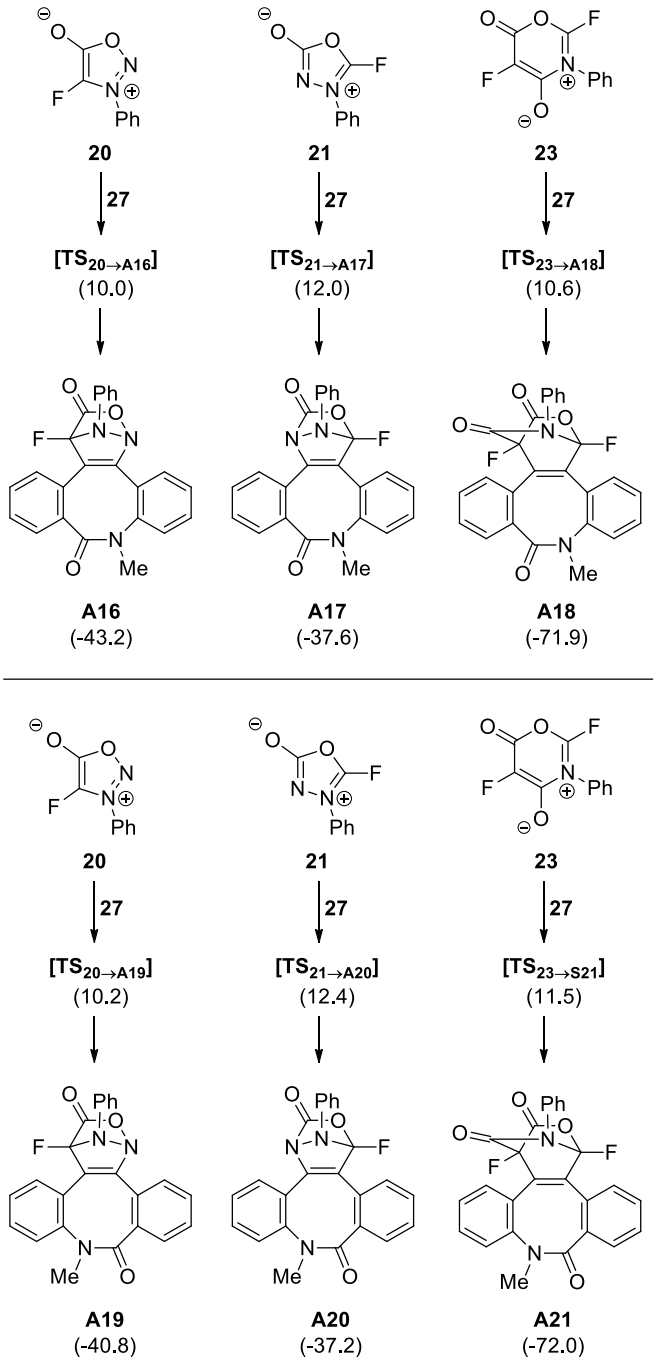

Figure A6.8. Computed free energy barriers for the cycloaddition reactions between dipoles **20**, **21**, and **23** *versus* BARAC (**27**) at the M06-2X/6-311++G(d,p)-level in water (SMD), giving the regioisomeric cycloadducts **A16**-**A18** and **A19**-**A21**. Free energies are given in kcal mol^{-1} (values in parentheses).

6.7. Bibliography

(1) Saha, M. L.; Pramanik, S. De, S.; Schmittel, M. *Chem. Soc. Rev.* **2013**, *42*, 6860-6909.

(2) (a) Sletten, E. M.; Bertozzi, C. R. *Angew. Chem.* **2009**, *121*, 7108-7133; *Angew. Chem. Int. Ed*. **2009**, *48*, 6974-6998; (b) Agarwal, P.; Bertozzi, C. R. *Bioconjugate Chem.* **2015**, *26*, 176-192; (c) Li, J.; Chen, P. R. *Nat. Chem. Biol.* **2016**, *12*, 129-137; (d) Gehringer, M.; Laufer, S. A. *Angew. Chem.* **2017**, *129*, 15709-15711; *Angew. Chem. Int. Ed.* **2017**, *56*, 15504-15505.

(3) (a) Prescher, J. A.; Bertozzi, C. R. *Nat. Chem. Biol*. **2005**, *1*, 13-21; (b) Plass, T.; Milles, S.; Koehler, C.; Schultz, C.; Lemke, E. A. *Angew. Chem.* **2011**, *123*, 3964-3967; *Angew. Chem. Int. Ed*. **2011**, *50*, 3878-3881; (c) Koo, H.; Lee, S.; Na, J. E.; Kim, S. H.; Hahn, S. K.; Choi, K.; Kwon, I. C.; Jeong, S. I.; Kim, K. *Angew. Chem.* **2012**, *124*, 12006-12010; *Angew. Chem. Int. Ed*. **2012**, *51*, 11836-11840; (d) Anderton, G. I.; Bangerter, A. S.; Davis, T. C.; Feng, Z.; Furtak, A. J.; Larsen, J. O.; Scroggin, T. L.; Heemstra, J. M. *Bioconjugate Chem.* **2015**, *26*, 1687-1691; (e) Wang, I.; Lazor, K. M.; DeMeester, K. E.; Liang, H.; Heiss, T. K.; Grimes, C. L. *J. Am. Chem. Soc.* **2017**, *139*, 13596-13599; (f) For a recent perspective on challenges and limitations of azide-alkyne bioconjugation: Pickens, C. J.; Johnson, S. N.; Pressnall, M. M.; Leon, M. A.; Berkland, C. J. *Bioconjugate Chem.* **2018**, *29*, 686-701.

(4) For a recent and excellent overview of newer and conventional bioconjugation reactions: Algar, W. R. *Chemoselective and Bioorthogonal Ligation Reactions*; W. R. Algar, P. Dawson, I. L. Medintz, Eds., Wiley-VCH, Weinheim, 2017, Vol. 1, Ch. 1, pp. 3-36.

(5) (a) Mackenzie, D. A.; Sherratt, A. R.; Chigrinova, M.; Kell, A. J.; Pezacki, J. P.; *Chem. Commun.* **2015**, *51*, 12501-12504; (a) Tang, T. S.-M.; Liu, H.-W.; Lo, K. K.-W. *Chem. Eur. J.* **2016**, *22*, 9649-9659; (b) Lee, L. C.-C.; Lau, J. C.-W.; Liu, H.-W.; Lo, K. K.-W. *Angew. Chem.* **2016**, *128*, 1058-1061; *Angew. Chem. Int. Ed*. **2016**, *55*, 1046-1049.

(6) (a) McGrath, N. A.; Raines, R. T. *Chem. Sci*. **2012**, *3*, 3237-3240; (b) Josa-Culleré, L.; Wainman, Y. A.; Brindle, K. M.; Leeper, F. J. *RSC Adv*. **2014**, *4*, 52241-52244; (c) Friscourt, F.; Fahrni, C. J.; Boons, G.-J.; *Chem. Eur. J.* **2015**, *21*, 13996-14001.

(7) (a) Wallace, S.; W. J. Chin, *Chem. Sci.* **2014**, *5*, 1742-1744; (b) Liu, H.; Audisio, D.; Plougastel, L.; Decuypere, E.; Buisson, D.-A.; Koniev, O.; Kolodych, S.; Wagner, A.; Elhabiri, M.; Krzyczmonik, A.; Forsback, S.; Solin, O.; Gouverneur, V.; Taran, F. *Angew. Chem.* **2016**, *128*, 12252-12256; *Angew. Chem. Int. Ed.* **2016**, *55*, 12073-12077; (c) Bernard, S.; Audisio, D.; Riomet, M.; Bregant, S.; Sallustrau, A.; Plougastel, L.; Decuypere, E.; Gabillet, S.; Kumar, R. A.; Elyian, J.; Trinh, M. N.; Koniev, O.; Wagner, A.; Kolodych, S.; Taran, F. *Angew. Chem.* **2017**, *129*, 15818-15822; *Angew. Chem. Int. Ed.* **2017**, *56*, 15612-15616; (d) For a recent overview on sydnone-alkyne cycloadditions: Decuypère, E.; Plougastel, L.; Audisio, D.; Taran, F. *Chem Comm*. **2017**, *53*, 11515-11527.

(8) For general and recent reviews on mesoionic dipole-based chemistry: (a) Gribble, G. W. *Synthetic Applications of 1,3-Dipolar Cycloaddition Chemistry Toward Heterocycles and Natural Products*; Padwa, A.; Pearson W. H., Eds., John Wiley & Sons, New York, **2002**, pp. 681-753; (b) Ávalos, M.; Babiano, R.; Cintas, P.; Jiménez, J. L.; Palacios, J. C. *Acc. Chem. Res.* **2005**, *38*, 460-468; (c) Lopchuk, J. M.; *Top. Heterocycl. Chem.* **2012**, *29*, 381-414.

(9) (a) Gordon, C. G.; Mackey, J. L.; Jewett, J. C.; Sletten, E. M.; Houk, K. N.; Bertozzi, C. R. *J. Am. Chem. Soc.* **2012**, *134*, 9199-9208; (b) Kamber, D. N.; Liang, Y.; Blizzard, R. J.; Liu, F.; Mehl, R. A.; Houk, K. N.; Prescher, J. A. *J. Am. Chem. Soc.* **2015**, *137*, 8388-8391; (c) Narayanam, M. K.; Liang, Y.; Houk, K. N.; Murphy, J. M. *Chem. Sci.* **2016**, *7*, 1257-1261; (d) Champagne, P. A.; Houk, K. N. *J. Org. Chem.* **2017**, *82*, 10980-10988.

(10) Zhao, Y.; Truhlar, D. G.*Theor. Chem. Acc*. **2008**, *120*, 215-241.

(11) Francl, M. M.; Pietro, W. J.; Hehre, W. J.; Binkley, J. S.; DeFrees, D. J.; Pople, J. A.; Gordon, M. S. *J. Chem. Phys*. **1982**, *77*, 3654-3665.

(12) (a) Marenich, A. V.; Cramer, C. J.; Truhlar, D. G. *J. Phys. Chem. B* **2009**, *113*, 4538-4543; (b) Marenich, A. V.; Cramer, C. J.; Truhlar, D. G., *J. Phys. Chem. B* **2009**, *113*, 6378-6396; (c) Ribeiro, R. F.; Marenich, A. V.; Cramer, C. J.; Truhlar, D. G. *J. Comput.-Aided Mater*. **2010**, *24*, 317-333; (d) Halim, M. A.; Shaw, D. M.; Poirier, R. A. *J. Mol. Struct. (THEOCHEM)* **2010**, *960*, 63-72; (e) G. Saielli, J. Phys. Chem. A 2010, 114, 7261-7265.

(13) (a) Putnam, R. W.; Filosa, J. A.; Ritucci, N. A. *Am. J. Physiol. Cell Physiol.* **2004**, *287*, C1493-C1526; (b) Kim, T. H.; Böhmer, M.; Hu, H.; Nishimura, N.; Schroeder, J. I. *Annu. Rev. Plant Biol.* **2010**, *61*, 561-591.

(14) (a) McCarthy, A. R.; Ollis, W. D.; Barnes, A. N. M.; Sutton, L. E.; Ainsworth, C. *J. Chem. Soc.* **1969**, 1185-1194; (b) McCarthy, A. R.; Ollis, W. D.; Ramsden, C. A.; *J. Chem. Soc.* **1974**, 624-627; (c) Ollis, W. D.; Stanforth, S. P.; Ramsden, C. A. *Tetrahedron* **1985**, *41*, 2239-2329 and references therein.

(15) (a) Ramsden, C. A. *Tetrahedron* **2013**, *69*, 4146-4159; (b) Oziminski, W. P.; Ramsden, C. A. *Tetrahedron* **2015**, *71*, 7191-7198.

(16) A SciFinder® search on monocyclic 6-oxo-1,3-oxazinium-4-olates (bicyclic systems and higher polycyclic structures were deliberately omitted) identified a set of 32 compounds with different substitution patterns (alkyl, aryl): (a) Friedrichsen, W.; Kujath, E.; Liebezeit, G.; Schmidt, R.; Schwarz, I. *Justus Liebigs Ann. Chem.* **1978**, 1655-1665; (b) Friedrichsen, W.; Krueger, C.; Kujath, E.; Liebezeit, G.; Mohr, S. *Tetrahedron Lett.* **1979**, 237-238; (c) Kappe, T.; Golser, W.; Hariri, M.; Stadlbauer, W.; *Chem. Ber.* **1979**, *112*, 1585-1594; (d) Friedrichsen, W.; Kujath, E.; Liebezeit, G.; *Zeit. Natur. Anorg. Chem. Org. Chem.* **1982**, *37B*, 222-233; (e) Friedrichsen, W.; Schildberg, M. *Heterocycles* **1983**, *20*, 431-434; (f) Gotthardt, H.; Flosbach, C.; *Chem. Ber.* **1988**, *121*, 951-960; (g) Stadlbauer, W.; Badawey, E.-S.; Hojas, G.; Roschger,; Kappe, T. *Molecules* **2001**, *6*, 338-352; (h) Sheibani, H.; Bernhardt, P. V.; Wentrup, C. *J. Org. Chem.* **2005**, *70*, 5859-5861; (i) Abaszadeh, M.; Sheibani, H.; Saidi, K.; Nejad, R. M. *Arkivoc* **2008**, 262-268.

(17) (a) Orozco-Valencia, A. U.; Gázquez, J. L.; Vela, A. *J. Phys. Chem. A* **2017**, *121*, 4019-4029; (b) Pearson, R. G. *Inorg. Chem*. **1988**, *27*, 734-740; (c) Pearson, R. G. *J. Org. Chem*. **1989**, *54*, 1423-1430; (d) Miranda-Quintana, R. A.; Ayers, P. W. *Theor. Chem. Acc*. **2016**, *135*:172.

(18) Favre, C.; De Cremoux, L.; Badaut, J.; Friscourt, F. *J. Org. Chem.* **2018**, *83*, 2058-2066

(19) (a) Johnson, E. R.; Keinan, S.; Mori-Sánchez, P.; Contreras-García, J.; Cohen, A. J.; Yang, W. *J. Am. Chem. Soc*. **2010**, *132*, 6498-6506; (b) Contreras-García, J.; Johnson, E. R.; Keinan, S.; Chaudret, R.: Piquemal, J.-P.; Beratan, D. N.; Yang, W. *J. Chem. Theory Comput*. **2011**, *7*, 625-632.

(20) Frisch, M. J.; Trucks, G. W.; Schlegel, H. B.; Scuseria, G. E.; Robb, M. A.; Cheeseman, J. R.; Scalmani, G.; Barone, V.; Mennucci, B.; Petersson, G. A.; Nakatsuji, H.; Caricato, M.; Li, X.; Hratchian, H. P.; Izmaylov, A. F.; Bloino, J.; Zheng, G.; Sonnenberg, J. L.; Hada, M.; Ehara, M.; Toyota, K.; Fukuda, R.; Hasegawa, J.; Ishida, M.; Nakajima, T.; Honda, Y.; Kitao, O.; Nakai, H.; Vreven, T. Jr.; Montgomery J. A.; Peralta, J. E.; Ogliaro, F.; Bearpark, M.; Heyd, J. J.; Brothers, E.; Kudin, N. K.; Staroverov, V. N.; Kobayashi, R.; Normand, J.; Raghavachari, K.; Rendell, A.; Burant, J. C.; Iyengar, S. S.; Tomasi, J.; Cossi, M.; Rega, N.; Millam, J. M.; Klene, M.; Knox, J. E.; Cross, J. B.; Bakken, V.; Adamo, C.; Jaramillo, J.; Gomperts, R.; Stratmann, R. E.; Yazyev, O.; Austin, A. J.; Cammi, R.; Pomelli, C.; Ochterski, J. W.; Martin, R. L.; Morokuma, K.; Zakrzewski, V. G.; Voth, G. A.; Salvador, P.; Dannenberg, J. J.; Dapprich, S.; Daniels, A. D.; Farkas, Ö.; Foresman, J. B.; Ortiz, J. V.; Cioslowski, J.; Fox, D. J.; Gaussian 09, Revision D.01; Gaussian, Inc.: Wallingford, CT, 2009.

(21) Pettersen, E. F.; Goddard, T. D.; Huang, C. C.; Couch, G. G.; Greenblatt, D. M.; Meng, E. C.; Ferrin, T. E. *J Comput. Chem*. **2004**, *13*, 1605-1612.

(22) Lu, T.; Chen, F. *J. Comp. Chem*. **2012**, *33*, 580-592.

(23) Humphrey, W.; Dalke, A.; Schulten, K. *J. Mol. Graphics* **1996**, *14*, 33-38.

7. General conclusions

Throughout this work, it has been experimentally demonstrated that bicyclic thioisomünchnones derived from thiazolidin-2-thiones react in a regioselective manner with asymmetrically-substituted dipolarophiles, both olefins and acetylenes. The analysis of energy barriers for the reactions of 2-phenyl-5,6-dihydrothiazolo[2,3-*b*]thiazol-4-ium-3-olate with asymmetric olefins and acetylenes shows that the reactivity is slightly higher in the case of double bonds, but similar when the dipole is 5,6-dihydrothiazolo[2,3-*b*]thiazol-4-ium-3-olate against triple bonds, because the lack of substitution at C2 reduces the steric repulsions. From a geometrical point of view, the cycloadditions with olefins and acetylenes show similar trends, where the favored regiochemistry proceeds via asynchronous and/or stepwise mechanisms. Regarding the competitiveness between the two regiochemistries, all the energy data show that the kinetically favored processes for double and triple bonds agree with the experimental results, where electron-withdrawing groups are placed on C8 of the isolated products. The similarity in energy differences between the competitive regiochemistries also points to a similar selectivity against olefins and acetylenes. However, there is an exception in the case of (*E*)-(2-nitrovinyl)benzene, that together with the lowest barrier found, it shows the most regioselective pathway as well. Regarding the values of charge transfer (between the NBOs) for the cycloadditions with both type of reagents, it is noteworthly that the saddle points for the favored regiochemistry show a net electron flux from dipole to dipolarophile and an opposite flux for the disfavored regiochemistry. Donation processes during the favored regiochemistry are superior for cycloadditions with double bonds, while retrodonation values for the opposite regiochemistry afford similar charge transfers. In the case of symmetrical dipolarophiles, the reaction of 2-phenyl-5,6-dihydrothiazolo[2,3-*b*]thiazol-4-ium-3-olate with ACDM shows a markedly higher barrier than for symmetrical olefins. The charge transfer analyses for the cycloadditions with 1-phenyl-1*H*-pyrrole-2,5-dione and dimethyl maleate lead to results opposite to those obtained with the asymmetric derivatives, i.e. the most favorable process is the cycloaddition of the mesoionic dipole with dimethyl maleate, where electron donation from the dipolarophile to dipole is largely superior to the reversed direction. Additionally, the influence of the isopropyl group of (*S*)-5-isopropyl-2-phenyl-5,6-dihydrothiazolo[2,3-*b*]thiazol-4-ium-3-olate *versus* double and triple bonds has also been evaluated. This influence could not verified experimentally through the reaction with acetylenes, because the initial 1:1 cycloadducts evolved further with concomitant lost of the newly generated chiral centers. The theoretical results are surprising, as the lower energy barriers were

obtained when methyl propiolate approaches to the most hindered face of the dipole. This can reasonably be ascribed to the small size of the dipolarophile and, as a result, the bond length with the isopropyl group is not enough to generate repulsive interactions, but rather van der Waals stabilization. This theoretical result led us to use bulky double bonds in cycloadditions with olefins. They were carried out experimentaly with both 1-phenyl-1*H*-pyrrole-2,5-dione and (*E*)-(2-nitrovinyl)benzene. In these cases, the facial selection could be detected experimentally and supported by DFT calculations.

In Chapter 5, we have unveiled the double reactivity of a mesoionic dipole derived from a proteinogenic aminoacid. This dual dipolar behavior has never been detected previously, and the present Thesis provides sufficient experimental and theoretical validations. The isolation of an adduct formed by the cycloaddition with a thiazolium-olate, whereas the other arises from a diazolium-olate, clearly evidences that there is an equilibrium between two species resulting from a rapid proton transfer. The theoretical analysis of these reactions indicates that such species behave actually as dipoles. Generally, the C-N-C dipole appears to be more reactive than the C-S-C one, because of a higher interaction energy between the dipole and dipolarophile. On the other hand, the latter is less stable, so that the diazolium-thiazolium equilibrium will most likely be shifted to the thiazolium-olate form.

Chapter 6 shows that the 1,3-dipolar cycloaddition reactions of sydnones, isosydnones, thiosydnones, and conjugated six-membered mesomeric betaines with strained acetylenes are inverse electron demanding processes, controlled by the $HOMO_{dipolarophile}$-$LUMO_{dipole}$ interaction. The incorporation of electron-withdrawing groups like fluorine atoms into the dipoles has yielded much faster reactions, thereby corroborating previous studies by different groups. Encouraged by these results, a series of dipoles that give rise to ultrafast cycloaddition reactions with cyclooctynes has been developed in a theoretical manner. These reagents, not taken into account to date, meet the fundamental requirements for their application as suitable reagents in bio-orthogonal chemistry, which opens the doors to further experimental explorations.